„From Lithium Phosphanide to a series of 2-amino-1$\lambda^3\sigma^2$-phosphaalkenes and Some *N*-Lithium Phosphaguanidinates – Syntheses, 2D NMR Spectroscopic Analyses and X-Ray Structure Determinations“

Von der Fakultät Chemie der Universität Stuttgart

zur Erlangung der Würde eines Doktors

der Naturwissenschaften (Dr. rer. nat.)

genehmigte Abhandlung

vorgelegt von

M. Sc. **Samer A. Tanash**

Huwwara/Jordanien

Hauptberichter: Prof. Dr. D. Gudat

Mitberichter: Prof. Dr. Th. Schleid

Prüfungsvorsitzender: Prof. Dr. J. Van Slageren

Tag der mündlichen Prüfung: 21.09.2017

Institut für Anorganische Chemie der Universität Stuttgart

2017

Selbständigkeitserklärung

Hiermit erkläre ich, daß ich die vorliegende Arbeit selbständig und nur unter Verwendung der angegebenen Literatur und Hilfsmittel angefertigt habe.

Stuttgart, den 26.07.2017 M. Sc. Samer Tanash

Die vorliegende Arbeit wurde am
Institut für Anorganische Chemie
der Universität Stuttgart
unter der Leitung von Herrn Professor
Dr. D. Gudat angefertigt.

Meinem Doktorvater,
Herrn Prof. Dr. Gerd Becker,
danke ich herzlich für die Themenstellung,
die Bereitstellung ausgezeichneter
Arbeitsbedingungen, wertvolle
Anregungen und Diskussionen sowie sein stetes
Interesse an dieser Arbeit.

Meinen Eltern,
meiner Schwester und meinen Brüdern,
meiner Frau,
meinen Söhnen und meinen Töchtern
gewidmet

Table of Contents

Abbreviations and Definitions……... 9
1. Introduction…… 11
1.1 Low Coordinate-phosphorus Compounds……... 11
1.2 Amidines and Guanidines…… 14
1.3 Phospha-amidines and Phospha-guanidines and their Anions……. 16
1.4 Normal and Inverse Polarisation Phosphorus-carbon Double Bonds…….. 18
2. Reactions of $1\lambda^3\sigma^2$-Phosphaalkene **1** with *tert*-Butylchlorodiphenylsilane and Trifluoromethylsulfonic Acid…… 21
2.1 Introduction…….. 21
2.2 Low Temperature NMR Investigation of 2-(Lithiumamido)-2-phenyl-$1\lambda^3\sigma^2$-phosphaalkene {**(*Z*)-/(*E*)-1**}…… 25
2.3 Studies on the Chemical Reactivity of 2-(Lithiumamido)-2-phenyl-$1\lambda^3\sigma^2$-phosphaalkene {**(*Z*)-/(*E*)-1**} against *tert*-Butylchlorodiphenylsilane…….. 30
2.3.1 Preparation and Reaction Mechanism…….. 30
2.3.2 NMR Spectroscopic Characterization……... 32
2.3.3 Crystal Data, Data Collection and Structure Analysis…….. 39
2.3.4 Discussion of Bond Lengths and Angles…….. 41
2.4 2-[(*tert*-Butyldiphenylsilyl)amino]-2-phenyl-$1\lambda^3\sigma^2$-phosphaalkene {**(*Z*)-/(*E*)-I.1**} by Decomposition of Compound **(*Z*)-/(*E*)-I.2**…….. 47
2.5 Formation of (*Z*)-/(*E*)-Isomeric 2-Amino-2-phenyl-$1\lambda^3\sigma^2$-phosphaalkene H~P=C(C_6H_5)–NH2 (**I.0**) in Reactions of 2-(Lithiumamido)-2-phenyl-$1\lambda^3\sigma^2$-phosphaalkene (**1**) with Acids…… 53
2.6 NMR Spectroscopic Analysis of the Diphosphanes (*Z*)-**I.01** and (*Z*)-**I.02** Originating from a Dimerisation of the Phosphaalkenes (*Z*)-/(*E*)-**I.0**……. 64
3. Reaction of (*Z*)-/(*E*)-2-(Lithiumamido)-2-phenyl-$1\lambda^3\sigma^2$-phosphaalkene (**1**) with Bis(η^5-pentamethylcyclopentadienyl)zirconium dichloride…….. 73
3.1 Introduction……. 73
3.2 Isolation and NMR Spectroscopic Characterization of the Zirconium Complex **II**……... 76
3.2.1 Preparation……... 76
3.2.2 NMR Spectroscopic Identification of the Solvent Included in the Solid State Adducts……... 78
3.3 X-ray Structure Determinations of the Solvates of Complex **II**..... 89
3.3.1 Crystal data, Measuring Techniques and Structure Analyses……... 89
3.3.2 Bond Distances and Bond Angles for (**II·C_7H_8**)…….. 91
3.3.3 Crystal Packing of the Solid State Adduct (**II·C_7H_8**) and its Relation to the PtS-Structure……... 93
3.3.4 Molecular Structure of Compound **II** in the Solid State Adduct (**2II·*n*-C_6H_{14}**)……. 97
3.3.5 Packing of Both Components of the Solid State Adduct (**2II·*n*-C_6H_{14}**)….. 107
4. Reaction of (1,2-Dimethoxyethane)lithium Phosphanide with Different Diorganylcarbodiimides……. 109
4.1 Introduction…….. 109
4.2 Reaction of (1,2-dimethoxyethane)Lithium Phosphanide with Bis(4-methylphenyl)carbodiimides……..... 113
4.2.1 Preparation and Reaction Mechanism……... 113
4.2.2 NMR Spectroscopic Characterization……... 115
4.2.3 Crystal data, Data Collection and Structure Analysis……... 120

4.2.4 Discussion of Bond Lengths and Angles…….. 122
4.3 Reaction of (1,2-dimethoxyethane)Lithium Phosphanide with *N,N′*-di-*tert*-Butylcarbodiimide…… 128
4.3.1 Preparation and Reaction Mechanism……... 128
4.3.2 NMR Spectroscopic Characterization……... 129
4.3.3 Crystal Data, Data Collection and Structure Analysis…….. 131
4.3.4 Discussion of Bond Lengths and Angles…….. 134
4.4 Reaction of (1,2-Dimethoxyethane)lithium Phosphanide with *N,N′*-dicyclohexyl- and diisopropylcarbodiimide……. 137
4.4.1 Preparation and Reaction Mechanism……... 137
4.4.2 NMR Spectroscopic Characterization……... 138
4.4.3 Crystal Data, Data Collection and Structure Analysis…….. 138
4.4.4 Discussion of Bond Lengths and Angles…….. 141
5. Experimental Section……. 147
5.1 General Considerations…… 147
5.2 Preparation of (1,2-Dimethoxyethane-*O,O′*)lithium Phosphanide…….. 150
5.2.1 2-[(1,2-Dimethoxyethane-*O,O′*)lithiumamido]-2-phenyl-1$\lambda^3\sigma^2$-Phosphaalkene……... 150
5.3 Procedures for the Preparation of New Compounds…… 151
5.3.1 *Z*-[*N,P*-Bis(*tert*-butyldiphenylsilyl)-2-amino-2-phenyl-1$\lambda^3\sigma^2$-phosphaalkene](**I.2**)……... 151
5.3.2 2-[(*tert*-Butyldiphenylsilyl)amino]-2-phenyl-1$\lambda^3\sigma^2$-phosphaalkene {(***Z***)-/(***E***)-**I.1**} by Decomposition of Compound (***Z***)-/(***E***)-**I.2**…… 153
5.3.3 Formation of (*Z*)-/(*E*)-Isomeric 2-Amino-2-phenyl-1$\lambda^3\sigma^2$-phosphaalkene H~P=C(C_6H_5)–NH_2 (**I.0**) in Reactions of 2-(Lithiumamido)-2-phenyl-1$\lambda^3\sigma^2$-phosphaalkene (**1**) with Acids……. 154
5.3.4 Formation of Diphosphanes (***Z***)-**I.01** and (***Z***)-**I.02** from a Dimerisation of the Phosphaalkenes (***Z***)-/(***E***)-**I.0**……... 156
5.3.5 [*N,N′*-(1-Amido-3-imido-1,3-diphenyl-2$\lambda^3\sigma^2$-phospha-1-propene)bis(η^5-pentamethylcyclopentadienyl)zirconium] (**II**)…… 157
5.3.6 Bis(1,2-dimethoxyethane)-1κ^2O^1,O^2;$^2\kappa^2O^3,O^4$]{bis[μ-*N,N′*-bis(4-methylphenyl)}-*C*-phosphanylformamidinato]-1:2κ^4N^1, N^2;1κ^2N^3;N^4} dilithium (**III**)……... 158
5.3.7 [*tert*-Butyl-[(*tert*-butylamino)phosphanylidenemethyl]amino]-(tetrahydrofuran-*O*)lithium (**IV**)……... 159
5.3.8 *Catena*-poly[μ-(*N,N′*-dicyclohexyl-*C*-phosphanidato-1*:2*κ^2P-formamidinato-1:2κ^2N,1:2$\kappa^2N′$)-1,2-bis(tetrahydrofuran-*O*]di-lithium (**V**)..... 161
5.3.9 *Catena*-poly[μ-(*N,N′*-diisopropyl-C-phosphanidato-1*:2*κ^2P-formamidinato-1:2κ^2N,1:2$\kappa^2N′$)-1,2-bis(tetrahydropyran-*O*]di-lithium (**VI**)..... 161
6. Summary…… 163
7. Zusammenfassung…….. 175
8. Appendix…… 189
9. References 227

List of symbols and abbreviations

J coupling constant

δ chemical shift

b.p boiling point

n-Bu *n*-butyl

^{t}Bu *tert*-butyl

°C degree celcius

Cal. calculated

Cp* pentamethylcyclopentadienyl

Cp^{o} ethyltetramethylcyclopentadienyl

Cp cyclopentadienyl

Cy cyclohexyl

Dipp diisopropyl

DME, dme 1,2-dimethoxyethane

DFT density functional theory

DABCO 1,4-diazabicyclo[2.2.2]octane

d doublet

dd doublet of doublets

ddd doublet of doublet of doublets

dddd doublet of doublet of doublet of doublets

eq. equivalent

Et ethyl

Gl. Gleichung

h hour

IR Infrared spectroscopy

*i*Pr *iso*-propyl

K Kelvin temperature

MHz Mega Herz

m.p melting point

mmol millimol

Me methyl

Mes 2,4,6-trimethylphenyl

Mes* 2,4,6-tri-*tert*-butylphenyl

m multiplet

NBO natural bond orbital

NMR nuclear magnetic resonance

Ph phenyl

p-Tolyl *para*-tolyl; 4-methylphenyl

pm picometer

q quartet

r.t room temperature

s singlet

t triplet

TMS trimethylsilyl

THF tetrahydrofuran

TMEDA/tmeda tetramethylethylendiamine

XRD X-ray diffraction

1. Introduction

1.1 *Low Coordinate–Phosphorus Compounds*

In 1669, *Henning Brand* a German alchemist discovered – by chance while he was distilling human urine – a substance that emits light when exposed to oxygen. He named this substance "Kaltes Feuer"– the cold fire. It was in the 17th century until the name changed to phosphorus which means "light bearer" [1]. Phosphorus has not only many applications in our life, but it is essential for life itself. As phosphate for example, it is a component of DNA, RNA and ATP. Phosphorus exhibits a variety of oxidation state, so it is important even for the phosphorus chemist to classify the organophosphorus compounds according to the number of their valences (λ) and coordination number (σ).

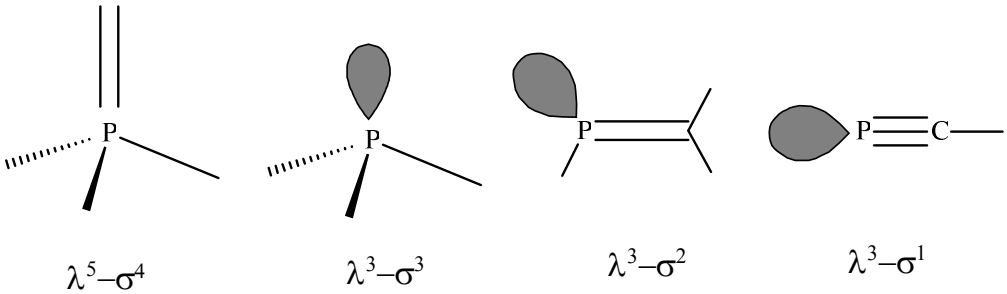

It was thought in the first half of the 20th century that low coordination phosphorus compounds of the type λ^3–σ^2 (phosphaalkenes) and λ^3–σ^1 (phosphaalkynes) does not exist. Nowadays, not only this type of compounds has been proven to exist, but even species like diphosphorus (P_2) and phosphinidenes (PH) could be stabilize by multiple-bonding to carbenes fragments [2 a)].

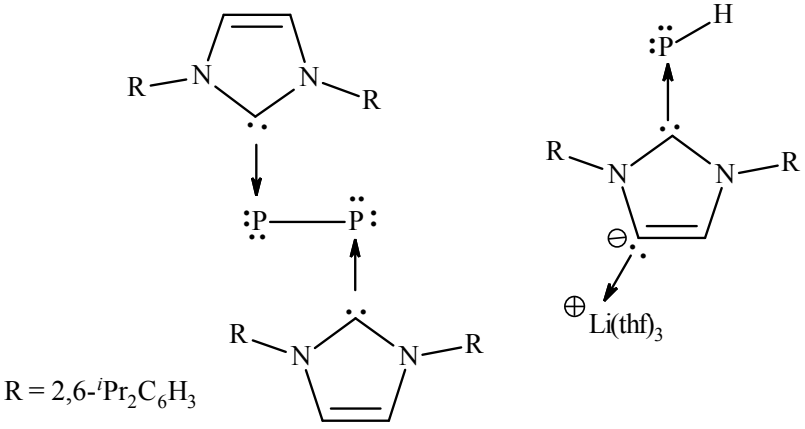

Figure 1.1 Representation of "carbene-stabilized" P2- and PH fragments (according to litature [2 a)]).

In fact, the chemistry of compounds with low-coordinate phosphorus atoms involved in phosphorus–carbon multiple bonding has rapidly developed and attracted growing interest in organophosphorus chemistry [2 b)].

The story of low coordinate phosphorus compounds began when *Gier* reported in 1961 the formation of minor amounts of phosphaacetylene (H−C≡P) from phosphine in an electric arc between graphite electrods, the gaseous products were collected at low temperature and separated by gas chromatography [3]. Three years later *Dimroth* and *Hoffmann* synthesized the first compound containing a partial P=C−double bonds (**1.1**) [4]. This compound draws its stability from the delocalization of the positive charge over the whole conjugated π-system. In 1966 *Märkl* prepared the first non-ionic, two coordinate Phosphorus(III) system (**1.2**) [5].

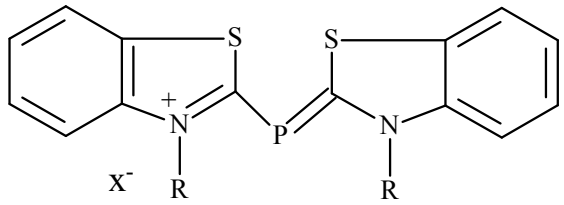

1.1

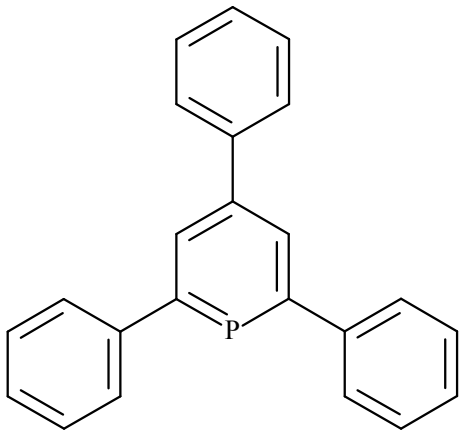

1.2

The great leap of the chemistry of the low coordinate phosphorus compounds occurred in the late 70es and early 80es of the last century. For example, by reacting $RP(SiMe_3)_2$ with $^tBuC(O)Cl$, *G. Becker* was able to isolate the first stable phosphaalkene (**1.3**) in 1976 [6].

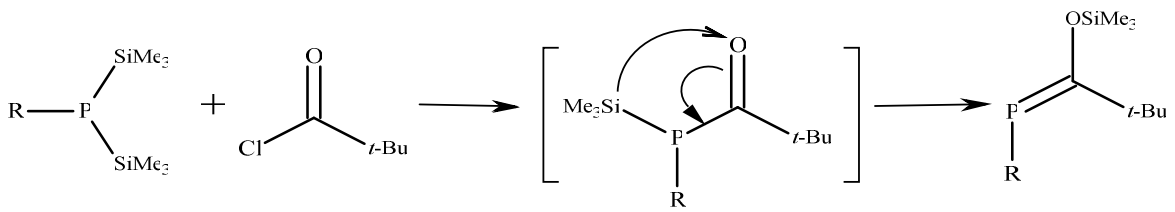

R= CH_3,^{t}Bu,Cy,Ph

1.3

The stability of this phosphaalkene results from two main factors, namely the presence of a hetero atom such as oxygen (*O*) attached to the sp^2-hybridized carbon atom of the double bond and the steric protection imposed by the use of bulky substituents. The importance of

steric protection is also illustrated, for example, by *Yoshifuji's* successful isolation of the first stable diphosphene using the extremely bulky 2,4,6-tri-*tert*-butylphenyl (Mes*) substituent attached to the phosphor atom (**1.4**) [7].

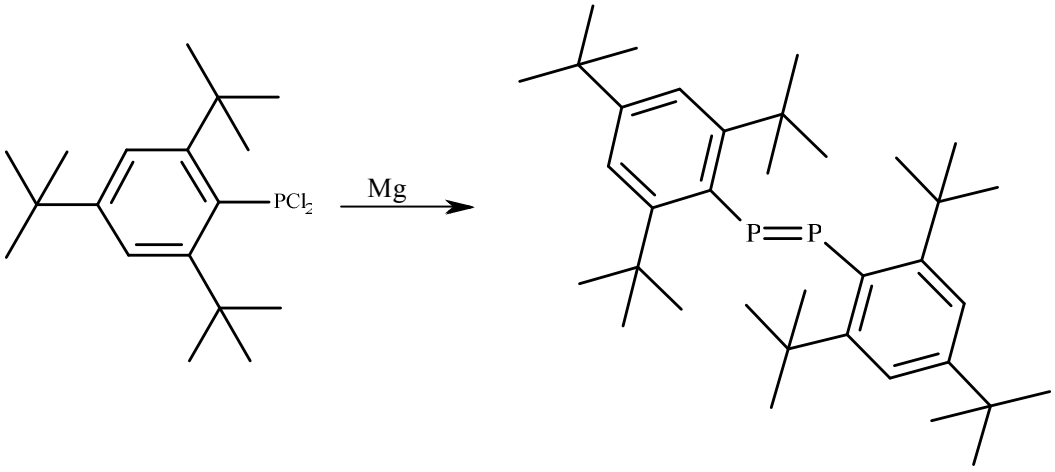

1.4

Last, but not least, the steric protection inposed by a bulky 2,4,6-trimethylphenyl group (Mes) substituent was a decisive factor that enabled the isolation of the first stable, all carbon substituted phosphaalkene (**1.5**) by *Bickelhaupt* et al. in 1978 [8].

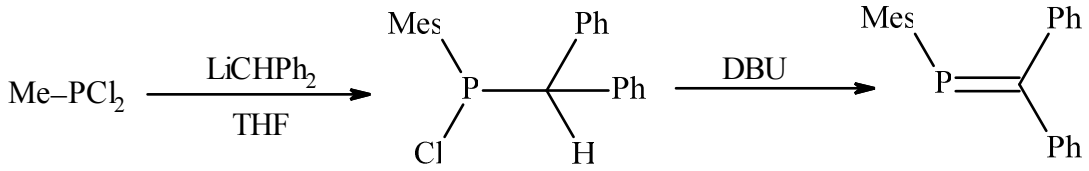

1.5

As mentioned previously, the siloxy substituent on the phosphaalkene carbon in **1.3** plays an essential role in the electronic stabilization of the phosphorus-carbon double bond. A similar stabilization can arise from substituents containing other heteroatoms. In particular, amino groups have been widely used. Since *C*-amino-substituted phosphaalkenes can be regardes as P-analogues of the well-known amidines and guanidines, we will shortly introduce these species before giving a more detailed account of the properties and synthetic routes of the amino-phosphaalkenes in **Sections 1.4** and **2.1**.

1.2 *Amidines and Guanidines*

Amidines are considered as nitrogen-analogous of the carboxylic acids. The first amidine (**1.6**) was first synthesized in 1858 via the reaction of aniline with *N*-phenylbenzimidoyl chloride [9].

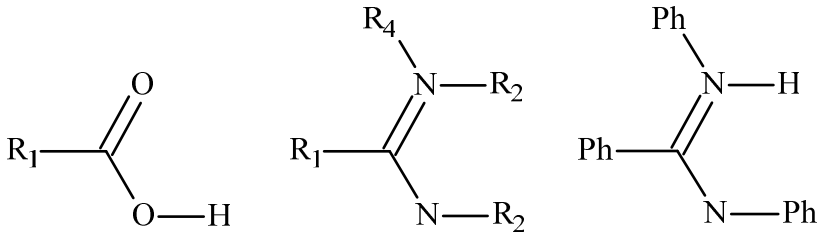

Carboxylic acid **Amidines** **1.6**

Dependant on the substituent on the nitrogen atoms, amidines can be classified as unsubstituted (**A**), mono-sbstituted (**B**) and (**C**), *N,N* or *N,N'* di-substituted (**D**) and (**E**) and tri-substituted (**F**).

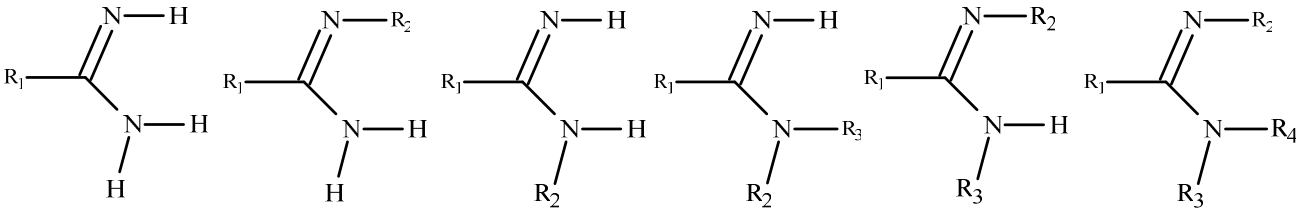

A **B** **C** **D** **E** **F**

Amidinate anions obtained by deprotonation of the primary or secondary amino group of an amidine have recently gathered attention as versaatile ligands for a variety of transition metal and main group metal complexes [10]. *Junk and co-worker* synthesized and studied some alkali metal formamidinates using different substituents and solvents.[11-13]. Furthermore, *Roesky* et al. reported the preparation of an amidinato silicon trichloride $[PhC(N^tBu)_2]SiCl_3$ as stable compound in good yield, which could readly be reduced to afford an isolable donor-stabilized chloro-silylene (1.7) [14].

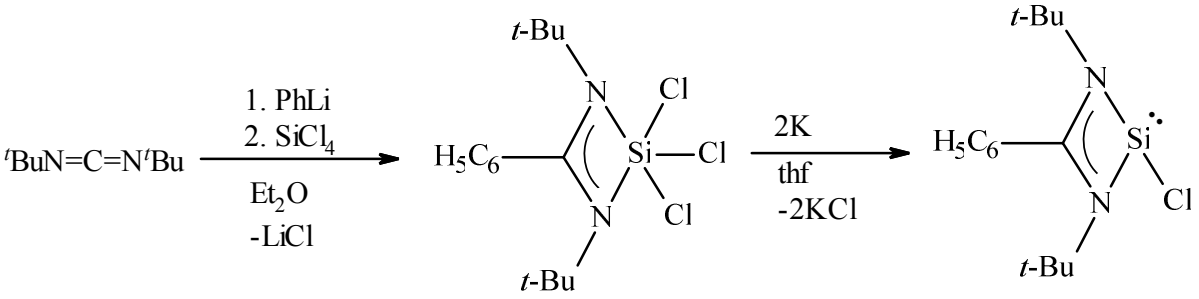

1.7

Introduction of further *amino*-substituent at the carbon atom formally converts an amidine into a quanidine which may be described by the generic formula ($R^1R^2N)(R^3R^4N)C=N-R^5$). Parent guanidine (with R1-R5 = H) was first synthesized in 1861 by the oxidative degradation of an aromatic natural product isolated from Peruvian guano [15], but its crystal structure was determined only 148 years later by *Yamada* and co-workers [16]. Guanidines can be synthesized through different methods (the most common one being the reaction of amines with carbodiimides) and are generally stronger bases than amidines.

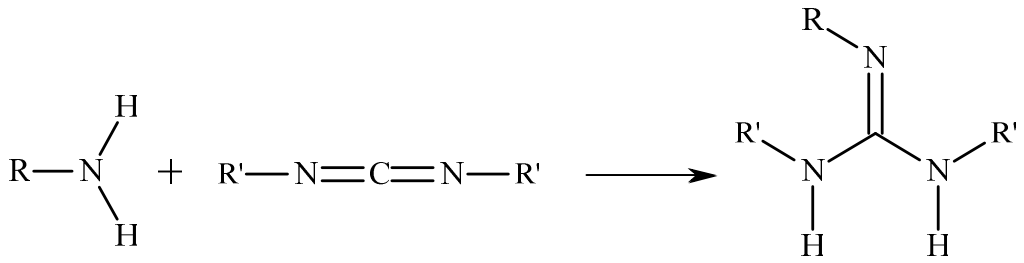

Iike amidines and amidinates, guanidines and guanidates are versatile ligands that may bind in different coordination modes to a wide range of metal ions from all parts of the periodic table. The coordination chemistry of guanidines and guanidates has been extensively reviewed [17, 18].

1.3 *Phospha-amidines and Phospha-guanidines and their Anions*

The presence of a phosphorus atom in an amidine or guanidine framework gives rise to special properties. In the phosphaguanidinates complexes for example the incorporation of the lone pair of electrons at phosphorus atom in the delocalization over the central vertex is not favored. The phosphaguanidinate ligands may therefore be considered as bifunctional compounds with independently reactive amidine and phosphane moieties [19].

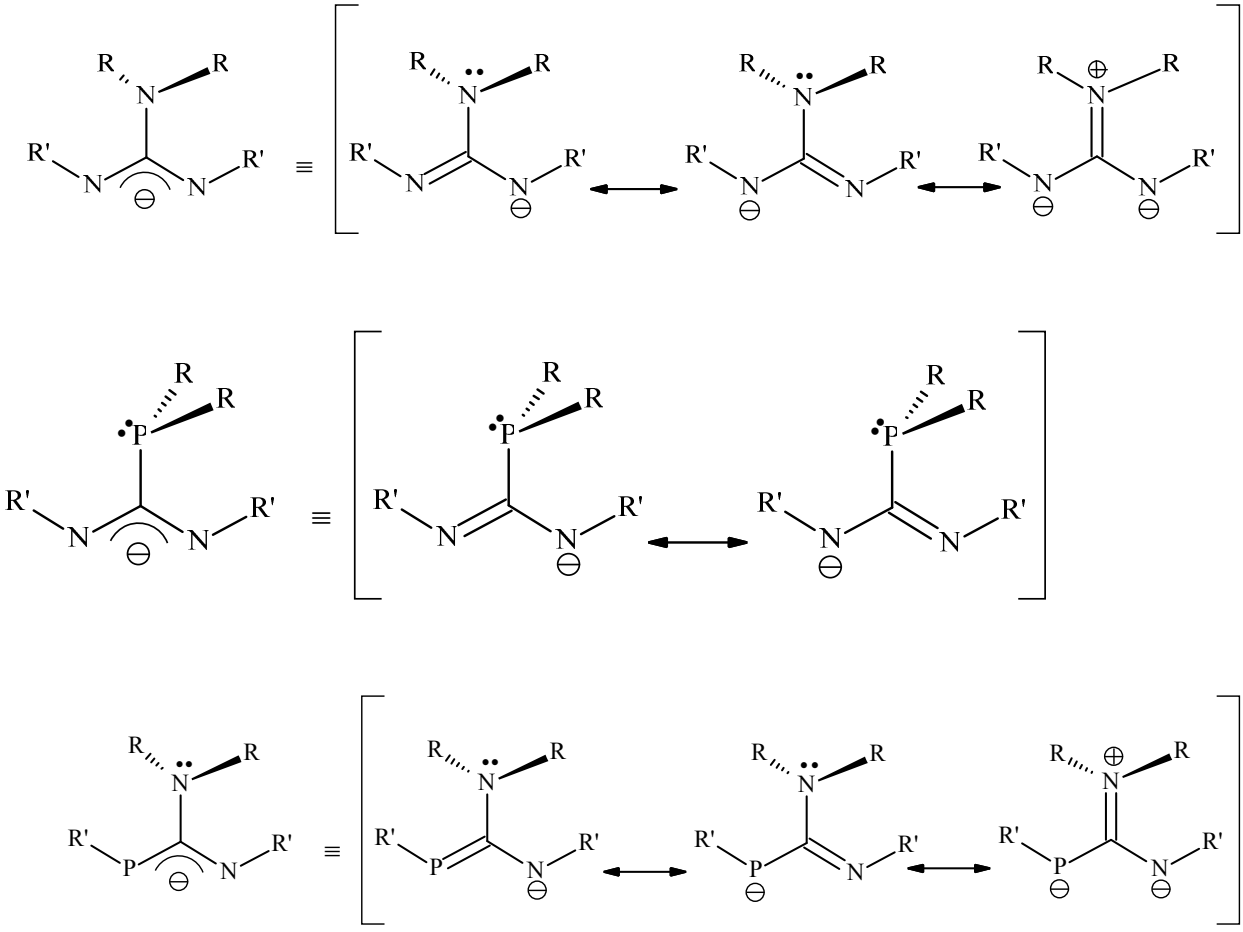

Figure 1.1 Different resonance structure for the guanidinate and phosphaguanidinate anions

This phenomenon leads to a change in the coordination modes of phosphaguanidinate ligands. one of the most characteristic features of these ligands are the coordination of a neutral phosphaguanidine ligand through the phosphorus atom (P-donation) (B, **Figure 1.2**) [20] and a chelating *P,N*-coordination mode (C and E, **Figurer 1.2**) of phosphaguanidinate ions [21, 22].

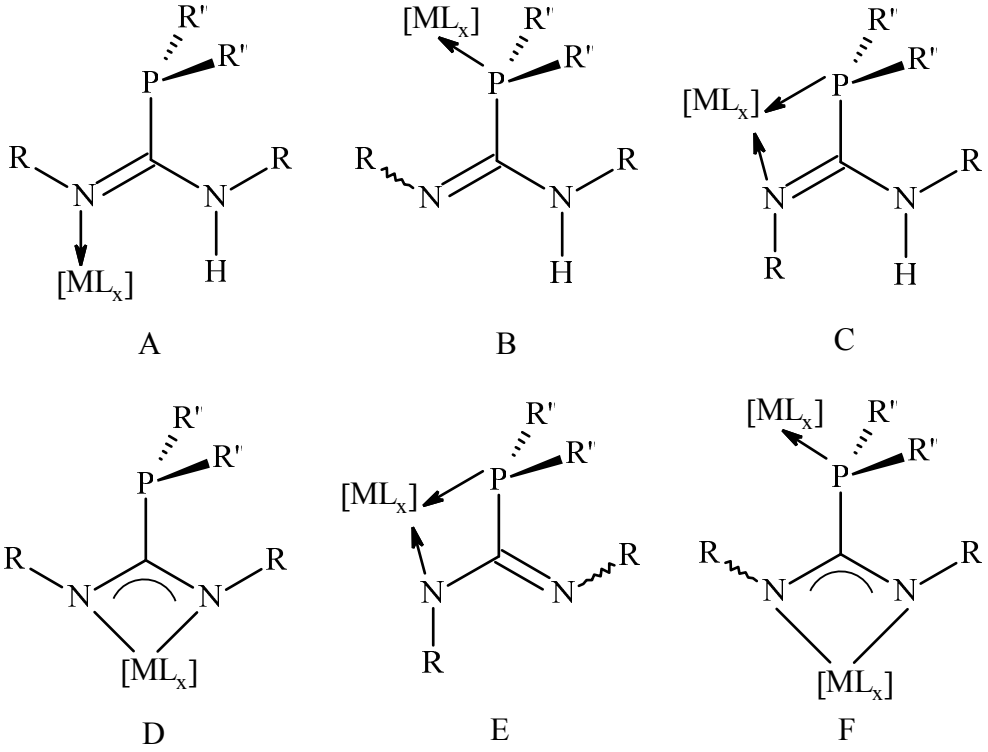

Figure 1.2 Some bonding modes for neutral and anionic phosphaguanidinate ligands

1.4 *Normal and Inverse Polarisation Phosphorus-Carbon Double Bonds*

Phosphaalkenes and phosphaalkynes are formal analogues of imines (R_2C=NR) and nitriles (R−C≡N) respectively, but their reactivity is more related to that of alkenes and alkynes. This is because: a) the energetic stabilization of the lone-pairs with respect to the π-orbital of the double bond and b) the decrease of the HOMO-LUMO-gap. Usually, the bond between phosphorus and carbon atom features an electron distribution $P^{\delta+}$–$C^{\delta-}$ as a result of small difference in electronegativities of carbon (2.5) and phosphorus (2.1), but due to on substituents influence the electron distribution may reversed ($P^{\delta-}$–$C^{\delta+}$) and such compounds are called "inversely polarized Phospha alkenes". In 1989 *Regitz* et al. synthesized the 2,3-Di-*tert*-butylcyclopropylidene phosphanes (**1.8**) which are considered as phosphaalkenes with an inversed polarization at the P=C double bond [23].

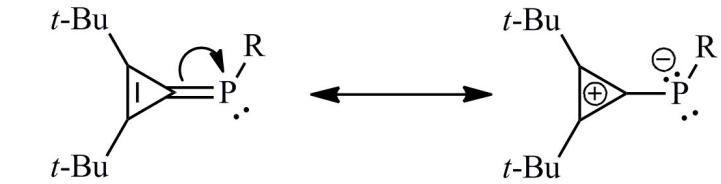

R = $SiMe_3$, Mes

1.8

A similar polarization of the P=C bond was also observed in *C*-aminosubstitueted phosphaalkenes [24]. In 1988 *Grobe* et al reported that (*P*-Trifluormethyl)diorganylamino-1λ^3-phosphaalkene compounds of the type F_3C–P=C(F)NR_2 show no sign of reactivity toward several H-acidic reagents such as HCl, ROH and R_2NH because of the P=C–N conjugation [25]. Surprisingly, the reaction of the compound F_3C–P=C(F)NMe_2 with $Cr(CO)_5$(THF) led to the formation of the complex $Cr(CO)_5$[F_3C–P=C(F)NMe_2], which converted to dineuclear complex in the organic solvents. Two years later the X-ray structure analysis reveals that the dineuclear complex (**1.9)** feature a unique η^1,μ^2-coordination mode at phosphorus atom [26].

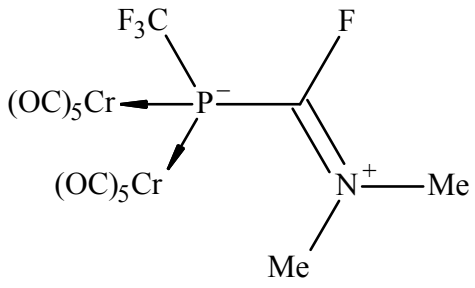

1.9

This new coordination mode can be explained only by assuming a negative charge at phosphorus atom which provides another electron pair. Therefore, the chemical properties of **1.9** mimic that of inversely polarized phosphaalkenes.

Furtherr experimental evidence can be gleaned from the paper published by *Weber* and co-worker about the reactivity of carbonyl functionalized phosphaalkenes $R(CO)P=C(NMe_2)_2$. The authors reported that the reaction of these compounds with several acids and alkylation reagents led to the formation of phosphanyl-substituted carbocations. These results were also attributed to the inversely polarized nature of the P=C bond in the starting material [27].
Keeping these observations in mind, several theoretical investigations have been performed to prove the presence of an inverse π-electron density in phosphaalkenes and its *amino*-substituted derivatives. For example, in 1991 *Chernega* et al. showed that the normal charge distribution of the π-bond at P=C unit in methylene phosphane (+0.039 e^- at P and −0.039 e^- at C) is reversed (−0.285 e^- at P and +0.013 e^- at C) in *C*-amino-$1\lambda^3$-phosphaalkenes [28].

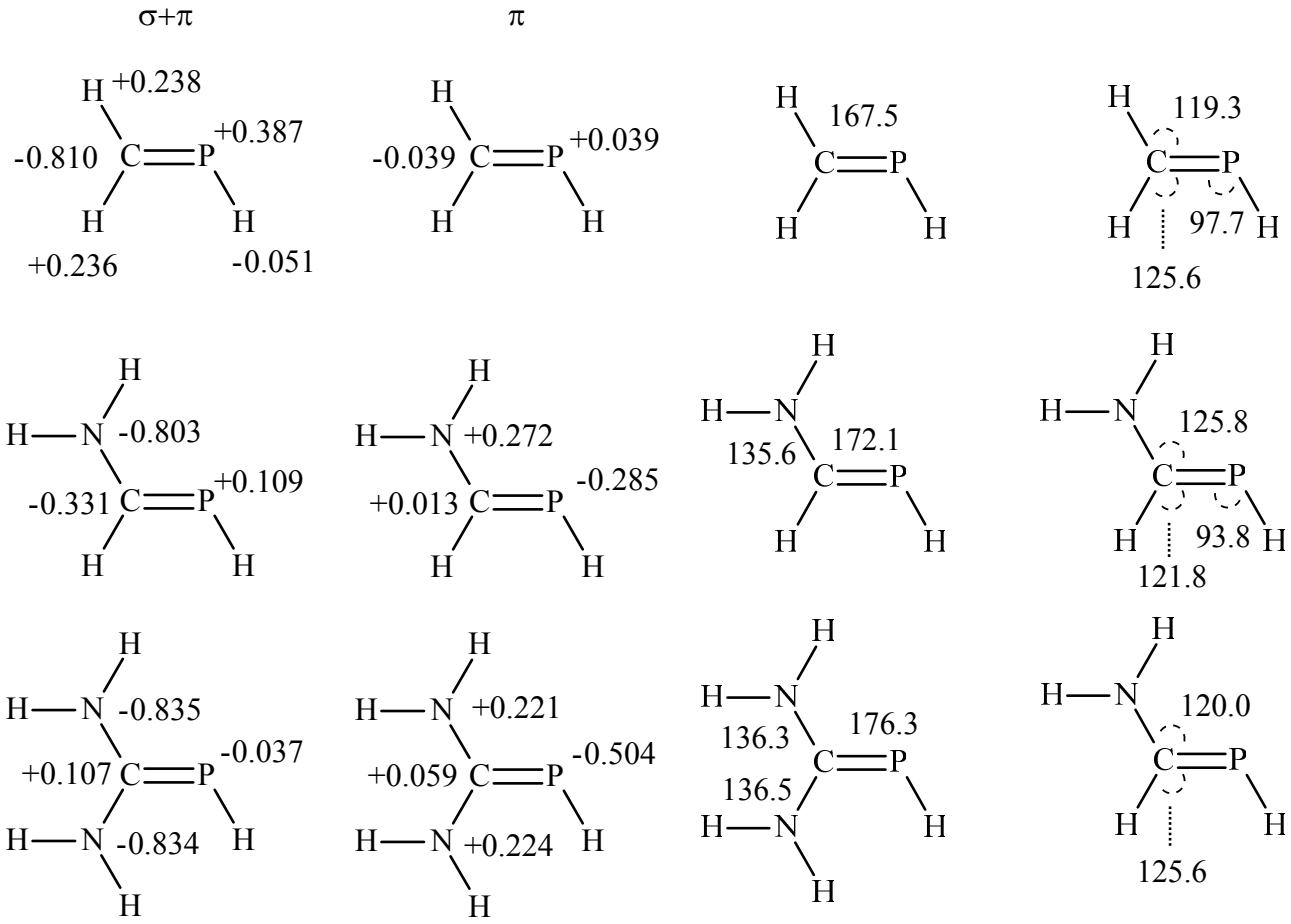

Figure 1.3 Charge distribution (left) and geometric parameters (right) of $HP=CH_2$, $HP=C(NH_2)H$, $HP=C(NH_2)_2$.

This effect is more pronounced (−0.504 e- at P and +0.059 e- at C) when two amino groups are attached to the carbon atom (**Figure 1.3**).

Actually, in most *C*-amino-1λ^3-phosphaalkenes a delocalization of the π-electron of the P=C bond over the P=C–N fragment is observed, this conjugation is only possible when the *p*-orbital of the nitrogen atom lies in the same plane of the P=C unit. An effective π-delocalization leads to an elongation of the P=C double bond from standard values between 165 and 167 pm to a values varies between 170 and 176 pm [28]. The P=C elongation is accompanied with C–N bond length shortening from values of 145 pm [29] to a values varies between 135 and 139 pm.

In addition to the influence of the effective π-conjugation of the nitrogen lone pair with the P=C double bond on the structural properties of the phosphaalkenes, another significant change in the ^{31}P NMR chemical shift values were also noticed.

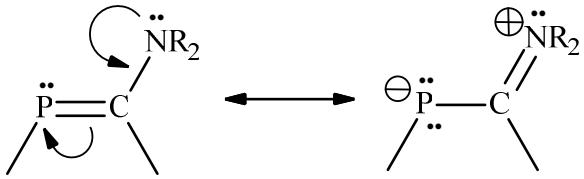

2 Reactions of $1\lambda^3\sigma^2$-Phosphaalkene 1 with *tert*-Butylchlorodiphenylsilane and Trifluoromethylsulfonic Acid

2.1 *Introduction*

Low coordinated phosphorus compounds with a P=C double bond can be stabilized either by introducing sterically protecting substituents (kinetic stabilization) or by electronic stabilization through π-delocalization. As mentioned in **section 1.1**, the first stable low coordinated phosphorus compounds were synthezied by several groups in the sixties and seventies of the last century. Since then, many stable *C*-aminophosphaalkenes have been synthesized in different ways. Using a catalytic amount of NaOH, the *C*-aminophosphaalkenes (**2.1**) can be obtained by treatment of $RP[Si(CH_3)_3]_2$ with an excess of *N*,*N*-dimethylformamide [30]. In the reaction of $MesP[Si(CH_3)_3]_2$ with an excess of *N*,*N*-dimethylformamide, Me_3SiCl must be used prior to work-up to remove the $LiOSiMe_3$ which is formed as by-product [31].

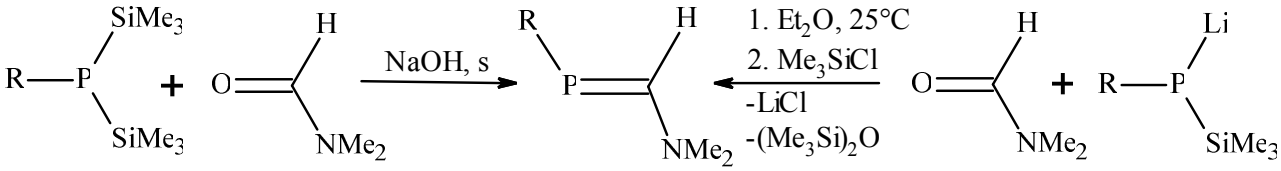

R = Mes, Ph and ^{t}Bu **2.1**

Another effective route to generate the *C*-aminophosphaalkenes (**2.2**) makes use of the reaction of carboxylic amide acetals with primary arylphosphanes at 60 °C [32]. It is worth mentioning that primary alkylphosphanes do not react with these acetals [33].

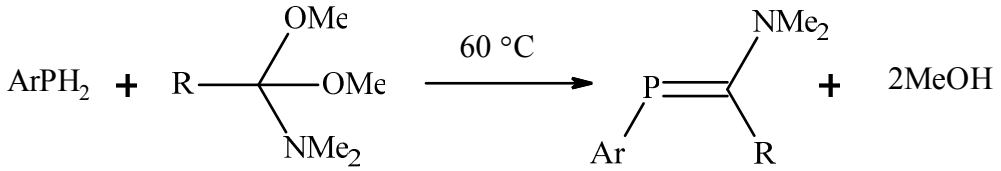

R = H; Ar = Mes, Ph, Mes*
R = Me; Ar = Ph, Mes*

2.2

Issleib et al reported the synthesis of a series of *C*-aminophosphaalkenes (**2.3**) from a condensation reaction of equimolar amounts of organosilylphosphanes with imidoyl

chlorides. The initial reaction is thought to occur via initial formation of imino phosphaamidines, followed by 1,3-silyl migration to yield the *C*-aminophosphaalkenes. Upon treatment with MeOH, phosphaalkenes with secondary *C*-amino substituents were isolated, but not fully characterized [34].

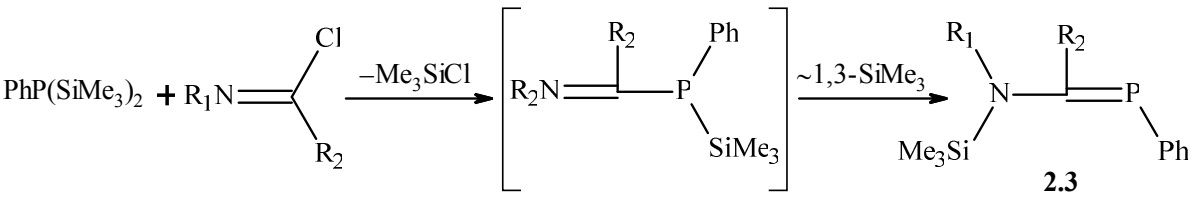

2.3

R_1 = Ph, Me, 2,6-$Et_2C_6H_3$, Cy, *p*-ClC_6H_4, *p*-$MeOC_6H_4$
R_2 = Ph, ^{t}Bu, Mes, *p*-ClC_6H_4, *p*-$MeOC_6H_4$

A completely new method to form *C*-aminophosphaalkenes was developed by *Bertrand* et al. Thermally stable and easy accessible *N*-arylformimidates were reacted with stoichiometric amount of primary arylphosphanides in the presence of butyllithium to afford the corresponding lithiated *C*-aminophosphaalkenes. Excess methanol was then added to give the desired *C*-aminophosphaalkenes (**2.4**) in an excellent yield [35].

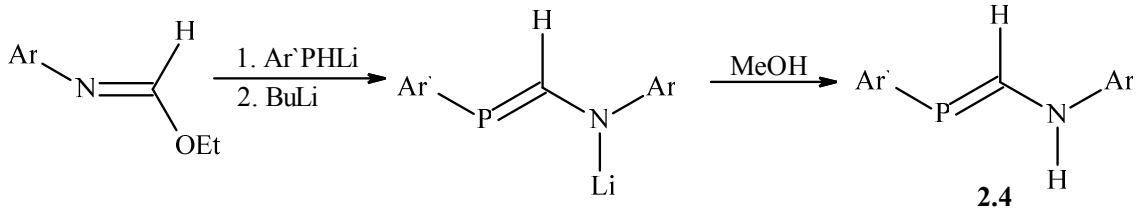

2.4

Ar = Ar´ = Mes
Ar = Dipp; Ar´ = Mes, Mes*

Lammertsma and co-workers reported that treatment of nitrilium triflates with Mes*PH_2 and then with NEt_3 afforded mixtures of diastreomiric *imino*-phosphane which tautomerized under the reaction condition to the *C*-aminophosphaalkenes (**2.5**) [36].

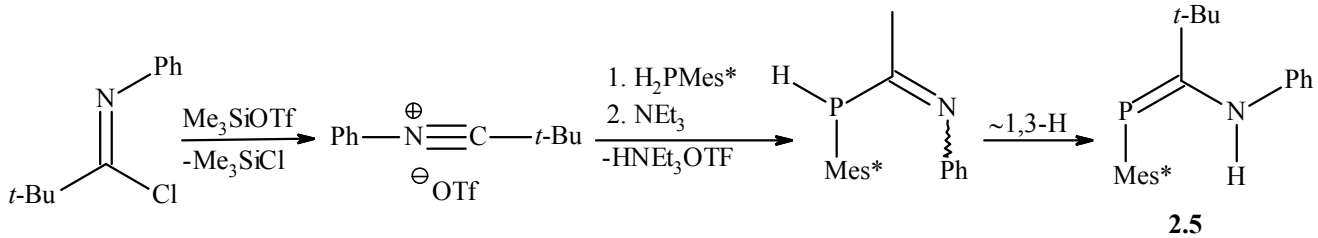

2.5

The final product, which was characterized by means of spectroscopic methods, was found to have one ^{31}P NMR signal at 102 ppm assigned to the (*Z*)-isomer. Theoretical calculations also confirmed that the (*Z*)-isomer is thermodynamically more stable than the (*E*)-isomer.

In contrast to the numerous examples of trisubstitueted *C*-aminophosphaalkenes [33], *C*-aminophosphaalkenes featuring only two non-hydrogen substituents attached either at phosphorus and nitrogen (*P*,*N*-disubstituted *C*-aminophosphaalkenes) or at the nitrogen atom (*N*,*N*′-disubstituted *C*-aminophosphaalkenes) are much rarer. The reaction of $R(Ph)PLi(thf)_x$ (R = H, $SiMe_3$) with acetonitrile (MeC≡N) in tetrahydrofuran afforded the corresponding ionic *C*-aminophosphaalkenes [37]. When R = H, the complex found to be a dimeric in the solid state as revealed by X-ray structure analysis, it has been treated further with trimethylsilylchloride ($ClSiMe_3$) to give the neutral *P*,*N*-disubstituted *C*-aminophosphaalkenes (**2.6**) in an very good yield [37].

Few examples for the monosubstituted *C*-aminophosphaalkenes were found in the literature, these examples encompass the phosphaalkenes (**2.7)** and (**2.8)** with NH_2 group. Phosphaalkene **2.7** was characterized by NMR spectroscopy wherease **2.8** was isolated as colourless crystals and characterized by X-ray structure analysis [37].

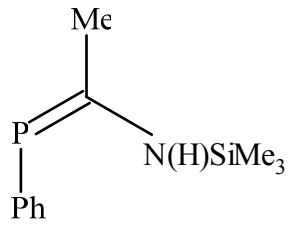

2.6

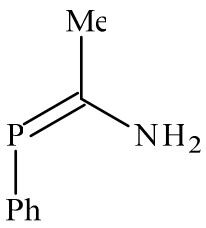

2.7

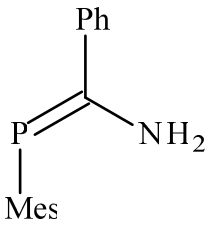

2.8

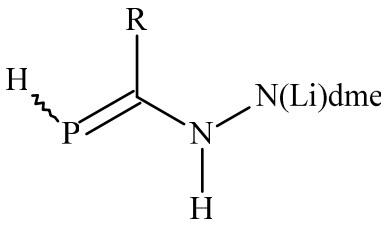

R = C_6H_5 **1**
R = $C(CH_3)_3$ **2.9**

In our research group, the 2-(lithiumamido)-2-organyl-l$\lambda^3\sigma^2$-phosphaalkenes (**2.9**) and **1** were synthesised by reacting lithium phosphanide with R–C≡N (R= $C(CH_3)_3$ or C_6H_5) in 1,2-dimethoxyethane [38]. Phosphaalkene **1,** which was crystallized with some difficulty from a mixture of 1,2-dimethoxyethane, *n*-pentane and a small amount of 1,3,5-trimethyl-1,3,5-triazinane, was found to crystalize as a dimeric complex with (*Z*)-configuration of the P=C bond [39]. The solution ^{31}P NMR spectrum reveals two signals in ratio of 5 : 1 at −28.5 ($^1J_{P,H}$ = 147) and −50.0 ppm ($^1J_{P,H}$ = 150 Hz), respectively, which were tentatively assigned to the (*Z*)- and (*E*)-isomers, respectively [39].

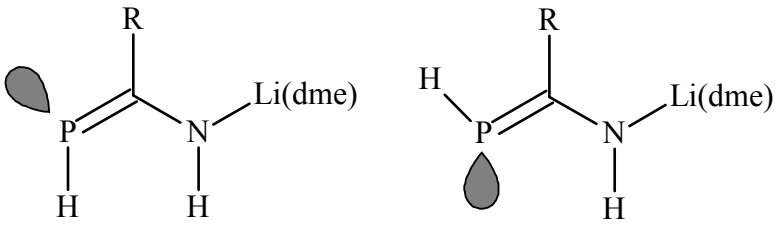

(***Z***)-**1** (***E***)-**1**

Remarkably, the signal at −50.0 ppm was very broad which indicates the presence of an exchange phenomenon that has until now not been investigated. The ^{1}H NMR spectrum shows beside the two doublets of the H–P groups of the *E*- (2.75) and *Z*-isomers (2.83 ppm) and the multiplet of the phenyl substituent (7.0 to 8.2 ppm) two additional doublets with different intensities at 6.08 and 7.41 ppm. Using a selective ^{31}P decoupling experiment it was possible to assign the doublet at high field with a $^{3}J_{P,H(N)}$ coupling constant of 16 Hz to the (*E*) isomer. This $^{3}J_{P,H(N)}$ coupling constant of the (*E*)-isomer of **1** is clearly larger than that of (***E***)-**2.9** (7 Hz). Unfortunately, in the ^{31}P NMR spectrum the $^{3}J_{P,H(N)}$ coupling constant of 16 Hz of the (*E*)-isomer of **1** was not appeared due to the strong broadening of the signal (line width about 110 Hz) [39].

2.2 *Low Temperature NMR Investigation of 2-(Lithiumamido)-2-phenyl-1$\lambda^3\sigma^2$-phosphaalkene {(Z)-/(E)-1}*

As mentioned in the last section, the remarkable broadening of the signal to a half-width of 190 Hz at −50.0 ppm in phosphaalkene **1** indicates the presence of an exchange phenomenon which up to now has not yet been investigated. The unsolved quistions in the spectral charaterization of **1** prompted us to study its NMR spectroscopic properties at low temperature. The synthesis of **1** was repeated as previously described [39] but now using a small excess of (1,2-dimethoxyethane)lithium phosphanide.

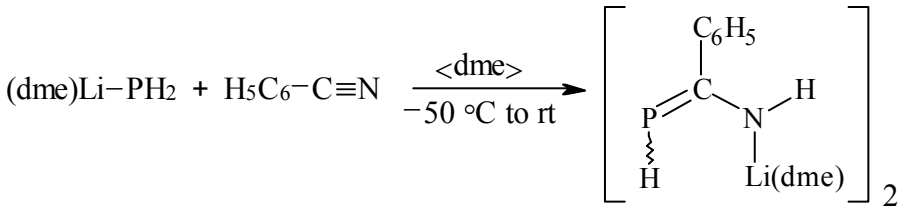

(*Z*)-/(*E*)-1

On cooling a diluted 1,2-dimethoxyethane solution of **1** from ambient temperature to 213K, the two signals visible in the room temperature $^{31}P\{^1H\}$ NMR spectrum broadened and eventually decoalesced into four signals at −25.6 ($^1J_{P,H}$ = 142 Hz), −32.1 (152 Hz), −35.4 (156 Hz), and −55.9 ppm (143 Hz) with an intensity ratio of 10.0 : 2.1 : 0.8: 2.3 (**Fig. 2.1**). Recording an ^{31}P NMR spectrum revealed that all signals split into doublets due to coupling with a P-bound hydrogen atom ($^1J_{P,H}$ = 142 - 156 Hz), while the signal at −35.4 ppm showed an additional splitting of 37 Hz attributable to a $^3J_{P,H(N)}$ long-range coupling to the hydrogen atom of the amido group. We can safely assume that the existence of four ^{31}P NMR signals is due to the presence of four different isomers formed as a result of restricted rotation around the P–C as well as the C–N bond. This exchange phenomenon is also observed in the ^1H NMR spectrum of the N–H and P–H-groups. At 213K four sets of doublets are detected in the high field region stemming from four different PH groups. This assignment is based on the $^1H,^{31}P$ HMQC experiment which clearly reveals four correlations between the ^{31}P NMR signals at −25.6, −32.1, −35.4 and −55.9 ppm on one side and four sets of ^1H doublets at 2.89, 2.71, 2.34 and 2.87 ppm on the other side (see footnote [5)] in **Table 2.1**. Depending on the arrangement of the individual substituents, we will denote these stereoisomers as ***Z*(P=C),*Z*(C–N)**, ***Z*(P=C),*E*(C–N)**, ***E*(P=C),*E*(C–N)**, ***E*(P=C),*Z*(C–N)**. Because of the additional coupling of 37 Hz, the signal at −35.4 ppm can be unambiguously assigned to

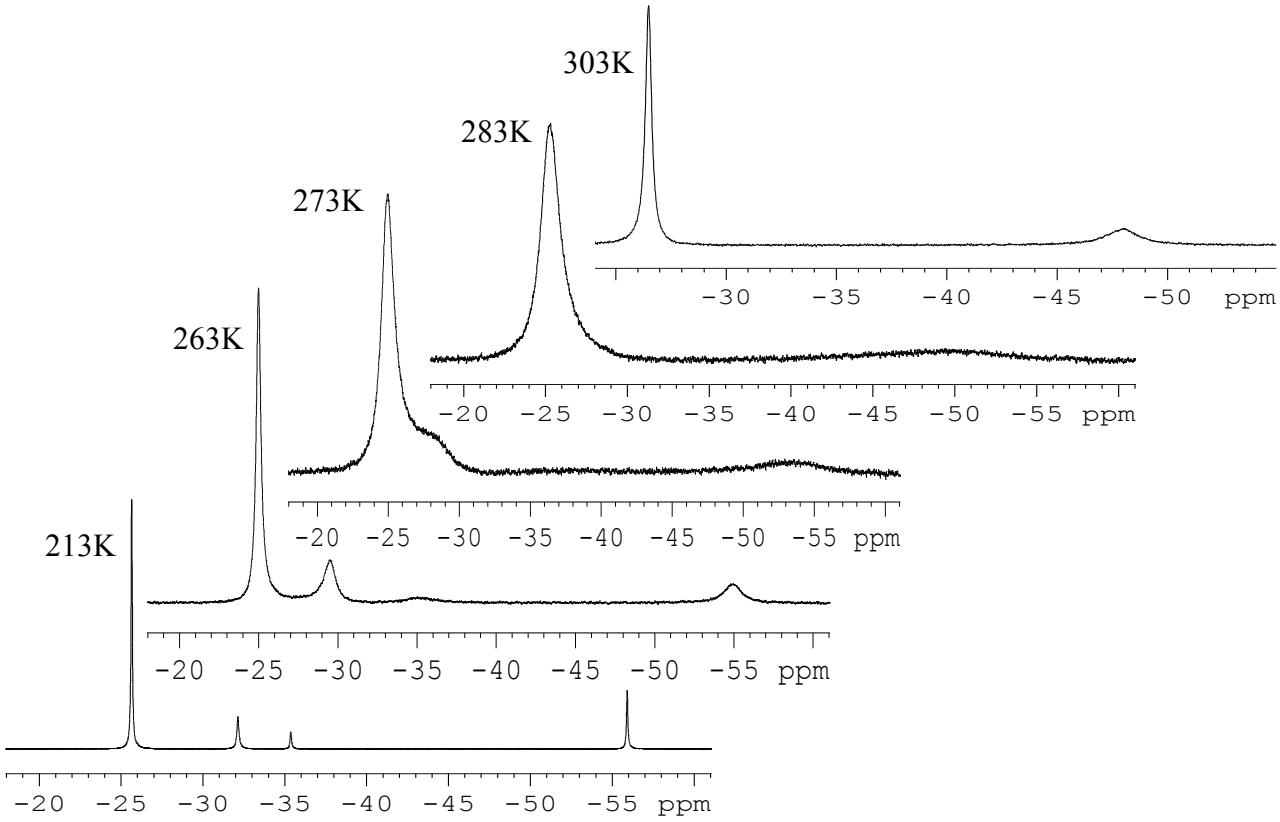

Figure 2.1 Temperature dependent 161.98MHz $^{31}P\{^{1}H\}$ NMR spectra of 2-(lithiumamido)-2-phenyl-1$\lambda^3\sigma^2$-phosphaalkene (**1**) dissolved in 1,2-dimethoxyethane and a small amount of [d_6]benzene which was added as reference
The figure depicts the alteration of the $^{31}P\{^{1}H\}$ NMR signals between 213K and 303K. Relevant NMR parameters have been compiled in **Table 2.1 b)**, **c)**. The resonances recorded at the lower temperature limit refer to the following isomers:
−25.6 ppm: ***Z*(P=C),*E*(C–N)**; −32.1 ppm: ***E*(P=C),*E*(C–N)**
−35.4 ppm: ***E*(P=C),*Z*(C–N)**; −55.9 ppm: ***Z*(P=C),*Z*(C–N)**

the ***E*(P=C),*Z*(C–N)** isomer. This assignment is based on the finding that in *C*-aminophosphaalkenes the $^{3}J_{P,H(N)}$ coupling constant is large when the lone pair at phosphorus and the hydrogen atom are arranged *cis* to each other [39,40].

The assignment of the remaining signals relies on the analysis of differences in the $^{1}J_{P,H}$ coupling constants, which are larger for the (*E*)- than the (*Z*)-isomers [39,40], the observation of different chemical shift values for the N–H hydrogen atoms in ***E*/*Z*(C–N)** isomers, and the finding that only the ***Z*(P=C)** isomers show strong $^{1}H,^{31}P$ HMQC correlations between the phosphorus and the *ortho*-hydrogen atoms in the phenyl substituents. Accordingly, the signal at −55.9 ppm was assigned to the ***Z*(P=C),*Z*(C–N)** isomer because the chemical shift value of its N–H group is alike that of the ***E*(P=C),*Z*(C–N)** isomer (6.10 *vs* 6.05 ppm).

Table 2.1 Results of an analysis of the temperature dependent 161.98MHz ^{31}P and 400.13MHz ^{1}H NMR spectra of 2-(lithiumamido)-2-phenyl-1$\lambda^3\sigma^2$-phosphaalkene (**1**) in 1,2-dimethoxyethane taken at 213K and 303K

Phosphaalkene **1** was prepared from benzonitrile and excess **(**1,2-dimethoxyethane)lithium phosphanide in a ratio of 1.0 : 1.18 between −60 °C and room temperature. A small amount of [d_6]benzene as a reference was added to the 1,2-dimethoxyethane solution which still contains some **(**1,2-Dimethoxyethane)lithium phosphanide (δ^{31}P −275.0 ppm, *t*, $^{1}J_{P,H}$ = 150 Hz; δ^{1}H(P) −1.2 ppm, *d*, $^{1}J_{P,H}$ = 148 Hz at 303K). The purpose of including two decimal places in several NMR shift values is not for accuracy but for easy identification of the corresponding signals in the spectrum.

Configuration/ conformation *E*(C–N)

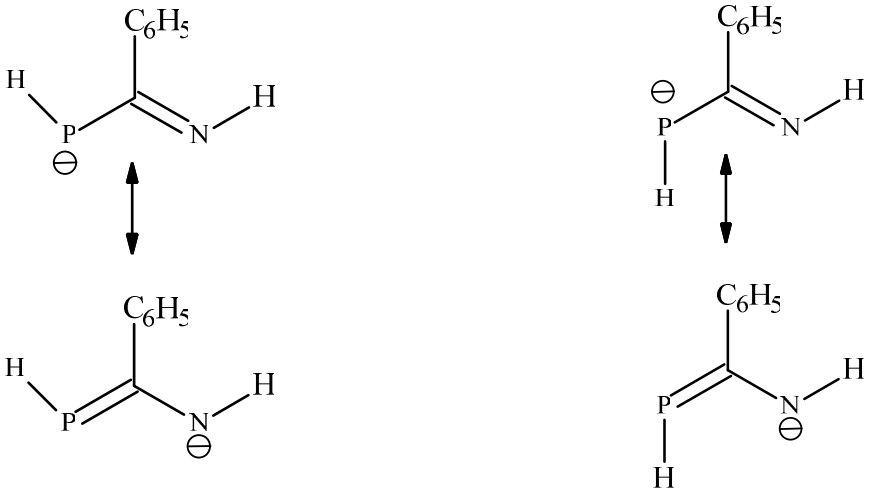

Isomer[1)]	***E*(P=C),*E*(C–N)**	***E*/*Z*(P=C),*E*(C–N)**	***Z*(P=C),*E*(C–N)**
temperature of measurement	213K	303K	213K
δ ^{31}P{^{1}H} (*int.*)[2)]	−32.1 ppm (*2.1*)	−26.5 ppm (*10.0*)	−25.6 ppm (*10.0*)
line width (^{31}P{^{1}H})	24 Hz	38 Hz	17 Hz
$^{1}J_{P,H}$	152 Hz	144 Hz	142 Hz
δ ^{1}H(P)	2.71 ppm[3)]	2.96 ppm[3)]	2.89 ppm[3)]
δ ^{1}H(N), *mult.*[4)], (*int.*)[2)]	7.32 ppm, (*d*), (*4.0*)	7.30 ppm, (*d*), (*10.9*)	7.40 ppm, (*s*), (*9.6*)
$^{3}J_{H(N),P}$	7 Hz	3 Hz	< line width
δ ^{1}H(C_{ortho}) (*int.*)[2)]	7.62 ppm[5)] (*4.6*)	7.75 ppm (*20.0*)	7.81 ppm[6)] (*20.0*)
^{1}H(C_{ortho}),^{31}P HMQC correlation	undetectable	strong	strong

Footnotes at the end of section **c)**

Configuration/ Conformation *Z*(C–N)

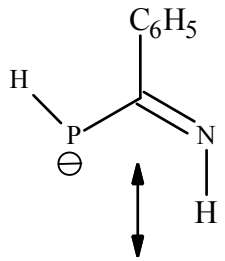
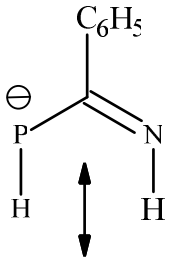
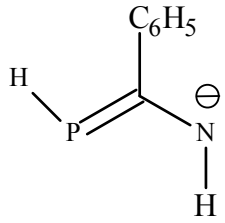
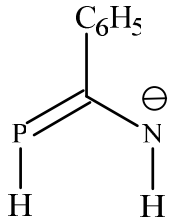

Isomer[1)]	***E*(P=C),*Z*(C–N)**	***E*/*Z*(P=C),*Z*(C–N)**	***Z*(P=C),*Z*(C–N)**
temperature of measurement	213K	303K	213K
δ ^{31}P{^{1}H} (*int.*)[2)]	−35.4 ppm (*0.8*)	−48.1 ppm (*2.8*)	−55.9 ppm (*2.5*)
line width (^{31}P{^{1}H})	16 Hz	190 Hz	17 Hz
$^{1}J_{P,H}$	156 Hz	about 149 Hz	143 Hz
δ ^{1}H(P)	2.34 ppm[3)]	2.73 ppm[3)]	2.87 ppm[3)]
δ ^{1}H(N), *mult.*[4)], (*int.*)[2)]	6.05 ppm, (*d*), (*0.4*)	5.97 ppm, (*d*), (*3.0*)	6.10 ppm, (*s*), (*2.2*)
$^{3}J_{H(N),P}$	37 Hz	17 Hz	< line width
δ ^{1}H(C_{ortho}) (*int.*)[2)]	undetectable	7.56 ppm (*7.0*)	7.58 ppm[5)] (*4.8*)
^{1}H(C_{ortho}),^{31}P HMQC correlation	undetectable	very weak	strong

[1)] For the sake of simplicity the ether complexed lithium cation of **1** is replaced by the negative charge of the anion. [2)] Intensities (*int.*) of the ^{31}P{^{1}H}, ^{1}H(N) and ^{1}H(C_{ortho}) signals relative to the most intense ^{31}P{^{1}H} (*10.0*) and ^{1}H(C_{ortho}) signals (*20.0*); [3)] δ^{1}H(P) values determined from the ^{1}H,^{31}P HMQC correlations; [4)] multiplicity: (*s*) singlet, (*d*) doublet; [5)] two broad lines with distances of 7 Hz and 5 Hz for ***E*(P=C),*E*(C–N)** and ***Z*(P=C),*Z*(C–N)**, respectively. [5)] Line width for ***Z*(P=C),*E*(C–N)** 14 Hz.

An analogous similarity is observed for the isomers ***Z*(P=C),*E*(C–N)** and ***E*(P=C),*E*(C–N)** which have nearly the same δ ^{1}H(N) values of 7.40 and 7.32 ppm. Furthermore, the δ ^{1}H values of the two P–H groups do not differ substantially (2.71 and 2.34 ppm) for the isomers ***E*(P=C)**. Similarly both the ***Z*(P=C)** isomers characterized by two δ ^{1}H values which are even closer to each other (2.89 and 2.87 ppm).

Additionally, in the ^{1}H,^{31}P HMQC experiment the two ***Z*(P=C)** isomers have a strong correlation between the phosphorus atom and the *ortho*-hydrogen atoms of the phenyl group whereas in the ***E*(P=C)** isomers no such correlation is observed. This difference is

readily explicable since in the ***Z*(P=C)** isomers the lone pair at phosphorus and the phenyl group are arranged *cis* to each other, whereas in the ***E*(P=C)** isomer the lone pair is *trans* to the phenyl group.

Finally, it has to be noted that for most *C*-aminophosphaalkenes the ***Z*(P=C)** isomer is more stable than ***E*(P=C)** isomer [33]. This observation is in agreement with the observed higher abundance of ***Z*(P=C)** over ***E*(P=C)** isomers (relative abundance 12.5 : 2.9 at 303K). Quantum chemical calculations for the ***Z*(P=C),*E*(C–N)** and ***Z*(P=C),*Z*(C–N)** isomers of **1** agree very well with this intensity ratio [41]. It can be assumed that at higher temperature a faster planar inversion of the hydrogen atom at nitrogen would result in a coalescence of the two NH doublets of the ***E*/*Z*(P=C),*Z*(C–N)** isomer at 5.97 ppm and the ***E*/*Z*(P=C),*E*(C–N)** isomer at 7.30 ppm (**Table 2.1**, 303K).

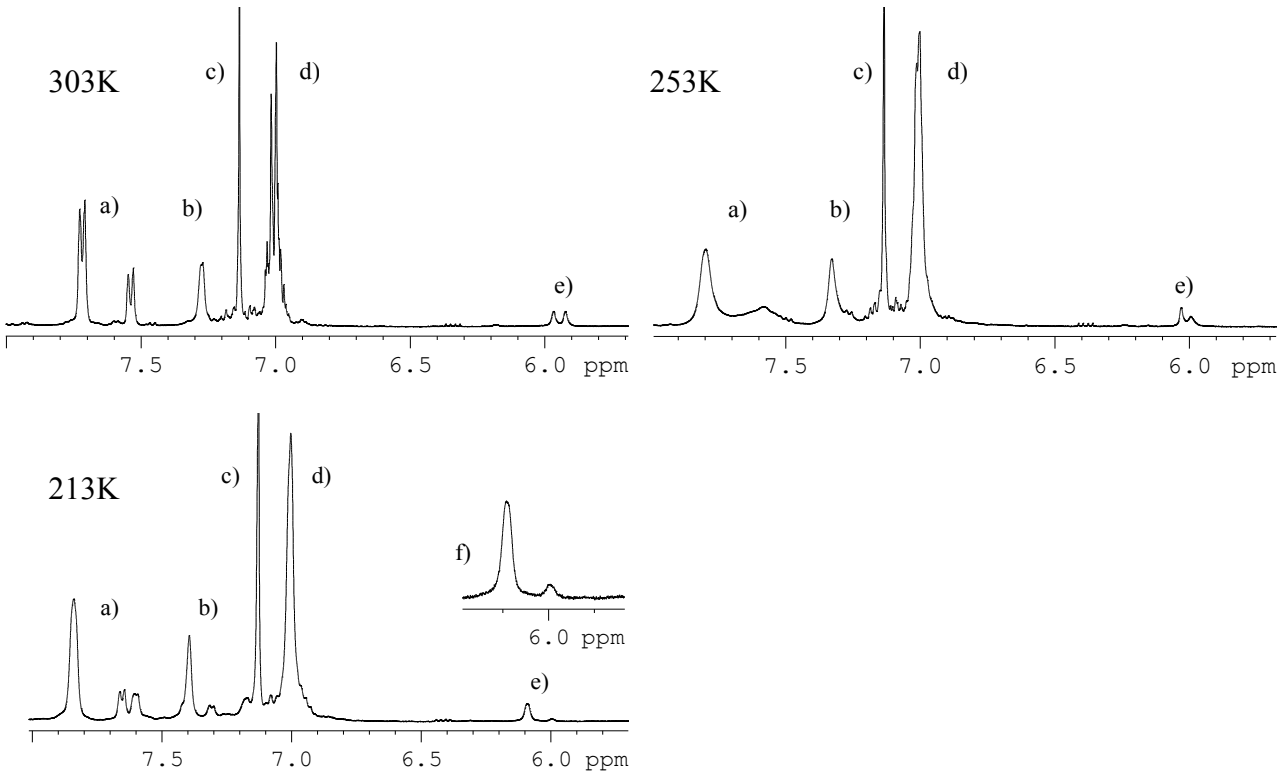

Figure 2.2 Variable temperature 400.13MHz ^{1}H NMR spectra of 2-(lithiumamido)-2-phenyl-1$\lambda^3\sigma^2$-phosphaalkene (**1**) dissolved in 1,2-dimethoxyethane with a small amount of [d_6]benzene which was added as reference. Relevant NMR parameters have been compiled in **Table 2.1.** Assignment: a) C–H$_{ortho}$ signals of the phenyl groups (7.5 → 8.0 ppm); b) N–H signals of the ***E*(C–N)** isomers (7.2 → 7.5 ppm); c) [d_6]benzene (7.13 ppm); d) C–H$_{meta}$ and C–H$_{para}$ signals of the phenyl groups (6.9 →7.1 ppm); e) N–H signals of the ***Z*(C–N)** isomers (5.9 → 6.2 ppm); f) expantion of the N–H region of the ***Z*(C–N)** isomers (5.8 → 6.4), the low field part of the ***E*(P=C),*Z*(C–N)** ^{1}H-doublet at 6.05 ppm ($^{3}J_{H(N),P}$ = 37 Hz) is covered by the singlet of the ***Z*(P=C),*Z*(C–N)** isomer at 6.10 ppm.

2.3 *Studies on the Chemical Reactivity of 2-(Lithiumamido)-2-phenyl-1$\lambda^3\sigma^2$-phosphaalkene {(Z)-/(E)-1} Against* tert-*Butylchlorodiphenylsilane*

2.3.1 *Preparation and Reaction Mechanism*

At −70 ºC to a 1,2-dimethoxyethane solution of 2-(lithiumamido)-2-phenyl-l$\lambda^3\sigma^2$-phosphaalkene (**1**) an equimolar amount of *tert*-butylchlorodiphenylsilane dissolved in the same solvent was added dropwise. The reaction mixture was stirred overnight and allowed to warm up slowly to ambient temperature. A colour change from deep red to orange indicated the completion of the reaction. The solvent was removed under reduced pressure and the residue was dissolved in a small amount of toluene. Solid lithium chloride was removed and the filtrate was concentrated under reduced pressure to one third of its original volume. On storing the solution at −13 ºC for several days pale yellow crystals precipitated in relatively high yield.

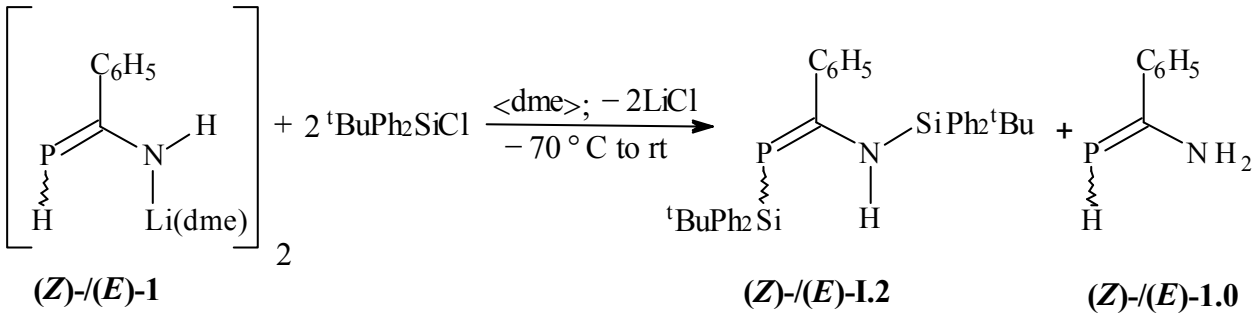

(*Z*)-/(*E*)-1 **(*Z*)-/(*E*)-I.2** **(*Z*)-/(*E*)-1.0**

Ph = C_6H_5

Unexpectedly, the disilylated (***Z***)-**I.2** with *two* silyl substituents, one bound to the nitrogen and one to the phosphorus atom of the 2-amino-2-phenyl-l$\lambda^3\sigma^2$-phosphaalkene framework, was isolated. In other words, the monosilylated compound **(*Z*)-/(*E*)-I.1** is not the main product although it can be detected in the ^{31}P NMR spectrum of the reaction mixture (**Figure 2.3**). Along with **I.1** and **I.2**, also the unsubstituted 2-amino-2-phenyl-1$\lambda^3\sigma^2$-phosphaalkene **I.0** is observed as further product in the reaction mixture. A plausible reaction mechanism being in line with the NMR spectroscopic results is given in **Scheme 2.1**.

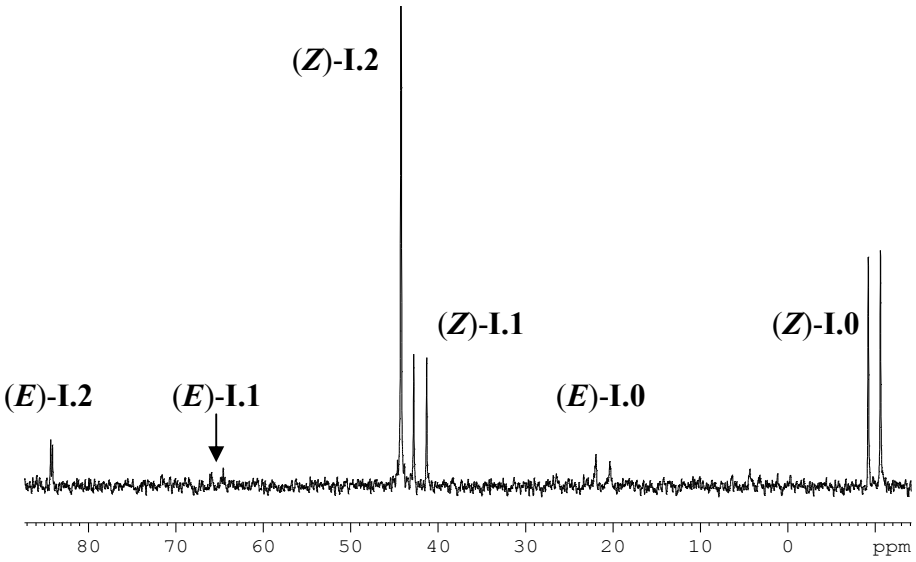

Figure 2.3 ^{31}P NMR spectrum showing the product distribution in the reaction of **(*Z*)-/(*E*)-1** with *tert*-butylchlorodiphenylsilane in 1,2-dimethoxyethane

A ^{31}P NMR spectrum taken from the reaction mixture two hours after beginning the experiment (**Fig. 2.3**) reveals the presence of six compounds which include not only the (*Z*)- and (*E*)-isomers of the isolated compound **I.2** but also the monosubstituted $l\lambda^3\sigma^2$-phosphaalkenes (*Z*)- and (*E*)-**I.1** and the *unsubstituted species* (*Z*)- and (*E*)-**I.0**. The NMR spectroscopic characterisation of the **1.1** and **1.0** will follow in detail in **Sections 2.4** and **2.5**.

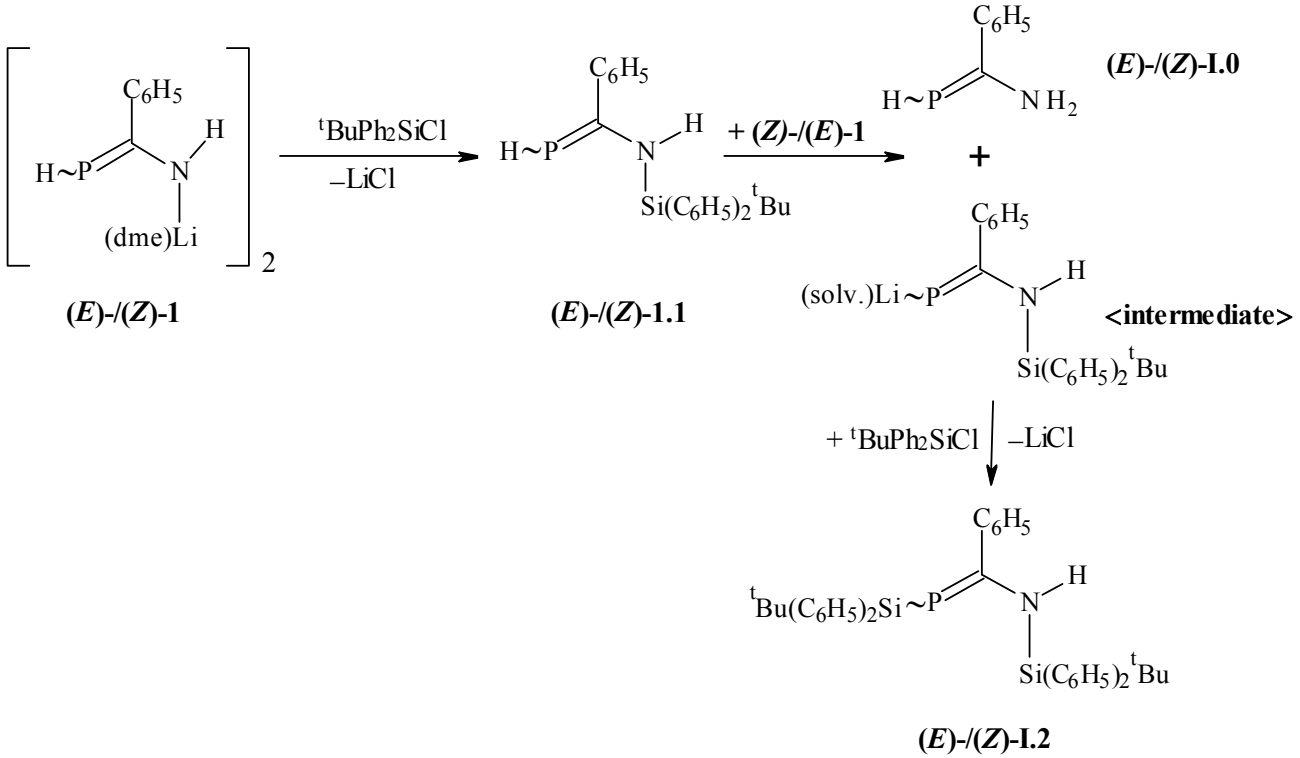

Scheme 2.1 Suggested mechanism for the reaction of phosphaalkene **1** with *tert*-butylchlorodiphenylsilane in 1,2-dimethoxyethane at −70 °C

2.3.2 *NMR Spectroscopic Characterization*

The NMR data of the $1\lambda^3\sigma^2$-phosphaalkenes (*Z*)- and (*E*)-**I.2** have been compiled in **Table 2.2**. The $^{31}P\{^1H\}$ NMR spectrum taken from a [d_8]tetrahydrofuran solution reveals two signals at 45.5 and 85.4 ppm with relative intensities of 7 : 1. Both resonances are accompanied by ^{29}Si satellites with $^1J_{P,Si}$-coupling constants of 81 and 77 Hz, respectively. Additionally, at the more intense resonance $^{13}C_{ipso}$ satellites ($^2J_{P,C}$ = 27 Hz) are observed. In the ^{31}P spectrum, the signal at 45.5 ppm remains a singlet but the less intense signal at 85.4 ppm splits into a doublet. This alteration is attributed to a coupling with the hydrogen atom of the NH group ($^3J_{P,H(N)}$ = 22 Hz). From a comparison with the very similar $^3J_{P,H(N)}$ values of compounds **(*E*)-I.0** at 213K and **(*E*)-I.1** at 298K given in **Table 2.11** and especially from the temperature dependent ^{31}P NMR spectrum of **(*E*)-I.0** (**Fig. 2.8**), it can be unambiguously inferred that the signal at 45.5 ppm comes from the (*Z*)- and that at 85.4 ppm from the (*E*)-isomer. The ^{29}Si NMR spectrum shows two doublets at –3.9 and –11.6 ppm that are attributable to the (*Z*)-isomer; the pertinent coupling constants of 81 Hz ($^1J_{P,Si}$) and 3 Hz ($^3J_{P,Si}$) differ considerably. For comparison, a $\delta^{29}Si$ value of −4.5 ppm and a $^1J_{P,Si}$ coupling constant of 70 Hz have been reported for the structurally similar 1,3-bis(2,6-diisopropylphenyl)-2-(trimethylsilyl)phos- phanylidene-2,3-dihydro-1H-imidazole [42].

At first the ^{29}Si NMR signals of the (*E*)-**I.2** isomer could not be detected but this was finally achieved in the $^1H,^{29}Si$ HSQC experiment (see below). Since the high field region of the ^1H NMR spectrum reveals two pairs of signals of very different intensity (7 : 1) for the *tert*-butylsilyl fragments at phosphorus and nitrogen, a straightforward assignment of the more intense pair at 0.87 and 0.00 ppm to the (*Z*)-isomer and that at 0.42 and 0.86 ppm to the less abundant (*E*)-isomer can be carried out. Furthermore, by an $^1H,^{31}P$ HMQC experiment a correlation of the *tert*-butylsilyl singlet at 0.87 ppm with the ^{31}P NMR signal of the (*Z*)-isomer at 45.5 ppm as well as a correlation between the resonances at 0.42 ppm and 85.4 ppm for the (*E*)-isomer was established. As a consequence the two *tert*-butylsilyl fragments which give rise to the ^1H-signals at 0.00 and 0.86 ppm are bound to nitrogen. Ultimately the above mentioned $^1H,^{29}Si$ HSQC experiment results in correlations of the two *tert*-butylsilyl singlets at 0.42 and 0.86 ppm with ^{29}Si resonances at − 0.62 ppm for the silicon atom at phosphorus and at −11.2 ppm for the silicon at the nitrogen atom of the (*E*)-isomer. This experiment also confirms the assignment of values given earlier for the (*Z*)-isomer.

Table 2.2 Assignment of ^{1}H, ^{13}C, ^{29}Si, and ^{15}N NMR signals of [*N*,*P*-bis(*tert*-butyldiphenylsilyl)-2-amino-2-phenyl-1$\lambda^3\sigma^2$-phosphaalkene] (**I.2**) based on ^{1}H-COSY, *^{1}H-EXSY* (*EX*); HSQC, HMQC, and HMBC correlations of the *tert*-butyl, amino and phenyl hydrogen atoms. The sample was prepared from crystals of the 1$\lambda^3\sigma^2$-phosphaalkene (**I.2**) which were washed with small amounts of *n*-hexane**,** dried in vacuo, and dissolved in [d_8]tetrahydrofuran.
δ-Values obtained from an *^{1}H-EXSY* (*EX*) experiment are given in italics or denoted with (*EX*). The purpose of including two decimal places in the NMR shift values presented here is not for accuracy but for easy identification of the corresponding signals in the spectrum.

Part α): *tert*-Butyl substituents and amino group

^{1}H atom, isomer	δ (ppm), multiplicity[a)]	^{1}H- COSY/ *^{1}H-EXSY* (*EX*)	HMQC(^{15}N)/(^{31}P), HSQC(^{13}C)/(^{29}Si)	HMBC
a) *$(H_3C)_3C$–Si fragment at P*				
($\underline{H}_3C)_3C$ (*Z*)	0.87 (*s*)[b)]		$^{13}\underline{C}H_3$ (26.8)	$^{13}\underline{C}H_3$(26.70) s[c)d)]
				$^{13}\underline{C}_{quar}$ (19.07) s[c)]
			$^{31}\underline{P}$ (45.5)[e)]	
			^{29}Si (– 3.9)[f)]	
($\underline{H}_3C)_3C$ (*E*)	0.42 (*s*)[b)]		$^{13}\underline{C}H_3$ (27.2)	$^{13}\underline{C}H_3$ (27.08) [c)d)]
				$^{13}\underline{C}_{quar}$ (19.78) [c)]
			$^{31}\underline{P}$ (85.4)[e)]	
			^{29}Si (– 0.62)	
b) *$(H_3C)_3C$–Si fragment at NH*				
($\underline{H}_3C)_3C$ (*Z*)	0.0 (*s*)		$^{13}\underline{C}H_3$ (25.8)	$^{13}\underline{C}H_3$ (25.70)[c)]
				$^{13}\underline{C}_{quar}$ (17.49)[c)]
			^{29}Si (– 11.6)[f)]	
($\underline{H}_3C)_3C$ (*E*)	0.86 (*s*)		$^{13}\underline{C}H_3$ (26.8)	$^{13}\underline{C}H_3$ (26.70)[c)]
				$^{13}\underline{C}_{quar}$ (18.20)[c)]
			^{29}Si (– 11.2)	
c) *N–H group*				
N–$\underline{H}$ (*Z*)	6.13 [b)]		^{15}N (−240.1[g)]	$^{13}\underline{C}_{ipso}$ (143.8)
	(*br*, *s*)		$^{31}\underline{P}$ (45.5) (*s*)	
N–$\underline{H}$ (*E*)	6.07 [b)]		^{15}N (unres.)[h)]	
	(*br*, *d*)[i)]		$^{31}\underline{P}$ (85.4) (*d*)[i)]	

[a)] singlet (*s*), doublet (*d*), triplet (*t*), multiplet (*m*), broad (*br*); [b)] in [d_8]tetrahydrofuran (*Z*) and (*E*) isomers with an intensity ratio of about 7:1, in [d_6]benzene with a ratio of about 9:1; [c)] HMBC correlations with the quarternary (*quar*) carbon atoms are weaker than those of the respective methyl carbon atoms. [d)] HMQC-/ HMBC-correlations: strong (s), medium (m), weak (w), very weak (vw). [e)] ^{31}P NMR spectrum of the (*Z*)-isomer: δ = 45.5 (*s*), ^{29}Si and $^{13}C_{ipso}$ (P=C–C_6H_5) satellites with $^{1}J_{P,Si}$ = 81 Hz and $^{2}J_{P,C}$ = 27 Hz, resp.; of the (*E*)-isomer: δ = 85.4 (*d*, $^{3}J_{P,H}$ = 22 Hz), after ^{1}H-decoupling ^{29}Si satellites with $^{1}J_{P,Si}$ = 77 Hz; [f)] ^{29}Si NMR spectrum (room temp.): δ = –3.9 (*d*), $^{1}J_{P,Si}$ = 81 Hz; δ = –11.62 (*d*), $^{3}J_{P,Si}$ = 3 Hz. ^{29}Si NMR signals of the (*E*)-isomer are undetectable. [g)] Solvent [d_6]benzene: δ^{1}H = 6.52 (*br*, *s*); $^{1}J_{H,15N}$ = 75 Hz; [h)] unresolved (unres.); [i)] $^{3}J_{P,H(N)}$ = 22 Hz.

Part β): Phenyl substituents at carbon (P=C) and silicon

^{1}H atom	δ- value (ppm), multiplicity[a)]	^{1}H- COSY *^{1}H-EXSY* (*EX*)	HMQC(^{15}N)/(^{31}P), HSQC(^{13}C)/(^{29}Si)	HMBC
d) *phenyl substituents at carbon (P=C)*				
C–H*ortho* (*Z*)	6.69 (*m*)	C–H*meta* (6.41)	^{13}C*ortho* (128.1) ^{31}P (45.5) s[d)]	^{13}C*ortho* (127.5) ^{13}C*para* (127.4) ^{13}P=C (208.2)
C–H*ortho* (*E*)	6.63 (unres.)[h)]	C–H*meta* (6.33)	^{13}C*ortho* (127.2)	^{13}C*para* (126.0)
C–H*meta* (*Z*)	6.42[b)] (*m*)	C–H*ortho* (6.69) C–H*para* (6.63)	^{13}C*meta* (126.2) ^{31}P (45.5) w[d)]	^{13}C*meta* (126.4) ^{13}C*ipso* (143.7)
C–H*meta* (*E*)	6.33[b)] (*m*)	C–H*ortho* (6.64) C–H*para* (6.60)	^{13}C*meta* (126.7)	^{13}C*meta* (126.8) ^{13}C*ipso* (144.6)
C–H*para* (*Z*)	6.64 (*m*)	C–H*meta* (6.42)	^{13}C*para* (127.3) ^{31}P (45.5) m[d)]	^{13}C*ortho* (128.0)
C–H*para* (*E*)	6.61 (unres.)[h)]	C–H*meta* (6.33)w[d)]	^{13}C*para* (unres.)[h)]	
e) *phenyl substituents at Si(P)*				
C–H*ortho* (*Z*)	8.05 (*m*)	C–H*meta* (7.31) *C–H*ortho (*7.19*)[k)]	^{13}C*ortho* (136.8) ^{31}P (45.5)[j)] w[d)] ^{29}Si (–4.0) s[d)]	^{13}C*ortho* (136.6) ^{13}C*para* (129.6)
C–H*ortho* (*E*)	7.19 (*EX*) (*m*)		^{13}C*ortho* (136.1)	
C–H*meta* (*Z*)	7.31 (*m*)	C–H*ortho* (8.05) *C–H*meta (*6.95*)[k)]	^{13}C*meta* (127.9) m[d)]	^{13}C*meta* (128.0) ^{13}C*ipso* (134.1)
C–H*meta* (*E*)	6.95 (*EX*) (*m*)		^{13}C*meta* (126.4) w[d)]	^{13}C*meta* (unres.)[h)] ^{13}C*ipso* (136.0)
C–H*para* (*Z*)	7.27 (*m*)	*C–H*para (*7.02*)[k)]	^{13}C*para* (129.5)	^{13}C*ortho* (136.6)
C–H*para* (*E*)	7.02 (*EX*)		^{13}C*para* (129.1) w[d)]	^{13}C*ortho* (unres.)[h)]

^{1}H atom	δ- value (ppm), multiplicity[a)]	^{1}H- COSY *^{1}H-EXSY* (*EX*)	HMQC(^{15}N)/(^{31}P), HSQC(^{13}C)/(^{29}Si)	HMBC
f) *phenyl substituents at Si(NH)*				
C–H$_{ortho}$ (*Z*)	7.02 (*m*)	C–H$_{meta}$ (unres.)[h)] *C–H*$_{ortho}$(*7.76*)[k)l)]	^{13}C$_{ortho}$ (135.2) ^{29}Si (–11.3) vw[d)]	^{13}C$_{ortho}$ (135.1) ^{13}C$_{para}$ (129.1)
C–H$_{ortho}$ (*E*)	7.76 (*EX*) (*m*)	C–H$_{meta}$ (7.26)	^{13}C$_{ortho}$ (135.9)	^{13}C$_{ortho}$ (135.9) ^{13}C$_{para}$ (129.2)
C–H$_{meta}$ (*Z*)	7.03 (*m*)	C–H$_{para}$ (7.11) *C–H*$_{meta}$ (*7.26*)[k)]	^{13}C$_{meta}$ (127.5)	^{13}C$_{meta}$ (127.1) ^{13}C$_{ipso}$ (133.0)
C–H$_{meta}$ (*E*)	7.26 (*EX*) (*m*)[m)]	C–H$_{para}$ (7.34)	^{13}C$_{meta}$ (127.2)	^{13}C$_{meta}$ (127.3) ^{13}C$_{ipso}$ (136.5)
C–H$_{para}$ (*Z*)	7.11 (*m*)	C–H$_{meta}$ (7.03)	^{13}C$_{para}$ (129.1)	^{13}C$_{ortho}$ (135.4)
C–H$_{para}$ (*E*)	7.34 (*m*)	C–H$_{meta}$ (7.26)	^{13}C$_{para}$ (unres.)[h)]	

[J)] $^{4}J_{P,H}$ ~ 2 Hz; [k)] δ-values obtained from an *^{1}H-EXSY* experiment; [l)] ^{1}H-NOESY correlation between C–H$_{ortho}$ (*E*) at 7.76 ppm and C–H$_{meta}$ (*E*) at 7.26 ppm; [m)] partially superimposed.

With respect to the (*E*)-isomer, which shows a doublet at 6.07 ppm and a $^{3}J_{P,H(N)}$ coupling constant of 22 Hz, the broad N–H signal of the (*Z*)-isomer at 6.13 ppm is shifted by approximately 0.6 ppm downfield. ^{1}H,^{31}P HMQC correlations allow to distinguish between three chemically different phenyl substituents in each isomer of **I.2**. Starting with the ^{31}P NMR signal of the (*Z*)-isomer at 45.5 ppm, correlations with two multiplets in the phenyl region at 6.69 ppm and 8.05 ppm are observed; these two multiplets arise from hydrogen atoms in an *ortho*-position. Since the ^{1}H,^{29}Si HSQC experiment provides a definite correlation between the low-field multiplet at 8.05 ppm and the ^{29}Si resonance at −4.0 ppm, the phenyl groups in question belong to the *tert*-butyldiphenylsilyl substituent at phosphorus. Consequently, the second multiplet at 6.69 ppm has to be attributed to the phenyl group at the carbon atom of the P=C unit. Furthermore, the ^{1}H,^{29}Si HSQC experiment allows also an assignment of the third multiplet at 7.02 ppm to phenyl groups of the *tert*-butyldiphenylsilyl substituent at nitrogen, since it correlates with the ^{29}Si resonance at −11.3 ppm.

Applying ^{1}H-COSY and *EXSY* as well as ^{1}H,^{13}C HSQC and ^{1}H,^{13}C HMBC NMR experiments, nearly all NMR parameters of the phenyl substituents of (*Z*)- and (*E*)-**I.2** could be assigned (**Table 2.2** part β).

Table 2.3 δ ^{13}C (ppm) and $^{n}J_{P,C}$ values (Hz) of (*Z*)- and (*E*)-[*N*,*P*-bis(*tert*-butyldiphenylsilyl)-2-amino-2-phenyl-1λ^{3}σ^{2}-phosphaalkene] (**I.2**). The purpose of including two decimal places in the NMR shift values presented here is not for accuracy but for easy identification of the corresponding signals in the spectrum.

^{13}C atom	**(*Z*)-isomer** δ ^{13}C (ppm)[a)]	**(*E*)-isomer** δ ^{13}C (ppm)[a)]
a) tert-*Butyl group at silicon*		
$(H_3\underline{C})_3C$–Si(P)	27.31 (*d*), $^{3}J_{P,C}$ = 4	27.74 (*d*), $^{3}J_{P,C}$ = 5
$(H_3\underline{C})_3C$–Si(NH)	26.33 (*s*) —	27.10 (*s*) —
$(H_3C)_3\underline{C}$–Si(P)	19.51 (*d*), $^{2}J_{P,C}$ = 16	20.36 (*d*), $^{2}J_{P,C}$ = 19
$(H_3C)_3\underline{C}$–Si(NH)	17.89 (*s*) —	18.71 (*s*) —
b) Phenyl substituents at carbon (P=C)		
$\underline{C}_{ipso}$	144.18 (*d*), $^{2}J_{P,C}$ = 28	148.98 (*d*), $^{2}J_{P,C}$ = 27
$\underline{C}_{ortho}$	128.58 (*d*), $^{3}J_{P,C}$ = 11	127.74 (*d*), $^{3}J_{P,C}$ = 2
$\underline{C}_{meta}$	126.69 (*s*) —	127.30 (*s*) —
$\underline{C}_{para}$	127.70 (*s*) —	126.65 (*s*)[b)] —
c) *Phenyl substituents at Si(P)*		
$\underline{C}_{ipso}$	134.52 (*d*), $^{2}J_{P,C}$ = 2	136.41 (*d*), $^{2}J_{P,C}$ = 2
$\underline{C}_{ortho}$	137.29 (*s*) —	136.36 (*d*), $^{3}J_{P,C}$ = 2
$\underline{C}_{meta}$	128.44 (*s*) —	126.91 (*s*) —
$\underline{C}_{para}$	130.04 (*s*) —	129.60 (*s*)[c)] —
d) *Phenyl substituents at Si(NH)*		
$\underline{C}_{ipso}$	133.47 (*s*)[d)] —	136.80 (*s*) —
$\underline{C}_{ortho}$	135.76 (*s*)[d)] —	136.70 (*s*) —
$\underline{C}_{meta}$	127.51 (*s*)[d)] —	127.71 (*s*) —
$\underline{C}_{para}$	129.53 (*s*)[d)] —	129.70 (*s*) —
c) *P=C fragment*		
P=$\underline{C}$	208.94 (*d*), $^{1}J_{P,C}$ = 78	209.37 (*d*), $^{1}J_{P,C}$ = 76[f)] —

[a)] additional data refer to signal multiplicities (in parentheses) and $J_{P,C}$ coupling constants in Hz; [b)] superimposed by the $\underline{C}_{meta}$ (*Z*) signal of the P=C phenyl substituent at 126.69 ppm; [c)] superimposed by the $\underline{C}_{para}$ (*Z*) signal of the Si(NH) phenyl substituent at 129.53 ppm; [d)] assignment based on signal intensity and position; [f)] doublet of *very* weak intensity.

The ^{15}N NMR signal of the (*Z*)-isomer was detected at −240.1 ppm; the low concentration of the (*E*)-isomer, however, prevented observation of its ^{15}N resonance.

The ^{13}C NMR spectrum of compound **I.2** (**Table 2.3**) shows not only strong signals of the (*Z*)-isomer but also weaker ones of the less abundantr (*E*)-isomer. As for the (Z)-isomer, in the high field region at 27.31 and 19.51 ppm, respectively, the methyl and the quaternary carbon atoms of the *tert*-butyldiphenylsilyl substituent at phosphorus are found. They are split into doublets due to coupling with the phosphorus atom ($^3J_{P,C}$ = 4, $^2J_{P,C}$ = 16 Hz). The methyl groups and the quaternary carbon atom of the analogous substituent at nitrogen give rise to singlets at 26.33 and 17.89 ppm, respectively. A similar pattern is observed for the signals of *ipso*-carbon atoms of the phenyl groups. They are split into doublets with a $^2J_{P,C}$ coupling constant of 28 and 2 Hz for phenyl groups bound to the carbon atom of the P=C unit or to the silicon atom at phosphorus, respectively. A singlet is observed for the *ipso*-carbons of the *tert*-butyldiphenylsilyl substituent at nitrogen. Except for the $^3J_{P,C}$ coupling constants between phosphorus and the *ortho*-carbon atoms of the phenyl substituent at the P=C unit and of the *tert*-butyldiphenylsilyl group at phosphorus, the (*E*)-isomer is on the whole characterized by very similar ^{13}C NMR data (**Table 2.3**). Finally, two doublets with $^1J_{P,C}$ coupling constants of 78 and 76 Hz are observed for the P=C unit of the (*Z*)- and (*E*)-isomers in the low field region at 208.94 and 209.37 ppm.

Table 2.4 contains a compilation of selected characteristic NMR parameters of the (*Z*)- and (*E*)-isomers of $1\lambda^3\sigma^2$-phosphaalkene **I.2** and structurally similar compounds. The low ^{31}P chemical shift of (***Z***)-**I.2** of 45.5 ppm compared to δ^{31}P values from 64 to 102 ppm of **(*Z*)-2.5**, **(*Z*)-2.6**, **(*Z*)-2.7** and **(*Z*)-2-8** can be attributed to the influence of the *tert*-butyldiphenylsilyl substituent at phosphorus. For the (*E*)-isomer of the **I.2**, **2.4'**, **2.4''** and **2.4'''** a reverse order is ascertained; an explanation for this observation cannot be given. In this context one should draw attention to a publication by *Weber* [33]; he reported the following chemical shift values for several [bis(dimethylamino)methylidene]phosphanes: $Ph_3SiP{=}C(NMe_2)_2$ −85.1; $HP{=}C(NMe_2)_2$ −62.6; $Me_3SiP{=}C(NMe_2)_2$ −47.1; ^{t}BuP=C(NMe$_2$)$_2$ 91.9 ppm.

Except for the **(*Z*)-2.7** and **(*Z*)-2.8** the ^{1}H chemical shift values of the H–N groups of both the isomers (***Z***)- and (***E***)-**I.2** compare very well with those listed in **Table 2.4**. The $^3J_{P,H(N)}$ coupling constant, however, is a characteristic feature of compound (***E***)-**I.2**. To the best of our knowledge no similar $^3J_{P,H(N)}$ values has been reported in the literature.

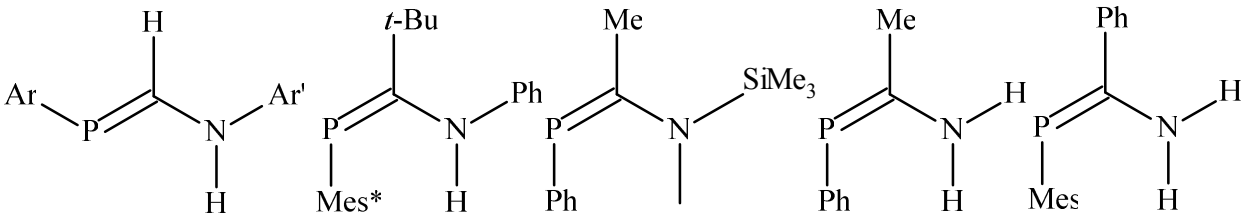

(*E*)-2.4 **(*Z*)-2.5** **(*Z*)-2.6** **(*Z*)-2.7** **(*Z*)-2.8**

Table 2.4 Selected NMR data of compounds with an P=C–N(H) unit
Chemical shift δ(ppm), coupling constant *J*(Hz)

Compound	$\delta^{31}P$	$\delta^{1}H$ (H–N)	$\delta^{13}C$ (P=C)	$^{1}J_{P,C}$	$^{3}J_{P,H(N)}$	solvent	Liter.
(***Z***)-**I.2**	45.70	6.13	208.94	78	–	[d_8]THF	
(***Z***)-**2.8**	64.4	4.4	186.6	60	–	*n*-pentane	[37]
(***Z***)-**2.7**	74.7	4.7	189.0	63	–	*n*-pentane	[37]
(***Z***)-**2.6**	94.7	5.8	193.6	64	–	*n*-pentane	[37]
(***Z***)-**2.5**	102.0	5.26	192.6	73	–	$CDCl_3$	[36]
(***E***)-**I.2**	85.45	6.07	209.37	76	22	[d_8]THF	
(***E***)-**2.4'** Ar = Dipp; Ar`= Mes*	75.6	5.17	166.9	65	–	C_6D_6	[35]
(***E***)-**2.4''** Ar = Dipp; Ar`= Mes*	57.2	6.20	173.1	67	–	C_6D_6	[35]
(***E***)-**2.4'''** Ar = Ar`= Mes	55.6	5.78	171.7	66	–	C_6D_6	[35]

2.3.3. *Crystal data, Data Collection and Structure Analysis*

Pale yellow block-shaped crystals suitable for an X-ray structure analysis were formed when a concentrated toluene solution of compound **I.2** was kept for several days at −13 ºC. Data for a structure determination were collected on a P4 diffractometer using graphite monochromatized MoK_{α} radiation (λ = 71.073). On the basis of unit cell dimensions and statistical tests on the distribution of E-values, the triclinic space group $P\bar{1}$ was chosen. To solve the crystal structure with statistical methods, the software package SHELXTL version 5.1 was applied [43 and 44]. This package also includes the program XP for an analysis of the molecular geometry and the preparation of drawings. All phosphorus, nitrogen, silicon and carbon atoms were located step by step and their positions as well as their isotropic replacement parameters were refined by full-matrix least-squares calculations. Thereafter, the structure determination was continued by introducing individual anisotropic U_{ij}-values. At the end of the structure refinement, the atomic coordinates of hydrogen atoms were calculated on the basis of an idealized geometry –using a N–H distance of 88 pm for the amino and a C–H distance of 95 or 98 pm for the phenyl and methyl groups, respectively, as well as tetrahedral angles and a staggered arrangement of bonds at carbon. Furthermore, the riding model applied ensures that a change in the carbon position is automatically transferred to the adjacent hydrogen atoms. Individual isotropic U-values for these hydrogen atoms were adopted from the respective carbon atoms and increased by a factor of 1.5 for the methyl groups and of 1.2 for the phenyl substituents. To take into account the incorporation of hydrogen atoms, the parameters of all heavier atoms were refined again, and final agreement factors of R1 = 0.0492 and wR2 = 0.1230 were achieved. Crystallographic parameters and details of data collection have been listed in **Table 2.5**. A complete listing of bond lengths (pm) and bond angles (deg), characteristic torsion angles as well as least-squares planes and angles between them can be found in **Table 8.2.1**. Final atomic coordinates and equivalent isotropic as well as anisotropic displacement parameters can be found in **Table 8.2.1** and **8.2.2**, respectively.

Table 2.5 Crystal data and details of structure refinement for *Z*-[*N*,*P*-bis(*tert*-butyldiphenylsilyl)-2-amino-2-phenyl-1$\lambda^3\sigma^2$-phosphaalkene] {(***Z***)-**I.2**}

Diffractometer	P4
Empirical formula; mol. Weight	$C_{39}H_{44}NPSi_2$; 613.9
Melting point (ºC)	176
Wavelength (pm)	71.073
Temp. of measurement (K)	173 ± 2
Crystal shape; crystal size (mm)	pale yellow blocks; 0.4 x 0.4 x 0.4
Crystal system; space group [45]	triclinic; *P* $\bar{1}$ *(No. 2)*
Unit cell dimensions a/pm	956.68(12)
b/pm	971.62(10)
c/pm	2193.8(2)
α/deg	85.235(9)
β/deg	80.980(10)
γ/deg	60.633(9)
Volume ($10^{-30}m^3$)	1755.1(3)
Z	2
Calculated density (10^3 kg/m^3)	1.16
Absorption coefficient μ (mm^{-1})	0.174
F(000)	656
Θ-Range for data collection (deg)	1.88 to 26.00
Limiting indices	$0 \le h \le 11$; $-10 \le k \le 11$; $-26 \le l \le 27$
Scan mode; scan width (deg)	ω; 2.4
Velocity (deg s^{-1})	3.0 to 60.0
Reflections collected	7314
Unique reflections	6877
Completeness to θ_{max}	1.00
Refinement method	Full-matrix least-squares on F^2
Data used	6877
Parameters refined (n)	394
Restraints	0
Goodness-of-fit (GOF) on F^2	1.031
Final R-indices:	
R1/wR2 using all data	0.0492/ 0.1230
with [I > 2 σ (I)]	0.0426/ 0.1198
Largest diff. peak;	0.510
deepest hole (10^{-30}e.m^{-3})	−0.454

Table 2.6 Selected Bond lengths (pm) and bond angles (deg) for *Z*-[*N*,*P*-bis(*tert*-butyldiphenylsilyl)-2-amino-2-phenyl-1$\lambda^3\sigma^2$-phosphaalkene] {(***Z***)-**I.2**}

a) Bond lengths

PCN-skeleton		C-phenyl		mean	Si–C_6H_5	*m* = 1	*m* = 2	mean
P–C	172.7(2)	C1–C2	139.8(2)	138.9	Si*m*–C*m*11	187.7(2)	189.1(2)	188.5
P–Si2	226.4(1)	C1–C6	139.1(2)		Si*m*–C*m*21	187.7(2)	189.4(2)	
C–C1	149.7(2)	C2–C3	138.7(9)		Si–$C(CH_3)_3$	*m* = 1	*m* = 2	mean
C–N	137.4(2)	C3–C4	137.9(3)		Si*m*–C*m*31	190.2(2)	190.8(2)	190.5
N–Si1	177.2(1)	C4–C5	138.3(3)					
N–H	88.0	C5–C6	139.3(2)					

b) Bond angles

C–P–Si2	106.1(1)	N–Si1–C111	111.7(1)	P–Si2–C211	111.0(1)
N–C–P	128.6(1)[a)]	N–Si1–C121	109.3(1)	P–Si2–C221	110.0(1)
P–C–C1	114.1(1)[a)]	N–Si1–C131	103.4(1)	P–Si2–C231	103.9(1)
N–C–C1	117.2(1)[a)]	C111–Si1–C121	110.7(1)	C211–Si2–C221	112.0(1)
C–N–Si1	134.4(1)	C111–Si1–C131	112.0(1)	C211–Si2–C231	110.7(1)
C–N–H	112.8	C121–Si1–C131	109.5(1)	C221–Si2–C231	108.9(1)
Si1–N–H	112.8				

[a)] sum of angles at C: 359.9°

2.3.4 *Discussion of bond lengths and Angles*

The X-ray structure analysis reveals that the (*Z*)-isomer of compound **I.2** predominating also in solution (see **Section 2.3.2**) had precipitated. **Figure 2.4** gives a stereoscopic view of the monomeric molecule.

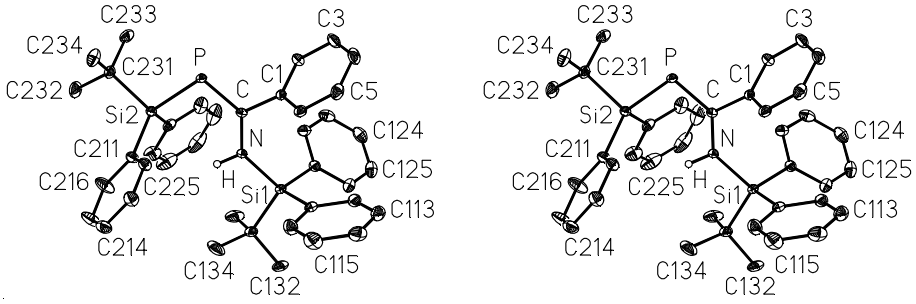

Figure 2.4 Molecular structure of *Z*-[*N*,*P*-bis(*tert*-butyldiphenylsilyl)-2-amino-2-phenyl-1$\lambda^3\sigma^2$-phosphaalkene] **(I.2)** in stereoscopic view
Thermal ellipsoids are at 30% probability; except for the N–H group all hydrogen atoms have been omitted for clarity. Absent atom numbering has to be complemented in a logical manner.

As reported in the literature, the P=C bond length of classical non-conjugated $1\lambda^3\sigma^2$-phosphaalkenes varies only slightly between 165 and 167 pm [48]. When, however, an amino substituent is bound to the *sp*^{2}-hybridized carbon atom, the possibility of an electronic interaction between the π-system of the P=C entity and the a priori non-bonding electron pair at nitrogen has to taken into consideration. This interaction is most efficient when the nitrogen atom is *sp*^{2}-hybridized and its *p*-orbital is perpendicularly arranged to the plane of the P=C system. As a result of such a conjugation, significant alteration of bond lengths is observed. The P=C double bond is elongated, whereas the adjacent C–N single bond gets shorter. Typical P–C and N–C distances fall within a range of 170 to 176 pm and 135 to 139 pm, respectively [33]; for comparison, a value of 145 pm is accepted as standard bond length for C_{Sp^2}–N_{Sp^2} [33].

The discussion about the influence of π-conjugation on bond lengths is based on several studies found in the literature [33, 37 and 49]. For example, in the 2-amino-$1\lambda^3\sigma^2$-phosphaalkene (*E*)-[Cp*(CO)$_2$Fe–P=C(C$_6$H$_5$)N(CH$_3$)$_2$] ((***E*)-2.10**, **Table 2.7**) published recently by *Weber* et al. [33], P=C and a N–C bond lengths of 171.7 and 139.9 pm, respectively, indicate an effective π–interaction between the P=C system and the nearly coplanar (dihedral angle 16.6°) dimethylamino group. When, however, the phenyl substituent at the sp^2-hybridized carbon atom is replaced by a bulky *tert*-butyl group (**(*Z*)-2.11**, **Table 2.7**), steric effects prevent a coplanar arrangement and the dimethylamino group and the P=C plane include an angle of 86.7°. At 169.7 and 144.8 pm, respectively, the P=C and C–N bond lengths approach values of non-conjugated $1\lambda^3\sigma^2$-phosphaalkenes.

P=C and C–N distances of 172.7 and 137.4 pm, respectively, have been determined for compound **(*Z*)-I.2**. An angle of 22.7° between the planes of the P=C system and the *tert*-butyldiphenylsilylamino substituent indicates an almost parallel arrangement. Furthermore, the P=C and C–N bond lengths of this compound are remarkably similar to those of the $1\lambda^3\sigma^2$-phosphaalkenes **(*Z*)-2.8**, **(*E*)-2.10** and **(*Z*)-2.12 (Table 2.7)**. Except for the *tert*-butyl derivative **(*Z*)-2.11** already discussed, major differences of nearly ±2.5 pm in the P=C and C–N bond lengths of compound **(*Z*)-I.2** and **(*E*)-2.10**, respectively, are considered to be insignificant. With these structural features in mind, compound **(*Z*)-I.2** might be classified as a typical inverse $1\lambda^3\sigma^2$-phosphaalkene.

Table 2.7 Selected bond lengths (pm) and bond angles (°) of some 2-amino-1$\lambda^3\sigma^2$-phosphaalkenes and differences to values of compound **(*Z*)-I.2**
"<diff.> denotes deviations of metrical parameters from those of (**Z**)-**I.2**."

Compound	P=C <diff.>	C–N <diff.>	P–C–N <diff.>	literature
(***Z***)-**I.2**	172.7(2) –	137.4(2) –	128.6 –	
(***Z***)-**2.8**	170.4 <−2.5>	135.7 <−1.7>	128.0 <−0.6>	[37]
(***E***)-**2.10**	171.7 <−1.0>	139.9 <2.5>	120.0 <−8.6>	[33]
(***Z***)-**2.12**	170.9 <−1.8>	136.7 <−0.7>	123.4 <−5.2>	[49]
(***Z***)-**2.11**	169.7 <−3.0>	144.8 <7.4>	120.8 <−7.8>	[33]

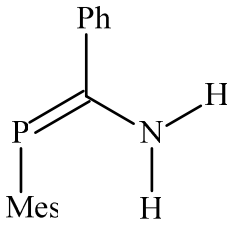

(*Z*)-2.8

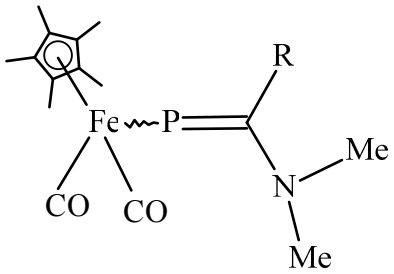

(*E*)-2.10 R = C_6H_5
(*Z*)-2.11 R = ^{t}Bu

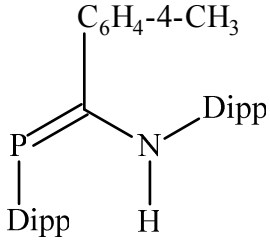

(*Z*)-2.12

A Si–P distance of 226.4(1) pm (**Table 2.6**) has been determined for the 2-amino-1$\lambda^3\sigma^2$-phosphaalkene (*Z*)-**I.2**. This bond-length agrees very well with the sum of covalent radii *r* [50] provided that the sum has been corrected for different electrongativity values (*x*) of phosphorus and silicon according to the *Schomaker-Stevenson* rule [51]. This rule which is based on an early proposal of *Pauling* and *Huggins* in 1937 [52] was modified later with respect to the scaling factors *c* by *Pauling* in 1960 [53].

$$d_{(Si–P)} = r_{kov.}\,(Si) + r_{kov.}\,(P) – c\,|\,x_P – x_{Si}\,|$$

Covalent radii ($r_{kov.}$): $r_{(Si)} = 117$, $r_{(P)} = 110$

Pauling electronegativities: $x_{Si} = 1.74$, $x_P = 2.06$

Adjustment factor: $c = 6$

$$225\text{ pm} = (117 + 110)\text{ pm} – 6\,|\,2.06 – 1.74\,|\text{ pm}$$

A considerable number of Si–P bond lengths are found in the literature; they all fall in a rather narrow range of 224 to 228 pm. A short compilation of those values is given in the thesis of *H. Kraft* [54, Table 8,p 36] of our research group. Some additional structure determinations,

however, deserve to be pointed out in detail. For example, the structure of the parent compound tris(trimethylsilyl)phosphane has been reported twice. Whereas *Rankin* et al [55] obtained a bond length of 225.9(1) pm by gas phase electron diffraction, the X-ray structure determination of *Bruckmann* and *Krüger* [56] gave a slightly shorter Si–P distance of 224.5(1) pm. Similar values were also obtained in our research group; an average value of 224.1(2) pm was observed for the three Si–P bond lengths in the bis(trimetylsiyl)tris(trimeth- ylsilyl)phosphane, the analogous compound bis(trimethylsilyl)trisisopropylsi- lylphosphane on the other hand shows a somewhat larger average P–Si distance of 225.1(2) pm [54]. Values of 226.0(1) and 227.0(1) pm were published by *Westerhausen*, *Löw* and *Schwarz* [57] for bis(triisopropylsilyl)phosphane. A fascinating compound has been prepared and studied structurally in *Niecke's* research group [58]. The special features of this phosphasilane (*E*)-Mes*–P=Si(*t*-Bu)–P(Mes*)–P(C_6H_5)$_2$ are the presence of a Si–P single and Si=P double bond; they have very different lengths of 225.4(3) and 209.4(3) pm. It should be mentioned that the research group of *Hänisch* studied intensively compounds that contains Si–P bonds. For example, different *N*-heterocyclic carbene (NHC) stabilized silylphosphinogallanes [(NHC)→Ga(Et_2)–P(H)–(Si*t*BuPh$_2$)] were reported, and the structure analysis of these compounds reveals Si–P bond lengths varies between 222.1(3) and 223.6(1) pm [59]. When, however, the phosphaalkene Me_3SiP=C(H)NMe_2 is used as a ligand in a $W(CO)_5$-complex, a Si–P distance of 224.6(2) pm has been determined [62]. Finally, the complex [$(CO)_5$W←P($SiMe_3$)=C(OEt)-(2-MeC_6H_4)] prepared by *Weber* et al. from Me_3Si–P=C(NMe_2)$_2$ and [$(CO)_5$W←C(OEt)-(2-MeC_6H_4)-] in 14% yield has to be mentioned; it has a slightly longer Si–P distance of 227.2(1) pm [63].

Early Ab intio calculations at the SCF level with a 3-21G* basis set published by *Gordon* et al. [60] for unsubstituted silylphosphane H_3Si–PH_2 predicted a Si–P distance of 225.8 pm.

Remarkably, calculation of *Grobe*, *Maulitz* et al [61] at the RHF/6-31+G* level reveal that the Si–P distances of (*E*)- and (*Z*)-(dimethylamino)fluoromethylidene(trimethylsilyl)phosphane do not differ substantially (227.3 *vs* 227.1 pm).

The discussion of Si–N bond lengths turns out to be more complicated than that of Si–P distances. To explain the experimentally obtained value of 177.2 pm for **(*Z*)-I.2**, one starts again with the sum of the covalent radii *r* of nitrogen (74 pm) and silicon (117 pm). In this case, however, one has to take into consideration that the nitrogen radius might be somewhat too large due to lone pair repulsions in compounds like hydrazine. At first, the *Schomaker-Stevenson* correction [51] modified in 1960 by *Pauling* [53] with respect to the scaling factors *c* gives a Si–N distance of 180.4 pm.

$$d_{(Si–N)} = r_{kov.}(Si) + r_{kov.}(N) – c\,|\,x_N – x_{Si}\,|$$

Covalent radii ($r_{kov.}$): $r_{(Si)} = 117$, $r_{(N)} = 74$

Pauling electronegativities: $x_{Si} = 1.74$, $x_N = 3.07$

Adjustment factor: $c = 8$

$$180.4 \text{ pm} = (117 + 74) \text{ pm} – 8\,|\,3.07 – 1.74\,|\text{ pm}$$

Since this value is too large and does not agree with the results of many structure determinations, *Blom* and *Haaland* [64] suggested a variance of the *Schomaker-Stevenson* rule now being generally applicable. Moreover, sometimes the authors used slightly different covalent radii.

$$d_{(Si–N)} = r_{kov.}(Si) + r_{kov.}(N) – c\,|\,x_N – x_{Si}\,|^{n}$$

Covalent radii ($r_{kov.}$): $r_{(Si)} = 115$, $r_{(N)} = 73$

Pauling electronegativities: $x_{Si} = 1.74$, $x_N = 3.07$

Adjustment factors: $c = 6$, $n = 1.4$

$$175 \text{ pm} = (115 + 73) \text{ pm} – 6\,|\,3.07 – 1.74\,|^{1.4} \text{ pm}$$

A significant number of different Si–N bond lengths has been reported in the literature. In contrast to the Si–P distances, however, these values are spread over a wide range of 170 to 180 pm. In general, Si–N bond lengths shorter than the calculated standard value of 175 pm [65] are considered to be influenced by a p(N)→σ*(Si–C) or p(N)→σ*(Si–H) back-bonding [66].

In the sixties and early seventies of the last century, a series of silyl- and trimethylsilylamines such as $(H_3Si)_3N$ [67], $H_3Si–N(CH_3)_2$ [68] or $Me_3Si–N(H)CH_3$ [69] has been studied by gas phase electron diffraction. The Si–N distances of these compounds vary only slightly between 171.5 (4) and 173.4 (5) pm. The research groups of *Lappert* [70], *Mootz* [71] and *Atwood* [72] determined with X-ray structure analyses an average Si–N bond length of 170.5 (3) pm for the dimeric complex $[(Me_3Si)_2N–Li(OEt_2)]_2$ and of 172.9 (4) pm for the trimer $[(Me_3Si)_2N–Li]_3$. Further examples of lithium triorganylsilylamides as well as of neutral silazanes and their derivatives are given in the theses of *Abele* [73] and *Oberprantacher* [74] from our research group. Relative long Si–N distances of 179.1 (2) and 179.4 (2) pm were obtained from the zinc complex $\{P[C(C_6H_5)\cdots N(SiMe_3)_3]_2\}_2Zn$ prepared and studied by *U. Hübler* [75]. The Relatively large Si–N distance of 177.2 (1) pm in **(*Z*)-I.2** might be attributed to steric effects in that two phenyl groups and a bulky *tert*-butyl substituent are bound to the silicon atom. Actually, a C–N–Si angle of 134.4° (1) and a P–C–N angle of 128.6° (1) are in accord with this explanation.

Figure 2.5 gives a stereoscopic view of the molecular packing. No intermolecular contacts significantly shorter than *van der Waals* distances were found. The arrangement of molecules can best be described as a distorted hexagonal primitive packing (**Figure 2.5 b)**.

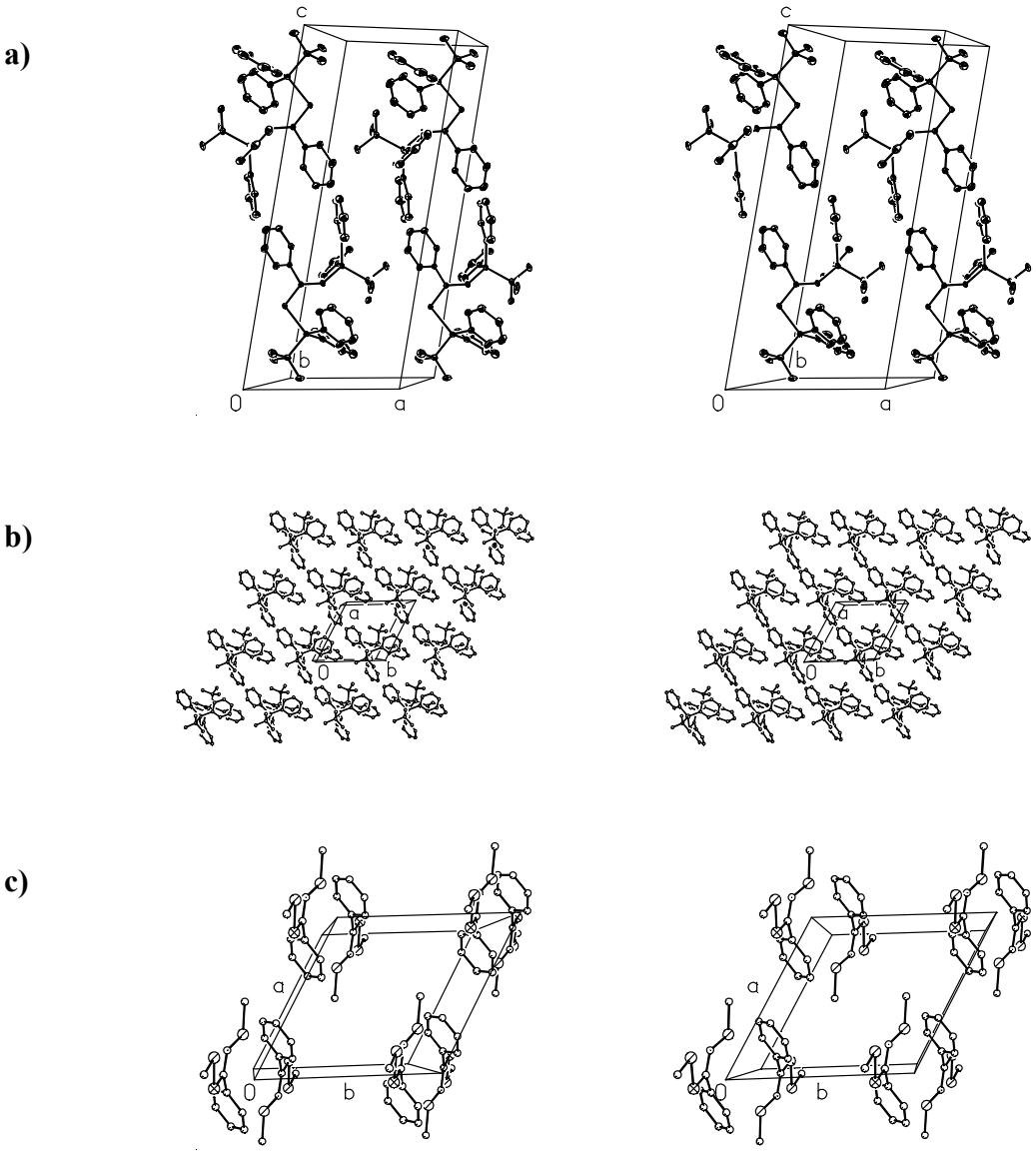

Figure 2.5 Arrangement of compound (**I**.**2**) molecules in the solid state
a) The figure shows two pairs of inverse molecules inside and outside the unit cell. Thermal ellipsoids are at 30% probability; all hydrogen atoms have been omitted for clarity.
b) The molecules set up a slightly distorted hexagonal primitive packing. Whereas angle γ (60.633°) is near its ideal value, the angles α and β deviate significantly from 90° Table 3.1.
c) The (001) layers are interrelated by centres of inversion. Note that in the two *tert*-butyldiphenylsilyl substituents the phenyl and methyl groups have been additionally omitted for clarity.

2.4 *2-[(*tert*-Butyldiphenylsilyl)amino]-2-phenyl-1λ³σ²-phosphaalkene {(Z)-/(E)-I.1} by Decomposition of Compound (Z)-/(E)-I.2*

To our surprise, the *P,N*-disilylated $1\lambda^3\sigma^2$-phosphaalkene **(*Z*)-/(*E*)-I.2** turned out to be unstable in [d_8]tetrahydrofuran and decomposed when being stored in this solvent for several weeks at room temperature. The $^{31}P\{^1H\}$ NMR spectrum showed a new singlet of low intensity at +43.8 ppm which appeared in the ^{31}P NMR spectrum as a doublet with a $^1J_{P,H}$-value of 150 Hz indicating the presence of a H~P=C entity. This observation motivated us to study the decomposition in detail.

Another sample freshly prepared by dissolving crystals of **(*Z*)-I.2** in [d_8]tetrahydrofuran was kept for about six months at +55 °C in a drying oven and the decomposition was monitored by ^{31}P NMR spectroscopy (**Figure 2.6**). After about three months, two new, rather strong signals at +43.8 and +66.8 ppm with $^1J_{P,H}$-coupling constants of 150 and 154 Hz, respectively, were detected. They show an intensity ratio of 1 : 0.27, whereas the signals of the isomers ***(Z)-/(E)*-I.2** had decreased accordingly.

Fortunately the origin of the new signals was established unambiguously by 2D NMR techniques. They stem from 2-[(*tert*-butyldiphenylsilyl)amino]-2-phenyl-$1\lambda^3\sigma^2$-phosphaalkene (**I.1**) present as a mixture of *(Z)*- and *(E)*-isomers (see below). The hydrogen atom that had replaced the former *tert*-butyldiphenylsilyl substituent in **I.2** does not originate from a deuterated solvent molecule but presumably from the *tert*-butyl group at silicon. We assume that the weak Si–P bond is cleaved, and a hydrogen atom from a *tert*-butyl substituent is transferred to phosphorus. Probably, this step is facilitated by the solvent molecule [d_8]tetrahydrofuran which intercepts the remaining but still bulky entity •Si(C_6H_5)$_2$–C(CH_3)$_2$-CH_2• under ring opening. Unfortunately, composition and structure of the phosphorus-free by-product (**I*$_{eli}$**) has not yet been resolved. The NMR data of (***Z***)/(***E***)-**I.1** have been compiled in **Tables 2.8** and **2.9** in so far as they could be detected.

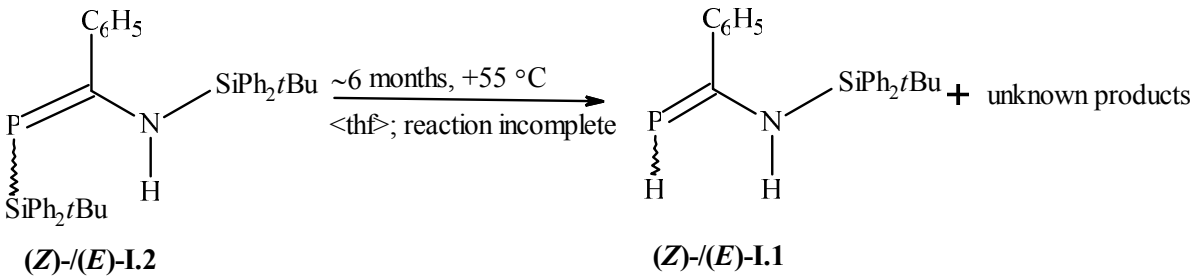

(*Z*)-/(*E*)-I.2 **(*Z*)-/(*E*)-I.1**

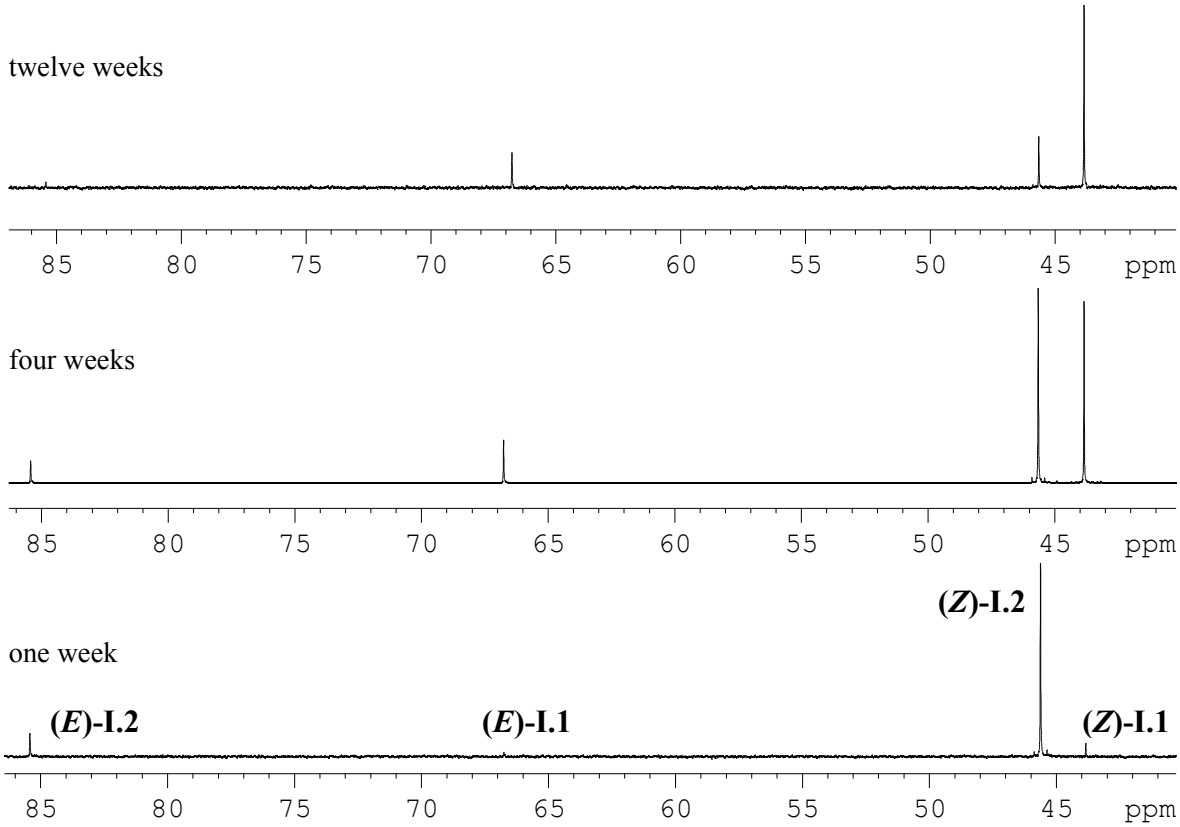

Figure 2.6 $^{31}P\{^{1}H\}$ NMR spectra illustrating the decomposition of the (***Z***)-/(***E***)-**I.2** in [d_8]tetrahydrofuran. The spectra have been taken at room temperature from a sample which had been prepared by dissolving crystals of (***Z***)-**I.2** in [d_8]tetrahydrofuran and was kept in a sealed NMR tube for several months at +55 ºC in a dry oven. Signal assignments: 2-[(*tert*-Butyldiphenylsilyl)amino]-2-phenyl-1$\lambda^3\sigma^2$-phosphaalkene (**I.1**), *N,P*-bis(*tert*-butyldiphenylsilyl)-2-amino-2-phenyl-1$\lambda^3\sigma^2$-phosphaalkene (**I.2)**

After about six months at +55 °C, the ^{31}P NMR signals of *(**Z**)*- and ***(E)*-I.1** showed still an intensity ratio of 1 : 0.27, but the decomposition of the 1$\lambda^3\sigma^2$-phosphaalkene **I.2** had proceeded to such an extent that the less abundant isomer **(*E*)-I.1** could be characterized adequately. Hydrogen coupling splits its ^{31}P NMR signal at +66.8 ppm into a doublet of doublets with two very different coupling constants of 154 and 19 Hz. The first value corresponds to the well known $^{1}J_{P,H}$ coupling, the second one has to be attributed to a coupling between phosphorus and the hydrogen atom at nitrogen ($^{3}J_{P,H(N)}$). Thus, even at this early stage the two ^{31}P NMR signals at +43.8 and +66.8 ppm can be assigned to the *(Z)*- and *(E)*-isomers of **I.1**, respectively.

Further analyses confirm this assignment. In the $^{1}H,^{31}P$ HMQC experiment, the ^{31}P doublet of the (*Z*)-isomer at 43.8 ppm reveals three cross peaks with ^{1}H NMR signals. The first cross peak with the ^{1}H doublet at 3.6 ppm; due to a coupling constant of 150 Hz it comes from the

Table 2.8 Assignment of ^{1}H, ^{13}C, and ^{29}Si NMR signals of the 2-[(*tert*-butyldiphenylsilyl)amino]-2-phenyl-1$\lambda^3\sigma^2$-phosphaalkene isomers (***Z***)- and (***E***)-**I.1**, based on ^{1}H-COSY, HSQC, HMQC, and HMBC correlations of the *tert*-butyl, amino and phosphanylidene hydrogen atoms

The purpose of including two decimal places in the NMR shift values presented here is not for accuracy but for easy identification of the corresponding signals in the spectrum.

Part α): P–H, N–H and *tert*-butyl group at silicon

^{1}H atom (isomer)	δ (ppm), multiplicity[a)]	^{1}H-COSY	HMQC/(^{31}P)[b)], HSQC(^{13}C)/(^{29}Si)[b)]	HMBC[b)]
a) *P–H group*				
P–H (*Z*)[c)]	3.63 (*dd*)[d)]	N–H (*Z*) (5.76) m[e)]	^{31}P (43.86) s[f)]	^{13}P=C (200.3) m[g)] $^{13}C_{ipso}$(145.1) vw[h)i)]
P–H (*E*)[c)]	3.61 (*dd*)[j)]	N–H (*E*) (5.72) m[k)]	^{31}P (66.76) s[l)]	
b) *N–H group*				
N–H (*Z*)	5.76 (*s, br*)		^{31}P (43.86) w[f)]	
N–H (*E*)	5.72 (*dd, br*)[m)n)]		^{31}P (66.76) s[l)]	
c) tert-*butyl substituent*[o)]				
(H_3C)$_3$C (*Z*)	0.83 (*s*)		$^{13}CH_3$ (26.54) s ^{29}Si (– 9.63) s	$^{13}CH_3$ (26.58) s $^{13}C_{quar}$ (19.06) m
(H_3C)$_3$C (*eli*)	0.86 (*s*)		$^{13}CH_3$ (26.72) s ^{29}Si (– 11.46) s	$^{13}CH_3$ (26.70) s $^{13}C_{quar}$ (18.47) m
(H_3C)$_3$C (*E*)	0.89 (*s*)		$^{13}CH_3$ (26.96) m ^{29}Si (– 9.86)	$^{13}CH_3$ (26.97) s $^{13}C_{quar}$ (18.65) m

[a)] singlet (*s*), doublet (*d*), triplet (*t*), multiplet (*m*), broad (*br*); [b)] HMQC, HSQC and HMBC correlation: strong (s), medium (m), weak (w), very weak (vw); [c)] intensity ratio of 1 : 0.27 for the isomers (***Z***)- and (***E***)-**I.1**; [d)] two slightly split peaks at 3.43 and 3.82; $^{1}J_{H,P}$ = 150 Hz, $^{4}J_{H,H(N)}$ = 1 Hz; [e)] correlation with the P–H (*Z*) peak at 3.8; [f)] ^{31}P: δ = 43.8 (*d*), $^{1}J_{H,P}$ = 150 Hz; [g)] $^{1}J_{P,C}$ = 54 Hz; [h)] phenyl substituent at the P=C carbon atom; [i)] $^{2}J_{P,C}$ = 27 Hz; [j)] three peaks discernible at 3.8, 3.8 and 3.4 (already partially covered), fourth peak at 3.4 completely covered by [d_8]tetrahydrofuran {δ(C–CHD–O) = 3.4, $^{1}J_{H,C}$ = 144.1, $^{2}J_{H,C}$ = 40 Hz; δ(C–CHD–C) = 1.5, $^{1}J_{H,C}$ = 131.3, $^{2}J_{H,C}$ = 37 Hz}, $^{1}J_{H,P}$ = 154 Hz, $^{4}J_{H,H(N)}$ = 3 Hz; [k)] correlation between the centre of the P–H (*E*) doublet at 3.8 and the centre of the N–H (*E*) doublet at 5.8 and also between the centres at 3.4 and 5.7; [l)] ^{31}P: δ = 66.8 (*dd*), $^{1}J_{H,P}$ = 153.6, $^{3}J_{P,H(N)}$ = 19 Hz; [m)] three broad peaks discernable at 5.69, 5.70 and 5.75 (already partially covered), fourth peak at 5.75 completely covered by the N–H resonance of the (*Z*) isomer; [n)] $^{4}J_{H,H(P)}$ = 3, $^{3}J_{H,P}$ = 20 Hz; [o)] The sample still contains a small but detectable amount of the starting compound (***Z***)-**I.2**

Part β): Phenyl substituents at the P=C carbon and silicon

^{1}H atom	δ- value (ppm), multiplicity[a)]	^{1}H- COSY	HMQC/(^{31}P)[b)], HSQC(^{13}C)/(^{29}Si)[b)]	HMBC[b)]
d) *phenyl substituent at the P=C carbon of the isomer* (***Z***)**-I.1**[p)]				
C–$\underline{H}_{ortho}$ (*Z*)	7.57[q)] (*m*)	C–$\underline{H}_{meta}$ (7.19) s	$^{13}\underline{C}_{ortho}$ (125.7) s[r)] $^{31}\underline{P}$ (43.88) s	$^{13}\underline{C}_{para}$ (136.4) w[s)] $^{13}\underline{C}_{ortho}$ –
C–$\underline{H}_{meta}$ (*Z*)	7.19 (*m*)	C–$\underline{H}_{ortho}$ (7.57) s C–$\underline{H}_{para}$ (7.67) s	$^{13}\underline{C}_{meta}$ (128.6) m	$^{13}\underline{C}_{ipso}$ (145.0) w[t)]
C–$\underline{H}_{para}$ (*Z*)	7.67 (*m*)	C–$\underline{H}_{meta}$ (7.19) s	$^{13}\underline{C}_{para}$ (136.4) s[s)u)]	–
e) *phenyl substituents at Si(NH)*				
C–$\underline{H}_{ortho}$ (*Z*)	7.56 (*m*)[w)]	C–$\underline{H}_{meta}$ (7.14) s	$^{13}\underline{C}_{ortho}$ (135.1) s[v)]	$^{13}\underline{C}_{ortho}$ (135.1) w $^{13}\underline{C}_{para}$ (129.3) s
C–$\underline{H}_{meta}$ (*Z*)	7.14 (*m*)	C–$\underline{H}_{ortho}$ (7.55) s	$^{13}\underline{C}_{meta}$ (127.6) s	$^{13}\underline{C}_{meta}$(127.7) vw $^{13}\underline{C}_{ipso}$ (137.1) m
C–$\underline{H}_{para}$ (*Z*)	7.14 (*m*)	–	$^{13}\underline{C}_{para}$ (129.3) m	$^{13}\underline{C}_{ortho}$ (135.1) w

[p)] The low concentration of the isomer (***E***)**-I.1** (ratio of 1 : 0.27 with respect to (***Z***)**-I.1**) prevents the detection and identification of its ^{13}C phenyl resonances. [q)] Partially covered by the C–$\underline{H}_{ortho}$ (*Z*) multiplet of the phenyl substituents at silicon (7.56); [r)] $^{3}J_{P,C}$ = 15 Hz; [s)] $^{5}J_{P,C}$ = 2 Hz; [t)] $^{2}J_{P,C}$ = 27 Hz; [u)] intensity ratio of 1.7 : 1.0 for the resonances of $^{13}\underline{C}_{ortho}$ and $^{13}\underline{C}_{para}$; [v)] intensity ratio of 1.0 : 0.8 for the ^{13}C phenyl resonances of the (*Z*) isomer and the second structurally still unknown compound; [w)] multiplet with more than five dominant lines as a consequence of superposition.

hydrogen atom at phosphorus. The second cross peak with a broad singlet at 5.76 ppm has to be attributed to the hydrogen atom at nitrogen because of signal shape and chemical shift value. The third cross peak is found between the ^{31}P resonances and the multiplet at 7.57 ppm of the two hydrogen atoms in *ortho*- position of the phenyl substituent at the P=C entity. This assignment is confirmed by a ^{1}H,^{13}C HSQC correlation between this multiplet and the doublet ($^{3}J_{P,C}$ = 15 Hz) of the pertinent carbon atom in *ortho*-position at 125.7 ppm. In the meantime, all ^{1}H and ^{13}C NMR signals of the phenyl substituent at the P=C entity of the (*Z)*-isomer were assigned in HSQC and HMBC experiments; an analogous analysis of the (*E*)-isomer remained unsuccessful because of its low concentration.

Since at least three decomposition compounds, i.e **(*Z*)-I.1** and **(*E*)-I.1** and a phosphorus-free organosilane , are present in solution, the *tert*-butyl region of the ^{1}H NMR spectrum is expected to show three different signals. Indeed, these are observed at 0.83, 0.86 and 0.89

ppm in an intensity ratios of 1.0 : 0.64 : 0.22. The corresponding ^{13}C NMR signals of the methyl and quarternary carbon atoms were assigned by means of HSQC and HMBC. Their intensity ratios of (1.0 : 0.72 : 0.19) and (1.0 : 0.71 : 0.23), respectively, agree very well with the aforementioned values and the intensity ratio of (1.0 : 0.27) known from the ^{31}P NMR spectrum (**Figure 2.7** a)).

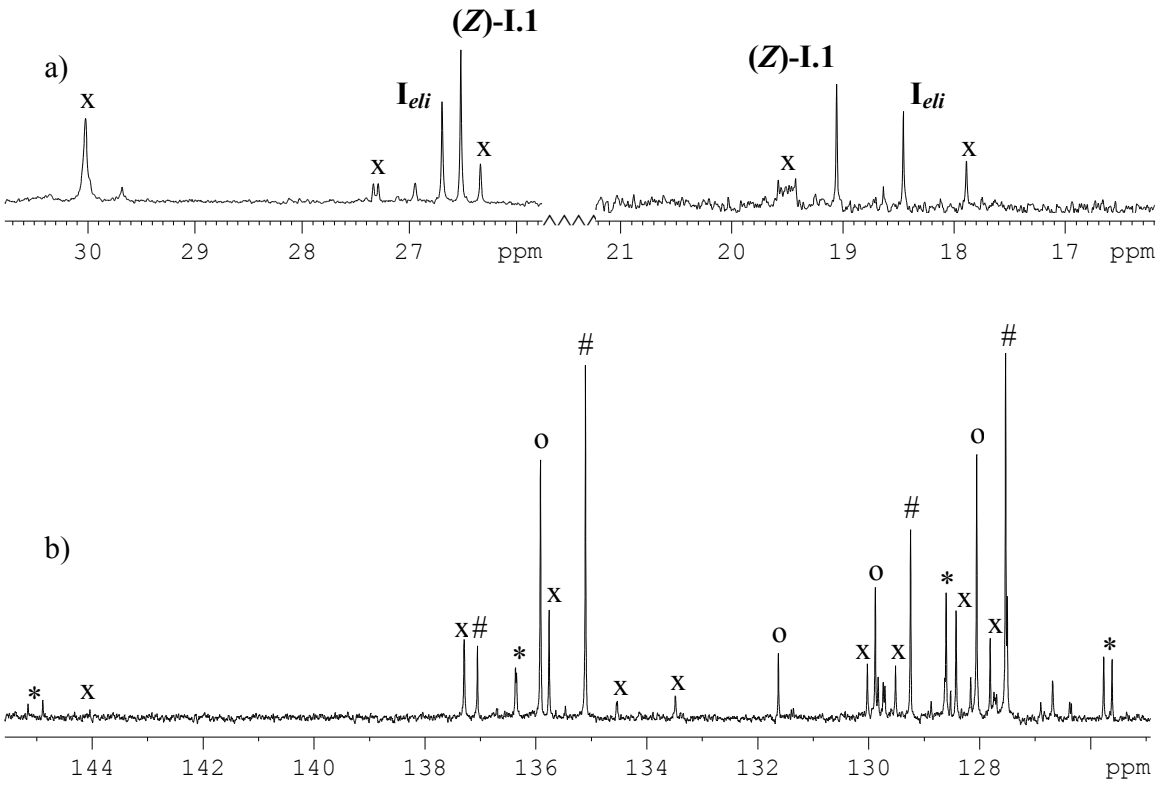

Figure 2.7 *tert*-Butyl (a) and phenyl regions (b) of the ^{13}C NMR spectrum of compounds (***Z***)-**I.1,** (***E***)-**I.1,** $\mathbf{I}_{eli}$ and undecomposed (***Z***)-**I.2**
The spectrum has been taken at room temperature from a [d_8]tetrahydrofuran solution of the crystalline $1\lambda^3\sigma^2$-phosphaalkene (***Z***)-**I.2** kept in a sealed NMR tube for four months at +55 ºC. The signals were marked as follows: (x) = (***Z***)-**I.2**, (*) = (***Z***)-**I.1**, (#) = (***E***)-**I.1**, (o) = signals of phosphorus-free unknown reaction products.

It has to be mentioned that the ^{13}C NMR signals of the two different phenyl substituents (**Table 2.9,** part b) and c)) could be assigned on the basis of carbon phosphorus coupling and intensity ratio. Indeed, for the isomer (***Z***)-**I.1** the ^{13}C NMR signals of the C_{ipso} (145.0), C_{ortho} (125.7), and C_{para} atoms (136.4 ppm) of the phenyl substituent at the P=C entity are all found to be doublets with coupling constants of $^2J_{P,C} = 27$, $^3J_{P,C} = 15$ and $^5J_{P,C} = 2$ Hz, respectively. The ^{13}C NMR signal of the two carbon atoms in *meta*-position is a singlet at 128.6 ppm. The phenyl substituents at the silicon atoms of the (*Z*)-isomer are assigned according to the

intensity ratio (**Table 2.9**, **Figure 2.7** b)). Furthermore, in the low field region of the ^{13}C NMR spectrum a signal at 200.3 ppm with a $^{1}J_{P,C}$ coupling constant of 54 Hz is observed. Since in the HMBC experiment a clearly visible correlation with the doublet of the P–H hydrogen atom of the (*Z*)-isomer at 3.63 ppm is detected it has to be assigned to the P=C carbon atom of **(*Z*)-I.1**. The ^{13}C NMR signals of the isomer **(*E*)-I.1** are undetectable because of low concentration.

Table 2.9 δ ^{13}C (ppm) and $^{n}J_{P,C}$ values (Hz) of (*Z*)- and (*E*)-2-[(*tert*-butyldiphenylsilyl)amino]-2-phenyl-1$\lambda^3\sigma^2$-phosphaalkene] (**I.1**). The signal assignmengts were verified by the analysis of 2D NMR spectra. The purpose of including two decimal places in the NMR shift values presented here is not for accuracy but for easy identification of the corresponding signals in the spectrum.

^{13}C atom	**(*Z*) isomer** δ ^{13}C (ppm), multiplicity[a)]	**(*E*) isomer** δ ^{13}C (ppm), multiplicity[a)]
a) tert-*butyl group at silicon*		
$(H_3\underline{C})_3C$–Si(NH)	26.52 (*s*)	26.94 (*s*)
$(H_3C)_3\underline{C}$–Si(NH)	19.06 (*s*)	18.64 (*s*)
b) *phenyl substituent at the P=C carbon atom*		
$\underline{C}_{ipso}$	145.0 (*d*), $^{2}J_{P,C} = 27$	[b)]
$\underline{C}_{ortho}$	125.7 (*d*), $^{3}J_{P,C} = 15$	
$\underline{C}_{meta}$	128.6 (*s*)	
$\underline{C}_{para}$	136.4 (*s*), $^{5}J_{P,C} = 2$	
c) *phenyl substituents at silicon*		
$\underline{C}_{ipso}$	137.1 (*s*)	[b)]
$\underline{C}_{ortho}$	135.1 (*s*)	
$\underline{C}_{meta}$	127.5 (*s*)	
$\underline{C}_{para}$	129.3 (*s*)	
d) *P=C fragment*		
<u>P=C</u>	200.1 (*d*), $^{1}J_{P,C} = 54$	[b)]

[a)] singlet (*s*), doublet (*d*); [b)] The concentration of (***E***)-**I.1** was too low as to detect the corresponding ^{13}C NMR signals.

2.5 *Formation of (Z)-/(E)-Isomeric 2-Amino-2-phenyl-1$\lambda^3\sigma^2$-phosphaalkene* H~P=C(C_6H_5)–NH_2 (I.0) *in Reactions of 2-(Lithiumamido)-2-phenyl-1$\lambda^3\sigma^2$-phosphaalkene (1) with Acids*

In our research group trifluoroacetic acid, has been successfully applied for several times as a proton source in order to replace lithium for hydrogen. For example, an NMR experiment reveals that treatment of a 1,2-dimethoxyethane solution of lithium-bis(methoxycarbonyl)phosphanide at −50 °C with a stoichiometric amount of this acid furnished bis(methoxycarbonyl)phosphane. Remarkably, the protonation of the anion takes place at phosphorus [76]. Similarly, from a reaction of lithium-bis[(*N*-trimethylsilyl)iminobenzoyl]phosphanide the neutral compound bis[(*N*-trimethylsilyl)iminobenzoyl]phosphane was isolated in 74% yield [76]. Another well known proton source is triethylammonium chloride. A slight excess of this acid was used by *Coles* and co-workers to prepare neutral phospha(III)guanidines at ambient temperature from the corresponding lithium derivatives dissolved in tetrahydrofuran [77].

In **Section 2.3.1** it has already been discussed that a 1,2-dimethoxyethane solution of the starting compound **1** reacts with an equimolar amount of *tert*-butylchlorodiphenylsilane between −70 °C and room temperature. As a consequence of a lithium–hydrogen exchange the *P*,*N*-disilylated 1$\lambda^3\sigma^2$-phosphaalkene **I.2** together with the unsilylated 2-amino-2-phenyl-1$\lambda^3\sigma^2$-phosphaalkene H~P=C(C_6H_5)–NH_2 **(I.0)** are formed. Keeping this result in mind, a controlled formation and NMR spectroscopic characterization of the first parent 2-amino-2-aryl-1$\lambda^3\sigma^2$-phosphaalkene was quite obvious. Therefore, a 1,2-dimethoxyethane solution of **1** was treated with different proton sources such as neat trifluoromethanesulfonic acid instead of trifluoroacetic acid as well as with triethylammonium chloride dissolved in the same solvent at ambient temperature. Similar results were also obtained in a reaction of **1** with (*tert*-butyldimethylsilyl)trifluoromethanesulfonate where it was found that a major part of the silyl ester had accidentally been hydrolysed.

Details of the sample preparation are given in the experimental part section **5.3.3** (*Samples A, B, and C*); in **Table 2.10** the results of the ^{31}P NMR experiments have been compiled. For a better comparison, analogous data of the aforementioned reaction of **1** with an equimolar amount of *tert*-butylchlorodiphenylsilane (**2**) have been included (*Sample D*). It should be mentioned that, beside the ^{31}P NMR signals of the compounds disscussed in **Table 2.10**, the spectra displayed further resonances which belong to minor impurities that could not be identified, these results are given in the experimental part, section **5.3.3**.

Indeed, the successful formation of the unsubstituted 2-amino-2-phenyl-1$\lambda^3\sigma^2$-phosphaalkene (**1.0**) via a lithium–hydrogen exchange is verified by these NMR spectroscopic observations:

α) In all $^{31}P\{^1H\}$ NMR spectra depicted in **Figure 2.8** a very strong signal at about −10 ppm is accompanied by a much weaker one at about +21 ppm. The intensity ratio is always 1: 0.2.

β) ^{1}H-coupling splits these two resonances into doublets with a $^1J_{P,H}$ coupling constant of 142 Hz or 161 Hz, respectively. Values of this magnitude are indicative of two-coordinate phosphorus atoms in P–H groups. The smaller coupling constant has to be attributed to the (*Z*)- and the larger one to the (*E*)-isomeric 1$\lambda^3\sigma^2$-phosphaalkene (for comparison see e.g. **Section 2.2**).

γ) Furthermore, in the ^{31}P NMR spectra of the *Samples A, B, and D* the doublet of the (*E*)-isomer at about +21 ppm is split into a triplet due to an additional $^3J_{P,H(N)}$ coupling of about 10 Hz. The unusual size of this coupling constant will be discussed later. In the ^{31}P NMR spectrum of *Sample C* the additional splitting of the doublet lines is not observed, presumably as a consequence of a rapid trimethylamine–induced exchange of the NH_2 hydrogen atoms.

δ) 2D NMR experiments are completely in agreement with the assignment derived above. These results have been compiled in **Table 2.10** and will be discussed in details below.

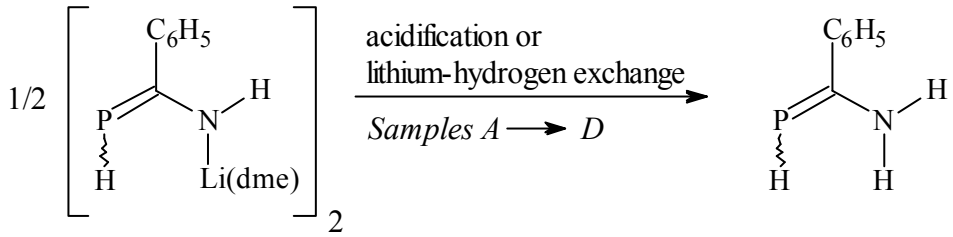

(***Z***)-/(***E***)-**1** (***Z***)-/(***E***)-**I.0**

Except for the doublets *a* to *d* of the (*Z*)-/(*E*)-isomeric dimers **I.01** and **I.02** *Sample A* prepared from neat trifluoromethanesulfonic acid and a 1,2-dimethoxyethane solution of 2-(lithiumamido)-2-phenyl-1$\lambda^3\sigma^2$-phosphaalkene (**1**), shows only two additional impurity signals (*e* and *f*, **Figure 2.8**) and in contrast to *Sample C* seems to be free of exchange phenomena. It was therefore considered to be most suitable for further ^{1}H and ^{13}C NMR studies in order to ensure the structure of the (*Z*)-/(*E*)-isomeric 1$\lambda^3\sigma^2$-phosphaalkene **I.0**. But initial attempts failed because of the presence of too large amount of the undeuterated solvent 1,2-dimethoxyethane. Most of it had to be removed *in vacuo* and replaced by [d_8]tetrahydrofuran (*Sample A'*, results in **Table 2.11**). However, we note that the δ^{31}P NMR values of the isomers (***Z***)- and (***E***)-**I.0** change from −10.2 and +20.9 ppm at +28 °C in

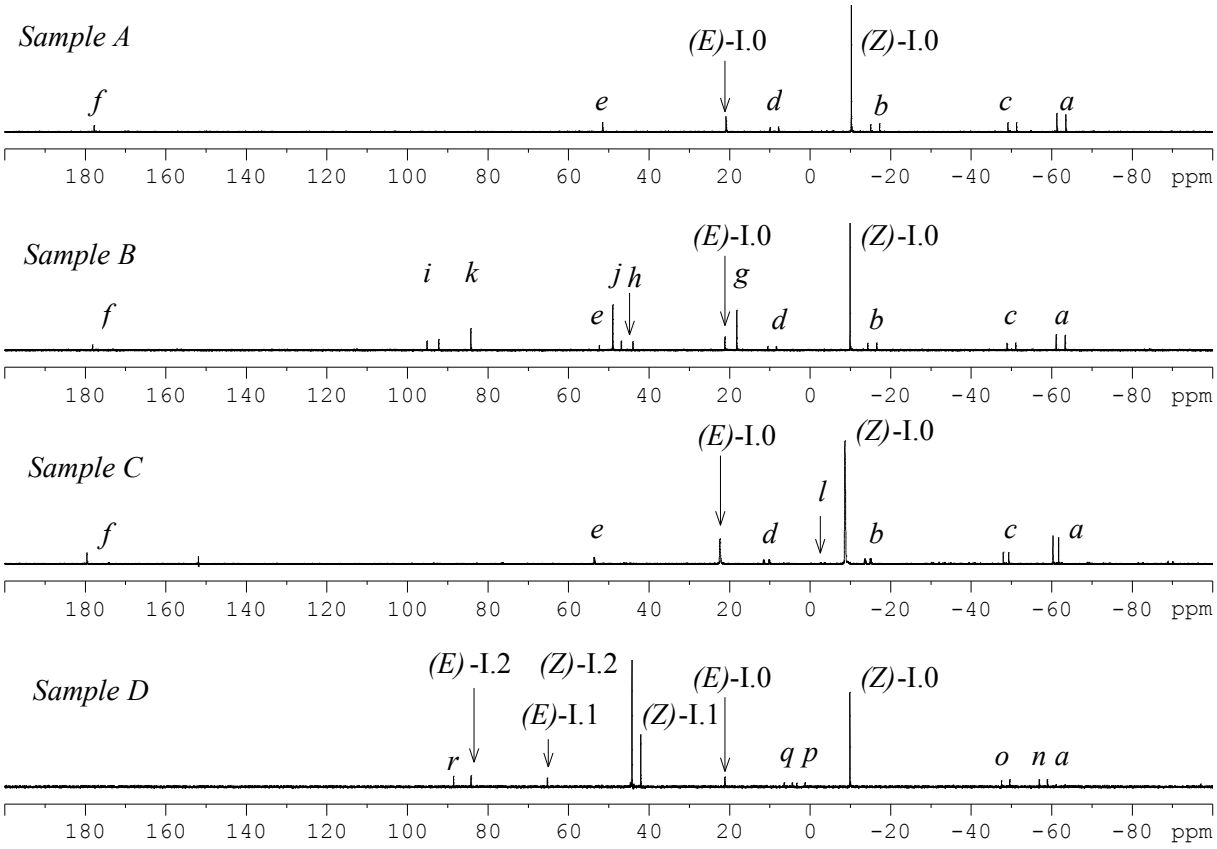

Figure 2.8 $^{31}P\{^{1}H\}$ NMR spectroscopic detection of (*Z*)-/(*E*)-isomeric 2-amino-2-phenyl-$1\lambda^3\sigma^2$-phosphaalkene H~P=C(C_6H_5)–NH_2 (**I.0**) in different reactions of the *N*-lithiumamido derivative **1**

The samples *A*→*D* were taken from the reactions of 2-(lithiumamido)-2-phenyl-$1\lambda^3\sigma^2$-phosphaalkene (**1**) with neat trifluoromethanesulfonic acid, largely hydrolysed (*tert*-butyldimethylsilyl)trifluoromethanesulfonate, triethylammonium chloride and *tert*-butylchlorodiphenylsilane, respectively; for details see experimental section 5.3.3. In the ^{31}P NMR spectra of the *Samples A, B, and C*, the signals of the (***Z***)-/(***E***)-isomeric dimers **I.01** and **I.02** of the $1\lambda^3\sigma^2$-phosphaalkenes (***Z***)-/(***E***)-**I.0** are marked with the letters *a*→ *d* ; these two compounds will be discussed in **Section 2.7**. The origin of signals marked with the letters *e* → *n* is unknown. In *Sample D*, the signals of the $1\lambda^3\sigma^2$-phosphaalkenes H~P=C(C_6H_5)–N(H)Si^{t}Bu(C_6H_5)$_2$ ((***Z***)-/(***E***)-**I.1**) and ^{t}Bu(H_5C_6)$_2$Si~P=C(C_6H_5)N(H)–Si^{t}Bu(C_6H_5)$_2$ ((***Z***)-/(***E***)-**I.2**) can also be detected; signal *m* at −186.5 ppm has not been depicted.

1,2-dimethoxyethane to −13.9 and +17.2 ppm, respectively, at −20 °C in [d_8]tetrahydrofuran (**Table 2.11**), whereas both $^1J_{P,H}$ coupling constants stay constant (142 and 161 Hz *vs* 142 and 162 Hz). Furthermore, slightly different intensity ratios for the two isomers of (1.0 : 0.20) and (1.0 : 0.15) are found in the different solvents.

Table 2.10 ^{31}P NMR spectroscopic characterization of (*Z*)-/(*E*)-isomeric 2-amino-2-phenyl-1$\lambda^3\sigma^2$-phosphaalkene H~P=C(C_6H_5)–NH_2 (**I.0**) in different reactions of its *N*-lithiumamido derivative **1** with acids (samples *A* – *C*) or with *tert*-butylchlorodiphenylsilane (**2**) (*Sample D*)

In this table *all* chemical shift values and coupling constants of signals observed in the spectra of the *Samples A, B, C, and D* (**Figure 2.8**) have been put together. Unlike the *Samples A, B, and D*, the ^{31}P NMR signals of *Sample C* are found to be relatively broad. Furthermore, the presence of triethylamine leads to a disappearance of the $J_{P,H(N)}$ coupling probably as a consequence of rapidly exchanging hydrogen atoms at nitrogen. Therefore in *Sample C* the isomer (***E***)-**I.0** shows only a doublet (*d*) and not a doublet of triplets (*dt*).

Please note that the intensity ratio of the phosphorus nuclei as given below, does not correlate with their frequency as a consequence of different relaxation times. For example, the ratio of (***Z***)-**I.01**, CH_{alk} to (***Z***)-**I.01**, P=C is found to be (2 : 1) instead of (1 : 1) as to be concluded from the same coupling constant.

^{31}P NMR signals of the (*Z*)-/(*E*)-isomeric compounds **I.0**, **I.01**, **I.02**, **I.1**, and **I.2**

I.0: H~P=C(C_6H_5)–NH_2 ; **I.01** and **I.02**: dimers of compound **I.0** (see **Section 2.6**);

I.1: H~P=C(C_6H_5)–N(H)Si^{t}Bu(C_6H_5)$_2$; **I.2**: ^{t}Bu(H_5C_6)$_2$Si~P=C(C_6H_5)–N(H)Si^{t}Bu(C_6H_5)$_2$

Compound or signal	*Sample*	δ ^{31}P	multiplicity[a] {^{1}H}/^{1}H coupl.	$J_{P,P}$	$^1J_{P,H}$	$J_{P,H}$	$J_{P,H(N)}$	intens. ratio
(***Z***)-**I.0**	*A*	–10.2	(*s*)/(*d*)	–	142	–	–	10.00
	B	–9.9	(*s*)/(*d*)	–	142[b]	–	–	10.00
	C[c]	–8.7	(*s*)/(*dd*)	–	142	16[d]	–	10.00
	D	–9.9[e]	(*s*)/(*d*)	–	141	–	–	10.00
(***E***)-**I.0**	*A*	20.9	(*s*)/(*dt*)	–	161	–	10	1.97
	B	21.2	(*s*)/(*dt*)	–	161	–	10	1.98
	C	22.4	(*s*)/(*d*)	–	161[f]	–	–	1.94
	D	21.2	(*s*)/(*dt*)	–	161	–	10	2.26
(***Z***)-**I.01,**	*A*	–62.4	(*d*)/(*dd*)	226	167	–	–	1.99
CH_{alk}	*B*	–62.2	(*d*)/(*dd*)	226	168	–	–	1.87
	C	–61.0	(*d*)/(*dd*)	226	167[g]	–	–	1.26
	D	–62.2[h)i]	(*d*)/(*d*)	226	–	–	–	0.41
(***Z***)-**I.01,**	*A*	–16.2	(*d*)/(*d*)	226	–	–	–	1.08
P=C	*B*	–15.4	(*d*)/(*d*)	226	–	–	–	0.99
	C	–14.2	(*d*)/(*d*)	227[f]	–	–	–	0.82
(***Z***)-**I.02,**	*A*	–50.2	(*d*)/(*dddd*)	216	170	28	6	0.95
CH_{alk}	*B*	–50.0	(*d*)/(*dddd*)	216.3	170.2	27.9	6.20	0.97
	C	–48.6	(*d*)/(*ddd*)	217.0	171.1	27.9[g]	–	0.65
(***Z***)-**I.02,**	*A*	8.9	(*d*)/(*d*)	216.5	–	–	–	0.48
P=C	*B*	9.5	(*d*)/(*d*)	216.7	–	–	–	0.51
	C	10.9	(*d*)/(*d*)	216.7	–	–	–	0.47
(***Z***)-**I.1**[j]	*D*	42.1	(*s*)/(*d*)	–	150.2	–	–	5.19

– Table continued on the next page –

(***E***)-**I.1**[j)]	*D*	65.2	(*s*)/(*dd*)	–	154.2	–	19.20	1.06
(***Z***)-I.**2**[j)]	*D*	44.2[k)]	(*s*)/(*s*)	–	–	–	–	17.52
(***E***)-**I.2**[j)]	*D*	84.2	(*s*)/(*d*)	–	–	–	21.40	1.50

[a)] singlet (*s*), doublet (*d*), triplet (*t*), quartet (*q*), multiplet (*m*); [b)] half-width of each resonance 7 Hz; [c)] formation of small amounts of phosphine (–243.9, *q*, 186 Hz; intensity ratio 0.07). [d)] In the ^{1}H-coupled spectrum are both resonances of the doublet very broad (half-width 40 Hz) and *presumably* split further to narrow doublets. [e)] Line-width: {^{1}H} 2.5, ^{1}H-coupled 7 Hz; [f)] half-width of each resonance 35 Hz; [g)] half-width of each resonance 12 Hz; [h)] weak doublet; [i)] further signals of **I.01**, **I.02** etc. undetectable; [j)] (***Z***)-/(***E***)-**I.1** and (***Z***)-/(***E***)-**I.2** in an intensity ratio of 6.25: 19.02 (0.33 : 1.0); [k)] $^{1}J_{P,Si}$ = 81 Hz.

By applying 2D NMR techniques it proved possible to assign all signals of the isomer (***Z***)-**I.0**, but only a few one of the (***E***)-**I.0** because of its low concentration. In the ^{1}H,^{31}P HMQC experiment, three cross peaks between the ^{31}P NMR signal of the (*Z*)-isomer at −13.9 ppm and three different ^{1}H signals at 3.76, 6.78 and 7.71 ppm were detected (**Table 2.11**). The first signal at 3.76 ppm stems from the H–P group ($^{1}J_{P,H}$ = 142 Hz), the second, relatively broad one at 6.78 ppm has to be attributed to the NH_2 group. This assignment is supported by additional ^{1}H,^{15}N HSQC and ^{1}H,^{15}N HMBC experiments which both unveil a strong correlation with an ^{15}N NMR signal at −278.1 ppm, respectively. The third signal, a multiplet at 7.71 ppm, comes from the *ortho*-hydrogen atoms of the phenyl substituent at the P=C group. On the basis of this ^{31}P, C–H$_{ortho}$ correlation, an assignment of the corresponding C–H$_{para}$ and C–H$_{meta}$ multiplets as well as of all ^{13}C NMR signals were possible by making use of ^{1}H-COSY and HSQC or/and HMBC experiments, respectively (**Table 2.11**).

With the exception of the $^{13}C_{meta}$ singlet at 127.9 ppm all other ^{13}C NMR signals are split into doublets by coupling with the ^{31}P nucleus. Their $^{n}J_{P,C}$ values decrease continuously with an increasing number of bonds (*n*). Accordingly, the doublets of the C(P), C_{ipso}, C_{ortho}, and C_{para} atoms have coupling constants of 59.6 (*n*= 1), 25.1 (*n*= 2), 15.9 (*n*= 3), and 3 Hz (*n*= 5). Whereas the δ^{13}C values of the phenyl carbon atoms are found in the specific region between 125 and 145 ppm, the doublet of the P=C carbon atom was undoubtly located at very low field (200.1 ppm). Such a strong downfield shift is characteristic for the P=C carbon atoms of the $1\lambda^3\sigma^2$-phosphaalkenes [39, 78-80]. Usually, the ^{31}P NMR resonances of this group of compounds also shows an analogously strong downfield shift. In 2-amino-$1\lambda^3\sigma^2$-phosphaalkenes, however, the phosphorus atom is embedded in a three-centre-four-electron-π system and experiences an additional negative partial charge. This alteration in electron distribution causes a pronounced highfield shift of the ^{31}P signals [33] and is expected to provoke a hindered rotation of the amino group which will be discussed later.

Table 2.11 Assignment of ^{1}H, ^{13}C, and ^{15}N NMR signals of (***Z***)-/(***E***)-isomeric 2-amino-2-phenyl-1$\lambda^3\sigma^2$-phosphaalkene H~P=C(C_6H_5)–NH_2 (**I.0**) based on ^{1}H-COSY, HSQC, HMQC, and HMBC correlations of the phosphanylidene, amino and phenyl hydrogen atoms

Unless otherwise stated the measurements were performed at −20 ºC. In contrast to (***Z***)-**I.0**, the low concentration of the (***E***)-isomer prevented a complete NMR characterization.

^{1}H atom (isomer)	δ (ppm), multiplicity[a)]	^{1}H-COSY[b)]	HMQC(^{15}N)/(^{31}P)[c)], HSQC(^{13}C)/(^{15}N)[c)]	HMBC[c)]
a) *P–H group*				
P–H (*Z*)	3.76 (*d*)[d)e)]		^{31}P (–13.9) s ^{15}N (−278.1) s[g)]	^{13}P=C (200.1) m[f)] $^{13}C_{ipso}$ (140.5) m[h)] $^{13}C_{ortho}$ (125.2) w[i)]
P–H (*E*)	3.28 (*d*)[e)j)]		^{31}P (+17.2) s	
b) *NH_2 group*				
N–H (*Z*)	6.78 (*s, br*)[b)k)]		^{15}N (−278.1) s[l)] ^{31}P (–13.9) vw	
N–H (*E*)	7.04 (*s, br*)[k)]		^{31}P (+17.2) vw	
c) *phenyl substituents at carbon (P=C)*				
C–H$_{ortho}$ (*Z*)	7.71 (*m*)	C–H$_{meta}$ (7.33)	$^{13}C_{ortho}$ (125.0) s ^{31}P (–13.9) m	$^{13}C_{ortho}$ (125.0) s $^{13}C_{para}$ (129.5) m[m)] ^{13}P=C (199.9) m[f)]
C–H$_{meta}$ (*Z*)	7.33 (*m*)	C–H$_{ortho}$ (7.71) C–H$_{para}$ (7.61)	$^{13}C_{meta}$ (127.9) s ^{31}P (–13.9) m	$^{13}C_{ipso}$ (140.5) m[h)]
C–H$_{para}$ (*Z*)	7.61 (*m*)	C–H$_{meta}$ (7.33)	$^{13}C_{para}$ (126.0) m[n)]	

[a)] singlet (*s*), doublet (*d*), triplet (*t*), multiplet (*m*), broad (*br*); [b)] NMR measurements at +28 ºC; [c)] HMQC, HSQC and HMBC correlations: strong (s), medium (m), weak (w), very weak (vw); [d)] two signals at 3.58 and 3.94 ppm, $^{1}J_{H,P}$ = 142 Hz; [e)] intensity ratio of the P–H signals of the (***Z***)- and (***E***)-isomers at −20 ºC (1: 0.15); [f)] $^{1}J_{P,C}$ = 60 Hz; [g)] HMQC correlation, NMR measurement at +28 ºC; [h)] $^{2}J_{P,C}$ = 25 Hz; [i)] $^{3}J_{P,C}$ = 16 Hz; [j)] two signals at 3.08 and 3.48 ppm (covered completely by the dme signal, $^{1}J_{H,P}$ = 162 Hz). [k)] The ^{1}H NMR spectrum of a freshly prepared sample shows a third broad N–H resonance of unknown origin at 6.91 ppm. When this sample has been stored at −25 ºC for one week, all resonances are found to be merged at +28 ºC. Since the ^{1}H NMR signal of the (***E***)-isomer is now superimposed by other resonances, the restricted rotation of its amino group can be detected only in the low temperature ^{31}P NMR spectrum, for further details see **Figure 2.9**). [l)] HSQC correlation, measurement at +28 ºC; [m)] doubtful result; [n)] $^{5}J_{P,C}$ = 3 Hz.

The isomer (***E***)-**I.0** shows only two ^{1}H, ^{31}P HMQC correlations. One was detected between the ^{31}P NMR signal at +17.2 and the ^{1}H doublet of the P–H unit centred at 3.3 ppm; the second one comes from the broad singlet of the NH_2 group at 7.0 ppm (**Table 2.11**). Further NMR experiments did not give any reliable results.

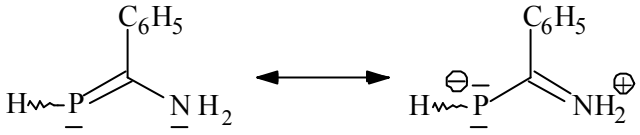

(***Z***)-/(***E***)-**I.0**

Even if not all signals of **(*E*)-I.0** were detected, the available data of this specie were found to be most suitable to provide proof of the hindered rotation of the amino group in an temperature dependant ^{31}P NMR experiment and to ensure additionally its structure with the amino group in β-position to phosphorus. At 293K, the ^{1}H coupled ^{31}P NMR spectrum of *Sample A'* exhibits a doublet of triplets with a chemical shift of 20.6 ppm (**Figure 2.9**). Whereas the $^{1}J_{P,H}$ coupling constant of 161 Hz is as to be expected, the $^{3}J_{P,H(N)}$ value of 10 Hz turns out to be unusually small, as had already been mentioned above. The triplett fine structure observed at room temperature, however, indicates that the two hydrogen atoms at nitrogen are chemically equivalent owing to free rotation of the amino group within the NMR time scale. On cooling *Sample A'* the fine structure of the triplett converts at 213K to a doublet of doublets. The interpretation of this phenomenon is really straightforward. As the temperature decreases, the rotation of the amino group becomes restricted and the two hydrogen atoms are no longer chemically equivalent: H_a is in a synperiplanar, H_b in an antiperiplanar position with respect to the C–N bond. The coupling of atom H_a with phosphorus ($^{3}J_{P,Ha(N)}$= 21 Hz), large compared to H_b, leads in the low temperature limit to a doublet of doublets. As expected, in the doublet of triplets at 293K the $^{3}J_{P,H(N)}$-coupling constant (10 Hz) is approximately half of that in the doublet of doublets. In the ^{1}H NMR spectrum an analogous temperature dependence of the amino signal cannot be ascertained because of a superposition with the very broad singlet of the (*Z*)-isomer. Since in the (*Z*)-isomer the $^{3}J_{P,H(N)}$ coupling is too small to be detected, the ^{31}P NMR signal split only into a doublet ($^{1}J_{P,H}$= 142 Hz), does not show a temperature dependence.

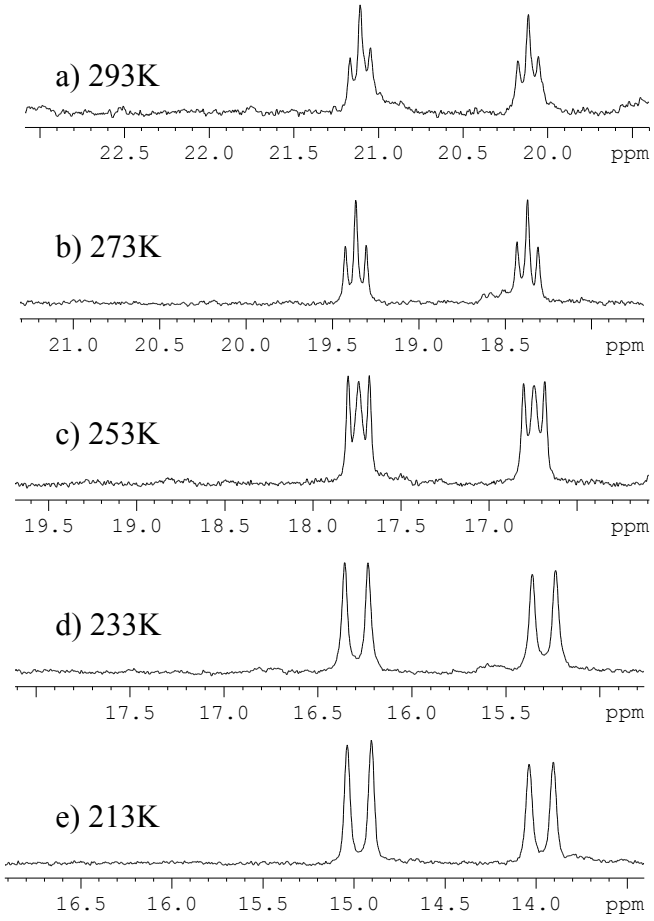

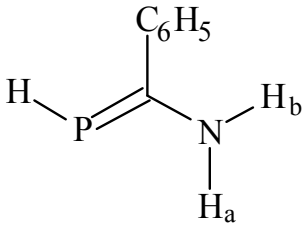

(***E***)-**I.0**

a) δ= 20.6; $^{1}J_{P,H}$= 161; $^{3}J_{P,H(N)}$= 10
b) δ= 18.9; $^{1}J_{P,H}$= 161; $^{3}J_{P,H(N)}$= 10
c) δ= 17.2; $^{1}J_{P,H}$= 161; $^{3}J_{P,H(N)}$= 10
d) δ= 15.8; $^{1}J_{P,H}$= 161; $^{3}J_{P,Ha(N)}$= 20
e) δ= 14.5; $^{1}J_{P,H}$= 162; $^{3}J_{P,Ha(N)}$= 21

Figure 2.9 Temperature dependent ^{31}P NMR spectrum of compound (***E***)-**I.0** in *Sample A'* The temperature dependent changes of the signal fine structure and the chemical shift values are a consequence of the hindered rotation of the amino group in β-position to the phosphorus (see text),

On the whole, the ^{31}P NMR chemical shift values of $1\lambda^3\sigma^2$-phosphaalkenes vary over a wide range from e.g. −99.9 ppm for (*Z*)-H–P=C(F)–NMe_3 [81] and +740.5 ppm for the nickel complex (η^5-C_5Me_5)(Et_3P)Ni–P=C($SiMe_3$)$_2$ [82]. In spite of that, some trends can be realized for $1\lambda^3\sigma^2$-phosphaalkenes and particularly for their 2-amino derivatives that exhibit an inverse π–electron density. Not only the substituents at phosphorus influence the chemical shift value but also the electronic properties of the substituents at the P=C carbon atom and those in *β*–position. Whereas for example compound Cl–P=C(Ph)$SiMe_3$ has a δ^{31}P value of +273 ppm, the chemical shift value changes considerably to +342 ppm [33] when the phenyl substituent is replaced by a second trimethylsilyl group. Moreover, a difference of 81 ppm in the δ^{31}P values of the (*Z*)- and (*E*)-isomeric compounds Ph–P=C(Ph)–NPh($SiMe_3$) was observed.

A plausible explanation of such a large difference might be that for steric reasons only the (*E*)-isomer can achieve a planar molecular structure which is required for the effectiveness of the three-centre four-electron π–system in an inverse polarized phosphaalkene [33]. With all of this in mind, a comparison of chemical shift values and coupling constants for the (*Z*)-/(*E*)-isomeric molecule H~P=C(C_6H_5)–NH_2 (**I.0**) as well as the fragments H~P=C(C_6H_5)–NH and P=C(C_6H_5)–NH of the (*Z*)-/(*E*)-isomeric compounds 2-(*tert*-butyldiphenylsilyl)amino-2-phenyl-1$\lambda^3\sigma^2$-phospha- alkene (**I.1**) and *N*,*P*-bis(*tert*-butyldiphenylsilyl)-2-amino-2-phenyl-1$\lambda^3\sigma^2$-phosphaalkene (**I.2**) is given in **Table 2.12**.

An inspection of this table discloses several characteristic features:

1. All δ^{31}P values fall into a narrow range between −20 and +100 ppm which is typical for inverse 1$\lambda^3\sigma^2$-phosphaalkenes. At −13.9 ppm isomer **(*Z*)-I.0** exhibits the strongest high-field shift, whereas the *tert*-butyldiphenylsilyl substituent at nitrogen causes a down-field shift in both the (*Z*)- and (*E*)-isomers of **I.1** and **I.2**. Remarkably, in all these 1$\lambda^3\sigma^2$-phosphaalkenes the (*E*)-isomer shows the more positive chemical shift.
2. The (*E*)-isomers of all three compounds are characterized by relatively large $^3J_{P,H(N)}$ coupling constants. They differ only slightly between 22 Hz for **(*E*)-I.2** and 19 Hz for **(*E*)-I.1**; such a coupling, however, cannot be detected in the accompanying (*Z*)-isomers. One should also note that for compound **(*E*)-I.0** only the value of 21 Hz obtained from an NMR measurement at 213K, should be taken into account – for details on the restricted rotation of the amino group see **Figure 2.9**. In our opinion, the observation of three relatively large and very similar $^3J_{P,H(N)}$ values is best explained as the consequence of a through-space coupling between the hydrogen atom at nitrogen and the free electron pair at phosphorus. Furthermore, values of 19 Hz and 22 Hz strongly indicate that in the isomers **(*E*)-I.1** and **(*E*)-I.2** even at ambient temperature the restricted rotation of the *tert*-butyldiphenylsilylamino group still exists with respect to the NMR time scale.

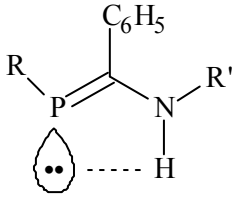

R, R' = H	**(*E*)-(I.0)**
R = H, R' = ^{t}BuPh$_2$Si	**(*E*)-(I.1)**
R, R' = ^{t}BuPh$_2$Si	**(*E*)-(I.2)**

Table 2.12 Comparison of chemical shift values δ (ppm) and coupling constants *J* (Hz) for the (*Z*)-/(*E*)-isomeric molecule H~P=C(C_6H_5)–NH_2 (**I.0**), 2-(*tert*-butyldiphenylsilyl)amino-2-phenyl-1$\lambda^3\sigma^2$-phosphaalkene (**I.1**), and [*N*,*P*-bis(*tert*-butyldiphenylsilyl)-2-amino-2-phenyl-1$\lambda^3\sigma^2$-phosphaalkene] **(I.2)**.

atom	NMR parameter	(*Z*)-**I.0** (253K)[a]	(*E*)-**I.0** (253K)[a]	(*Z*)-**I.1** (298K)[a]	(*E*)-**I.1** (298K)[a]	(*Z*)-**I.2** (298K)[a]	(*E*)-**I.2** (298K)[a]
^{31}P	δ	−13.9(*d*)[b]	213K: 14.5(*dd*)[c]	43.8(*d*)	66.8(*dd*)	45.7(*s*)	85.5(*d*)
	$^1J_{P,H}$	142	162	150	154	–	–
	$^3J_{P,H(N)}$		21		19		22
			293K: 20.6(*dt*)[c]				
			161				
			10				
^{15}N	δ	−278.1[d]	[e]	[e]	[e]	−240.1[f]	[e]
^{1}H(P)	δ	3.76(*d*)	3.28(*d*)	3.63(*dd*)	3.61(*dd*)	–	–
	$^1J_{P,H}$	142	162	150	154	–	–
	$^4J_{H,H(N)}$			1	3	–	–
^{1}H(N)	δ	6.9(*s*,*br*)	[g]	5.76(*s*)	5.72(*dd*,*br*)	6.13(*s*,*br*)	6.07(*d*)
	$^3J_{P,H(N)}$		(21)[h]		20		22
	$^4J_{H,H(P)}$				3		
Phenylmethylidene substituent at phosphorus (H_5C_6–P=C)							
$^1H_{ortho}$	δ	7.7(*m*)	[e]	7.6(*m*)	[e]	6.7(*m*)	6.6(*m*)
$^1H_{meta}$	δ	7.3(*m*)	[e]	7.2(*m*)	[e]	6.4(*m*)	6.3(*m*)
$^1H_{para}$	δ	7.6(*m*)	[e]	7.7(*m*)	[e]	6.6(*m*)	6.6(*m*)
^{13}P=C	δ	200.5(*d*)	[e]	200.1(*d*)	[e]	208.9(*d*)	209.4(*d*)
	$^1J_{P,C}$	60		54		78	76
$^{13}C_{ipso}$	δ	141.1(*d*)	[e]	145.0(*d*)	[e]	144.2(*d*)	149.0(*d*)
	$^2J_{P,C}$	25		27		28	27
$^{13}C_{ortho}$	δ	125.5(*d*)	[e]	125.7(*d*)	[e]	128.6(*d*)	127.7(*d*)
	$^3J_{P,C}$	16		15		11	2
$^{13}C_{meta}$	δ	128.3(*s*)	[e]	128.6(*s*)	[e]	126.7(*s*)	127.3(*s*)
$^{13}C_{para}$	δ	126.5(*d*)	[e]	136.4(*d*)	[e]	127.7(*s*)	126.7(*s*)
	$^5J_{P,C}$	3		2			

[a] temperature of measurement unless otherwise stated; [b] multiplicity: singlet (*s*), doublet (*d*), triplet (*t*), multiplet (*m*), broad (*br*); [c] for details see **Figure 2.9**; [d] HSQC-correlation at 298K; [e] undetectable; [f] HMQC-correlation; [g] amino signal of the (*E*)-isomer covered by the very broad singlet of the (*Z*)-isomer; [h] $^3J_{P,H(N)}$-coupling constant from the ^{31}P NMR spectrum at 213K (see above).

3. Similar to a large number of $1\lambda^3\sigma^2$-phosphaalkenes [80] the ^{13}C NMR signals of the P=C unit are shifted downfield into a narrow range between 200 and 210 ppm. Differences, however, are observed for the $^1J_{P,C}$ coupling constants. At 60 Hz and 54 Hz, respectively, they are smaller in the isomers **(*Z*)-I.0** and **(*Z*)-I.1** which have a hydrogen atom at phosphorus, than for compound **(*Z*)-I.2** where a *tert*-butyldiphenylsilyl substituent is bound each to phosphorus and nitrogen. Due to low concentrations, the ^{13}C values of the (*E*)-isomers could not be determined.

2.6 *NMR Spectroscopic Analysis of the Diphosphanes (Z)-I.01 and (Z)-I.02 Originating from a Dimerisation of the Phosphaalkenes (Z)-/(E)-I.0*

In **Section 2.5** it has already been pointed out that the generation of the unsubstituted (*Z*)-/(*E*)-isomeric 2-amino-2-phenyl-1$\lambda^3\sigma^2$-phosphaalkene (**I.0**) is accompanied by the formation of two additional products **I.01** and **I.02**. In the $^{31}P\{^1H\}$ NMR spectra of the *Samples A, B,* and *C* (**Figure 2.7**), each compound is characterized by a pair of doublets, marked with the small letters *a* (δ ^{31}P −61.6) and *b* (δ ^{31}P −18.3 ppm) for **I.01** or *c* (−49.2) and *d* (+7.2 ppm) for **I.02**. From $^1J_{P,P}$ coupling constants of 229 Hz and 218 Hz the presence of two different diphosphanes can be inferred. In the ^1H-coupled ^{31}P NMR spectrum, however, a further large splitting of the doublets *a* (−61.6) and *c* (−49.2) is observed. At 168 Hz and 170 Hz, the two coupling constants indicate the presence of a P–H group in each diphosphanes; their magnitude implies that one phosphorus atom of each P–P unit is most probably three coordinate. The remaining signals at −18.3 (*b*) and +7.2 ppm (*d*) might very well be attributed to the phosphorus atoms of 2-amino-1$\lambda^3\sigma^2$-phosphaalkene units. For comparison, compound (***Z***)-**I.0** shows a very similar value of −13.9 ppm.

A careful literature search reveals a similar P–P bond formation with a 2-amino-1$\lambda^3\sigma^2$-phosphaalkene as one of the two starting compounds. In 1997 *Regitz* et al. reported the generation of two diastereomeric diphosphanes (**2.13**) *via* a so-called *ene* reaction using the 2-dimethylamino-2-methyl-1$\lambda^3\sigma^2$-phosphaalkene as *ene* component and a 1-bis(trimethylsilyl)amino-1$\lambda^3\sigma^2$-phosphaalkene as enophile [83]. Very surprisingly, the reaction proceeds even at room temperature within a few days. The two diasteromers are formed in a ratio of 60 : 40. The $^{31}P\{^1H\}$ NMR spectrum of the major diastereomer exhibits two doublets at +65.0 {P–$NSiMe_3$} and −21.8 ppm (P–C_6H_5) with a $^1J_{P,P}$-coupling constant of 221 Hz. NMR data of the minor diastereomer are 57.8 and −14.0 ppm together with a $^1J_{P,P}$ coupling constant of 203 Hz.

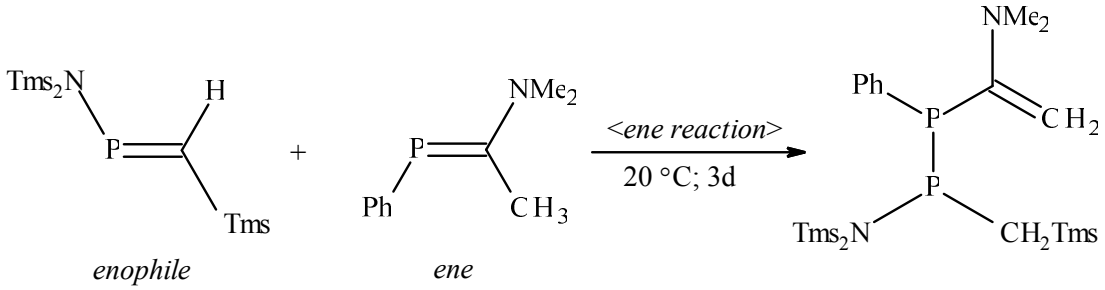

enophile *ene*

2.13 (two diastereoisomers)

Tms = $SiMe_3$

The presence of compounds **I.01** and **I.02** already in the 1,2-dimethoxyethane solution of the freshly generated 2-amino-2-phenyl-1$\lambda^3\sigma^2$-phosphaalkene (**I.0**) indicates an acid-catalyzed P–P bond formation. With this observation in mind the following reaction mechanism might be suggested which deviates from the *ene* mechanism published by *Regitz* et al. [83] in that here a dimerization of two identical 2-amino-2-phenyl-1$\lambda^3\sigma^2$-phosphaalkene molecules has to be considered.

As already pointed out, in the 2-amino-2-phenyl-1$\lambda^3\sigma^2$-phosphaalkene the a priori nonbonding electron pair at nitrogen and the π–system of the P=C group interact in such a way that slight excess and depletion of π-electron density at the phosphorus and nitrogen atoms, respectively; therefore, compounds of this type are called ″inverse 1$\lambda^3\sigma^2$-phosphaalkenes″ (**Scheme 2.2, a**). With respect to standard bond lengths, the C–N distance is shorter, and the P=C bond elongated. A protonation of the amino group results in a strong perturbation of the mesomeric 4-electron-3-centre π-system so that the phosphorus atom looses its excess negative charge (**b**). It can now be attacked by the nucleophilic phosphorus atom of an unprotonated 2-amino-2-phenyl-1$\lambda^3\sigma^2$-phosphaalkene molecule. After P–P bond formation and the transiently generated carbanion receives a proton from the neighbouring NH_3^+-substituent (**c**), the whole system is stabilized with release of a proton and restoring the P=C double bond; it is (*Z*)-configurated. The reaction leads to a (*Z*)-[(*C*-amino-*C*-phenyl)methylphosphanyl](2-amino-2-phenyl)-1$\lambda^3\sigma^2$-phosphaalkene. Since, however, two chiral centres at the P–H phosphorus and the methyl carbon atom are created, the symbols (***R***) or (***S***) have to be introduced in order to classify the diastereomers **(*Z*)-I.01** and **(*Z*)-I.02** further (**see Scheme 2.2**).

Initially the concentration of the two diasteromers **I.01** and **I.02** is relatively low with respect to that of (*Z*)-/(*E*)-isomeric 2-amino-2-phenyl-1$\lambda^3\sigma^2$-phosphaalkene **I.0** but it increases considerably when e.g. *Sample A* (lithium derivative **1** and neat trifluoromethanesulfonic acid; **Table 2.10**) is stored for one week even at −30 °C. The ratio of the two diasteromers remains almost constant (1.0 : 0.6). Since these compounds could not be isolated, their structures were ascertained as far as possible in solution by 2D NMR spectroscopic techniques.

For the sake of simplicity, the results of the NMR spectroscopic studies (**Table 2.13**) are discussed first for diastereomer **I.01**. The analysis starts with the ^{31}P NMR signal at −61.6 ppm. It is converted into a doublet of doublets when ^{1}H coupling is allowed.

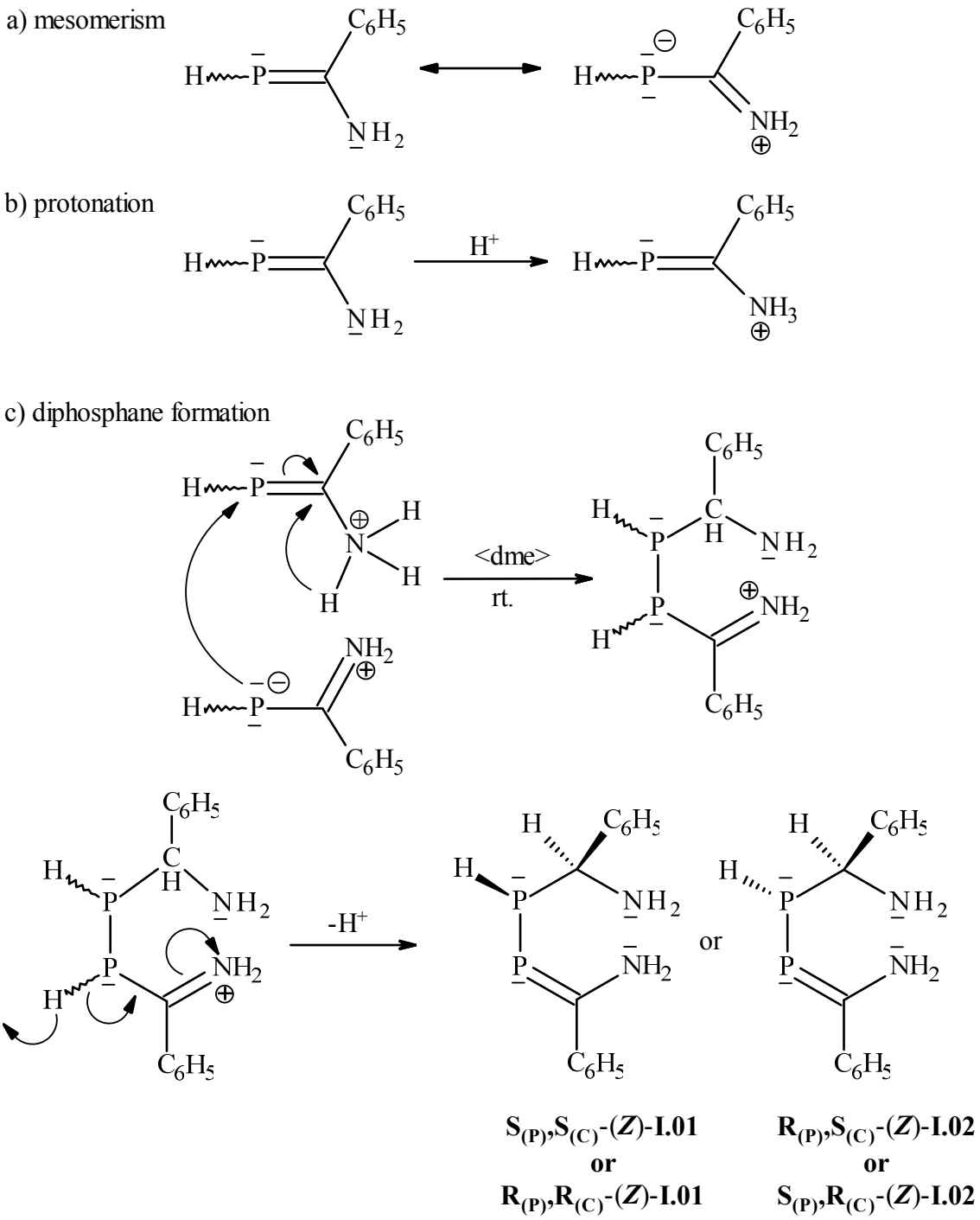

Scheme 2.2 Plausible reaction mechanism explaining the P–P bond formation of the two diastereomers (*Z*)-**I.01** and (*Z*)-**I.02**

As already mentioned, the coupling constants $^{1}J_{P,P}$ and $^{1}J_{P,H}$ are 229 and 168 Hz. The $^{1}H,^{31}P$ HMQC experiment reveals a strong correlation with the ^{1}H signal at 4.48 ppm; it is split into a doublet of doublets of doublets with $^{1}J_{P,H}$, $^{3}J_{H(P),H(C)}$, and $^{2}J_{H(P),P}$ coupling constants of 167.5, 9 and 4 Hz, respectively (see below). Furthermore, two additional correlations with ^{1}H signals at 5.86 and 8.76 ppm were detected. The first signal is a doublet of triplets and correlates in

Table 2.13 Selected ^{1}H NMR data of the diastereomers (***Z***)-**I.01** and **(*Z*)-I.02**. Signal assignments were obtained from ^{1}H-COSY-, HMQC-, HSQC- and HMBC-correlations
The positions of the two phenyl substituents either at the methyl (C–H$_{alk}$) or the 1λ^{3}σ^{2}-phosphaalkene carbon atom are designated as (C–H$_{alk}$) and (P=C), respectively. All NMR spectroscopic measurements were performed at –20 ºC.

a) Diastereomer I.01

^{1}H atom	δ (ppm), multiplicity[b)]	^{1}H-COSY	HMQC(^{15}N)/(^{31}P), HSQC(^{13}C)/(^{15}N)	HMBC
a) *E–H groups (E= P, C$_{alk}$, N)*				
P–H	4.48 (*ddd*)[c)]	C–H$_{alk}$ (5.86) s	^{31}P (–61.6)[d)] s	^{13}P=C (202.0) w
			^{31}P (–18.3)[e)] m	^{13}C$_{ipso(CH)}$ (141.8) m
C–H$_{alk}$	5.86 (*dt*)[f)]	P–H (4.48) s	^{31}P (–61.6) m	^{13}C$_{ortho(CH)}$ (125.1) s
		N–H (8.76) m	^{13}C–H$_{alk}$ (+63.1) s	^{13}C$_{ipso(CH)}$ (141.9) m
		C–H$_{ortho(CH)}$ (7.31) w		^{13}P=C (201.7) s
N–H[g)]	8.76 (*s,br*)	C–H$_{alk}$ (5.86) m	^{31}P (–61.6) s	
			^{31}P (–18.3) m	
			^{15}N (–246.1)[h)] s	
b) *phenyl substituents at the C–H$_{alk}$ and P=C group, respectively*				
C–H$_{ortho(CH)}$	7.31 (*m*)	C–H$_{meta(CH)}$ (7.39) w	^{13}C$_{ortho(CH)}$ (125.1) s	^{13}C$_{ortho(CH)}$ (125.1) s
		C–H$_{para(CH)}$ (7.22) m	^{31}P (–61.6) s	^{13}C$_{para(CH)}$ (126.7) s
				^{13}C$_{ipso(CH)}$ (141.9) s
				^{13}C–H$_{alk}$ (62.6) w
C–H$_{meta(CH)}$	7.39 (*m*)	C–H$_{ortho(CH)}$ (7.31) w	^{13}C$_{meta(CH)}$ (128.2) s	^{13}C$_{meta(CH)}$ (128.2) s
				^{13}C$_{ipso(CH)}$ (141.8) s
C–H$_{para(CH)}$	7.22 (*m*)	C–H$_{ortho(CH)}$ (7.31) m	^{13}C$_{para(CH)}$ (126.8) s	^{13}C$_{ortho(CH)}$ (125.1) s
			^{31}P (–61.6) m	
C–H$_{ortho(P=C)}$	7.87 (*m*)	C–H$_{meta(P=C)}$ (7.45) s	^{13}C$_{ortho(P=C)}$ (126.2) s	^{13}C$_{ortho(P=C)}$ (126.3) s
			^{31}P (–18.3) s	^{13}C$_{meta(P=C)}$ (128.2) m
				^{13}C$_{para(P=C)}$ (130.1) s
				^{13}P=C (202.0) w
C–H$_{meta(P=C)}$	7.45 (*m*)	C–H$_{ortho(P=C)}$ (7.87) s	^{13}C$_{meta(P=C)}$ (128.2) s	^{13}C$_{ortho(P=C)}$ (126.3) w
			^{31}P (–18.3) w	^{13}C$_{meta(P=C)}$ (128.1) s
				^{13}C$_{ipso(P=C)}$ (135.7) s
C–H$_{para(P=C)}$	7.48 (*m*)	C–H$_{ortho(P=C)}$ (7.87) m	^{13}C$_{para(P=C)}$ (130.1) s	^{13}C$_{ortho(P=C)}$ (126.0) m
			^{31}P (–18.3) w	^{13}C$_{meta(P=C)}$ (128.1) s
				^{13}C$_{ipso(P=C)}$ (135.8) m

[a)] ^{1}H-COSY-, HMQC-, HSQC- and HMBC-correlations: strong (s), medium (m), weak (w); [b)] singlet (*s*), doublet (*d*), triplet (*t*), multiplet (*m*), broad (*br*); [c)] $^{1}J_{P,H}$ = 168 Hz, $^{3}J_{H(P),H(C)}$ = 9 Hz; $^{2}J_{H(P),P}$ = 4 Hz; [d)] $^{1}J_{P,P}$ = 229 Hz, $^{1}J_{P,H}$ = 168 Hz; [e)] $^{1}J_{P,P}$ = 228 Hz broad resonance with a line width of about 11 Hz; [f)] doublet ($^{3}J_{H(P),H(C)}$ = 9 Hz) of triplets ($^{4}J_{H(C),H(C)}$ = 2 Hz) arising most probably from coupling with two hydrogen atoms C–H$_{ortho}$ of the phenyl substituent. [g)] Only the signal of one hydrogen atom in the NH_2 groups could be assigned. [h)] By HMQC-correlation only one ^{15}N-signal could be detected for the mixture of the two diasteromers **I.01** and **I.02**.

—**Table 2.13 b) Diastereomer I.02** on the next page —

the HSQC experiment with a ^{13}C NMR doublet at +63.1 ppm ($^{2}J_{P,C}$ = 25 Hz). A ^{13}C NMR signal in a region near +60 ppm can be attributed to a carbon atom of a methyl group at a $\lambda^3\sigma^3$-phosphorus atom.

Another indication for a correct assignment comes from the ^{1}H-COSY experiment where a strong correlation between the two hydrogen atoms at the $\lambda^3\sigma^3$-phosphorus (4.48 ppm) and the methyl carbon atom (5.86 ppm) is found. Additionally, the signals of both these hydrogen atoms give HMBC-correlations with the ^{13}C doublet of the P=C group (202.5 ppm; $^{1}J_{P,C}$ = 77 Hz) and the ^{13}C doublet of doublets of the *ipso*-carbon atom (142.6 ppm; $^{2}J_{P,C}$ = 19 Hz; $^{3}J_{P,C}$ = 2 Hz) in the CH-part of the molecule; an analogous correlation with the *ortho*-carbon atoms (125.64 ppm; $^{3}J_{P,C}$ = 4 Hz) could be detected only for the hydrogen atom of the P–C<u>H</u> entity {**Tables 2.13 a)** and **2.14**}. The doublet of the <u>P</u>=C phosphorus atom at −18.3 ppm has a HMQC correlation with the signal of the P–H group at 4.48 ppm. Three cross peaks with the hydrogen atoms of the phenyl group in the P=C part of the molecule at 7.87, 7,45 and 7.48 ppm together with a cross peak to the N–H fragment at 8.76 ppm (see below) were also observed. Further details can be taken from **Table 2.13 a)**.

The NMR spectroscopic analysis of the NH_2 signals turned out to be very difficult and could not yet be completed in a satisfactory way. Despite the assumption that two amino groups are present in diastereomer **I.01**– one in the (P)CH-part and the other in the P=C-part of the molecule – the ^{1}H,^{31}P HMQC experiment gives only correlations of strong to medium intensity between the two ^{31}P NMR signals at −61.6 and −18.3 ppm and a broad singlet at 8.76 ppm {**Table 2.13 a)**}. As already pointed out above, this signal correlates in the ^{1}H-COSY spectrum with the C<u>H</u>-hydrogen atom (5.86 ppm) of the substituted methyl group at phosphorus (δ^{31}P −61.6 ppm). Very surprisingly, integration of the signals at 4.48 (P–<u>H</u>), 5.86 (C–H_{alk}) and 8.76 ppm at temperatures of −40 °C and 0 °C results in an intensity ratio of 0.9 : 1.1 : 1.0 and 1.0 : 1.0 : 1.0, respectively.

b) Diastereomer I.02

^{1}H atom	δ (ppm), multiplicity[b)]	^{1}H-COSY	HMQC(^{15}N)/(^{31}P), HSQC(^{13}C)/(^{15}N)	HMBC
c) *E–H groups (E= P, C, N)*				
P–H	3.73 (*ddd*)[i)]	C–H$_{alk}$ (5.54) s	^{31}P (–49.2)[j)] s	^{13}P=C (201.4) w
			^{31}P (7.2)[k)] w	^{13}C$_{ipso(CH)}$ (141.7) m
C–H$_{alk}$	5.54 (*dd*)[l)]	P–H (3.73) s	^{31}P (–49.2) s	^{13}C$_{ortho(CH)}$ (126.2) m
		N–H (8.32) m	^{31}P (7.2) m	^{13}C$_{ipso(CH)}$ (141.8) m
			^{13}C–H$_{alk}$ (69.8) m	
N–H[m)]	8.32 (*s*)	C–H$_{alk}$ (5.54) m	^{31}P (–49.2) s	
			^{31}P (7.2) m	
			^{15}N (−244.7) s	
d) *phenyl substituents at the C–H$_{alk}$ and P=C group, respectively*				
C–H$_{ortho(CH)}$	7.64 (*m*)	C–H$_{meta(CH)}$ (7.36) s	^{13}C$_{ortho(CH)}$ (126.2) s	^{13}C–H$_{alk}$ (69.9) m
			^{31}P (–49.0) m	^{13}C$_{ortho(CH)}$ (126.6) s
				^{13}C$_{para(CH)}$ (129.7) w[n)]
C–H$_{meta(CH)}$	7.36 (*m*)	C–H$_{ortho(CH)}$ (7.64) s	^{13}C$_{meta(CH)}$ (128.0) s	^{13}C$_{meta(CH)}$ (128.2) s
		C–H$_{para(CH)}$ (7.28) w		^{13}C$_{ipso(CH)}$ (141.7) s
C–H$_{para(CH)}$	7.28 (*m*)	C–H$_{meta(CH)}$ (7.36) w	^{13}C$_{para(CH)}$ (129.8) w	^{13}C$_{ortho(CH)}$ (126.2) m
				^{13}C$_{ipso(P=C)}$ (141.8) m
C–H$_{ortho(P=C)}$	7.79 (*m*)	C–H$_{meta(P=C)}$ (7.41) s	^{13}C$_{ortho(P=C)}$ (126.0) s	^{13}C$_{ortho(P=C)}$ (126.0) m
			^{31}P (7.1) s	^{13}C$_{para(P=C)}$ (130.0) m
				^{13}P=C (201.8) m
C–H$_{meta(P=C)}$	7.41 (*m*)	C–H$_{ortho(CH)}$ (7.79) s	^{13}C$_{meta(P=C)}$ (128.2) s	^{13}C$_{meta(P=C)}$ (128.2) s
		C–H$_{para(P=C)}$ (7.48) w[n)]		^{13}C$_{ipso(P=C)}$ (136.1) s
C–H$_{para(P=C)}$	7.48 (*m*)	C–H$_{meta(P=C)}$ (7.41) s	^{13}C$_{para(P=C)}$ (130.2) s	^{13}C$_{ortho(P=C)}$ (126.1) m
				^{13}C$_{meta(P=C)}$ (128.2) s
				^{13}C$_{ipso(P=C)}$ (136.2) m

[i)] $^{1}J_{P,H}$ = 170, $^{3}J_{H(P),H(C)}$ = 19; $^{2}J_{H(P),P}$ = 3 Hz; [j)] $^{1}J_{P,P}$ = 218, $^{1}J_{P,H}$ = 170; $^{2}J_{P,H(C)}$ = 28; $^{3}J_{P,H(N)}$ = 6 Hz; [k)] $^{1}J_{P,P}$ = 218 Hz broad resonances with a line width of about 11 Hz; [l)] substituted methyl group at 1λ^{3}σ^{3}-phosphorus: $^{3}J_{H(P),H(C)}$ = 20; $^{2}J_{P,H(C)}$= 28 Hz. At 293 K, each line of the doublet of doublets is split into a triplet {$^{4}J_{H(C),H(C)}$ = 2 Hz} most probably due to coupling with two hydrogen atoms C–H$_{ortho}$ of the phenyl substituent. [m)] Only the signal of one hydrogen atom in the NH_2 group could be assigned. [n)] Assignment questionable

Since in the ^{15}N HMQC experiment a strong correlation with a ^{15}N signal at −244.7 ppm was detected, the broad singlet at 8.76 ppm undoubtly arises from an N–H group. Because of its downfield shift the hydrogen atom is supposed to be involved in a *possibly* unsymmetrical N–H···N bridge {see e.g. [84]}; unfortunatily we can not assure this assumption.

The second diastereomer **I.02** was NMR spectroscopically analysed in an analogous way {**Table 2.13 b)**}. Many results are similar and do not deserve special comments. Differences, however, were noticed with respect to the fine structure of the ^{1}H-coupled ^{31}P NMR signals, the $^{3}J_{H(P),H(C)}$ coupling between the two hydrogen atoms at the phosphorus and the adjacent methyl carbon atom and last but not least the lower concentration of diastereomer **I.02**. Whereas the slightly broadened ^{31}P NMR doublet of diastereomer **I.01** at −61.6 ppm (229 Hz) shows only one additional splitting in the ^{1}H-coupled spectrum ($^{1}J_{P,H}$ = 168 Hz), the analogous multiplet of diastereomer **I.02** at −49.2 ppm is found to be a doublet ($^{1}J_{P,P}$ = 218 Hz) of doublets ($^{1}J_{P,H}$ = 170 Hz) of doublets ($^{2}J_{P,H(C)}$ = 28 Hz) of doublets ($J_{P,H}$ = 6 Hz). To observe a fourth coupling of 6 Hz is very amazing, since such a small splitting cannot be detected in the relatively broad signal of the hydrogen atom in question. After a careful consideration of several possibilities the constant of 6 Hz was attributed to the $^{4}J_{P,H(N)}$ coupling with the hydrogen atom in the NH_2 group. Furthermore, in both diastereomers **I.01** and **I.02**, the ^{1}H-signal of the P–H group at 4.48 and 3.73 ppm, respectively, is split into a doublet ($^{1}J_{P,H}$) of doublets ($^{3}J_{H(P),H(C)}$) of doublets ($^{2}J_{H(P)-P}$). This assignment is based on the correlations between the ^{1}H-signals and the ^{31}P resonances in the ^{1}H,^{31}P HMQC experiment.
Surprisingly, the two diastereomers **(*Z*)-I.01** and **(*Z*)-I.02** differ considerably in their $^{3}J_{H(P),H(C)}$ coupling between the hydrogen atoms at phosphorus and the adjacent methine group. At 9 Hz and 20 Hz, the larger value is more than twice the smaller one. Studies on the interdependence of the $^{3}J_{H,H}$ coupling constant and the hydrogen positions at adjacent atoms are well known from the literature [85]. They come to the result that the coupling constant is larger in case the two hydrogen atoms are in an almost eclipsed (synperiplanar) and not in a

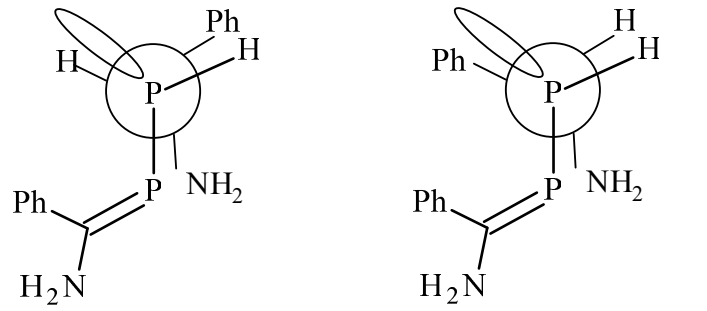

$R_{(P)}$,$S_{(C)}$-(*Z*)-/(*E*)-I.01
or
$S_{(P)}$,$R_{(C)}$-(*Z*)-/(*E*)-I.01

$S_{(P)}$,$S_{(C)}$-(*Z*)-/(*E*)-I.02
or
$R_{(P)}$,$R_{(C)}$-(*Z*)-/(*E*)-I.02

Figure 2.10 Newman projection of the two diastereomers of the diphosphanes **(*Z*)-I.01** and **(*Z*)-I.02**

synclinal position. Accordingly, the diastereomers **(*Z*)-I.01** ($^3J_{H(P),H(C)}$ = 9 Hz) and **(*Z*)-I.02** (20 Hz) are assigned as **$R_{(P)}$, $R_{(C)}$ / $S_{(P)}$, $S_{(C)}$** and **$R_{(P)}$, $S_{(C)}$/ $S_{(P)}$, $R_{(C)}$** isomers (see **Scheme 2.2**). The diastereomers **(*Z*)-I.01** and **(*Z*)-I.02** show also very different $^2J_{P,H(C)}$ coupling constants. Whereas such a coupling cannot be detected in compound (***Z***)-**I.01**, it exhibits a rather large value of 28 Hz in diphosphane (***Z***)-**I.02**. In case the constitution of diastereomer (***Z***)-**I.02** as just derived is correct, the two hydrogen atoms at phosphorus and the carbon atom of the substituted methyl group adopt a synperipalanr position (**Scheme 2.2**). With respect to the non-bonding electron pair (i.e. the fourth coordination site) at phosphorus it is the synclinal position. Unfortunately, the diagnostic value of a $^2J_{P,H(C)}$ coupling constant is unknown – at least for us. Therefore, no conclusions can be drawn from the different coupling constants.

As in diastereomer **I.01** the broad lowfield ^{1}H signal at 8.32 ppm is assigned to the hydrogen atom of the NH_2 group. In the ^{1}H,^{15}N-HSQC experiment the same correlation to the ^{15}N signal at −244.7 ppm could be detected as before. Again it turned out to be impossible to locate the ^{1}H NMR positions of the remaining hydrogen atoms at nitrogen.

In **Table 2.14** the NMR parameters of the (*Z*)-/(*E*)-isomeric 2-amino-1$\lambda^3\sigma^2$-phosphaalkene **I.0** and the diphosphanes **(*Z*)-I.01** and **(*Z*)-I.02** have been compiled in order to allow for comparison a better assignment of the analogous signals of monomer and dimer. At first one should be aware that the insertion of the P=C group of one molecule into the P–H bond of a second one is accompanied by the generation of a three-coordinate phosphorus atom. Only the NMR signal of this phosphorus atom is shifted highfield from −13.9 ppm in **(*Z*)-I.0** or +14.5 ppm in **(*E*)-I.0** to −61.6 ppm in **(*Z*)-I.01** or −49.2 ppm in **(*Z*)-I.02**, whereas the phosphorus atom of the P=C group in the two monomers and the two dimers are observed in an identical region near 0 ppm (−13.9 or +14.5 vs −18.3 or +7.2 ppm). Secondly, the conversion of the H~P=C entity into an H~P(P)–CH fragment entails the presence of an aliphatic carbon atom in an substituted methyl group. Therefore two new ^{13}C NMR signals at +62.7 ppm for **(*Z*)-I.01** and +70.2 ppm for **(*Z*).I.02** coupled to phosphorus by 25 Hz and 26 Hz emerge. The ^{13}C NMR signals of the P=C groups are all observed in the low-field region near 200 ppm; the $^1J_{P,C}$ value increases slightly from 60 Hz for the **(*Z*)-I.0** to 79 Hz for **I.01** and **I.02**. Finally, the very complicated NMR spectroscopic problems concerning the two amino groups and the presence of only one hydrogen atom H in each diastereomer has already been set out in detail. Last but not least it has to be pointed out that the diastereomers **(*Z*)-I.01** and **(*Z*)-I.02** are unstable in tetrahydrofuran solution when stored at room temperature for a couple of weeks.

Table 2.14 Comparison of ^{31}P and ^{31}C data of the amino-phosphaalkenes[a] (***Z***)/(***E***)-**I.0**, (***Z***)-**I.01** and (***Z***)-**I.02**

The data were obtained at 253K. The sample had been prepared from trifluoromethanesulfonic acid and the lithium derivative (***Z***)/(***E***)-**1** in 1,2-dimethoxyethane at –40 °C, the solvent had been subsequently replaced by [d_8]tetrahydrofuran.

	(***Z***)-**I.0**	(***E***)-**I.0**	(***Z***)-**I.01**		(***Z***)-**I.02**	
			CH-part[b]	P=C part[a]	CH-part[b]	P=C part[a]
^{31}P						
δ	–13.9 (*d*)	+14.5 (*dd*)[b]	–61.6 (*dd*)	–18.3(*d*)	–49.2 (*dddd*)	+7.2
$^{1}J_{P,P}$	–		229	228	218	218
$^{1}J_{P,H}$	142	162	168	–	170	–
$^{2}J_{P,H(C)}$		–	–	–	28	–
$^{3}J_{P,H(C)}$		21[c]	–	–	–	–
$^{3}J_{P,H(N)}$					6	
^{13}C						
δ P=C	200.55 (*d*)	–	–	202.54 (*d*)	–	202.21 (*d*)
$^{1}J_{P,C}$	60	–	–	77		79
δ C_{ipso}	141.1 (*d*)	–	142.6 (*dd*)	136.4 (*d*)	142.3 (*dd*)	136.9 (*d*)
$^{2}J_{P,C}$	25	–	19	19	4	19
$^{3}J_{P,C}$	–	–	2	–	1	–
δ C_{ortho}	125.48 (*d*)	–	125.64 (*d*)	126.6	126.45 (*d*)	126.32 (*d*)
$^{3}J_{P,C}$	16	–	4	14	3	14
δ C_{meta}	128.3 (*s*)	–	[d]	[d]	[d]	[d]
δ C_{para}	126.5 (*d*)	–	127.3 (*d*)	130.55 (*d*)	129.88 (*d*)	130.36 (*d*)
$^{5}J_{P,C}$	3	–	3	3	3	3
δ C–H_{alk}	–	–	63.72 (*d*)[e]	–	70.37 (*d*)[e]	–
$^{1}J_{P,C}$	–		25	–	26	–
^{1}H (P–H, C–H_{alk} and N–H groups)						
δ P–H	3.76 (*d*)	3.28 (*d*)	4.48 (*ddd*)	–	3.73 (*ddd*)	–
$^{1}J_{P,H}$	142	162	168	–	170	–
$^{3}J_{H(P),H(C)}$	–	–	9	–	19	–
$^{2}J_{H(P),P}$	–	–	4	–	3	–
δ C–H_{alk}	–	–	5.86 (*dt*)	–	5.54 (*dd*)	–
$^{3}J_{H(P),H(C)}$	–	–	9	–	20	–
$^{2}J_{P,H(C)}$	–	–	undetectable	–	28	–
$^{4}J_{H(C),H(C)}$	–	–	2[f]	–	2[f),g]	–
δ N–H	–	–	8.76 (*s*,*br*)	–	8.32 (*s*,*br*)	–
δ NH_2[h]	6.78 (*s*,*br*)	7.04 (*s*,*br*)				

[a] part of the molecule with the C–H_{alk} and the P=C entity, respectively; [b] values at 213K (restricted rotation of the amino group, see **Figure 2.8**); [c] $^{3}J_{P,Ha(N)}$; detectable coupling with only one hydrogen atom at nitrogen; [d] four singlets at 128.5, 128.60, 128.65 and 128.9; correct assignment not possible; [e] *amino*-substituted methyl group at phosphorus; [f] coupling with the *ortho*-hydrogen atoms of the phenyl substituent at the methyl carbon atom; [g] detectable at 293K, see footnote [l] of **Table 2.13 b)**; [h] see footnote [k] of **Table 2.11**.

3. Reaction of (*Z*)-/(*E*)-2-(Lithiumamido)-2-phenyl-1$\lambda^3\sigma^2$-phosphaalkene (1) with Bis(η^5-pentamethylcyclopentadienyl)zirconium dichloride

3.1 *Introduction*

After the successful preparation of (*Z*)-/(*E*)-[*N*,*P*-bis(*tert*-butyldiphenylsilyl)-2-amino-2-phenyl-1$\lambda^3\sigma^2$-phosphaalkene] (**I.2**) from (*Z*)-/(*E*) [H~P=C(C_6H_5)–N(H)Li(dme)]$_2$ (**1**) and the respective chlorosilane, it was intended next to check its reactivity against an appropriate transition metal chloride. For this, the well known and commercially available complex bis(η^5-pentamethylcyclopentadienyl)zirconium dichloride appeared to be an excellent choice. To come straight to the result, the reaction furnished the zirconium complex of the up to now unknown chelate ligand 1-amido-3-imido-1,3-diphenyl-2$\lambda^3\sigma^2$-phosphapropene.

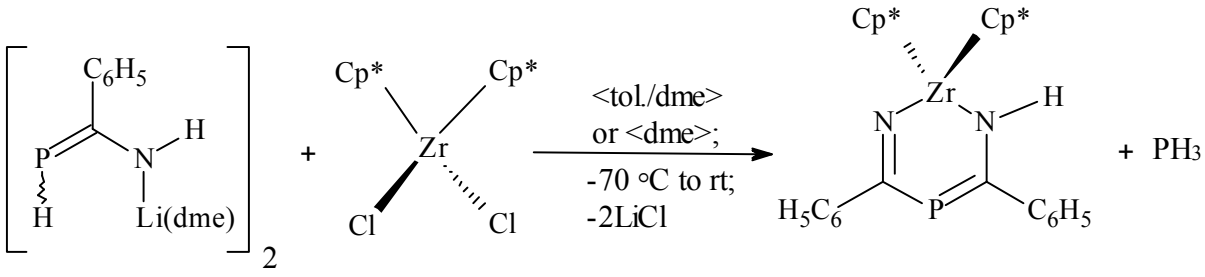

(*Z*)-/(*E*)-**1** **II**

To throw some light on the chemical background and to lay a firm foundation for the comparison of NMR parameters and structural data later on, the introduction of some similar compounds found in the literature is advantageous. In order to avoid going into too much detail, the early seminal work of *Issleib*, *Hey-Hawkins*, *Lappert* and others is not discussed. A short survey on these contributions is given in the review of *Stephan* [86].

In her thesis, *Seidl* [39] reacted bis(tetrahydrofuran)lithium-bis(trimethylsilyl)phosphanide between −60 °C and room temperature with two equivalents of benzonitrile in 1,2-dimethoxyethane as solvent and isolated (1,2-dimethoxyethane-*O,O'*)lithium-bis(*N*-trimethylsilyliminobenzoyl)phosphanide (**3.7**) in 69% yield. Since the solvent-coordinated lithium cation is bound almost symmetrically to the two nitrogen atoms of a trimethylsilylimino and a trimethysilylamido group, complex **3.7** has to be considered as *P*-analogous to the acetylacetonato (NacNac) ligand with delocalized π-system. With trifluoroacetic acid the lithium cation of the N—Li←N fragment has been exchanged for hydrogen. A characteristic structural feature of compound **3.8** obtained in 74% yield is the intramolecular N—H···N bridge which is present in solution and in the solid state.

Furthermore, the coordinate complex **3.9** was synthesised in two different ways, either by reacting zinc chloride or zinc bis[bis(trimethylsilyl)amide] with a stoichometric amount of bis(*N*-trimethylsilyliminobenzoyl)phosphane (**3.7)** in 1,2-dimethoxyethane.

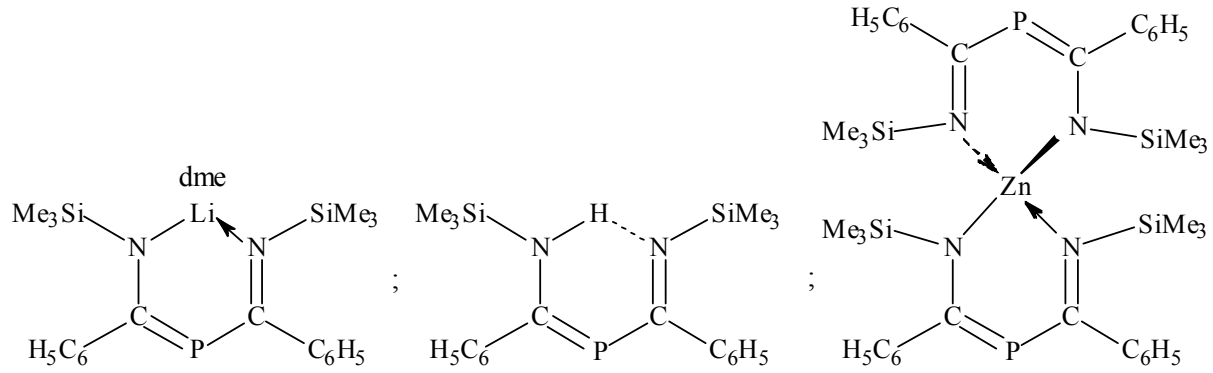

3.7 **3.8** **3.9**

In 1989, *Bergman* et al. started to report on efforts to gain access to the unsaturated, highly reactive compounds $Cp^*_2Zr{=}O$ and $Cp^*_2Zr{=}S$. Since an isolation of these complexes failed, they applied trapping reagents to demonstrate at least an intermediate formation. When, for example, a toluene or benzene solution of the starting material $Cp^*_2Zr(C_6H_5)(OH)$ was heated up to 160 ºC in the presence of three to four equivalents of benzonitrile, the elimination of benzene gives the zirconium-oxygen complex $Cp^*_2Zr{=}O$. Subsequent trapping is achieved with two equivalents of benzonitrile (complex **3.10**). The first step is a [2+2] cycloaddition of the C≡N triple bond to the Zr=O unit, the second one an insertion of a benzonitrile molecule into the Zr–N bond [87]. One year later, the sulphur congener (**3.11**) was prepared in a similar way [88].

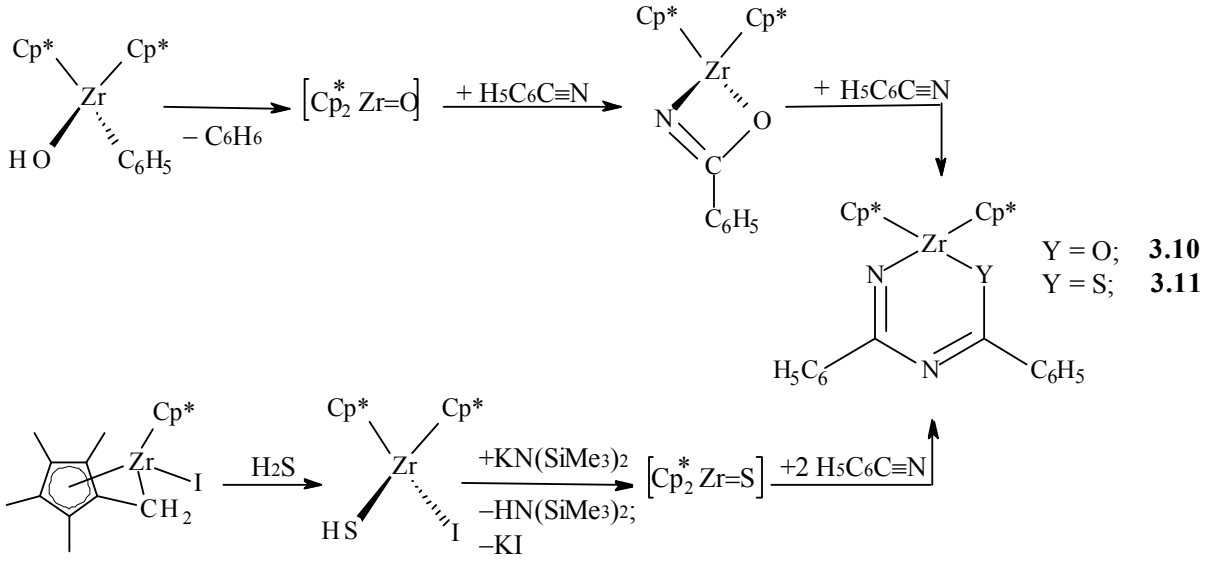

Keeping these results in mind, *Stephan* and co-workers tried to obtain the analogous complex $Cp^*_2Zr{=}PR$ in a similar way. They reacted compound $Cp^*_2ZrCl_2$ with two equivalents of lithium 2,4,6-trimethylphenylphosphanide in benzene. Since there was evidence for the formation of the aforementioned intermediate, they trapped it by addition of two equivalents of acetonitrile at room temperature and isolated needlelike orange of complex **3.12**. Again, the reaction proceeds in two steps: [2+2] cycloaddition of the C≡N to the Zr=PR bond and subsequent insertion of a second molecule of acetonitrile into the Zr–P bond of the four-membered heterocycle. Complex **3.12** is not stable in solution and decomposes to unidentified products within one week [90, 91]. In this respect, it is noteworthy that on the basis of the transient phosphinidene complex a rather large number of very different metallaphosphaheterocycles have been obtained [91].

Finally, the authors succeeded in the isolation of a stable phosphinidene complex just by replacing lithium 2,4,6-trimethylphenylphosphanidene with the 2,4,6-tri-*tert*-butylphenyl derivative and performing the reaction in the presence of trimethylphosphine. Black crystals of the complex $[Cp^*_2Zr(PMe_3)(=P–C_6H_2{}^tBu_3\text{-}2,4,6)]$ (**3.13**) were obtained in 40% yield.

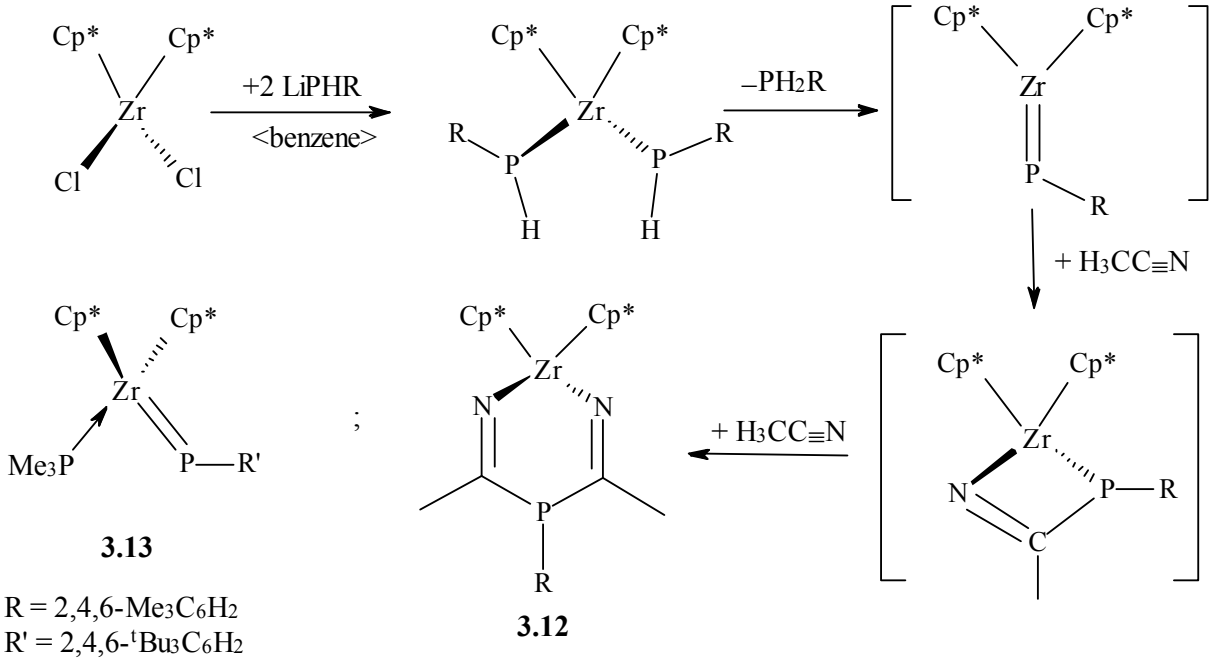

3.2 *Isolation and NMR Spectroscopic Characterization of the Zirconium Complex II*

3.2.1. *Preparation*

At −78 ºC, a solution of two equivalents of (*Z*)-/(*E*) 2-(lithiumamido)-2-phenyl-1$\lambda^3\sigma^2$-phosphaalkene (**1**) in 1,2-dimethoxyethane was added dropwise with stirring to a suspension of bis(η^5-pentamethylcyclopentadienyl)zirconium dichloride in toluene. The reaction mixture was allowed to warm up slowly to ambient temperature; its colour changed from deep red to wine red. To separate lithium chloride from the reaction product all volatile components were removed under reduced pressure and the resulting residue was extracted with an appropriate solvent. Thereafter, the solution was concentrated to one third of its original volume and cooled to −13 ºC. After several days red prisms containing the complex [(1-amido-3-imido-1,3-diphenyl-2$\lambda^3\sigma^2$-phospha-1-propene-*N*,*N*′)bis(η^5-pentamethylcyclopentadienyl)zirconium] (**II**) had precipitated and were isolated in about 50% yield.

Suitable crystals for X-ray structure determinations were obtained from a concentrated toluene solution (**II**·$\mathbf{C_7H_8}$)$_{Tol}$ and from a *n*-hexane solution which contained only a very small amount of toluene (**II**·$\mathbf{C_7H_8}$)$_{Hex}$. In a similar procedure, crystals of a second solvate (**2II**·***n*-$\mathbf{C_6H_{14}}$**)** were obtained. At first, in the preparation step only the solvent 1,2-dimethoxyethane and not a mixture of 1,2-dimethoxyethane and toluene was applied for a partial dissolution of bis(η^5-pentamethylcyclopentadienyl)zirconium dichloride. In the subsequent crystallisation step, a concentrated *n*-hexane solution was kept for several days at −13 ºC. Again, the isolated solid turned out to contain solvent molecules; a ratio of 2 : 1 was determined NMR spectroscopically for zirconium complex **II** and *n*-hexane (see below).

In complex **II**, the up to now unknown chelate ligand [1-amido-3-imido-1,3-diphenyl-2$\lambda^3\sigma^2$-phospha-1-propene] coordinates to the bis(η^5-pentamethylcyclopentadienyl)zirconium fragment via the two negatively charged nitrogen atoms of the amido and the imido group. This ligand differs from the 1,3-diimido-1,3-dimethyl-2-(2,4,6-trimethylphenyl)-2$\lambda^3\sigma^3$-phospha-propane ligand prepared by *Stephan* et al. [90] in a formal 1,3-shift of the hydrogen atom from the amido group to the two-coordinate phosphorus atom of complex **II**. One should be aware that *Stephan* et al. [90] started their reaction with a lithium organylphosphanide and intercepted the intermediate phosphinidene complex Cp*$_2$Zr=P–R with two equivalents of acetonitrile.

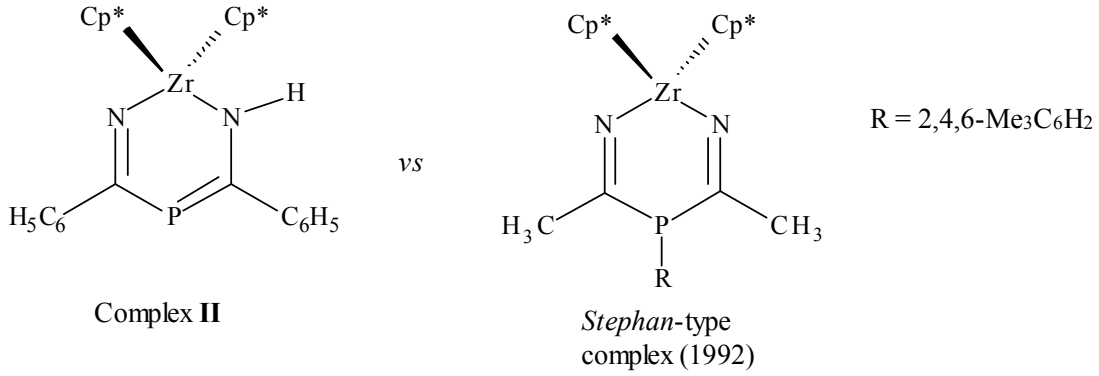

Complex **II**

Stephan-type complex (1992)

In case of complex **II,** [2-lithiumamido-2-phenyl-1$\lambda^3\sigma^2$-phosphaalkene] (**1**) prepared from lithiumphosphanide and benzonitrile was applied as starting compound. Therefore, a different reaction mechanism has to be worked out.

We assume that at first, two 2-amido-2-phenyl-1$\lambda^3\sigma^2$-phosphaalkene substituents replace two chlorine atoms at the zirconium centre. In a second step, the close proximity of the two ligands facilitates the addition of the P–H unit of one H~P=C entity to the P=C bond of the other one to establish a six-membered metallaphosphacycle with a freshly formed P–C bond. Finally, elimination of phosphane leaves a C=N bond.

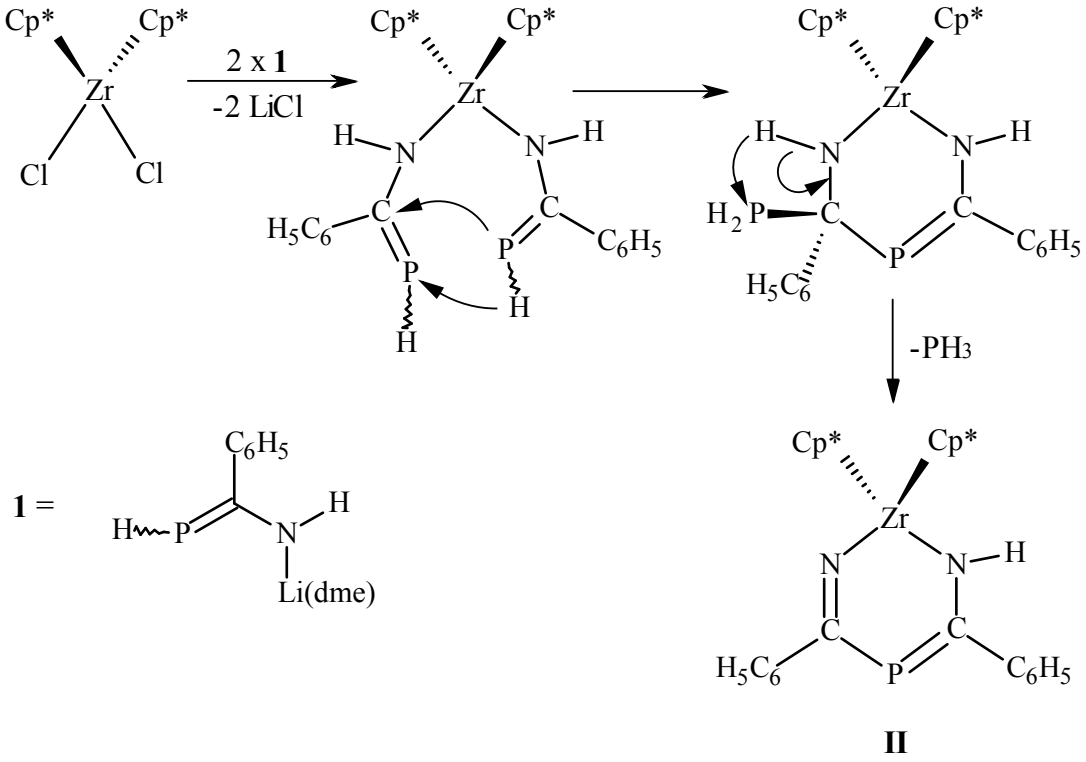

II

Scheme 3.1 Suggested mechanism for the reaction of compound **1** with bis(η^5-pentamethylcyclopentadienyl)zirconium dichloride

To sum up, the reaction of bis(η^5-pentamethylcyclopentadienyl)zirconium dichloride with two equivalents of 2-(lithiumamido)-2-phenyl-1$\lambda^3\sigma^2$-phosphaalkene (**1**) gives complex **II** and phosphane as volatile gas (**Scheme 3.1**). In this context it is worth to mention that the formation of substituted phosphanes is very often observed in zirconium chemistry; impressive examples are found in *Stephan's* review on "Zirconium-phosphorus Chemistry" [90].

3.2.2. *NMR Spectroscopic Identification of the Solvent Included in the Solid State Adducts*

The $^{31}P\{^1H\}$ NMR spectrum of the reaction mixture reveals a sharp singlet at +38.4 ppm and a second one of low intensity at −240.0 ppm. When ^1H coupling is allowed, the signal at +38.4 ppm remains unchanged whereas the second one is converted into a quartet with a $^1J_{P,H}$ coupling constant of 244 Hz, indicating the presence of phosphane (PH_3). Furthermore, a *very weak* ABX pattern of still unknown origin at about –10 ppm was also detected.

When crystals of (**II·C_7H_8**) are dissolved in [d_6]benzene the ^{31}P NMR spectrum shows –as expected– a sharp singlet at +38.4 ppm. The very intense high field ^1H signal at 1.7 ppm (**Figure 3.1**) comes from the methyl groups of the two pentamethylcyclopentadienyl ligands at zirconium. The broad resonance of relatively low intensity at 6.19 ppm is attributed to the N–H hydrogen atom. Furthermore, two multiplets at 7.9 and 8.4 ppm are assigned to the *ortho*-hydrogen atoms of two chemically different phenyl groups on both sides of the chelate ligand.

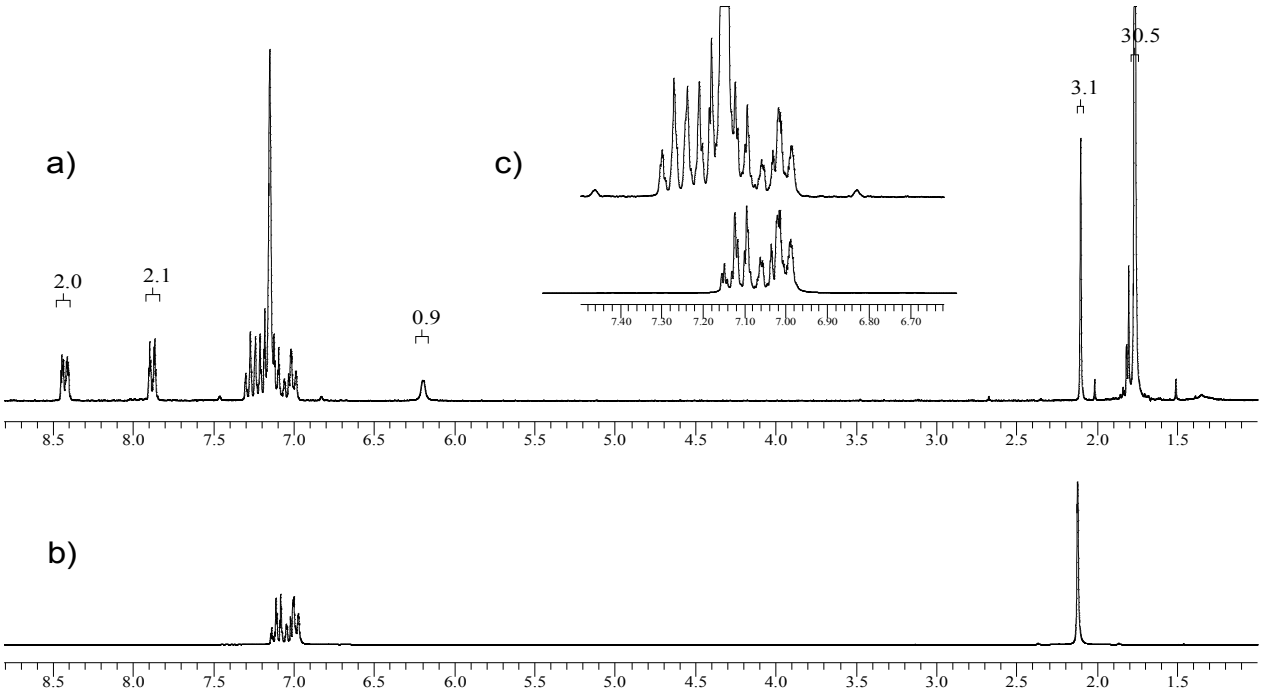

Figure 3.1 ^{1}H NMR spectrum of (**II**·C_7H_8)
a) Full ^{1}H NMR spectrum of (**II**·C_7H_8)$_{Tol}$ crystals dissolved in [d_6]benzene.
b) Full spectrum of pure toluene.
c) Expansion of the phenyl region of both spectra. The signals of the *ortho*-hydrogen atoms at 7.9 and 8.4 ppm arising from two different phenyl substituents at the complex ligand are not depicted.

In addition to the ^{1}H signals of complex **II**, two further signals at 2.1 and 7.1 ppm are observed. By comparison with the ^{1}H NMR spectrum of pure toluene (**Figure 3.1 b)**) they are unambiguously assigned to the toluene molecules in the solid state adduct. The signal intensities indicate definitely a complex to solvent ratio of 1 : 1.

As the inclusion of toluene into the crystal was found to introduce molecular disorder which interfered with the pollution and interpretation of the crystal structure (see below), complex **II** was prepared again in pure 1,2-dimethoxyethane and crystals were precipitated at −13 °C from a concentrated *n*-hexane solution. After the isolation of another crop of red prisms in about 50% yield, the ^{1}H NMR spectrum (**Figure 3.2 a)**) revealed that again a solvate (**2II**·***n***-C_6H_{14}) which now contained two molecules of *n*-hexane per formula unit of complex had been obtained.

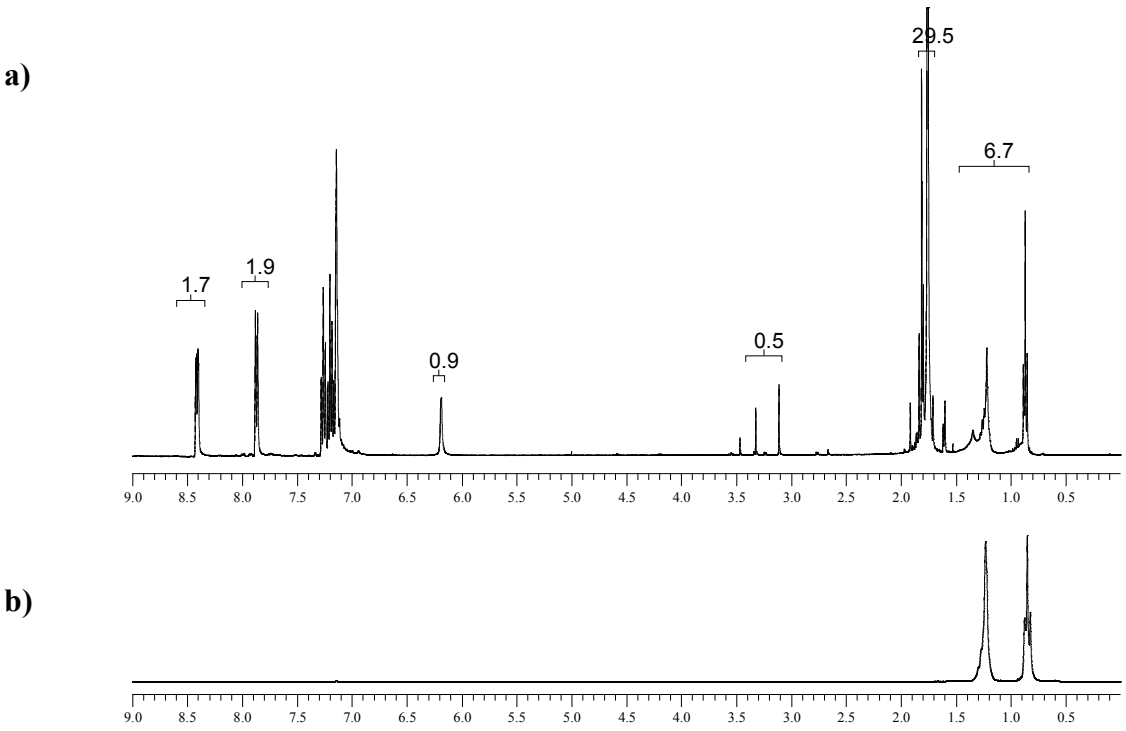

Figure 3.2 ^{1}H NMR spectrum of **(2II· *n*-C_6H_{14})**
a) Full spectrum of crystals isolated from a *n*-hexane solution and dissolved in [d_6]benzene
The spectrum shows a small amount of 1,2-dimethoxyethane (0.5) which is supposed to replace *n*-hexane in the solid.
b) Full spectrum of *n*-hexane

Similar to (**II**·C_7H_8) (**Figure 3.1 a)**), the signals of complex **II** are accompanied by two multiplets at 0.82 and 1.25 ppm arising from *n*-hexane. A ratio of *approximately* 2 : 1 for complex **II** to solvent is derived from the intensities of appropriate signals. In addition, the presence of a small amount of 1,2-dimethoxyethane is detected.

In order to establish the ratio of compound **II** to the included solvent molecules in the solid state adducts, several characteristic ^{1}H NMR signals had to be assigned in advance. For the following detailed analysis, a [d_6]benzene (**Table 3.1**) as well as a [d_2]dichloromethane solution (**Table 3.2**) had been prepared.

The most intense ^{1}H NMR signal of the [d_6]benzene solution at 1.8 ppm can unambiguously be attributed to the two pentamethylcyclopentadienyl ligands at zirconium. The corresponding ^{13}C NMR signals of the methyl and the ring carbon atoms are observed at 11.4 and 119.2 ppm, respectively. Due to its shape and low intensity (of about 1 : 30 with respect to ten

methyl groups), the broad signal at 6.19 ppm is assigned to the hydrogen atom of the N–H group (**Table 3.1**). This assumption is corroborated in the ^{15}N HMQC experiment exhibiting a definite cross peak with the ^{15}N signal of the amido group at −170 ppm which is split into a doublet by a $^{1}J_{15N,1H}$ coupling constant of 63 Hz (**Table 3.1, Figure 3.3 a)**). Since an additional HMBC correlation between the ^{1}H signal of the methyl substituents at the η^5-cyclopentadienyl ligands at 1.8 ppm and the ^{15}N singlet of the imido group at −281 ppm is observed, a rapid 1,3-shift of the N–H hydrogen atom between the two different nitrogen atoms has to be excluded.

Two lowfield multiplets at 7.87 and 8.41 ppm, each of which showing double the intensity of the broad N–H singlet, come from the hydrogen atoms in *ortho*-position of the phenyl substituents and demonstrate again the presence of different (H_5C_6)C–N entities in the chelate ligand. A correct assignment to the entity with a C–N single or double bond is possible by means of 2D NMR spectroscopic methods in that the N–H singlet at 6.19 ppm reveals definite HMBC correlations *only* with two ^{13}C NMR signals at 147.7 and 203.2 ppm (**Figure 3.3 b)**). Both signals are split into doublets by a $^{2}J_{P,C}$ and a $^{1}J_{P,C}$ coupling constant of 35 Hz and 75 Hz, respectively, and arise from carbon atoms in *ipso*-position of the phenyl group and the carbon atom in the P–C double bond in the P=C(Ph)–NH entity.

a)

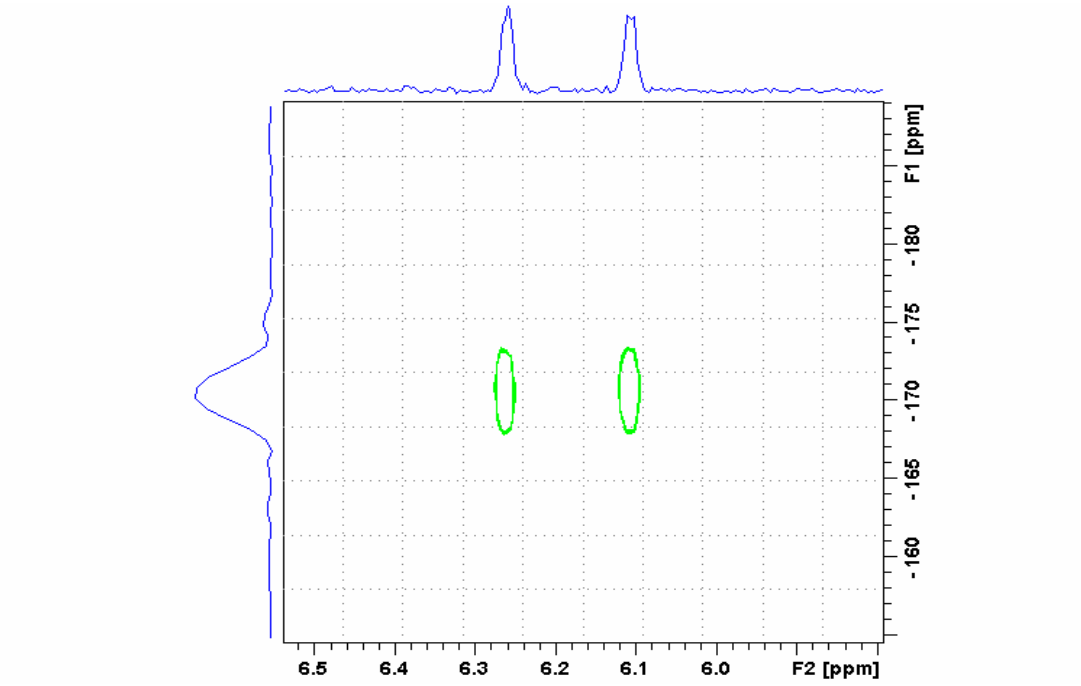

b)

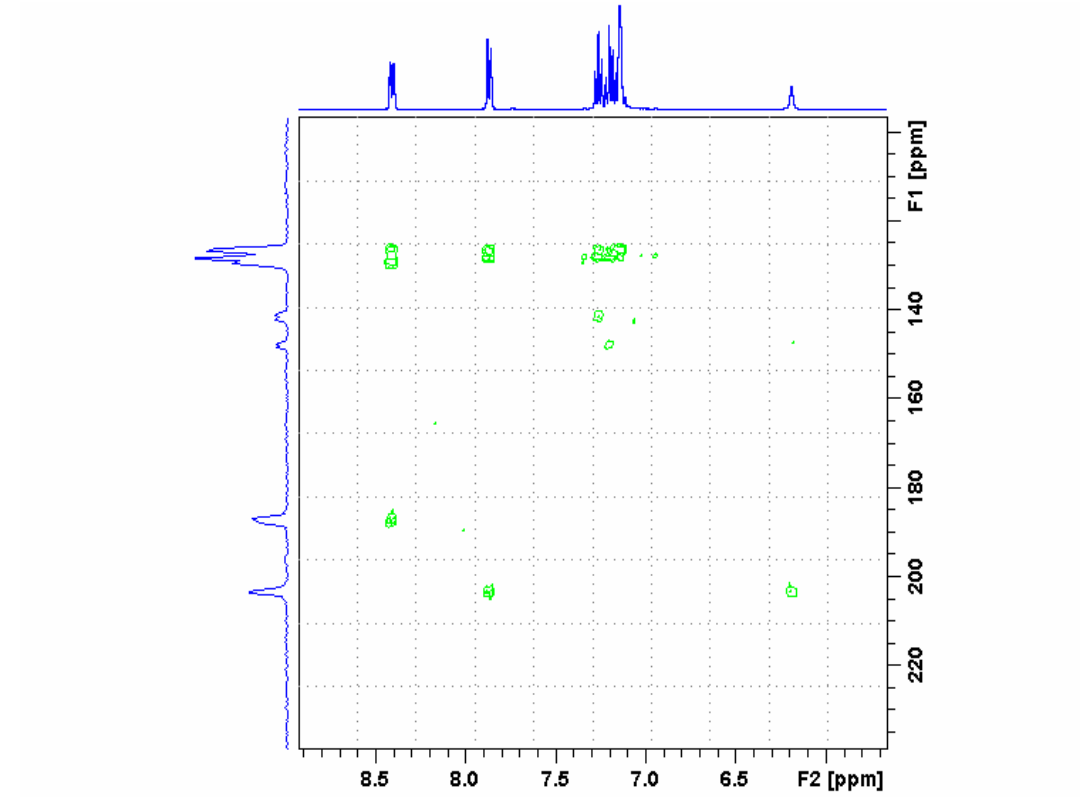

Figure 3.3 Section of $^{1}H,^{15}N$ HMQC NMR spectrum **a)** and $^{1}H,^{13}C$ HMBC NMR spectrum **b)** of complex **II** dissolved in [d_6]benzene

Table 3.1 Assignment of ^{1}H, ^{13}C and ^{15}N NMR signals of the 1-amido-3-imido-1,3-diphenyl-2$\lambda^3\sigma^2$-phospha-1-propene ligand in complex **(II)** based on ^{1}H-COSY, HSQC, HMQC, and HMBC correlations
All measurements were carried out in [d_6]benzene.

^{1}H-atom	δ (ppm), multiplicity[a)]	^{1}H-COSY[b)]	HMQC (^{15}N)/(^{31}P)[b)]; HSQC (^{13}C)[b)]	HMBC[b)]
a) *H_5C_6–C(=P)–NH entity*				
N–H	6.19 (*br s*)		^{15}N–H (–170.0)[c)d)] s ^{31}P (38.4) s	$^{13}C_{ipso}$ (147.7) w ^{13}P=C (203.2) s
C–H$_{ortho}$	7.87 (*m*)	C–H$_{meta}$ (7.20) s C–H$_{para}$ (7.13) m	$^{13}C_{ortho}$ (126.4) s ^{31}P (38.4) m	$^{13}C_{ortho}$ (126.5) s $^{13}C_{para}$ (128.5) s ^{13}P=C (203.0) s
C–H$_{meta}$	7.20 (*m*)	C–H$_{ortho}$ (7.87) s C–H$_{para}$ (7.13) m	$^{13}C_{meta}$ (128.1) s	$^{13}C_{meta}$ (128.2) s $^{13}C_{ipso}$ (147.7) m
C–H$_{para}$	7.13[e)] (*m*)	C–H$_{ortho}$ (7.87) m C–H$_{meta}$ (7.20) m	$^{13}C_{para}$ (128.3) s	$^{13}C_{ortho}$ (126.5) s
b) *H_5C_6–C(P)=N entity*				
C–H$_{ortho}$	8.41 (*m*)	C–H$_{meta}$ (7.26) s C–H$_{para}$ (7.15) m	$^{13}C_{ortho}$ (126.1) s ^{31}P (38.4) s	$^{13}C_{ortho}$ (126.1) s $^{13}C_{para}$ (129.0) s ^{13}C=N (187.3) s
C–H$_{meta}$	7.26 (*m*)	C–H$_{ortho}$ (8.41) s C–H$_{para}$ (7.15) m	$^{13}C_{meta}$ (128.0) s ^{31}P (38.4) w	$^{13}C_{meta}$ (128.1) s $^{13}C_{ipso}$ (141.4) m
C–H$_{para}$	7.15[e)] (*m*)	C–H$_{ortho}$ (8.41) m C–H$_{meta}$ (7.26) m	$^{13}C_{para}$ (128.5) s	$^{13}C_{ortho}$ (126.2) s

[a)] Broad singlet (*br s*), multiplett (*m*); [b)] correlation intensity: strong (s), medium (m), weak (w); [c)] $^{1}J_{1H,15N}$ = 63 Hz; [d)] no HMQC correlation with the ^{15}N=C signal but a HMBC correlation between the ^{1}H singlet of the methyl substituents at the η^5-cyclopentadienyl ligands and the ^{15}N=C signal (−281.0 ppm); [e)] partially superimposed by the C_6D_5H signal, centre determined with the help of an *approximate* $^{3}J_{H,H}$ coupling constant of 8 Hz.

In the HMBC experiment, the $^{13}C_{ipso}$ NMR signal at 147.7 ppm correlates with the multiplet of the hydrogen atoms in *meta*-position at 7.20 ppm. The ^{1}H-COSY spectrum exhibits a cross peaks between this signal and the one of the *ortho*-hydrogen atoms at 7.87 ppm and the multiplet of the *para*-hydrogen atoms at 7.13 ppm which is partially superimposed by the

signal of the residual protonated solvent C_6D_5H. The corresponding ^{13}C chemical shift values were determined by means of HSQC experiments.

Starting with the second lowfield multiplet at 8.41 ppm, which comes from the two hydrogen atoms in *ortho*-position of the phenyl substituent at the P–C=N entity of the chelate ligand, a similar procedure yields the remaining ^{1}H and ^{13}C NMR data listed in (**Table 3.1**).

In order to resolve some unclear points regarding the assignment of ^{1}H NMR multiplets of the two different *para*-hydrogen atoms and their HSQC correlations (see **Table 3.1**) a solution of the solid state adduct (**II·C_7H_8**) in [d_2]dichloromethane was prepared and the NMR spectroscopic analysis repeated. ^{13}C chemical shift values and $^{n}J_{P,C}$ coupling constant obtained from the [d_2]dichloromethane solution are compiled in **Table 3.2** and found to be nearly identical with analogous data of the [d_6]benzene solution. In addition to the lowfield singlet of toluene, a slowly increasing signal at 123.9 ppm is observed which probably arises from a reaction of the zirconium complex with the solvent.

Table 3.2 ^{13}C chemical shifts (ppm) and $^{n}J_{P,C}$ coupling constants (Hz, in brackets) of complex **II**

^{13}C-atom	[d_6]benzene δ ^{13}C ($J_{P,C}$ in Hz)	[d_2]dichloromethane δ ^{13}C ($J_{P,C}$ in Hz)
$(H_3\underline{C})_5\underline{C}_5$	11.4	10.8
$(H_3C)_5\underline{C}_5$	119.2	118.9
a) *H_5C_6–C(=P)–NH entity*		
P=C	204.1 (75)	203.3 (73)
$\underline{C}_{ipso}$	148.4 (35.3)	147.0 (35)
$\underline{C}_{ortho}$	127.2 (12)	126.4 (12)
$\underline{C}_{meta}$	129.0 (–)	128.3 (–)
$\underline{C}_{para}$	129.1 (2)	128.6 (2)
b) *H_5C_6–C(P)=N entity*		
C=N	188.1 (72)	185.9 (70)
$\underline{C}_{ipso}$	142.1 (40)	141.1 (41)
$\underline{C}_{ortho}$	126.9 (16)	126.0 (15)
$\underline{C}_{meta}$	128.8 (1)	128.0 (1)
$\underline{C}_{para}$	130.0 (2)	129.2 (2)

The ^{13}C NMR data of **II** reveal some noteworthy features:

α) The $^{1}J_{P,C}$ coupling constants do not differ significantly in spite of different bond order {P=C 73 Hz; (N=)C–P 70 Hz}.

β) The ^{13}C NMR signals of both phenyl substituent show notable differences. The signals of carbon atoms in *ortho*-, *meta*- or *para*-position, however, are shifted slightly highfield into a narrow region from 125 to 130 ppm. Except for the *meta*-position the $^{n}J_{P,C}$ coupling constants decrease with increasing distances to phosphorus.

γ) The ^{15}N signals of two different nitrogen atoms at −281 (C=N) and −170 ppm (N–H) were detected in HMQC experiments (see above).

In order to verify the correct assignment of the ^{1}H NMR multiplets of the two phenyl substituents, one at the P=C–NH and the other at the P–C=N entity, the lowfield region of the spectrum was simulated by applying the program TOPSPIN-daisy Version 2.0.0 [92]. The comparison of experimental and simulated spectra in **Figure 3.4** shows an excellent conformity. A detailed listing of the simulated data is given in **Table 3.3**

Table 3.3 Parameters for the calculation of the lowfield ^{1}H NMR spectrum of complex **II**

^{1}H NMR parameter	phenyl substituent at P=C–NH	phenyl substituent at P–C=N	^{1}H NMR parameter	phenyl substituent at P=C–NH	phenyl substituent at P–C=N
δ (C–H$_{ortho}$)	7.87	8.41	δ (C–H$_{meta}$)	7.20	7.26
^{4}J(H$_o$,P)	1.2	2.7	^{5}J(H$_m$,P)	0.5	0.8
^{3}J(H$_o$,H$_m$)	8.1	8.4	^{3}J(H$_m$,H$_p$)	7.7	7.7
^{4}J(H$_o$,H$_p$)	1.3	1.4	^{4}J(H$_m$,H$_m'$)	1.3 [85]	1.3 [85]
^{4}J(H$_o$,H$_o'$)	1.3 [85]	1.3 [85]	δ (C–H$_{para}$)	7.13	7.15
^{5}J(H$_o$,H$_m'$)	0.5 [85]	0.5 [85]	^{6}J(H$_p$,P)	1.0	—

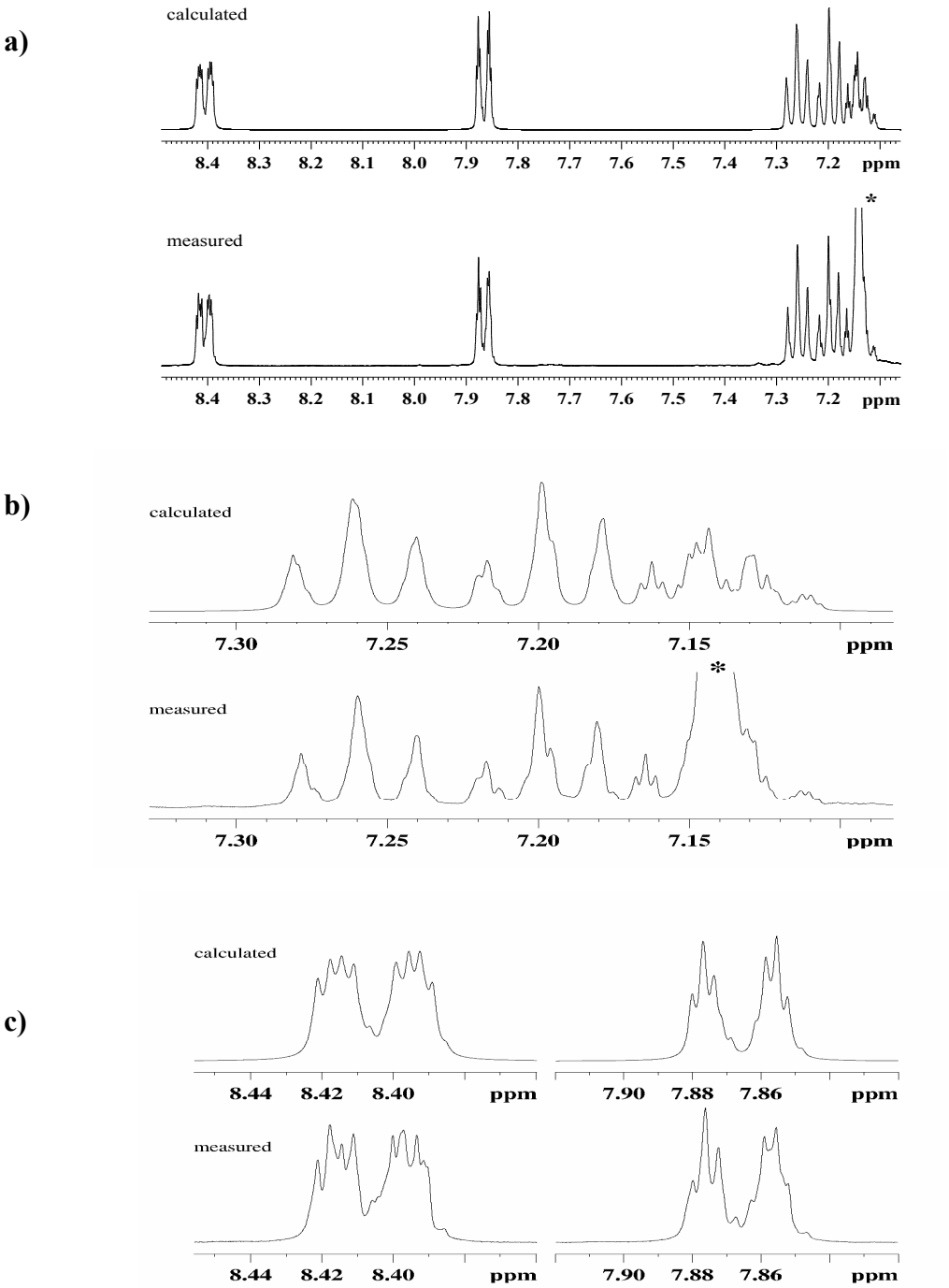

Figure 3.4 Comparison between calculated and measured ^{1}H NMR spectra of the two different phenyl substituents of complex **II**
The $C_6D_5\underline{H}$ signal in the experimentally obtained spectrum is marked with an asterisk (*).
The calculated spectra were obtained with the help of the program TOPSPIN-daisy Version 2.0.0 [92].
a) Full spectra of the phenyl region
b) Multiplets of the *meta*- (7.17 → 7.30 ppm) and *para*-hydrogen atoms (7.10 → 7.17 ppm) in detail
c) Multiplets of the *ortho*-hydrogen atoms in detail (7.84 → 7.89 ppm)

In **Table 3.4** a selected NMR data of some compounds that contain an (O)N=C–P=C–N(O) fragment were listed. The ^{31}P chemical shift values vary between −18.7 for **(*E*)-3.3** and +136.8 ppm for **3.14**, thus value of +38.4 for **II** lies almost in the middle part of **Table 3.4** and agrees very well with values observed for **3.5**. Except the ^{13}C NMR signals of **3.6**, the values which compiled in **Table 3.4** vary in rather narrow range. Since for **II** a ^{13}C NMR signals at 204.1 or 203.3 ppm were obtained, they lie in the expected range. As previously mentioned, the $^{1}J_{P,C}$ coupling constant of bothe carbon atoms (P=C and P–C) does not vary substantially in agreement with values reported for **3.14** in which a difference of 5 Hz was observed.

Table 3.4 Selected NMR data of compounds with an N=C–P=C–N(H) unit
Chemical shift δ(ppm), coupling constant *J*(Hz)

compound	δ ^{31}P	δ $^{13}C_{P=C}$	$^{1}J_{P,C}$	δ $^{13}C_{P-C}$	$^{1}J_{P,C}$	Solv.	Lit.
II	+38.4	204.1	75	188.1	72	C_6D_6	
		203.3	73	185.9	70	CD_2Cl_2	
3.1	−17.4	201.0	68	198.2	85	d_8-THF	40
3.2	−0.8	206.7	83			d_8-THF	40
(*Z*)-3.3	3.5	199.1	62			C_6D_6	79
(*E*)-3.3	−18.7	199.2	53			d_8-THF	
		198.4	70				
3.4							
L = thf	28.7	—	—			d-Tol.	41
L = dme	25.3	188.8	73			C_6D_6	42
3.5							
a- R = *t*-Bu	36.7	202.6	241			C_6D_6/dme	43
b- R = Ad	36.7	203.6	241			C_6D_6/dme	43
c- R = ph	38.9	202.8	225			d_8-THF	44
d- R = Mes	48.5	204.1	234			d_8-THF	43
3.6							
R = Me	71.6	233.1	87			d_8-THF/Digl.	45
R = *t*-Bu	52.6	247.0	103			C_6D_6	46
R = Ph	64.2	224.9	87			C_6D_6	47
R = Mes	86.4	233.7	90			C_6D_6	48
3.7	63.3	208.3	83			d_8-THF	42
3.8	58.1	205.8	76			C_6D_6	42, 43
3.9	58.2	212.8	88			d_8-THF	42
3.14	136.8	220.4	103	189.6	98	C_6D_6	49

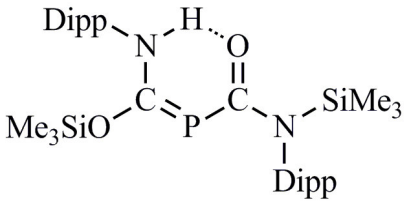

3.1

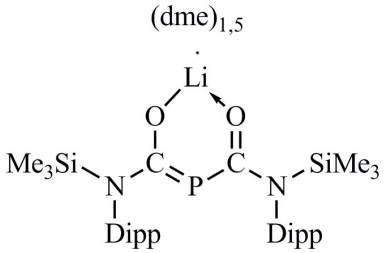

3.2

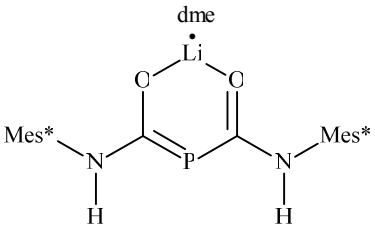

(*Z*)-3.3

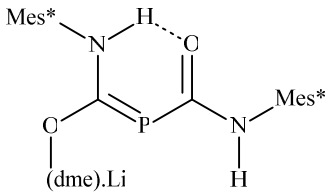

(*E*)-3.3

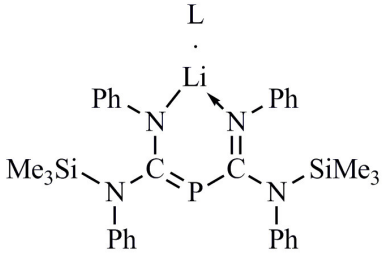

3.4

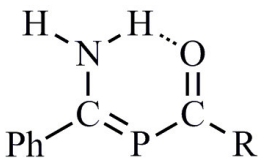

3.5

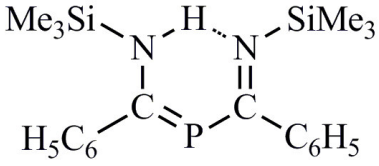

3.8

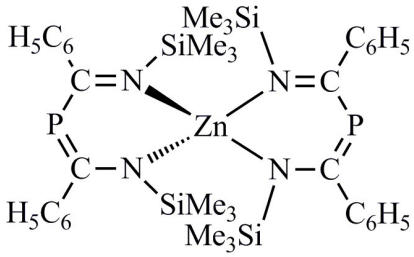

3.9

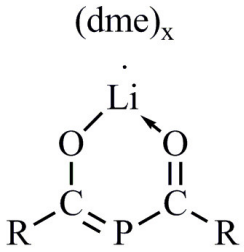

3.6

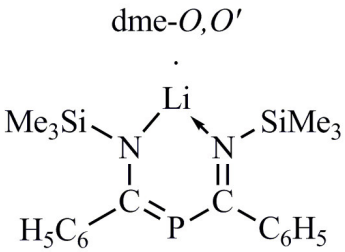

3.7

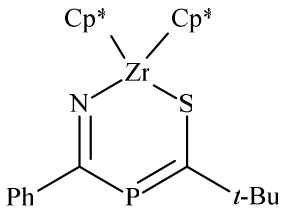

3.14

3.3 X-ray Structure Determinations of the solvates of Complex II

As already pointed out in **Section 3.2.1**, red prisms of the solvate (**II·C_7H_8**) precipitated at −13 °C from a solution of complex **II** in either pure toluene or *n*-hexane which contained a small amount of toluene. In order to distinguish between these two crops of crystals the terms (**II·C_7H_8**)$_{Tol}$ and (**II·C_7H_8**)$_{Hex}$ are introduced. Similarly, the solvate isolated in red prisms again from a solution of pure *n*-hexane is denoted as (**2II·*n*-C_6H_{14}**).

3.3.1 Crystal data, Measuring Techniques and Structure Analyses

Data for the structure determination of (**II·C_7H_8**)$_{Tol}$ were collected at ambient temperature on a four-circle diffractometer P21 (Syntex, Cupertino, USA), whereas low temperature data sets of (**II·C_7H_8**)$_{Hex}$ and (**2II·*n*-C_6H_{14}**) were obtained at 100K on a Kappa II Dou diffractometer. Graphite monochromatized Mo-Kα-radiation (λ = 71.073 pm) was used; lattice parameters were calculated from the exact positions of a selected number of reflections (**Table 3.5**) and refined thereafter. For (**II·C_7H_8**)$_{Tol}$ and (**II·C_7H_8**)$_{Hex}$, the monoclinic space group *C2/c* was derived from unit cell dimensions and systematic absences. For the solid state adduct (**2II·*n*-C_6H_{14}**) lattice parameters and statistical tests on the distribution of E-values suggested the triclinic space group $P\bar{1}$. The crystal structures were solved by statistical methods applying the software package SHELXTL version 5.1 [43 and 44] which also includes the program XP for the analysis of molecular geometry and the preparation of drawings.

After the zirconium, phosphorus, nitrogen and carbon atoms had been located step by step and their positions as well as their isotropic replacement parameters had been refined by full-matrix least-squares calculations, the structure determinations were continued applying individual anisotropic Uij-values. At the end, the atomic coordinates of hydrogen atoms could either be taken from a difference Fourier map and were refined together with their isotropic replacement parameters, or were calculated on the basis of an idealized geometry. The calculation procedure including the riding model has already been described in general in **Section 2.3.3**. Finally, the parameters of all heavier atoms were subjected to a last least squares refinement to take into account the incorporation of hydrogen atoms.

For the structures determinations discussed here the hydrogen problem was solved in detail as follows:

In case of the solid state adduct (**II·C_6H_8**)$_{Tol}$, the hydrogen positions of the methyl groups at the η^5-cyclopentadienyl ligands and the phenyl substituents at the P–C–N entities were

Table 3.5 Crystal data and details of structure refinement for the solid state adducts **(II·C_7H_8)$_{Tol}$**, **(II·C_7H_8)$_{Hex}$**, and **(2II·*n*-C_6H_{14})**

Compound	**(II·C_7H_8)$_{Tol}$**	**(II·C_7H_8)$_{Hex}$**	**(2II·*n*-C_6H_{14})**
Diffractometer	P21	Kappa II Dou	Kappa II Dou
Empirical formula	$C_{41}H_{49}N_2PZr$	$C_{41}H_{49}N_2PZr$	$C_{37}H_{48}N_2PZr$
Molecular weight	692.01	692.01	642.99
Melting point (ºC)	103	103	103
Wavelength (pm)	71.073	71.073	71.073
Temp. of measurement (K)	293 ± 2	100 ± 2	100 ± 2
Crystal shape;	red prism;	red prism;	red prism;
crystal size (mm)	0.31 x 0.28 x 0.24	0.24 x 0.21 x 0.21	0.37 x 0.27 x 0.2
Crystal system	monoclinic	monoclinic	triclinic
Space group [45]	*C2/c (No. 15)*	*C2/c (No. 15)*	*P* $\bar{1}$ *(No. 2)*
Unit cell dimensions a/pm	1615.75(14)	1614.53(7)	959.08(6)
b/pm	1090.53(3)	1090.18(5)	960.45(6)
c/pm	1987.78(4)	1989.05(10)	1946.5(1)
α/deg	90	90	92.921(4)
β/deg	99.136(1)	98.976(2)	91.254(3)
γ/deg	90	90	112.084(3)
Volume ($10^{-30}m^3$)	3458.1(3)	3458.1(3)	1657.7(2)
Z	(4 + 8 x 0.5)	(4 + 8 x 0.5)	(2 + 2 x 0.5)
Calculated density (10^3 kg/m^3)	1.329	1.329	1.288
Absorption coefficient μ (mm^{-1})	0.396	0.396	0.407
F(000)	1456	1456	678
Θ-Range for data coll. (deg)	2.57 to 28.28	2.07 to 28.31	2.1 to 28.37
Limiting indices	$-21 \le h \le 21$	$-21 \le h \le 15$	$-12 \le h \le 12$
	$-14 \le k \le 14$	$-14 \le k \le 12$	$-12 \le h \le 12$
	$-26 \le l \le 26$	$-26 \le l \le 26$	$-25 \le h \le 25$
Systematic absenses	*hkl:* $h+k = 2n+1$	*hkl:* $h+k = 2n+1$	none
	h0l: $h,l = 2n+1$	*h0l:* $h,l = 2n+1$	
Scan modes	Wyckoff scan	Omega + Phi	Omega + Phi
Scan width (deg)	0.8	wide scan	wide scan
Velocity (deg s^{-1})	5 to 29	0.1	0.1
Reflections collected	7874	15088	56749
Unique reflections	4267	4282	8251
Completeness to θ_{max}	0.996	0.997	0.995
Max. and minimum transmission	not det.	0.9208; 0.9127	0.9230; 0.8653
Data used for refinement [a]	4267	4282	8251
Parameters refined (n)	242	285	420
Restraints	0	0	15[b]
Goodness-of-fit (GOF) on F^2	1.033	1.055	1.016
Final R-indices:			
R1/wR2 using all data	0.0378; 0.0847	0.0555; 0.0870	0.0580; 0.0937
with [I > 2 σ (I)]	0.0306; 0.0806	0.0366; 0.0818	0.0401; 0.0874
Largest diff. peak;	0.544	0.616	0.860
deepest hole (10^{-30}e.m^{-3})	−0.12	−0.385	−0.576

[a] Full-matrix least-squares on F^2; [b] restrains concerning very similar C–C bond lengths of the disordered phenyl substituent and the disordered solvent molecule, respectively.

calculated with fixed C–H distances of 96 and 93 pm, respectively. The isotropic displacement parameters got the values of the corresponding carbon atoms multiplied by a factor of 1.2. A calculation of the hydrogen positions of the disordered toluene molecule was considered to be meaningless. The low temperature structure determination of the solid state adduct $(\mathbf{II}\cdot\mathbf{C_6H_8})_{Hex}$ allowed to localize the hydrogen atoms of compound **II** and to refine these parameters as well as their individual isotropic U-values. The hydrogen atoms of the toluene molecule were included mathematically given an overall distance of 96 pm and isotropic U-values of the adjacent methyl and phenyl carbon atoms increased by a factor of 1.5 and 1.2, respectively.

Very remarkably, in the structure determination of $(\mathbf{2II}\cdot\boldsymbol{n}\text{-}\mathbf{C_6H_{14}})$ the hydrogen atom of the NH groups could be located and its parameters were refined freely. The hydrogen positions of the methyl and phenyl substituents as well as the *n*-hexane molecules, however, were calculated as described above using C–H distances of 95 pm for methyl and 99 pm for phenyl and *n*-hexane; except for the strongly disordered solvent molecules, the isotropic U-values were received again from the corresponding carbon atoms and increased by a factor of 1.5 and 1.2 for the methyl and methylen carbons. Already in this section it has to be pointed out that one of the two phenyl substituents shows an additional rotation disorder.

Crystallographic parameters and details of data collection have been summarized in **Table 3.5**. Atomic coordinates and isotropic as well as anisotropic displacement parameters are given in **Tables 8.3.2, 8.3.3 and 8.4.3** for $(\mathbf{II}\cdot\mathbf{C_7H_8})_{Tol}$, $(\mathbf{II}\cdot\mathbf{C_6H_8})_{Hex}$ and $(\mathbf{2II}\cdot\boldsymbol{n}\text{-}\mathbf{C_6H_{14}})$, respectively, of the Appendix. Complete bond distances, bond angles and characteristic torsion angles of $(\mathbf{II}\cdot\mathbf{C_7H_8})_{Tol}$ and $(\mathbf{II}\cdot\mathbf{C_7H_8})_{Hex}$, respectively, have been put together in **Table 8.3.1**, for $(\mathbf{2II}\cdot\boldsymbol{n}\text{-}\mathbf{C_6H_{14}})$ they are given in **Table 8.4.1**.

3.3.2 *Bond Distances and Bond Angles for (II·C$_7$H$_8$)*

The X-ray structure determinations of the solid state adduct $(\mathbf{II}\cdot\mathbf{C_7H_8})_{Tol}$ at ambient temperature and of $(\mathbf{II}\cdot\mathbf{C_7H_8})_{Hex}$ at (100±2)K substantiate the results of the NMR spectroscopic studies in that the complex [(1-amido-3-imido-1,3-diphenyl-2$\lambda^3\sigma^2$-phospha-1-propene-*N*,*N*′)bis(η^5-pentamethylcyclopentadienyl)zirconium] (**II**) had been formed. The central zirconium atom is nearly tetrahedrally coordinated by two η^5-pentamethylcyclopentadienyl ligands and the two nitrogen atoms of the yet unknown chelate ring. Both structure determinations give almost identical results but nevertheless they are somewhat disappointing since disorder is associated with the solvent as well as the complex molecule.

a)

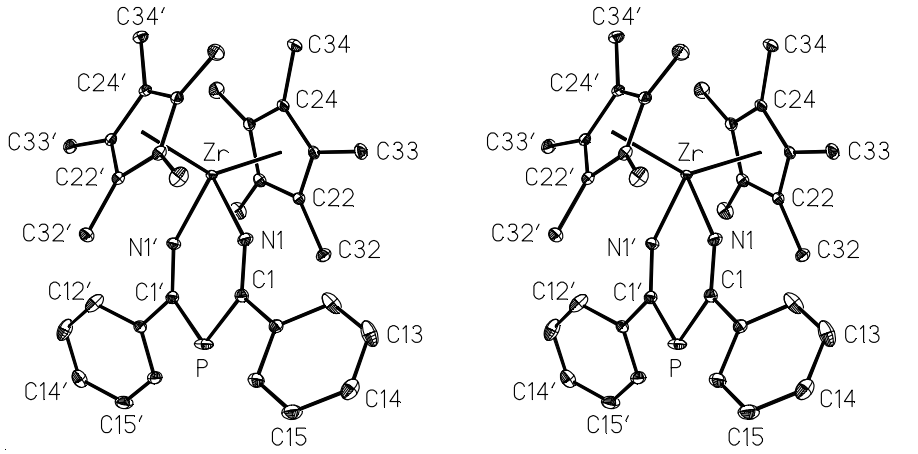

b)

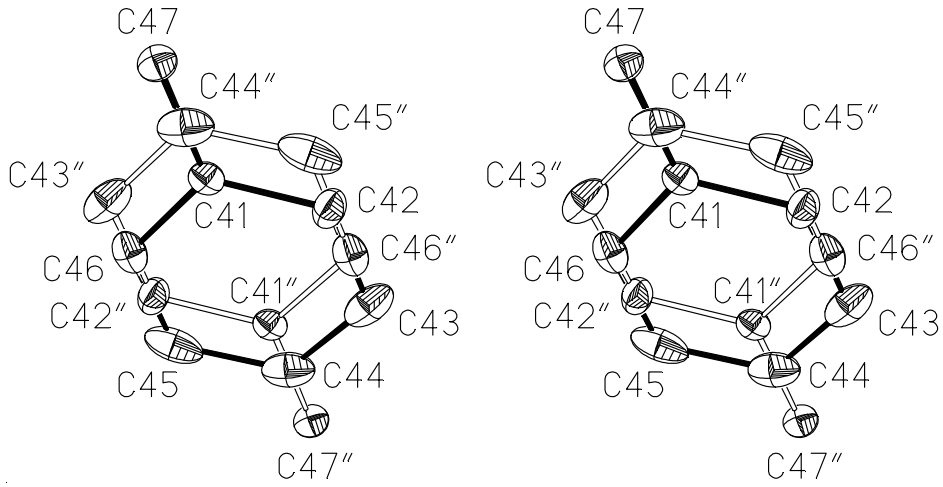

Figure 3.5 Structure of the complex molecule [(1-amido-3-imido-1,3-diphenyl-2$\lambda^3\sigma^2$-phospha-1-propene-*N,N′*)bis(η^5-pentamethylcyclopentadienyl)zirconium] (**II**) in (**II**·C_7H_8) **a)** and disorderd toluene molecules **b)** in stereoscopic view
All thermal ellipsoids are of 30% probability, but for a better presentation the size of the solvent molecule has been increased. Hydrogen atoms have been omitted for clarity. Absent atom numbering has to be complemented in a logical manner. The a priori unsymmetrical complex molecules (**a)**) reside on twofold axes of the unit cell. Atoms of the second half of the ligand generated by the symmetry operation (−x + 1, y, −z + 3/2) are marked with (′). Similarly, disorder also occurs with the toluene molecules (**b)**) on centres of inversion (": −x + ½, −y + 3/2, −z + 2).

Therefore only a relatively short discussion is given for the low temperature structure of (**II**·C_7H_8)$_{Hex}$.

Due to the symmetry of space group *C2/c*, the solvent molecule toluene is placed on a centre of inversion and the complex molecule resides on a twofold axis which goes through the phosphorus and zirconium atoms (**Figure 3.5 a)** and **b)**). As a consequence, the P=C–NH and P–C=N entities of disordered molecules of **II** are superimposed and only an approximate molecular skeleton (**Figure 3.5**) with averaged distances and angles can be obtained. Fortunately, analogous investigations on (**2II**·***n***-C_6H_{14}) show the most important part of the

structure, namely the unsubstituted 1-amido-3-imido-2$\lambda^3\sigma^2$-phospha-1-propene ligand to be free of disorder and allowed to determine specific bond lengths and angles as well as averaged values, representing the mean of the corresponding data for the P=C–NH and the P–C=N entities (**Table 3.7**, see below). The effective distances and angles obtained for (**2II·*n*-C_6H_{14}**) are in good agreement with the mean values calculated for (**II·C_7H_8**)$_{Hex}$, with maximum deviations of 0.5 pm and 0.6° for bond lengths and bond angles, respectively (**Table 8.4.2** of the appendix, parameters of (**II·C_7H_8**)$_{Tol}$ were also included although the data sets were obtained at different temperature (293K)).

Despite the successful resolution of the disorder in the complex molecule **II**, the treatment of the disordered solvent in (**II·C_7H_8**) still posed problems and took quite a while. Its shape, a six membered ring with two methyl groups in 1,4-position, aroused at first suspicion that an impurity of the solvent used might have been included or an unknown component might have been formed under the catalysis of bis(η^5-pentamethylcyclopentadienyl)zirconium dichloride. Furthermore, in this stage of structure refinement some unusually large isotropic displacement parameters could not be explained. By chance, however, studying several literature articles on crystals with included toluene [93] gave the idea that the strange pattern might be caused by two toluene molecules with an occupancy factor of 0.5 which are superimposed in such a way that the methyl groups are placed opposite to each other (**Figure 3.5 b)**). Additional NMR spectroscopic studies (**Section 3.2.2**) confirmed the presence of toluene at a 1 : 1 ratio of complex to solvent molecules. The final refinement of bond lengths and bond angles turned out to be without major problems even if the standard deviations are rather high (**Table 8.3.1**).

3.3.3 *Crystal Packing of the Solid State Adduct (II·C_7H_8) and its Relation to the PtS-Structure*

A careful analysis how the two components of the solid state adduct (**II·C_7H_8**) are structurally arranged reveals at first that the complex molecules are packed in (001) layers which are separated by (001) layers of toluene molecules. All complex molecules of a layer are equally lined up along twofold axes but the corresponding P···Zr vector changes its direction from layer to layer (**Figure 3.6)**. To our surprise the packing of the two components of the solid state adduct represent a well known but slightly distorted inorganic structure type. When the zirconium atoms, depicted in **Figure 3.7** as black spheres, are considered to be the centres of the complex molecules and the pairs of disordered toluene molecules are replaced by

Table 3.6 Selected distances (in pm) and angles (deg) for [(1-amido-3-imido-1,3-diphenyl-2$\lambda^3\sigma^2$-phospha-1-propene-*N,N′*)bis(η^5-pentamethylcyclopentadienyl)zirconium]–toluene (1/1) (≙ **II·C$_7$H$_8$**) determined from crystals of (**II·C$_7$H$_8$**)$_{Hex}$ at (100 ±2)K and (**II·C$_7$H$_8$**)$_{Tol}$ at 273K, respectively.
M_{Cp}: centre of the η^5-pentamethylcyclopentadienyl ligand; (′): symmetry operation (–x+1; y; –z+3/2).

a) Distances

chelate ligand at zirconium			
	(**II·C$_7$H$_8$**)$_{Hex}$ / (**II·C$_7$H$_8$**)$_{Tol}$	(**II·C$_7$H$_8$**)$_{Hex}$ / (**II·C$_7$H$_8$**)$_{Tol}$	
Zr–N1	210.2(2) / 210.4(2)	C1···C1′	280.5 / 281.9
N1–C1	130.3(3) / 130.2(2)	N1···N1′	275.5 / 276.2
P–C1	179.3(2) / 180.1(2)	Zr···M_{Cp}	224.5 / 224.9
C1–C11	150.2(3) / 150.1(2)		
phenyl substituent			
	(**II·C$_7$H$_8$**)$_{Hex}$ / (**II·C$_7$H$_8$**)$_{Tol}$		(**II·C$_7$H$_8$**)$_{Hex}$ / (**II·C$_7$H$_8$**)$_{Tol}$
C11–C12[a)]	139.1(3) / 139.2(3)	C13–C14	137.3(4) / 137.7(3)
C11–C16	138.9(3) / 139.4(3)	C14–C15	137.3(4) / 137.8(3)
C12–C13	138.6(3) / 138.5(3)	C15–C16	138.0(4) / 138.9(3)
H^5-pentamethylcyclopentadienyl ligand			
	(**II·C$_7$H$_8$**)$_{Hex}$ / (**II·C$_7$H$_8$**)$_{Tol}$		(**II·C$_7$H$_8$**)$_{Hex}$ / (**II·C$_7$H$_8$**)$_{Tol}$
C21–C22[b)]	141.5(3) / 141.4(2)	C21–C31[c)]	149.8(3) / 149.8(2)
C21–C25	141.9(3) / 142.5(2)	C22–C32	149.6(3) / 149.9(2)
C22–C23	142.4(3) / 142.3(2)	C23–C33	150.0(3) / 150.3(2)
C23–C24	141.8(3) / 142.0(2)	C24–C34	150.1(3) / 150.2(2)
C24–C25	142.0(3) / 142.4(2)	C25–C35	150.1(3) / 150.6(2)

mean values: [a)]C–C_{phenyl} 138.2 / 138.2; [b)]C–$C_{cycl.}$ 141.9 / 142.1; [c)]C–CH_3 149.9 / 150.2;

b) Bond angles

chelate ligand			
	(**II·C$_7$H$_8$**)$_{Hex}$ / (**II·C$_7$H$_8$**)$_{Tol}$		(**II·C$_7$H$_8$**)$_{Hex}$ / (**II·C$_7$H$_8$**)$_{Tol}$
M_{Cp}′···Zr···M_{Cp}	139.5 / 139.6	N1–C1–P[a)]	127.3(2) / 127.2(2)
N1–Zr···M_{Cp}	105.8 / 104.5	N1–C1–C11	118.8(2) / 119.2(2)
N1–Zr–N1′	81.8(1) / 82.0(2)	P–C1–C11	113.8(1) / 113.5(1)
Zr–N1–C1	140.1(2) / 140.1(2)	C1′–P–C1	102.9(1) / 103.0(1)

dummy atoms, depicted as white spheres, at the respective centres of inversion, one can without difficulty recognize the reproduction of a PtS-structure: Pairs of planar toluene molecules represent four coordinate Pt^{+2} cations in a planar environment and build up a cubic close packing, whereas spherical complex molecules represent four coordinate S^{-2} anions in a distorted tetrahedral environment (**Figure 3.7**).

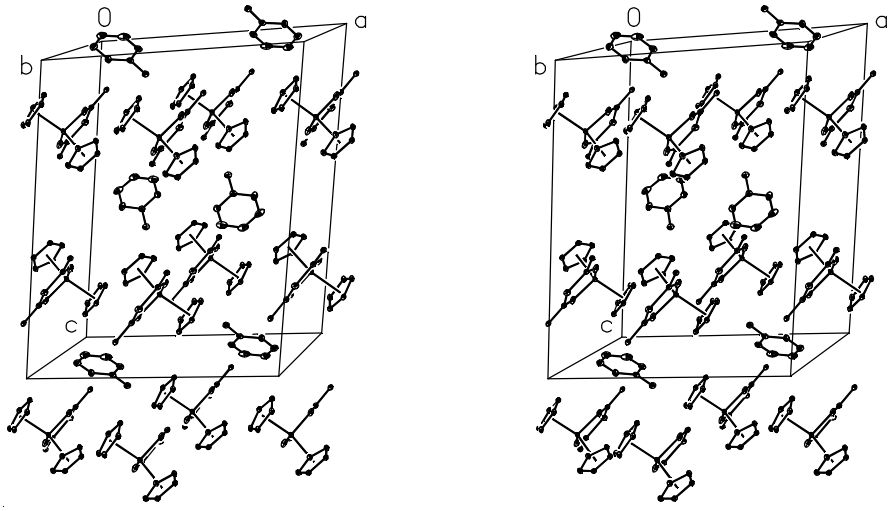

Figure 3.6 Packing of complex and solvent molecules in the structure of the solid state adduct (**II**·C_7H_8)
Thermal ellipsoids are of 30% probability. Except for the *ipso*-carbon atoms the phenyl groups of the 1-amido-3-imido-1,3-diphenyl-2$\lambda^3\sigma^2$-phospha-1-propene ligands, the methyl groups of the η^5-pentamethylcyclopentadienyl substituents and the hydrogen atoms of the disordered N−H unit and of the toluene molecules have been omitted for clarity. Only one toluene molecule of a pair of molecules each disordered with an occupancy factor of 0.5 and interrelated by a centre of inversion is depicted.

It is worth while to point out that the platinum(II) sulphide (PtS) structure can easily be derived from the well known calcium fluoride (CaF_2) structure. Whereas in the latter the fluoride anions (F^-) occupy all tetrahedral voids of a cubic close packed arrangement of Ca^{2+} cations the sulphide anions (S^{-2}) of the PtS structure leave half of them vacant (**Figure 3.8)**.

a)

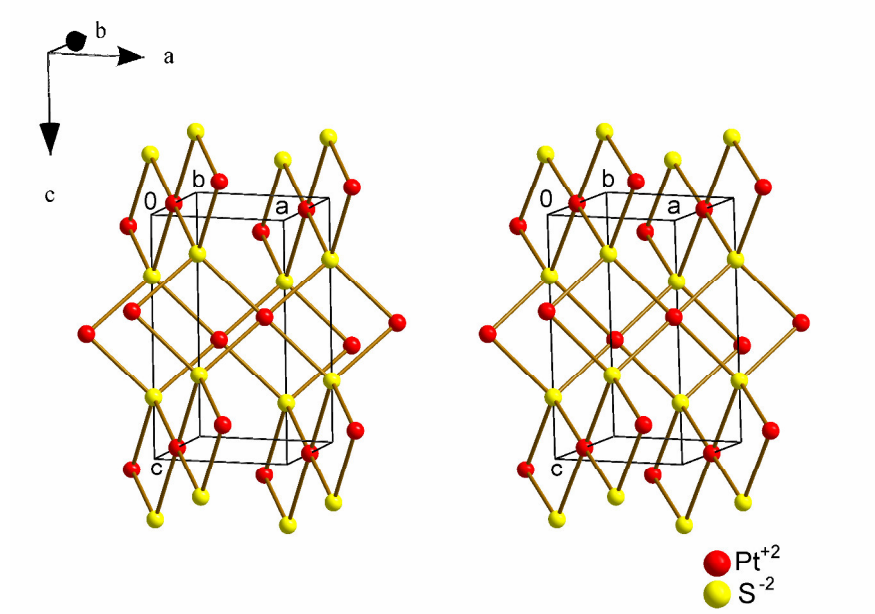

b)

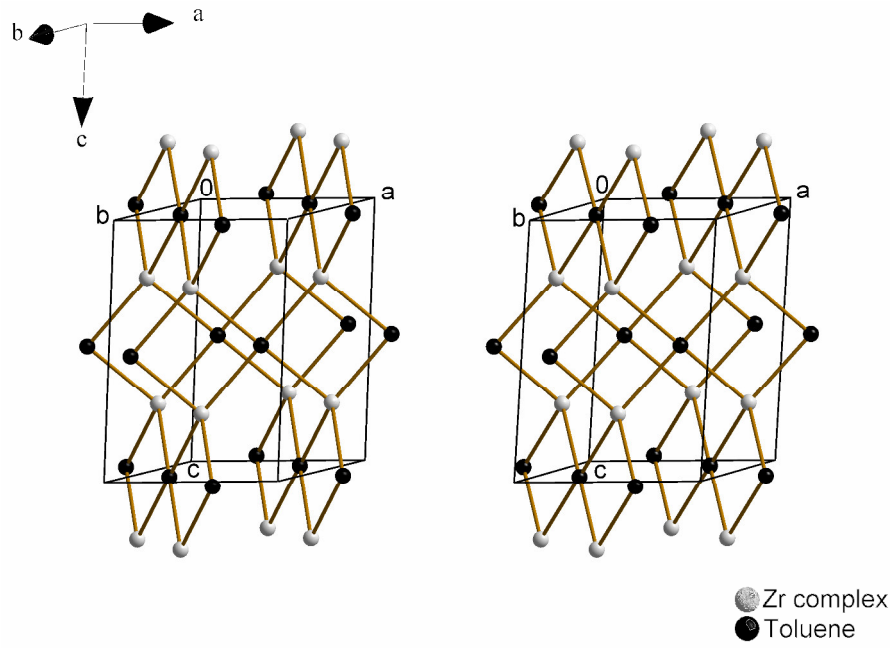

Figure 3.7 Crystallization of the solid state adduct **(II·C_7H_8)** in a slightly distorted PtS-type structure

Please note that on viewing **Figures 3.7 a)** and **b)** the origin of the unit cell has to be in the background.

a) Structure of platinum(II) sulphide, for details see **Figure 3.8**.

b) Results of the detailed structure analysis of **(II·C_7H_8) –** for a comparison see **Figure 3.6**

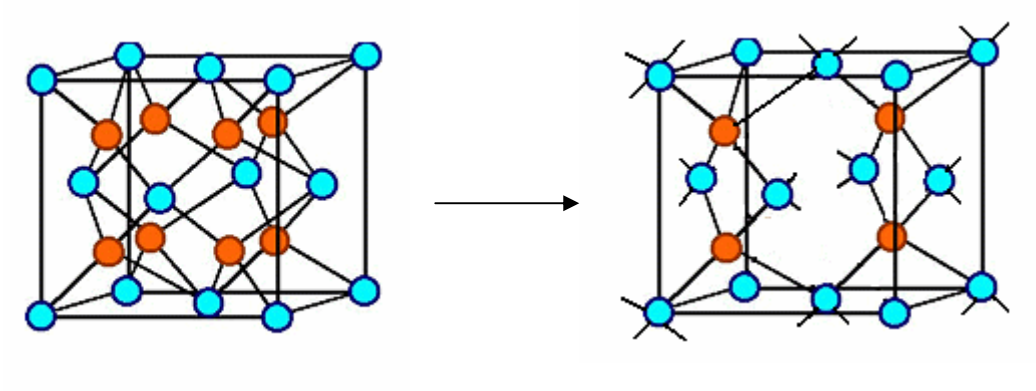

CaF_2 Pt(S□)

Figure 3.8 Relation between CaF_2 and PtS structures
The metal cations (Ca^{+2}, Pt^{+2}) are cubic close packed, the anions, occupy all (F^{-}) or half (S^{-2}) of the tetrahedral voids. For further details see [94].

3.3.4 *Molecular Structure of Compound II in the Solid State Adduct (2II·n-C_6H_{14})*

Crystals suitable for an X-ray structure analysis of the solid state adduct (**2II·*n*-C_6H_{14}**) precipitated at −13 °C from a concentrated *n*-hexane solution of complex **II** which had been prepared in pure toluene-free 1,2-dimethoxyethane (see **Section 3.2.1**). Crystallographic parameters and details of data collection have been summarized in **Table 3.5**. A complete compilation of bond lengths and bond angles as well as characteristic torsion angles is given **Table 8.4.1**. As already pointed out in **Section 3.3.2**, complex **II** in (**2II·*n*-C_6H_{14}**) does not show any sign of disorder with respect to the unsubstituted skeleton of the chelate ligand. Therefore, the hydrogen atom of the amido group could be detected experimentally.

The two η^5-pentamethylcyclopentadienyl substituents are bound to the zirconium metal, with Zr–Cp (centroid) distances of 224.7 and 224.3 pm are compare very well with those of other $Cp_2Zr(IV)$ complexes [107, 108].

Even a short look through the data compiled in **Table 3.7** indicates a rather complicated bonding situation within the chelate ring of compound **II**. In contrast to the structure of [bis{(*N*-trimethylsilyl)iminobenzoyl}phosphanid-*N*,*N*′](1,2-dimethoxyethane-*O*,*O*′)lithium (**3.7**) which due to the pioneering work of *U. Hübler* née *Seidl* [39] shows almost identical P–C {180.9(5) and 180.1(5) pm}, C–N {130.1(6) and 132.3(6) pm} and N–Li distances {202.9(9) and 202.3(9) pm} in both P–C–N–Li entities, the analogous bond lengths of **II** differ to a considerable degree. At the P=C–N(H) side, the P=C distance {176.9(2) pm} is elongated and the C–N distance {131.9(3) pm} considerably shortened in comparison to the standard values of a double (128 pm) and a single bond (145 pm), respectively. Such a strong

bond order equalization is indicative of efficient π–delocalization within the 2-amido-1$\lambda^3\sigma^2$-phosphaalkene fragment. It is by far stronger than in an 1-*tert*-butyl-2-dimethylamino-1$\lambda^3\sigma^2$-phosphaalkene (**2.4**) for which the following bond lengths have been determined at low temperature: P=C 170.4(2), C–N 134.8(2), N–CH_3 144.5(3) and 145.3(3), P–C(^{t}Bu) 188.6(2) pm [30]. A slightly higher degree of bond order equalization is realized for *N*,*P*-bis(*tert*-butyldiphenylsilyl) substituted **(*Z*)-I.2** {P=C 172.7(2), C–N 137.4(2) pm, **Table 2.6** in **Section 2.3.3**}. In that respect, the strong π–delocalization in the P=C–N(H) entity of complex **II** might be a consequence of the negatively charged amido group.

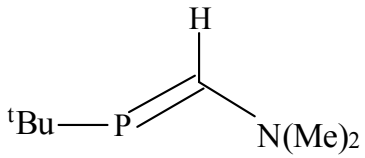

2.4

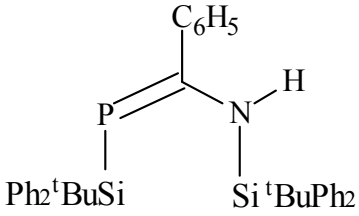

(*Z*)-I.2

Table 3.7 Selected bond distances (pm) and bond angles (deg), for **[**(1-amido-3-imido-1,3-diphenyl-2$\lambda^3\sigma^2$-phospha-1-propene-*N*,*N*′)bis(η^5-penta- methylcyclopentadienyl)zirconium]–*n*-hexane (2 / 2 x 0.5) (≙ **2II· *n*-C_6H_{14}**)
M_{Cp3}, M_{Cp5} : centres of the η^5-pentamethylcyclopentadienyl ligands

a) Distances

chelate ligand at zirconium						
	n = 1	*n* = 2				
Zr–N*n*	221.2(2)	199.6(2)	N1–H1	92.0(3)	Zr···M_{Cp3}	224.7(3)
N*n*–C*n*	131.9(3)	128.1(3)	C1···C2	282.5(2)	Zr···M_{Cp5}	224.3(2)
P–C*n*	176.9(2)	183.5(2)	N1···N2	275.6(2)		
C*n*–C*n*1	150.5(3)	150.2(3)				

b) Bond angles

chelate ligand at zirconium					
	n = 1	*n* = 2		*n* = 1	*n* = 2
M_{Cp3}···Zr···M_{Cp5}	139.2	—	N*n*–C*n*–P	131.1(2)	122.5(2)
N*n*–Zr···M_{Cp3}	104.0	106.4	N*n*–C*n*–C*n*1	116.9(2)	120.9(2)
N*n*–Zr···M_{Cp5}	103.8	106.7	P–C*n*–C*n*1	112.0(2)	116.6(2)
N1–Zr–N2	81.7(2)	—	C*n*1–P–C2	103.2(1)	—
Zr–N*n*–C*n*	133.0(2)	148.5(2)			

a)

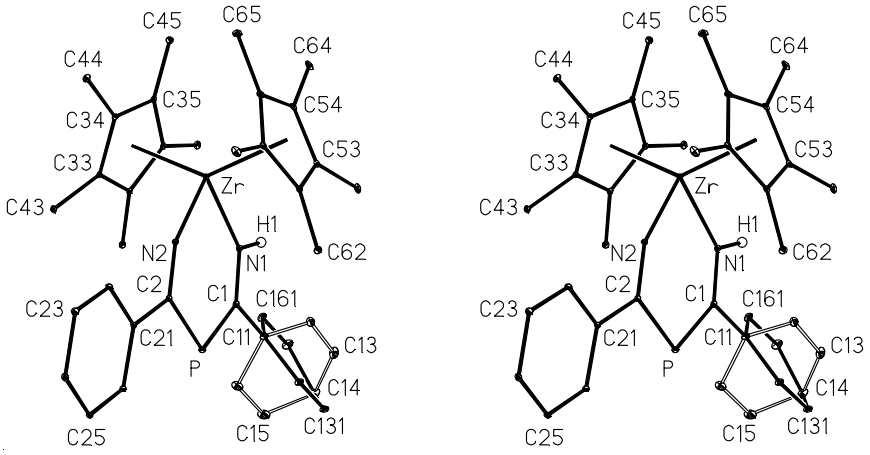

b)

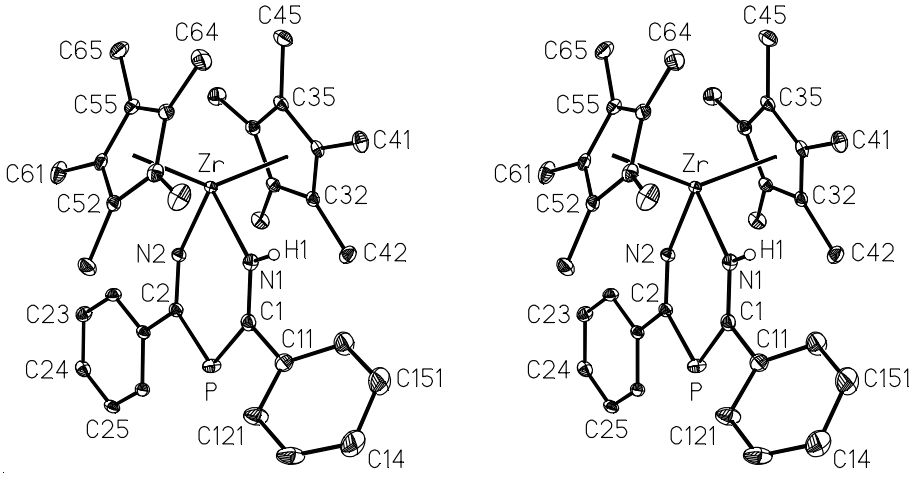

Figure 3.9 Structure of the two components of the solid state adduct [*N*,*N*′-(1-amido-3-imido-1,3-diphenyl-2$\lambda^3\sigma^2$-phospha-1-propene)]bis(η^5-pentamethylcyclopentadienyl)zirconium–*n*-hexane (1 / 0.5) (≙ **2II·*n*-C_6H_{14}**) in stereoscopic view
Except for the N–H unit all hydrogen atoms are omitted for clarity. Absent atom numbering has to be complemented in a logical manner.
a) Complex molecule **(II)**. Displacement ellipsoids are of 3% probability. The phenyl substituent with the carbon atoms C1*m*.. (m = 1→ 6) is found to be disordered.
b) Complex molecule **(II)**. Displacement ellipsoids are of 30% probability. With regard to the disordered phenyl substituent C1*m*... (m = 1→ 6) only the conformer with carbon atoms of the higher occupancy factor of 0.524 is depicted.

In the P–C=N entity, however, the bonding situation is found to be completely different in that the P–C distance of 183.5 and the C=N distance of 128.1 pm do not deviate significantly from the standard values of a P–C single and a C=N double bond. Very surprisingly, the general distribution of bond lengths agrees fairly well with that determined for the enole tautomers of 1-[*N*-(trimethylsilyl)iminobenzoyl]-2-phenyl-2-[*N*-(trimethylsilyl)amino]-1$\lambda^3\sigma^2$-phosphaalkene (**3.8**) and of 1-(2,4,6-trimethylbenzoyl)-2-amino-2-phenyl-1$\lambda^3\sigma^2$-phospha-

alkene (**3.5**). This similarity provides a reason to regard the chelate ligand of complex **II** as carboxylic acid derivative of a 2-amino-1$\lambda^3\sigma^2$-phosphaalkene and to use the alternative name "2-amido-1-(imidobenzoyl)-2-phenyl-1$\lambda^3\sigma^2$-phosphaalkene".

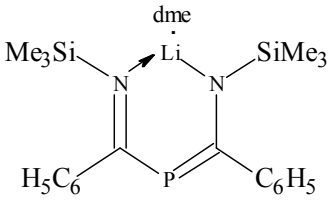

3.7

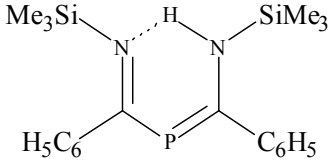

3.8

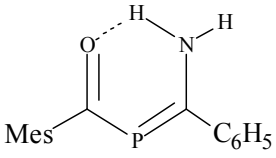

3.5

Mes = $C_6H_2Me_3$-2,4,6

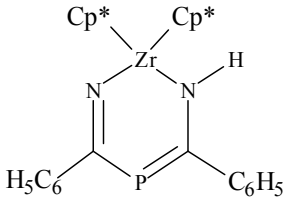

II

According to a literature survey, the Zr–N distances are distributed into three typical sections, even if sometimes a small area of overlap can be observed. The shortest Zr–N distances were reported for compounds of the *Type I* in which an organylimido group is attached to a thf-complexed zirconocene entity (see below). The first publication comes from *Bergman* and co-workers [95] who in 1993 used bulky substituents such as *N*-*tert*-butyl or *N*-2,6-dimethylphenyl for kinetic stabilization. In their intention to study metathesis reactions of ketimines, the authors started with dimethylzirconocene, converted it with *tert*-butylamine into (*tert*-butylam- ido)methylzirconocene and eliminated methane at +85 °C to afford $(\eta^5\text{-}C_5H_5)_2Zr(thf)=N^tBu$. A further method of preparation has been introduced by exchanging e.g. the bulky *tert*-butylimido for the less bulky *p*-tolylimido group. In this case dimerization is prevented by increasing the bulk of at least one cyclopentadienyl ligand by its pentamethyl analogue [96]. distances of 182 to 188 pm have been reported for the Zr=N double bond and the Zr–N–C(R) sequence is found to be almost linear (168° to 175°).

Compounds of *Type II* come from the research group of *Lappert* [97] and some years later from *Erker* and co-workers [98, 99]. They comprise zirconocene complexes with one or two alkylideneamido ligands bound to the central metal atom. As early as 1971, *Lappert* et al. published the preparation of $[(\eta^5\text{-}C_5H_5)_2Zr(Cl)\{N=C(C_6H_5)_2\}]$ and $[(\eta^5\text{-}C_5H_5)_2Zr\{N=C(C_6H_5)_2\}_2$ from $(\eta^5\text{-}C_5H_5)_2ZrCl_2$ and one or two equivalents of lithium (diphenylmethylidene)amide [97]. Alternatively, in an exchange reaction two dimethylamido groups at the zirconium centre might be replaced by diphenylmethylideneamido substituents. *Erker* and co-workers applied more sophisticated synthetic routes [98, 99]. The complex $(\eta^5\text{-}C_5H_5)_2Zr(Cl)N=CHC_6H_5$ was stereospecifically obtained via a hydrozirconation of benzonitrile with $(\eta^5\text{-}C_5H_5)_2Zr(H)Cl$. *Lappert's* compound $(\eta^5\text{-}C_5H_5)_2Zr\{N=C(C_6H_5)_2\}_2$ could additionally be prepared by photolysis of either $(\eta^5\text{-}C_5H_5)_2Zr(C_6H_5)_2$ or $(\eta^5\text{-}C_5H_5)_2Zr(CO)_2$ in

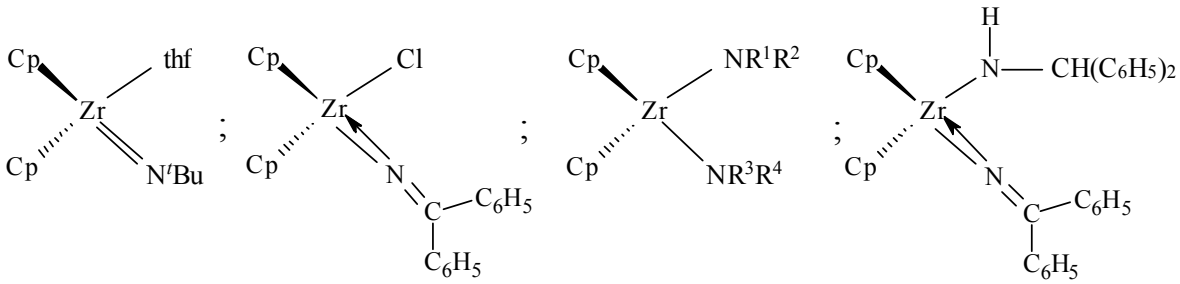

Type I *Type II* *Type III* *Type II / Type III*

the presence of benzophenone azine $(H_5C_6)_2C{=}N{-}N{=}C(C_6H_5)_2$ [99]. The research group of *Hey-Hawkins* [102] achieved the synthesis and isolation of an analogous complex via the insertion of acetonitrile into the Zr–P bond of {(η^5-$EtMe_4C_5)_2$Zr(Cl)P(H)Cy (Cy = cyclohexyl)}. A very slow elimination of the P(H)Cy radical converted (η^5-$EtMe_4C_5)_2$Zr(Cl)N=C(CH_3)-P(H)Cy isolated first, into [(η^5-$EtMe_4C_5)_2$Zr(Cl)N=C(CH_3)-]$_2$. The Zr–N(=C) distances of *Type II* complexes fall into a narrow range from 200 to 206 pm, in other words these bond lengths are intermediate between those of a Zr=N double and a Zr–N single bond. The sequence Zr–N=C is almost linear; the N=C distances show values between 125 and 126 pm.

Henderson and co-workers [100] attributed the short Zr–N bond length (200.7 pm) and almost linear Zr–N–C arrangement in the zirconocene ketimide complexes [Cp_2Zr(Cl)N=C(^{t}Bu)CH_3] and Cp_2Zr(Cl)N=C(^{t}Bu)Ph [101] as well as in the zirconocene amide Cp_2Zr(Cl)N(CH_2Ph)$_2$ to the efficient π-overlap between the acceptor orbital on the zirconium and a filled donor orbital on the nitrogen atom.

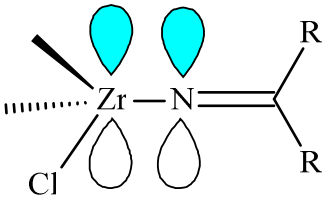

Segerer et al. explained also the short Zr–N bond length of 202.9(2) pm in the zirconocene complex (*Z*)-[$Cp^{\circ}{}_2$Zr(Cl){N=C(Me)(PHCy)}] by a similar nitrogen zirconium interaction which is facilitated by almost linear arrangement (174.2°(2)) of the Zr–N–C fragment [102]. Finally, the *Bergman* group assumed that the longer Zr–N in CpCp*(thf)Zr=N–^{t}Bu (184.6 pm) compared to Cp_2(thf)Zr=N–^{t}Bu (182.6 pm) is attributed to the fact that the Cp* substituent counteracts the π–donating ability of the imido group and induced therefore a slight reduction in the Zr–N bond order.

In complexes of *Type III*, one or two diorganylamino substituents are connected with the bis(η^5-cyclopentadienyl)zirconium fragment via single bonds. For the $(\eta^5\text{-}C_5H_5)_2Zr\text{–}NR_2$ entity, *Henderson*, *Mulvey* and co-workers [100] reported in 2000 the determination of a mean Zr–N single bond distance using the Cambridge Structural Database [103] and obtained a value of typically 216 pm, at least as they argued. From a series of different examples, however, it can safely be assumed that the Zr–N single bond may vary considerably in length. The authors themselves published a very short distance of merely 206.8 pm for $(\eta^5\text{-}C_5H_5)_2Zr(Cl)N(CH_2C_6H_5)_2$ which is already very near to the typical values of *Type II* complexes. Studies of *Bergman* and others [96] reveal Zr–N bond lengths of 209.3(4) and 209.1(4) pm for the diazametallacycle $(\eta^5\text{-}C_5H_5)_2Zr\{N(C_6H_4Me\text{-}4)\}_2CHC_6H_5$; the dinuclear complex $(\eta^5\text{-}C_5H_5)_2Zr\{N(C_6H_4{}^t\!Bu)\text{-}4\}_2\text{-}Zr(\eta^5\text{-}C_5H_5)_2$ which is the dimer of the corresponding imido compound, shows almost identical values of 209.3(2) and 209.8(2) pm [95]. The situation, however, becomes extremely bewildering when two Zr–N single bonds of strongly differing lengths are present in the same complex. This, for example, is the case with $(\eta^5\text{-}C_5Me_5)(\eta^5\text{-}C_5H_5)Zr\{N(H){}^t\!Bu\}\{N(C_6H_5)\text{–}C(C_6H_5)=CH_2\}$ which shows values of 207.0(3) and 223.9(2) pm for Zr–N(H)^{t}Bu and Zr–N(C_6H_5), respectively [96]. In order to explain this phenomenon, *Bergman* et al. stated that the elongation might be attributed to a delocalization of the nitrogen lone pair into the π-system of the eneamido ligand.

Another compound which has to be attributed to *Type II* as well as *Type III* complexes has been reported by *Rosental* and others [104] from [η^2-bis(trimethylsilyl)ethyne]bis(η^5-cyclopentadienyl)(pyridine)zirconium and benzophenone imine in *n*-hexane at ambient temperature. After 5 h orange-red needles were isolated in 93% yield. An X-ray structure analysis resulted in Zr–N distances of 204.3(3) and 208.9(3) pm for the Zr–N(=C) and Zr–N(H) bond, respectively. At 125.7(5) pm the length of the N=C double bond is as to be expected. Whereas the Zr–N=C angle is found to be almost linear (170.4(3)°), the second Zr–N(H)–C angle has a value of 138.5(3)° only.

The chelate ring of compound **II** shows a Zr–N(H)–C and Zr–N=C fragments and must therefore likewise be considered as a mixed *type-II*/*type-III* complex. But in contrast to the aforementioned examples, the Zr–N=C unit is no longer linear but – with a nitrogen valence angle of only 148.5(2)° – significantly bent. A literature survey produced three chelate complexes with similar structures but only for the last one bond lengths and bond angles have been published (see below).

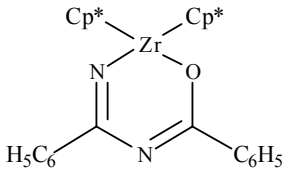

3.10

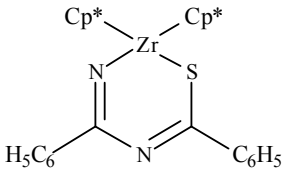

3.11

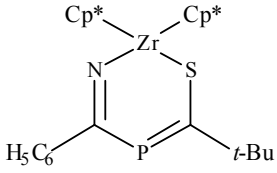

3.14

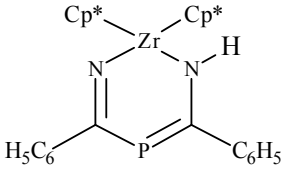

II

α) Bis(η^5-pentamethylcyclopentadienyl)[(3-imido-1-oxido-1,3-diphenyl-2-aza-1-propene)-*N*, *O*]zirconium (**3.10**) was prepared by *Bergman* and co-workers [87, 105] from bis(η^5-pentamethylcyclopentadienyl)hydroxyphenylzirconium and benzonitrile at 160 °C in a Pyrex bomb using benzene as solvent. The intermediate $Cp^*_2Zr{=}O$ was not isolated and underwent a rapid [2+2+2]-cycloaddition. After 24 h, the reaction mixture was worked up as usual; compound **3.10** precipitated at −40 °C from diethylether in large yellow rodlike crystals. An X-ray structure determination showed disorder of oxygen and nitrogen atoms at zirconium to the same positions so that due to disorder reliable Zr–N and Zr–O bond lengths were not accessible. Unfortunately, the structure of the bis(*tert*-butyl) derivative prepared in benzene from bis(η^5-pentamethylcyclopentadienyl)zirconiumhydroxidetrifluoromethylsulfonate, potassium bis(trimethylsilyl)amide and trimethylacetonitrile, has not been determined [88].

β) Bis(η^5-pentamethylcyclopentadienyl)[(3-imido-1,3-diphenyl-1-sulfanido-2-aza-1-propene)*N*,*S*]zirconium (**3.11**) was also synthesized by *Bergman* et al. as the sulphur derivative of the aforementioned complex **3.10** [105]. They started with (η^5-pentamethylcyclopentadienyl)zirconium iodidesulfanide and treated its benzene solution with potassium bis(trimethylsilyl)amide in the presence of benzonitrile. Again the intermediate — now $Cp^*_2Zr{=}S$ — underwent a [2+2+2]-cycloaddition to give complex **3.11**. Orange-yellow crystals precipitated from a solvent mixture of benzene and *n*-hexane but unfortunately their structure was not determined.

γ) Bis(η^5-pentamethylcyclopentadienyl)[(1-*tert*-butyl-3-imido-3-phenyl-1-sulfanido-2$\lambda^3\sigma^2$-phospha-1-propene)]zirconium (**3.14**). As reported by *Nixon* et al. [106] the complex $Cp^*_2Zr(py){=}S$ already discussed above, reacts in toluene with *tert*-butyl-1$\lambda^3\sigma^2$-phosphalkyne to yield the four-membered heterocycle $Cp^*_2Zr[–S–C(^t\text{Bu})=P–]$ in 61% yield. Subsequent addition of benzonitrile to a toluene solution of this compound at ambient temperature led to the formation of **3.14**. After 48 h all volatiles were removed and red crystals suitable for an X-ray structure determination were obtained from toluene at −30 °C.

Apart from the sulfur atom in the chelate ring of complex **3.14** which replaces the NH-group in compound **II**, both structures are almost identical. As can be taken from a comparison of bond lengths and bond angles (**Table 3.8**), especially the Zr–N(=C) (199.6 for **II** *vs* 198.8 pm for **3.14**), N=C (128.1 *vs* 128 pm) and P–C distances (183.5 *vs* 185 pm) differ by about 1% only. A larger deviation is observed for the P=C double bond distance; a value of 176.9 pm for **II** and 170 pm for **3.14** indicate only weak π-conjugation in the S–P=C but a strong one in the N(H)–P=C fragment.

Table 3.8 Comparison of characteristic bond lengths (pm) and bond angles (°) of the structurally similar complexes **II** and **3.14** [106]

Bond/angle	**II**	bond/angle	**3.14**
Zr–N	199.6(2)	Zr–N	198.8(1)
Zr–N(H)	221.2(2)	Zr–S	258.5(3)
N(H)–C	131.9(2)	S–C	175(1)
N=C	128.1(3)	N=C	128(1)
P=C	176.9(2)	P=C	170(1)
P–C	183.5(2)	P–C	185(1)
N–Zr–N(H)	81.7(2)	N–Zr–S	82.3(3)
Zr–N(H)–C	133.0(2)	Zr–S–C	116.3
(H)N–C=P	131.1(2)	S–C=P	132.9(8)
C=P–C	103.2(1)	C–P=C	107.7
P–C=N	122.5(2)	P–C=N	123.1(9)
C=N–Zr	148.5(2)	C=N–Zr	157.0

With all of this in mind, the presence of two significantly different Zr–N bond lengths in complex **II** can be attributed to difference in the interaction between the acceptor orbital on the zirconium with the filled π-donor orbitals on the two nitrogen atoms. In other words, the Zr–N1 bond length of 221.2 pm indicates that the π-interaction between zirconium and the nitrogen atom N1 is weak or completely absent and the nitrogen lone pair is therefore available for the delocalization over the P=C–NH entity. The short Zr–N2 bond (199.6 pm) indicates, however, the presence of strong π-interaction although the Zr–N2–C2 angle is 148.5°. This effect can be explained if one assumes donation from the C=N π-orbital to zirconium, which is perfectly in accord with the absence of π-delocalization in this part of the chelate ligand. Consequently the bonding in complex **II** may be represented by superposition of the canonical **II-A→II-D** of which **II-A** to **II-C** yield probably the dominating bonding contributions (see below).

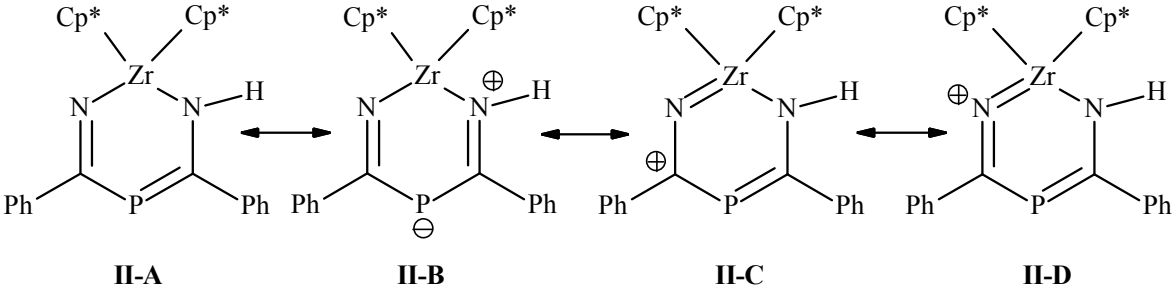

To exclude, however, even a slight superposition of the two sides of the chelate ligand, quantumchemical DFT calculations with the functional B3LYP were performed (Prof. Dr. M. Niemeyer, Universität Mainz). To reduce computation time, the voluminous pentamethylcyclopentadienyl ligands were substituted by ordinary cyclopentadienyl rings. Further details concerning the calculation are discreibed in the experimental section. The results of quantum chemical calculations for the model compound (**II**$_{Mod.}$) $Cp_2Zr\{N{=}C(C_6H_5)P{=}C(C_6H_5)NH\}$ and for the doubly negatively charged chelate ligand $\{N{=}C(C_6H_5)P{=}C(C_6H_5)NH\}^{-2}$ are summarized in **Table 3.9**. To our surprise the agreement between experimentally determined and calculated molecular parameters is found to be within the scope of expectation. The largest deviations between experiment and calculation are of 2.2 and 3.4 pm in the C–N(H) {131.9 *vs* 134.1 pm} and the Zr–N(=C) {199.6 *vs* 196.2 pm} bond.

Quantum chemical calculations yield not only bond lengths and bond angles but also the so-called Wiberg bond indices which allow to estimate the strength of a bond. In accordance with the discussion on bond lengths given above, Wiberg bond indices (**Table 3.9**) of 1.29 and 1.04 for the P=C and P–C distances indicate that the character of the double bond (177.9 pm) in the P=C–N(H) entity is strongly reduced whereas the strength of the P–C bond (184.4 pm) in the P–C=N entity corresponds to that of a single bond. A similar pattern is found for both the C–N bonds of the chelate ring: Wiberg indices of 1.41 in the P=C–N(H) and 1.62 in the P–C=N entity indicate a strongly shortened single bond (134.1 pm) and a slightly weakened double bond (128.4 pm). The absence of a bond order equalization is also found for the N–Zr–N entity. At values of 221.2 pm for Zr–N(H) and 199.6 pm for Zr–N(=C) both bond lengths differ by more than 10 percent. The corresponding Wiberg indices of 0.49 and 1.1, respectively, reveals a remarkable weakened Zr–N(H) single bond and a slightly shortened Zr–N(=C) single bond. An interpretation of this is feasible in connection with a comparison with relevant Zr–N distances of already published compounds.

Table 3.9 Characteristic bond lengths (pm), angles and dihedral angles (°) in the solid state adduct **2II·*n*-C_6H_{14}** and DFT-calculated parameters (pm, °)a) for the model compounds $Cp_2Zr\{N{=}C(C_6H_5)P{=}C(C_6H_5)NH\}$ (**$II_{Mod.}$**) and $\{N{=}C(C_6H_5)P{=}C(C_6H_5)NH\}^{-2}$ (**L^{-2}**)

	(**2II·*n*-C_6H_{14}**)	**$II_{Mod.}$**	**L^{-2}**
Zr–N1	221.2(2)	221.9[0.489]	
Zr–N2	199.6(2)	196.2[1.085]	
N1–C1	131.9(3)	134.1[1.409]	133.4[1.501]
N2–C2	128.1(3)	128.4[1.623]	123.9[2.163]
N1–H1	92	102.2[0.802]	102.6[0.878]
P–C1	176.9(2)	177.8[1.287]	179.1[1.269]
P–C2	183.5(2)	184.4[1.049]	200.2[0.785]
Zr···M_{Cp3}	224.7	228.2	
Zr···M_{Cp5}	224.3	228.5	
C1–C11	150.3(3)	150.1[1.039]	149.8[1.059]
C2–C21	150.2(3)	150.0[1.045]	152.0[0.971]
C1···C2	282.5(2)	283.6	
N1···N2	275.6(2)	273.3	
C1–P–C2	103.2	103.1	111.4
N2–C2–P–C1	−0.9	0.7	−118.2
P–C1–C11–C161	141.9	131.8	133.4
P–C1–C21–C26	−4.9	−7.9	−45.9

a) Wiberg bond indices are given in brackets

3.3.5 Packing of Both Components of the Solid State Adduct (2II·n-C_6H_{14})

Figures 3.10 and **3.11** depict stereoscopic views of the crystal packing; no intermolecular contacts significantly shorter than the *van der Waals* distances were found.

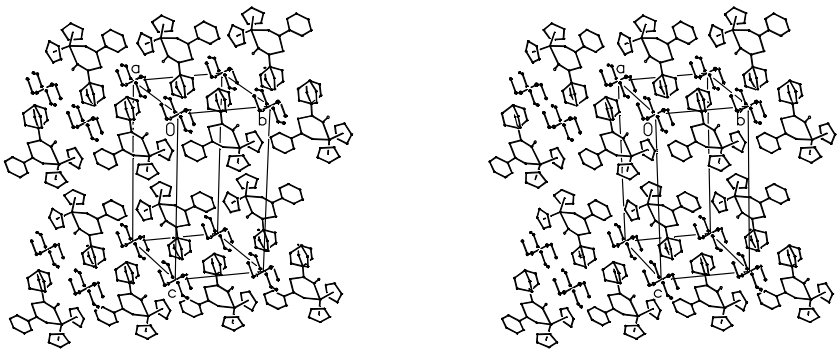

Figure 3.10 Structure of (**2II·*n*-C_6H_{14}**)** in stereoscopic view

The simplified figure depicts the arrangement of complex and solvent molecules. Both are disordered in that one of the two phenyl substituents of the 1-amido-3-imido-1,3-diphenyl-$2\lambda^3\sigma^2$-phospha-1-propene ligand at zirconium and the centrosymmetric *n*-hexane molecule each occupy two positions. For clarity, methyl groups of the η^5- pentamethylcyclopentadienyl substituents and all hydrogen atoms except that of the N−H unit have been omitted. Thermal ellipsoids are of 30% probability.

The complex molecules are arranged in (001) layers which by centres of inversion e.g. in (0, 0, 0) or (0.5, 0.5, 0) are combined to double layers (**Figure 3.10**). Whereas the η^5-pentamethylcyclopentadienyl substituents and the not disordered phenyl groups build up the upper and lower slab of the double layer, the disordered phenyl substituents and the disordered *n*-hexane molecules in cavities of the structure are located in between. The solvent molecules are surrounded by four disordered phenyl substituents but attempts to correlate the different positions of the two species according to their slightly differing occupancy factors have failed.

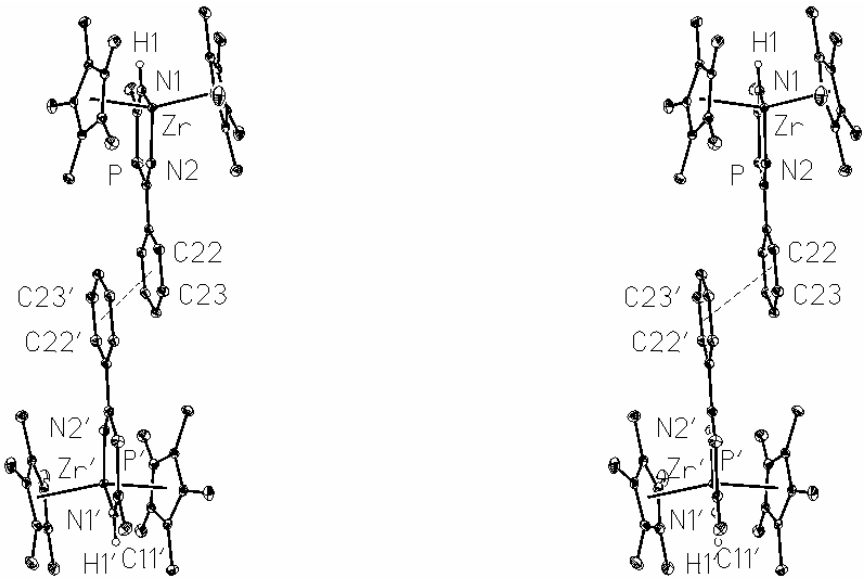

Figure 3.11 Arrangement of complex molecules of two different double layers in the structure of (**2II·*n*-C_6H_{14}**)
Thermal ellipsoids are at 30% probability; except for the NH-groups all hydrogen atoms have been omitted for clarity; only the *ipso*-carbon atom C11 and C11′ of the phenyl group at C1 and C1′ are depicted. In view of a separation of 362.3 pm (dashed Line) between the centres of the two inverse phenyl substituents C2m and C2m' (m = 1→ 6) an electronic π–π interaction can be assumed.

Finally, to perceive if there is an electronic π–π interaction between the centres of the two inverse phenyl substituents of two different double layers, the distance between the two centres was measured. At 362.3 pm separation distance between them, an electronic π–π interaction can be assumed (**Figure 3.11**).

4 Reaction of (1,2-Dimethoxyethane)lithium Phosphanide with Different Diorganylcarbodiimides

4.1 *Introduction*

To date, beside the reactions of (1,2-dimethoxyethane)lithiumphosphanide with pivalo- and benzonitrile also its reaction with an equimolar amount of *N*,*N*′-bis(trimethylsilyl)carbodiimide has been studied [109]. This reaction proceeded via trimethylsilyl/lithium exchange to yield a mixture of phosphane and tris(trimethylsilyl)phosphane together with a lithium cyanomethylsilylamide which was isolated and characterised by a single-crystal X-ray diffraction study.

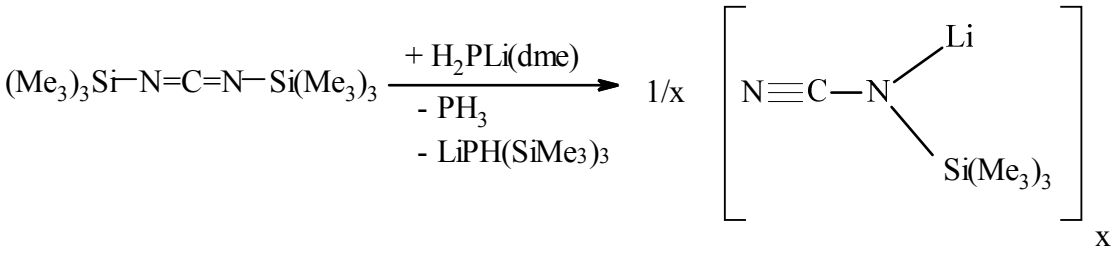

Probably, the presence of a good leaving group (trimethylsilyl) at the nitrogen atom facilitates the exchange process. The question in our mind was what would happen if we use diorganylcarbodiimides (which lack a good leaving group) instead of *N*,*N*′-bis(trimethylsilyl)carbodiimide?. In this chapter, the reactions of some diorganylcarbodiimide with (1,2-dimethoxyethane)lithiumphosphanide will be studied in detail in order to answer this question. Prior to a presentation of the results of these studies, we will shed some light on similar reactions found in the literature.

Issleib et al. were one of the first groups involved in the preparation of neutral phospha(III)guanidines; they reported that addition of trialkylsilyl-phosphanes to diphenylcarbodiimide yields, depending on the nitrogen substituents, either silylated phospha(III)guanidines or isomeric phosphaalkenes [110].

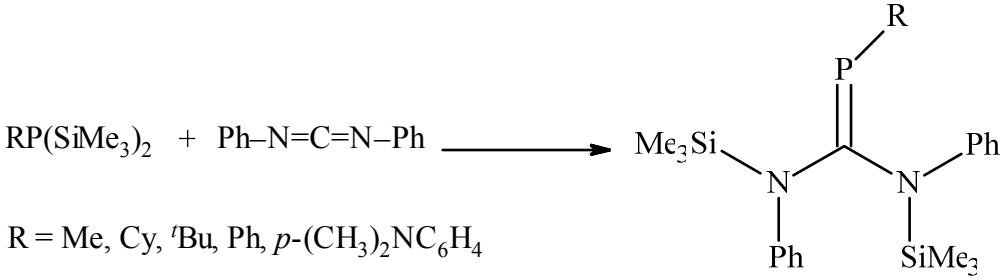

However, *N*,*N*′-dialkyl or *N*-alkyl-*N*′-aryl substituted phosphaguanidines could not be obtained in this way because the less electrophilic *N*,*N*′-dialkyl or *N*-alkyl-*N*′-aryl carbodiimides did not accept nuecleophilic attack of a phosphane [111]. However, amides of the alkali metals (M = Li, Na or K) or the amides of the heavier group two elements (M = Ca, Sr or Ba) can effectively catalyze the addition of phosphane P–H bonds to carbodiimides [111 - 113]. Another route to prepare neutral phosphaguanidines involves the reaction of *in situ* generated phosphanides (via deprotonation of secondary phosphines) with carbodiimides followed by protolysis of the resulting phosphaguanidinate anion [114,115.21,77]. In fact, most of the neutral phosphaguanidines were prepared by this way; for example, *Coles* and co-workers synthesized in 2002 a phosphaguanidinate complex $Li(Ph_2PC\{N^iPr\}_2)(THF)_2$ and reacted it with $[HNEt_3]Cl$ to produce the neutral phosphaguanidine $Ph_2PC(=N^iPr)(NH^iPr)$ [114]. One year later, $Ph_2PC(=NCy)(NHCy)$ was isolated using the same procedure [21].

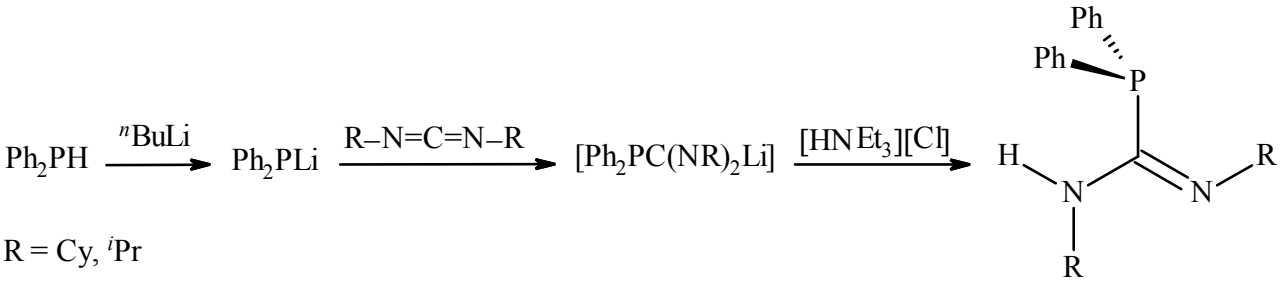

With different substituents at nitrogen atoms, *Jones* and co-workers could isolate two new phosphaguanidines $R_2PC(=NAr)N(H)Ar$ (R = Ph or cyclohexyl, Ar = 2,6-$^iPr_2C_6H_3$) from the reaction of R_2PLi with Ar–N=C=N–Ar followed by aqueous work-up [115]. Phosphaguanidines can be also obtained from the reaction of *tert*-butylamine with the phosphaazaallene ^tBu–P=C=N–^tBu between 25 °C and 35 °C. [116-118].

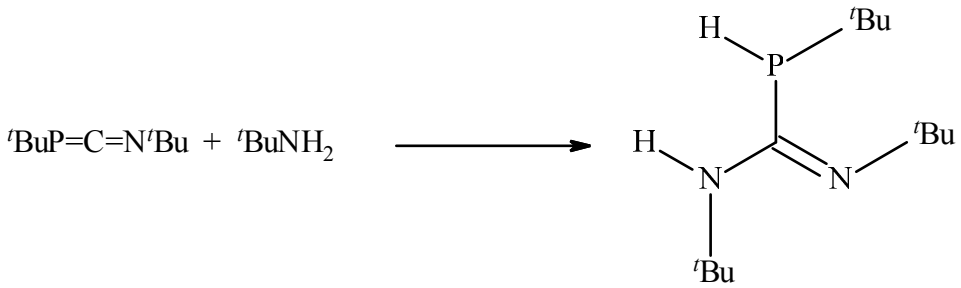

Another route to prepare phosphaguanidines involves the reaction of sodium phosphanides RPHNa (R = Ph, Mes**)** with the imidinium salt $[EtO\text{-}C(N(CH_3)_2)_2]BF_4$ [119].

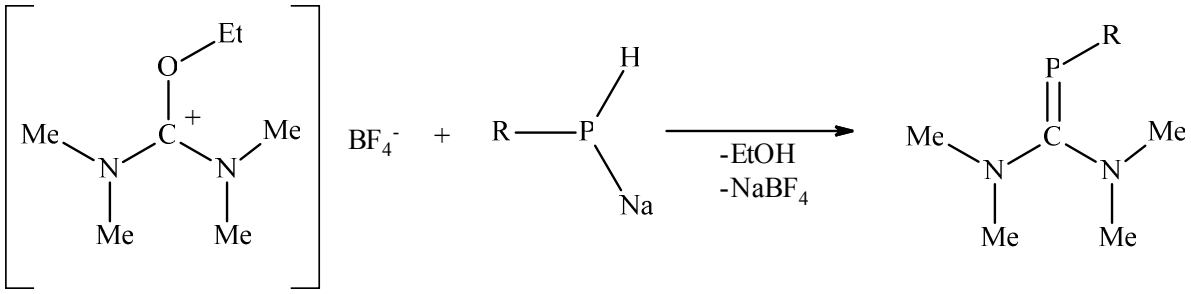

Furthermore, several neutral phosphaguanidines could be generated from the reaction of *α*,*α*-dihalo amines and silylated phosphanes, under elimination of trimethylsilyl halides [120-122]. In contrast to the large number of neutral phosphaguanidines found in literature, few examples of negatively charged phosphaguanidinates were reported. These examples include the dimeric complex $[Li(Ph_2PC\{N^iPr\}_2)(THF)]_2$ reported by *Coles* et al. which was prepared by addition of a THF solution of "Ph_2PLi" to ^{i}Pr–N=C=N–^{i}Pr or by deprotonation of the corresponding neutral phosphaguanidine with *n*-butylithium; displacement of the coordinated THF with tetramethylethylendiamine (TMEDA) to afford the monomeric complex $Li(Ph_2PC\{N^iPr\}_2)(TMEDA)$ [19].

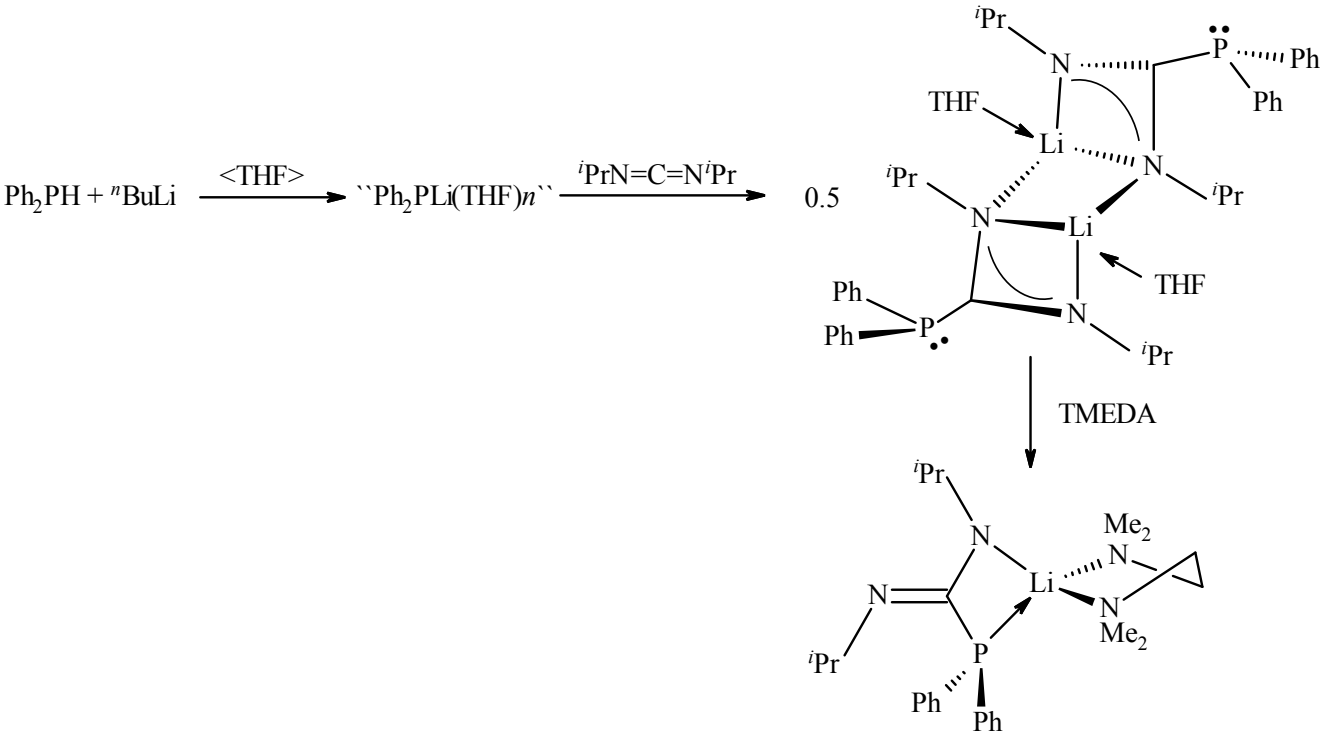

Also the calcium phosphaguanidinates $[(THF)_2Ca\{Ph_2PC(NR)_2\}_2]$ (R = ^{i}Pr or cyclohexyl) were synthesized from the reaction of $[(THF)_2Ca(PPh_2)]$ with the corresponding carbodiimides [123]. A new and completely unexpected access to phospha(III)guanidinates was demonstrated by *Goicoechea* and co-workers, they treated the hydrogen heptaphosphide

dianion $[HP_7]^2$ with a range of bulky carbodiimides to give the *exo*-functionalized cluster anions $[P_7C(NHR)(NR)]^{2-}$ (R = Dipp, ^{i}Pr and Cy) in one step [124]. Further reaction of $[P_7C(NHDipp)(NDipp)]^{2-}$ with proton sources such as $[NH_4][BPh_4]$ or $[H(OEt_2)_2][BAr^F{}_4]$ affords the protonated monoionic compound $[HP_7C(NHDipp)(Ndipp)]^-$.

4.2 *Reaction of (1,2-dimethoxyethane)Lithium Phosphanide with Bis(4-methylphenyl)carbodiimide*

4.2.1 *Preparation and Reaction Mechanism*

To a solution of (1,2-dimethoxyethane)lithium phosphanide ((dme)Li–PH_2) in 1,2-dimethoxyethane an equimolar amount of bis(4-methylphenyl)carbodiimide dissolved in the same solvent was added dropwise at −70 ºC. The reaction mixture was stirred overnight and allowed to warm up slowly to ambient temperature. A change from colourless to green-yellow indicates the completion of the reaction. Green-yellow crystals of the complex [bis(1,2-dimethoxyethane)-1κ^2O^1,O^2;2κ^2O^3,O^4]{bis[μ-*N*,*N*′-bis(4-methyl-phenyl)}-*C*-phosphanylformamidinato]-1:2κ^4-N^1,N^2;1κ^2N^3;N^4}dilithium (**III**) precipitated immediately on the wall of the flask after the solvent had been reduced to one third of its original volume under reduced pressure. Compound **III** was isolated as a dimer in an excellent yield approaching 98%.

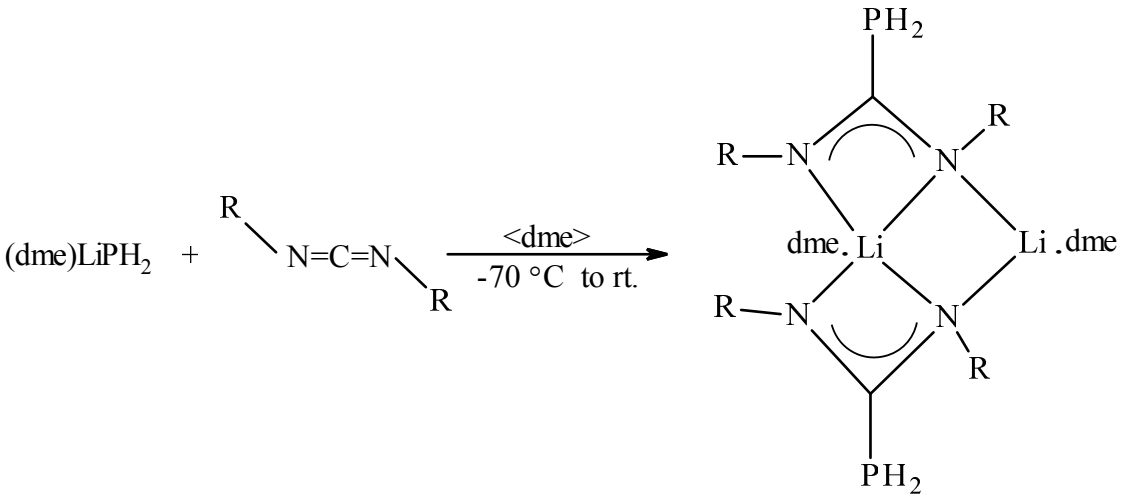

R = 4-methyl-phenyl **III**

The reaction proceeds presumably via nuecleophilic attack of the phosphanide anion at the *sp*-hybridized carbon atom of the carbodiimide. A single-crystal X-ray diffraction study revealed that one lithium cation is coordinated by a dme-ligand and the four nitrogen atoms of the bidentate monophosphaguanidinate anions to accomplish a coordination number of six. A second lithium cation binds to another dme-ligand and two nitrogen atoms from different phosphaguadinate entities to assume a coordination number of 4. The whole assembly can formally be described as a "lithium lithiate".

The formation of the dimeric complex **III** can be best explained by discussing a paper published by *Mews* and co-workers on the synthesis and structural characterisation of various lithium fluoroarylamidinato complexes with different coordination modes [129]. To understand the structural variety of the dimeric complexes the authors assumed that these complexes were generated from a monomeric complex [$RC(NR')_2Li.2D$] (**Scheme 4.1**) by loss of one donor molecule from each lithium centre. They suggested that initially an asymmetric ladder-type dimer (**b**) is formed in which both ligands occupying three coordination sites (with N11, N21 being monodentate, N12,N22 bidentate).

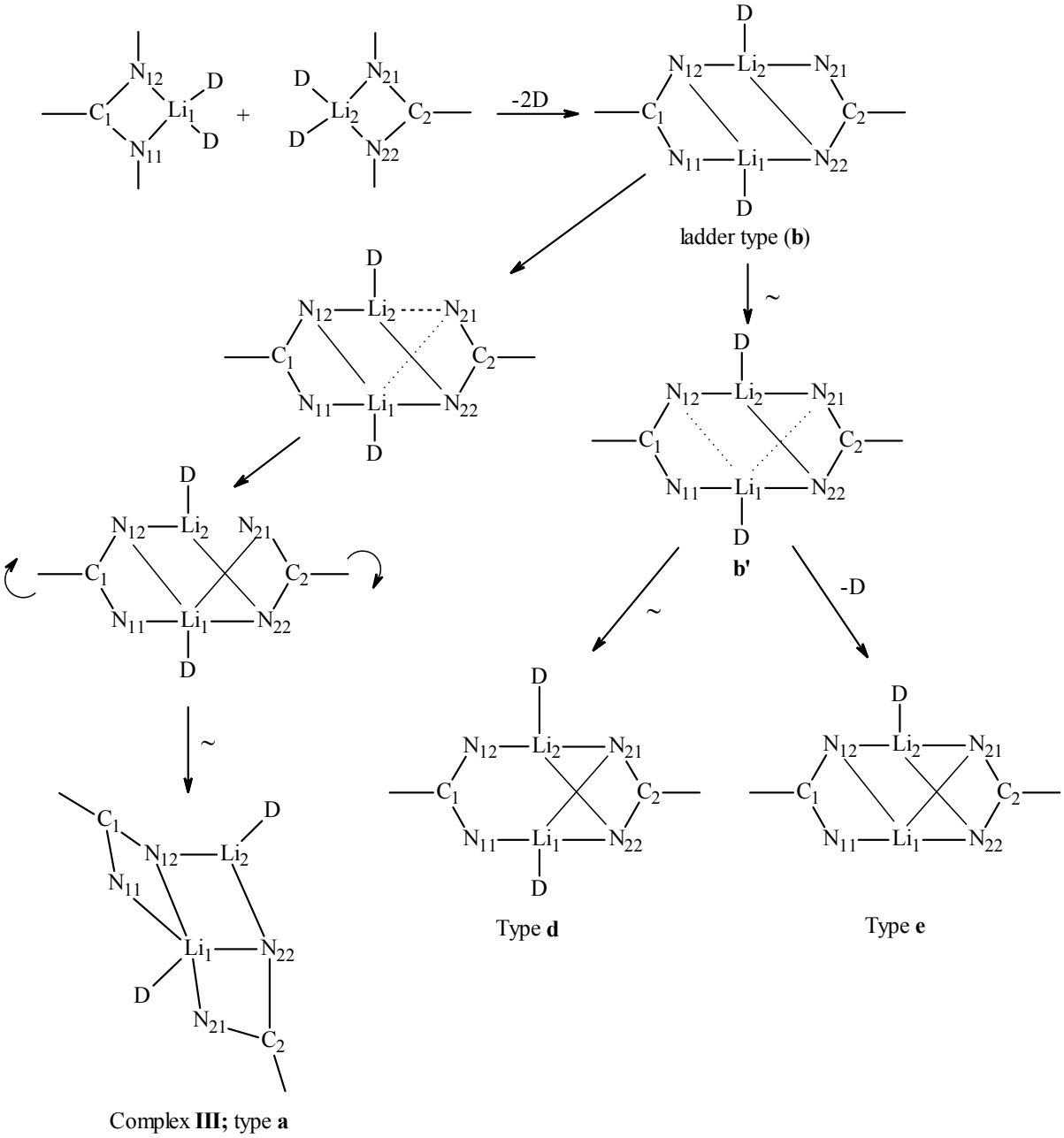

Scheme 4.1 Structural relationship between monomeric and dimeric amidinato-complexes

Cleavage of the Li1−N12 bond and formation of new nitrogen lithium bond (N21−Li1) (**b′**) afforded then an unsymmetrical "twisted" complex **d**. Type **e** results from **b′** by loss of a further donor molecule (D) from Li1; the empty coordination site at is then filled by the former N12. Applying this into our case and starting from a ladder complex (b), bond breaking between Li1 and N21 and bond formation between Li2 and N21 is formed, and finally twisting of the amidinate moiety (N21−C2−N22) to the front give the new structure in which both ligands connect to one corner (Li2) of the central (Li2N2) four-membered ring.

4.2.2 *NMR Spectroscopic Characterization*

The $^{31}P\{^{1}H\}$ NMR spectrum of crystals of complex **III** dissolved in [d_8]tetrahydrofuran reveals one sharp signal at −152.2 ppm (**Table 4.1 a**)) beside additional weaker signals at lower field (the overall intensity of these signals with respect to that of **III** was 0.30 : 1 at 303K). When ^{1}H coupling is allowed, the ^{31}P NMR signal splits into a triplet with a $^{1}J_{P,H}$ coupling constant of 210 Hz indicating the presence of a PH_2 group. These values agree very well with those reported by *Issleib* and co-workers for the first phosphaguanidine H_2P–C(=NPh)NHPh which has a ^{31}P chemical shift of −148 ppm and a $^{1}J_{P,H}$ coupling constant of 220 Hz [125]. Additionally, the (*Z*)-[phosphanyl-*N*-(2,4,6-tri-*tert*-butylphenyl)imi-noformiato-*O*]lithium complex, which had prepared in our research group, exhibits a ^{31}P NMR triplet at –144,9 ppm with a $^{1}J_{P,H}$ coupling constant of 207 Hz in [d_8]tetrahydrofuran solution [79]. These values also compares very well with our results. Attempt to assign the signals of the impurities failed (**Figure 4.1**).

In the ^{1}H NMR spectrum a doublet ($^{1}J_{P,H}$ = 210 Hz) at 3.0 ppm was attributed to the hydrogen atoms of the PH_2 group. This assignment was confirmed by the appropriate cross peak in the $^{1}H,^{31}P$ HMQC spectrum. Furthermore, the hydrogen atoms of the PH_2 group exhibit in the $^{1}H,^{15}N$ HMQC experiment a correlation with a ^{15}N signal at −164.2 ppm assigned to the nitrogen atoms of the N_2C fragment. In the $^{1}H,^{13}C$ HMBC experiment a correlation with the ^{13}C carbonyl signal located at 165.5 ppm (*d*, $^{1}J_{P,C}$ = 36 Hz) was observed (**Table 4.1 a)**). The signal of the methyl protons of the *p*-tolyl groups were found at 2.3 ppm as a sharp singlet, the intensity ratio of this signal compared to that of $P\underline{H}_2$ and C–$\underline{H}_{ortho}$ groups agrees very well with our assignment (see footnote [e] **Table 4.1**). In the ^{1}H-COSY spectrum, the ^{1}H signal of the PH_2 group at 3.0 ppm show a clear cross peak with a multiplet at 6.7 ppm, this signal should be attributed to the C–$\underline{H}_{ortho}$ of the *p*-tolyl groups. Indeed, this assignment was

confirmed by the presence of a strong correlation in the $^{1}H,^{13}C$ HSQC experiment between this multiplet and a ^{13}C singlet at 122.9 ppm attributed to the $^{13}C_{ortho}$ carbon atoms. Finally, the signal of C–H_{meta} hydrogen atoms could be also assigned since a weak but visible correlation in the ^{1}H-COSY spectrum between the C–H_{ortho} at 6.7 ppm and a multiplet at 6.9 ppm was observed.

Table 4.1 Assignment of ^{1}H, ^{13}C, ^{31}P, and ^{15}N NMR signals of [d_8]tetrahydrofuran/ 1,2-dimethoxyethane solvated [μ-*N*,*N*′-bis(4-methylphenyl)-*C*-phosphanylformamidinato-(*N,N'*)]lithium (**III**) **(a)** and *N*,*N*′-bis(4-methylphenyl)carbodiimide **(b)** based on ^{1}H-COSY, HSQC, HMQC, and HMBC correlations of phosphanyl, phenyl and methyl hydrogen atoms

^{1}H atom	δ (ppm), multiplicity[a]	^{1}H-COSY	HMQC(^{15}N)/(^{31}P), HSQC(^{13}C)	HMBC
PH_2	3.00 (*d*)[b]	C–H_{ortho} (6.7) s[c]	^{31}P(–152.2) s[c] ^{15}N(−164.2) s[c]	$^{13}CN_2$(P) (165.2)[d] m[c] $^{13}C_{ipso}$ (152.0) vw[c] $^{13}C_{ortho}$ (122.7) s[c]
C–H_{ortho}	6.71 (*m*)	C–H_{meta} (6.9) w[c] $CH_{3\ para}$ (2.35) w[c]	$^{13}C_{ortho}$ (122.9) s[c] ^{31}P(–152.2) s[c] ^{15}N(−164.2) s[c]	$^{13}C_{ortho}$ (122.9) m[c] $^{13}C_{para}$ (127.6) s[c]
C–H_{meta}	6.91 (*m*)	C–H_{ortho} (6.7) w[c] $CH_{3\ para}$ (2.3) w[c]	$^{13}C_{meta}$ (128.4) s[c]	$^{13}C_{meta}$ (128.3) m[c] $^{13}C_{ipso}$ (151.4) s[c]
$CH_{3\ para}$	2.27 (*s*)[e]		$^{13}CH_{3\ para}$ (19.9) s[c]	$^{13}C_{meta}$ (128.4, br)[a] m[c] $^{13}C_{ipso}$ (151.5) w[c]

[a] singlet (*s*), doublet (*d*), multiplets (*m*), broad (*br*); [b] $^{1}J_{P,H}$ = 210 Hz; [c] COSY/HMQC/HMBC cross peak intensities: strong (s), medium (m), weak (w), very weak (vw); [d] $^{1}J_{P,C}$ = 36 Hz; [e] integral ratio for PH_2 : (C–H_{ortho})$_4$: ($CH_{3\ para}$)$_2$ approximately 2.0 : 4.6 : 6.3

b) *N*,*N*′-bis(p-tolyl)carbodiimide dissolved in [d_8]tetrahydrofuran

^{1}H atom	δ-value (ppm), multiplicity[a]	^{1}H- COSY	HMQC(^{15}N), HSQC(^{13}C)	HMBC
CH_3	2.33 (*s*)	C–H_{meta} (7.2) m[c] C–H_{ortho} (7.1) w[c]	$^{13}CH_3$ (19.7) s[c]	$^{13}C_{meta}$ (129.7) s[c] $^{13}C_{para}$ (135.1) s[c]
C–H_{ortho}	7.08 (*m*)	C–H_{meta} (7.2) s[c]	$^{13}C_{ortho}$ (123.2) s[c] $^{15}N_{=C}$ (–279.5) m[c]	$^{13}C_{ortho}$ (123.2) s[c] $^{13}C_{para}$ (135.1) s[c]
C–H_{meta}	7.16 (*m*)	C–H_{ortho} (7.1) s[c]	$^{13}C_{meta}$ (129.7) s[c]	$^{13}CH_3$ (19.7) s[c] $^{13}C_{ipso}$ (135.9) s[c] $^{13}C_{meta}$ (129.7) w[c]

[a] and [c] as above

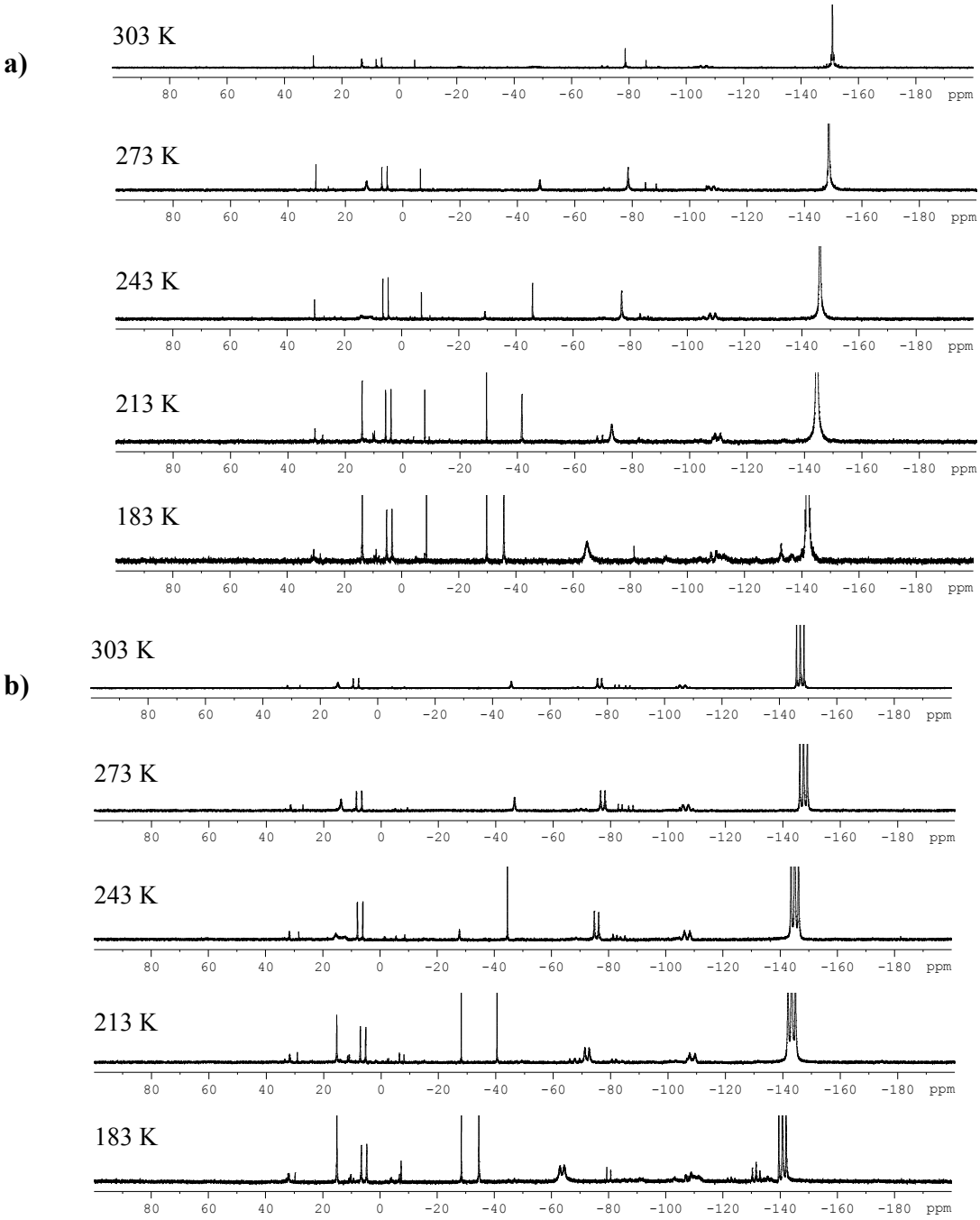

Figure 4.1 Temperature dependence of the ^{1}H-decoupled (**a**) and the ^{1}H coupled (**b**) ^{31}P NMR spectrum of compound **III** dissolved in [d_8]tetrahydrofuran

In the high field region of the ^{13}C NMR spectrum, a singlet at 19.9 ppm attributable to the methyl carbon atoms was observed (**Table 4.2**). The signals of the phenyl substituents were also assigned using the 2D NMR techniques; apart from the signal of the *ipso*-carbon at 152.0 ppm the other signals were found in the narrow range between 122.9 and 128.4 ppm. Furthermore, in the low field region of the ^{13}C NMR spectrum a signal at 165.5 ppm with a

Table 4.2 Compilation of $\delta^{13}C$ (ppm) and $^{n}J_{P,C}$ values (Hz) and further heteronuclear NMR data (δ ^{7}Li, δ ^{15}N, and δ ^{31}P) of complex **III** and *N*,*N*′-bis(4-methylphenyl)carbodiimides measured in [d_8]tetrahydrofuran.

^{13}C atom	**complex (III)** δ 13C[a)]	***N*,*N*′-bis(4-methylphenyl)carbodiimide**
$^{13}\underline{C}N_2(P)$	165.2 (*d*), $^{1}J_{P,C} = 36$	
$^{13}\underline{C}_{ipso}$	152.0 (*s*)	136.4 (*s*)
$^{13}\underline{C}_{ortho}$	122.9 (*s*)	123.2 (*s*)
$^{13}\underline{C}_{meta}$	128.4 (*s*)	129.7 (*s*)
$^{13}\underline{C}_{para}$	127.6 (*s*)	135.1 (*s*)
$C\underline{H}_{3\ para}$	19.9 (*s*)	19.7(*s*)
other nuclei		
^{31}P	–152.2 (*s*)[b)]	—
^{15}N	−164.2 (*s*)	—
^{7}Li	1.1 (*s*)	—

[a)] signal multiplicity (in parentheses): singlet (*s*), doublet (*d*); [b)] triplet in the ^{1}H coupled ^{31}P NMR spectrum ($^{1}J_{P,H} = 210$ Hz).

$^{1}J_{P,C}$ coupling constant of 36 Hz is observed. This signal has to be assigned to the $^{13}\underline{C}N2$ carbon since in the HMBC experiment a clear correlation with the doublet of the PH_2 hydrogen atoms is detected. Remarkably, the ^{13}C chemical shift value of 165.2 ppm of **III** compared very well with that obtained for (*Z*)-[phosphanyl-*N*-(2,4,6-tri-*tert*-butylphenyl)iminoformiato-*O*]lithium complex (168.3 ppm), whereas the $^{1}J_{P,C}$ coupling constants differ significantly (36 Hz for **III** *vs* 10 Hz).

The ^{1}H and ^{13}C NMR spectra displayed further weak signals of additional components. Apart from the presence of unreacted starting material (bis(4-methylphenylcarbodiimide) was ruled out, further structural assignment was unfeasible.

Since the complex contains two lithium atoms with different environments (one with coordination number four and the other with six) one expects to see two signals in the ^{7}Li NMR spectrum, but the ^{7}Li NMR spectrum of complex **III** shows only one singlet at 1.1 ppm. A similar observation was also reported by *Klingebiel* and co-workers. They reported that the crystalline THF solvate of the dimeric compound $[(t\text{Bu})_2\text{SiFLiN}t\text{Bu}]_2$ exhibits two different lithium atoms with four- and two-coordinate ligation spheres which are dynamically averaged in toluene solution at +32 °C as evidenced by the observation of a single ^{7}Li resonance at 0.91 ppm [126]. Low temperature ^{7}Li NMR of complex **III** was also

investigated, as the sample cooled down the signal at 1.1 pm becomes more broad and other signals with low intensity was also observed (**Figure 4.2**). Unfortunately, the origin of these signals could not be established but at least suggest that complex **III** is present in a number of isomeric forms in solution at low temperature. Last but not least, the explanation of the presence of one ^{7}Li NMR signal at room temperature might be the rapid fluctuation between the four and six coordinated lithium atoms (**Figure 4.3**).

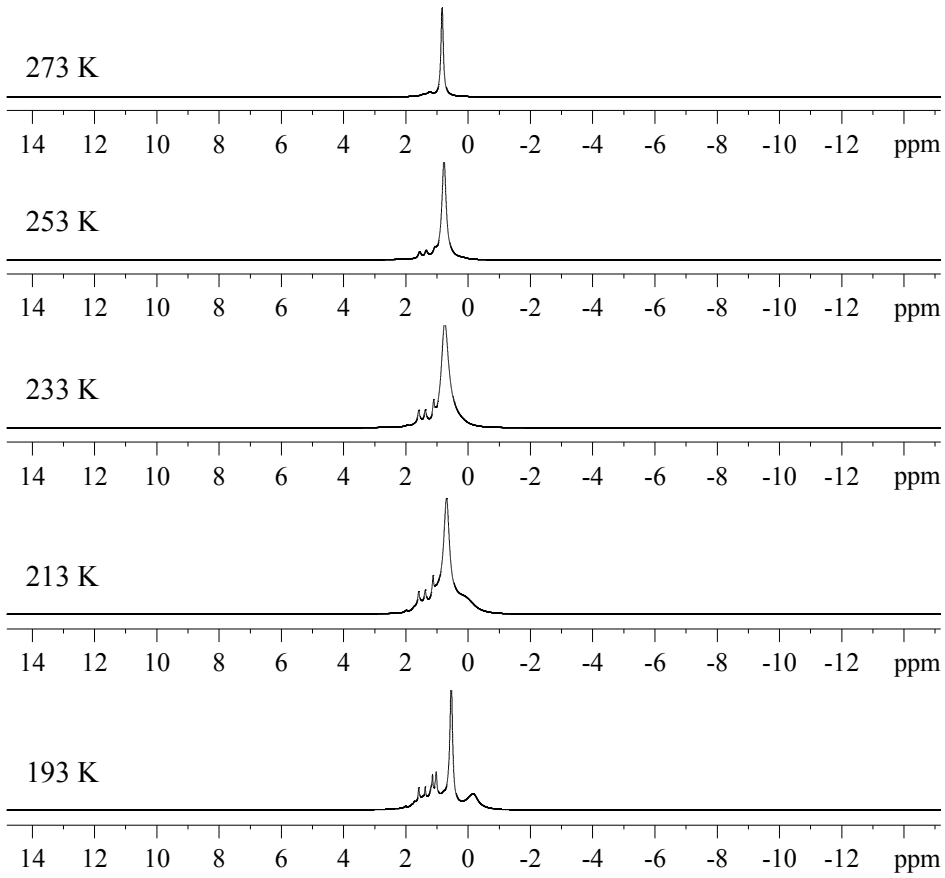

Figure 4.2 Temperature dependent ^{7}Li NMR spectra of complex **III** dissolved in [d_8]tetrahydrofuran
The figure depicts the alteration of the ^{7}Li NMR signal between 193K and 273K.

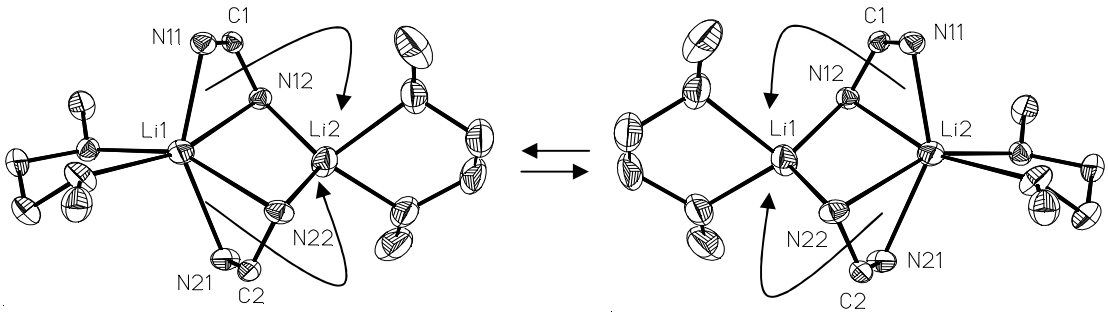

Figure 4.3 Studies of complex **III** in solution
Hypothetical pathway for the dynamic equilibration between the different coordination environment of Li1 and Li2 in complex **III** based on observed the solid-state structure.

4.2.3 *Crystal data, Data Collection and Structure analysis*

Crystals suitable for an X-ray structural analysis of complex **III** precipitated at room temperature on the wall flask during reduction of the volume of the reaction mixture one third of its original value. Data for a structure determination were collected on a P4 diffractometer using graphite monochromatized MoK_α radiation (λ = 71.073). On the basis of unit cell dimensions and statistical tests on the distribution of E-values, the triclinic space group $P\bar{1}$ was chosen. Further general information regarding structure analysis were described in the experimental part. The hydrogen atoms of methylene groups of the 1,2-dimethoxyethane were fixed at a distance of 99 pm, assuming tetrahedral angles at the carbon atoms and a staggered arrangement of adjacent CH_2 units. Furthermore, the riding model applied ensures that a change in the carbon position is automatically transferred to the adjacent hydrogen atoms. Individual isotropic U-values for these hydrogen atoms were set by multiplying the values for the respective carbon atoms by factors of 1.5 for the methyl groups at *para*-position, 1.2 for the phenyl and methylene substituents, and 1.3 for the methyl groups of the solvent molecules. To account for the incorporation of hydrogen atoms, the parameters of all heavier atoms were refined again, and final agreement factors of R1 = 0.0738 and wR2 = 0.1550 were achieved. Crystallographic parameters and details of data collection are listed in **Table 4.3**. Final atomic coordinates and equivalent isotropic as well as anisotropic displacement parameters can be found in **Table 7.5.2**.

Table 4.3 Crystal data and details of structure refinement for [bis(1,2-dimethoxyethane)-1κ^2*O*^{1},*O*^{2};2κ^2*O*^{3},*O*^{4}]{bis[μ-*N*,*N*′-bis(4-methylphenyl)}-*C*-phosphanylform-amidinato]-1:2κ^4*N*^{1}, *N*^{2};1κ^2*N*^{3};*N*^{4}}dilithium **III**

Diffractometer	P4
Empirical formula; Molecular weight	$C_{38}H_{52}Li_2N_4O_4P_2$; 704.66
Melting point (ºC)	147
Wavelength (pm)	71.073
Temp. of measurement (K)	173 ± 2
Shape and crystal size (mm)	colourless rod 0.4 x 0.2 x 0.2
Crystal system	triclinic
Space group [45]	*P* ī *(No. 2)*
Unit cell dimensions a/pm	1015.45(12)
b/pm	1292.7(3)
c/pm	1689.3(2)
α/º	86.842(15)
β/º	79.783 (11)
γ/º	67.668 (13)
Volume (10^{-30}m^3)	2018.5(6)
Z	2
Calculated density (10^3 kg/m^3)	1.159
Absorption coefficient (μ/mm^{-1})	0.149
F(000)	752
Θ-Range for data collection (deg)	1.70 to 25.00
Limiting indices	$0 \le h \le 12$, $-14 \le k \le 15$, $-19 \le l \le 20$
Systematic absences	none
Scan modes	ω-scan
Scan width (deg)	2.4
Velocity (deg s^{-1})	3.0 to 60.0
Reflections collected	7519
Unique reflections	7079
Completeness to θ_{max}	0.995
Max. and minimum transmission	not detected
Refinement method	[a]
Data used	7079
Parameters refined (n)	467
Restraints	0
Goodness-of-fit (GOF) on F^2	0.980
R-indices (all data): R1	0.0550,
wR2	0.1472
Final R-indices: R1	0.0738,
[I > 2 σ (I)] wR2	0.1550
Largest diff. peak;	0.482
Deepest hole (10^{-30}e.m^{-3})	−0.368

4.2.4 *Discussion of Bond Lengths and Angles*

Figure 4.4 shows the non-stereoscopic **a)** and stereoscopic view **b)** of complex **III** as determined by X-ray structure analysis. Complex **III** is dimeric in the solid state with three folded four-membered rings forming the core; the central four-membered ring, which is formed by the two lithium atoms and two nitrogen atoms (Li1,N12,Li2,N22), shares two adjacent edges with the two other rings formed by the amidinate ligands (Li1,N11,C1,N12) and Li1,N21,C2,N22). The outer rings are arranged on opposite sides of the plane of the central four-membered ring. The most striking feature of the structure of complex **III** is the inequivalence of the coordination spheres of the two lithium atoms. The Li1 atom is six coordinated by all nitrogen atoms of the dimer (N11, N12, N21 and N22) and one 1,2-dimethoxyethane molecule, whereas the Li2 atom is four coordinated by the two nitrogen atoms N12 and N22 and a second molecule of 1,2-dimethoxyethane.

According to the Cambridge Crystal Data Catalogue (CCDC) there is no phosphaguanidinate complex with such structure, and only a few similar structures of amidinates and related compounds were found. *Edelmann* et al. reported that bidentate organosulfinimidamide ligands show *in general* three structural classes:

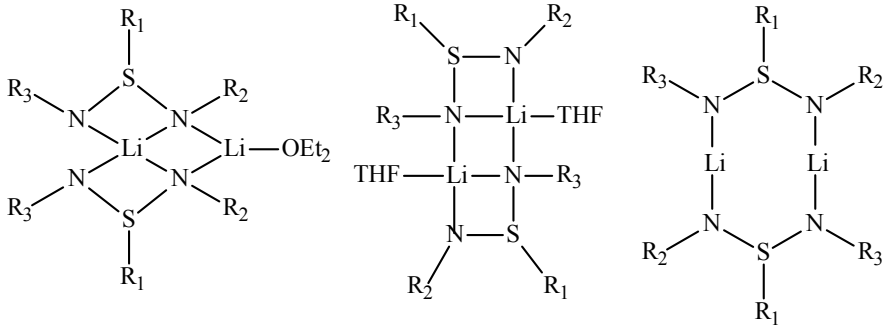

the *twisted tricyclic* structure **a**, a *ladder* or *step* structure **b**, and an *eight-membered ring* structure **c** [127]. Dimeric amidinate or guanidinate complexes normally adopt the *ladder-type* arrangement (type **b**) with an anti-arrangement about the central 4-membered ring [19, ref. therein].

a)

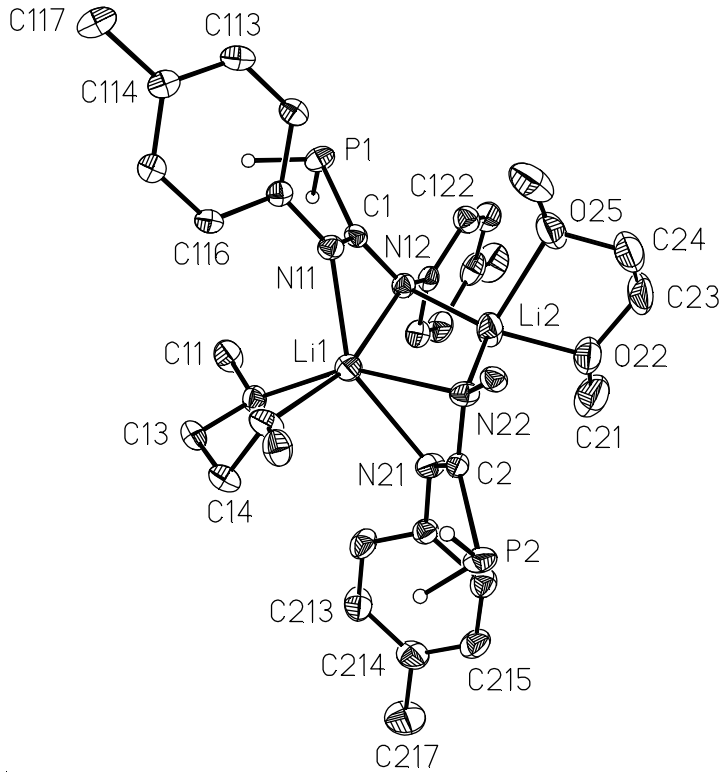

b)

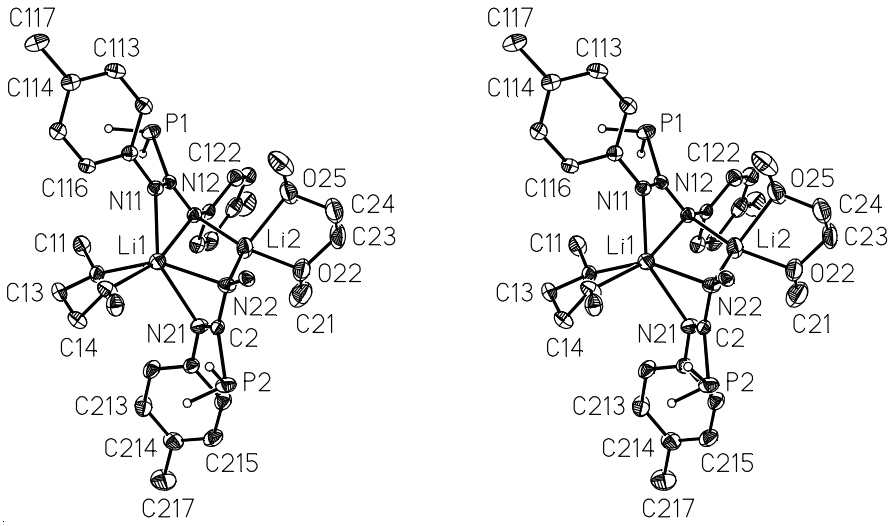

Figure 4.4 Non-stereoscopic (a) and stereoscopic view (b) of the complex [bis(1,2-dimethoxyethane)-1κ^2*O*^{1},*O*^{2};2κ^2*O*^{3},*O*^{4}]{bis[μ-*N*,*N*′-bis(4-methylphenyl)}-*C*-phosphanylform-amidinato]-1:2κ^4*N*^{1}, *N*^{2};1κ^2*N*^{3};*N*^{4}}dilithium **III**. Thermal ellipsoids are at 30% probability; except for the PH_2-groups all hydrogen atoms are omitted for clarity. Only the *ipso* carbon of the phenyl group at N22 is shown. Absent atom numbering has to be complemented logically.

As an example of compounds with a structure of type **a**, the group of *Edelmann* isolated two lithiumsulfinimidamides $[(Me_3SiN)_2S(C_6H_5)Li]_2 \cdot Et_2O$ and $[(Me_3SiN)(^tBuN)S(C_6H_5)Li]_2 \cdot Et_2O$. In both compounds two inequivalent lithium atoms were observed; one is four coordinated by nitrogen atoms and the other is three coordinated by two nitrogen atoms and an oxygen atom of an ether molecule. Furthermore, *Stalke* and co-workers reported the isolation of two compounds which also exhibit the structure of **a** type [128]. The first compound $\{[(H_5C_6)S(NC_6H_{11})(NSiMe_3)]Li\}_2 \cdot Et_2O$ is analogous to that reported by *Edelman*, the second one is $[(H_5C_6)S(NSiMe_3)_2]LiNa \cdot dme$. It should be noted that in the mixed Li, Na complex $[(H_5C_6)S(NSiMe_3)_2]LiNa \cdot dme$, one of the coordinate lithium ions has been formally replaced by sodium. Using *n*-butyllithium to lithiate the bulky guanidine ligand ($Cy_2NC\{NAr\}\{NHAr\}$, *Jones* et al. were able to isolate the dimeric solvent free guanidinate complex as another example of structural type **a** in good yield [115].

Table 4.4 Bond lengths (pm) and bond angles (deg), characteristic torsion angles as well as least-squares planes and angles between these planes for [bis(1,2-dimethoxyethane)-1κ^2*O*^{1},*O*^{2};2κ^2*O*^{3},*O*^{4}]{bis[μ-*N*,*N*′-bis(4-methylphenyl)}-*C*-phosphanylform-amidinato]1:2κ^4*N*^{1},*N*^{2};1κ^2*N*^{3};*N*^{4}}dilithium **III**.

a) Bond lengths

Amidinate ligands							
	n = 1	*n* = 2	mean		*m*/*n* = 1	*m*/*n* = 2	mean
P*n*–C*n*	188.9(2)	188.2(2)	188.6	Li1–N11	211.6(5)	—	—
P*n*–H*n*1	134(3)	128(3)	132.0	Li1–N1*m*		232.6(5)	233.2
P*n*–H*n*2	129(2)	138(3)		Li1–N2*m*	231.7(5)	235.2(5)	
C*n*–N*n*1	132.5(3)	131.9(3)	132.8	Li2–N*n*2	201.9(5)	203.7(5)	202.8
C*n*–N*n*2	133.5(3)	133.2(3)			*m* = 2	*m* = 5	
N*n*1–C*n*11	140.5(3)	140.8(3)	140.9	Li1–O1*m*	212.0(5)	222.4(5)	217.2
N*n*2–C*n*21	141.2(3)	140.9(3)		Li2–O2*m*	200.0(5)	208.6(6)	204.3

b) Bond angles

Amidinate-ligands				Coordination at Li1		
	n = 1	*n* = 2	mean			mean
C*n*–P*n*–H*n*1	98.0(1)	94.0(1)	96.0	N11–Li1–N12	61.2(1)	59.3
C*n*–P*n*–H*n*2	98.0(1)	94.0(1)		N21–Li1–N22	57.4(1)	
H*n*1–P*n*–H*n*2	97.0(2)	100.0(2)	99.0	O12–Li1–O15	76.2(2)	—
N*n*1–C*n*–P*n*	122.2(2)	122.2(2)	121.8	N11–Li1–N21	148.6(2)	155.2
N*n*2–C*n*–P*n*	120.6(2)	122.1(2)		N12–Li1–O15	163.4(2)	
N*n*1–C*n*–N*n*2	117.0(2)	115.5(2)	116.3	N22–Li1–O12	153.6(2)	

Coordination at Li2					
N12–Li2–N22	117.3(2)	O22–Li2–O25	81.8(2)	N21–Li2–O25	163.9(2)
N12–Li2–O22	123.5(2)	N12–Li2–O25	101.3(2)	N21–Li2–N12	92.5(2)
N22–Li2–O22	114.0(2)	N22–Li2–O25	109.7(3)	N21–Li2–N22	55.8(2)
				N21–Li2–O22	97.5(2)

A complete compilation of the bond lengths and bond angles as well as characteristic torsion angles is given in **Table 8.5.1** of the appendix. To discuss the structure in detail we will start from the core which is the four-membered ring (Li1,N12,Li2,N22). The ring is slightly folded but the deviations from planarity are not very significant (displacement from a least squares plane are −6.1, 7.7 −9.2 and 7.6 pm for Li1, N12, Li2 and N22, respectively). The ring is not square but kite-shaped since the two edges adjacent to the 6-coordinate Li1 atom (Li1−N12, Li1−N22) are obviously by 28.9 and 33.3 pm longer than the remaining ones (Li2−N12 and Li2−N22). The phosphaguanidinato ligands are likewise not planar.

The average P–C distance of 188.6 pm in complex **III** is remarkably elongated from the standard P–Csp^2 bond length of 183.5 pm, but at the same time consistent with P–C bond distances of related phosphaguanidines compounds found in literature [123]. The C−N bond distances in complex **III** varies in rather narrow range between 131.9 and 133.5 pm with

average C–N bond length of 132.8 pm. This bond distances indicate equal delocalization of the π-electrons over N⋯C⋯N unit.

The N–Li distances cover generally a rather broad range and vary according to Cambridge Crystallographic Data Centre (CCDC) between 145 and 280 pm with a mean of 207 pm [130]. A short compilation of N–Li distances in N2Li2 4-membered rings lithiumamides and –imides is given in a paper published by *Becker* and co-workers [109]. The authors found that these values vary between 192 and 214 pm and determined an average value of 204 pm. In the same paper they also described the isolation and structural characterization of polymeric (tetrahydrofuran)lithium cyanotrimethylsilylamide which reveals N–Li distances of 198.3 and 206.1 pm. In the phosphaguanidinato dimeric complex $[Li(Ph_2PC\{N^iPr\}_2)(THF)]_2$ reported by *Coles* et al., values between 202.4 and 217.5 pm were reported [19].

In complex **III** a significantly different N–Li distances were determined, the four-coordinate Li atom (Li2) exhibits N–Li distances of 201.9 and 203.7 pm which lie in the normal range. The six-coordinate lithium atom features one N–Li distance which is only slightly elongated (211.6 pm for Li1–N11) while the remaining ones are significantly larger (232.6, 231.7 and 235.2 pm for Li1–N12, Li1–N21 and Li1–N22, respectively). This general trend can be considered as a typical consequence of the increased coordination number of Li1.

Each PH_2 group in complex **III** comprise two different P–H bond distances; 134 and 129 pm for P1–H11/12 as well as 128 and 138 pm for P2–H21/22. It is worthy to mention that these distances vary in a wide range and that values of 142 pm for example were determined according to the infra red and electron diffraction methods for parent PH_3 [132, 133]. The sums of bond angles of 291° at phosphorus atom suggest a high *p*-orbital contribution form phosphorus atom in the P–H bond as well as high s-character of the non-bonding electrons at phosphorus atom.

Because of the high coordination number of the Li1 atom, the distances to the oxygen atoms of the 1,2-dimethoxyethane molecule are elongated (212.0(5) and 222.4(5) pm, respectively) when compared for example with Li–O bond distances (192.0 (9) to 197.8 (8)) reported for a series of fluoroarylamidinato and guanidinato lithium complexes [19, 129]. The angle at Li1 is restricted (76.2º). The other solvent molecule binds to Li2 at distances of 208.6(6) (Li2–O22) and 200.0(5) pm (Li2–O25) and the O22–Li2–O25 angle is 81.8º(2). These values are comparable to those of lithium-ether complexes [133] with average Li–O bond distances of 196.2 pm for a lithium atom of tetrahedral geometry. The six coordinated lithium atom Li1, on the other hand, which has a Li–O bond distances of 212.0 and 222.4 pm also agrees very well with that of 226.5 pm for lithium atoms with distorted octahedral geometry [133].

The geometry of the five-membered rings formed by the coordination of the 1,2-dimethoxyethane ligands to the lithium atoms can be easily determined based on the values of torsion angles. *Allmann* reported in an article published in 1977 that the sequence (+ α, – β, 0, + β, – α) is characteristic for the *envelope* conformation, whereas the presence of a *twisted* conformation is indicated by a (+ α, –β, γ, + β, – α) sequence [134]. With values of (−53.7, +29.4, 0.1, −28.7, +55.9) and (+49.9, −25.3, −5.1, +33.1, −56.3), an envelop confirmation is realized. The packing of the molecules in the unit cell is shown in the stereoscopic drawing in **Figure 4.5**; no intermolecular contacts significantly shorter than van der waals distances were found.

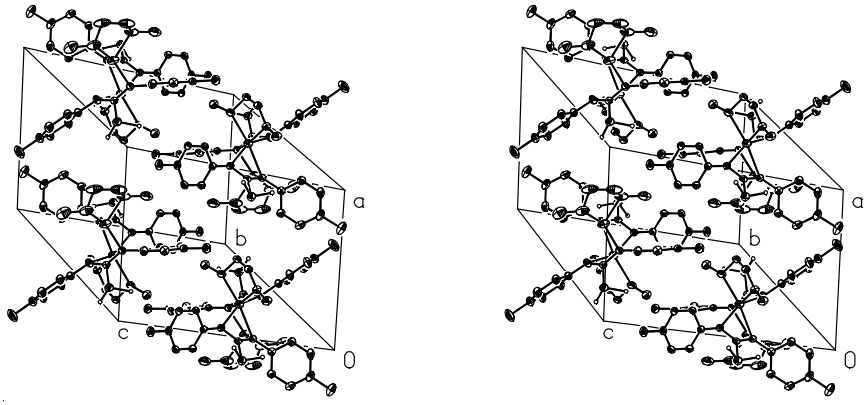

Figure 4.5 Unit cell content of the complex **III**. Thermal ellipsoids are at 30% probability; except for the PH_2-groups all hydrogen atoms are omitted for clarity.

4.3 *Reaction of (1,2-dimethoxyethane)Lithium Phosphanide with N,N′-di-*tert*-Butylcarbodiimide*

4.3.1 *Preparation and reaction Mechanism*

A solution of *N,N′*-di-*tert*-butylcarbodiimide dissolved in 1,2-dimethoxyethane was added dropwise at −70 ºC to a solution of lithium phosphanide in the same solvent. The reaction mixture was stirred overnight and allowed to warm up slowly to room temperature. No colour change was noticed during the reaction, but a ^{31}P NMR spectrum shows a new doublet at −63.8 ppm meanwhile the lithium phosphanide signal had completely disappeared. This indicates that the reaction is completed and the complex bis[μ-(*N,N′*-di-*tert*-butyl-*C*-phosphanidatoformamidin)-1κ^1*P*; 2κ^1*P′*;1:2κ^2*N*; 1:2κ^2*N′*]1,2-bis(tetrahydrofuran-*O*)dilithium (**IV)** was formed. The solvent was removed under reduced pressure and the residue dissolved in a small amount of tetrahydrofuran. On storing the solution at −13 ºC for several days, colourless crystals precipitated in a relatively high yield.

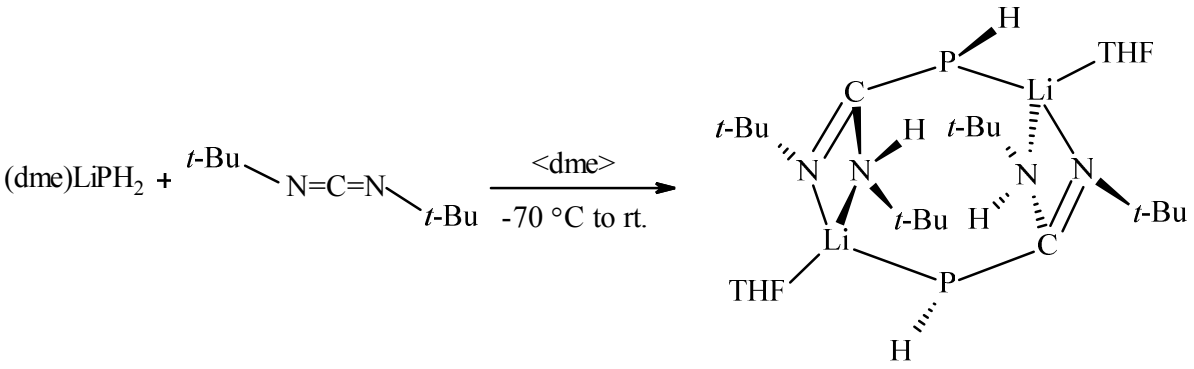

IV

The product was identified by spectroscopic and single-crystal X-ray diffraction studies as the dimeric complex **IV**. The reaction product **IV** exhibits a symmetrical structure composed of two anionic phosphanido-amidine ligands bridged by two lithium ions that bind to an additional THF molecule. In contrast to the reaction of lithium phosphanide with bis(4-methylphenyl)carbodiimide which proceeds via nuecleophilic attack of the phosphanide anion at the *sp*-hybridized carbon atom of the carbodiimide to afford complex **III**, two possibilities for the generation of **IV** should be considered: 1) addition of a PH bond to a C=N bond of the carbodiimide or 2) nuecleophilic attack of the phosphide anion at the *sp*-hybridized carbon atom of the carbodiimide and subsequent 1,3-H-shift from phosphorus to one of the nitrogen atoms.

4.3.2 *NMR Spectroscopic Characterization*

The ^{31}P NMR spectrum of **IV** dissolved in a very small amount of 1,2-dimethoxyethane and diluted with [d_6]benzene reveals a doublet at −63.8 ppm with a $^{1}J_{P,H}$ coupling constant of 153 Hz (**Table 4.5 a)**). Surprisingly, the chemical shift and coupling constant are in very good agreement with the values for HP=C(NMe$_3$)$_2$ which exhibits a ^{31}P NMR doublet at −62.6 ppm and a $^{1}J_{P,H}$ coupling constant of 159 Hz [135]. In contrast the $^{1}J_{P,H}$ coupling constant for compound **IV** is considered to be very small when compared with 1$\lambda^3\sigma^3$-phosphaguanidines such as (Me$_3$Si)HP–C{=NPh}{NPh(SiMe$_3$)} [125] and (^{t}Bu)HP–C{=N^{t}Bu}{NH(^{t}Bu)} [116] which have $^{1}J_{P,H}$ coupling constants of 216 and 210 Hz, respectively. It is worthy to mention that the complex (1,2-Dimethoxyethan-1κ^2*O,O′*)(1,2-dimethoxyethan-2κ^2*O,O′*)-(*Z*)-[phosphanidyl-*N*-(2,4,6-tri-*tert*-butylphenyl)iminoformiato-1κ^2*N,O*-2κ*P*]dilithium which also comprises a (Li)HP–C fragment shows a ^{31}P NMR doublet at −124 ppm with a $^{1}J_{P,H}$ coupling constant of 176 Hz [79]. Furthermore, the $^{1}J_{P,H}$ coupling constant for complex **IV** agrees very well with those observed for complex **V** and **VI** (**Section 4.4.2**) which exhibit values of about 158 Hz.

The ^{31}P NMR signal of **IV** correlates in the ^{31}P,^{1}H HMQC experiment with the ^{1}H signal at 3.04 ppm. this signal which appears as doublet with $^{1}J_{P,H}$ coupling constant of 153 Hz can be unambiguously attributed to the hydrogen atom attached to phosphorus. Furthermore, the broad ^{1}H signal at 3.53 ppm attributable to the hydrogen atom of the amino group correlates with a ^{15}N NMR doublet ($^{1}J_{^{15}N,H}$ = 70 Hz) at −261.1 ppm. A second ^{15}N NMR signal at −120.2 ppm is assigned to the imino nitrogen was also detected in the ^{15}N NMR spectrum. Additionally, very intense high field ^{1}H signals at 1.47 and 1.81 ppm can be easily assigned to the hydrogen atoms of the two different *tert*-butyl substituents. The signal at 1.47 ppm exhibits a long-range correlation with the ^{15}N NMR signal of the amino nitrogen atom at −261.1 ppm and the signal at 1.81 ppm correlates with the ^{15}N NMR signal of the N=C group at −120.2 ppm. For comparison, the NMR parameters of the di-*tert*-butylcarbodiimide were compiled also in **Table 4.5 b)**.

Table 4.5 Assignment of ^{1}H, ^{13}C, ^{31}P, and ^{15}N NMR signals of dme-complexed [μ-(*N,N′*-di-*tert*-butyl-*C*-phosphanidatoformamidin)lithium] **(IV) a)** and *N,N′*-di-*tert*-butylcarbodiimide **b)** based on ^{1}H-COSY, HSQC, HMQC, and HMBC correlations

a) [μ-(*N,N′*-di-*tert*-butyl-*C*-phosphanidatoformamidin)lithium] **(IV)**

^{1}H atom	δ (ppm), multiplicity[a)]	^{1}H- COSY	HMQC(^{15}N)/(^{31}P), HSQC(^{13}C)	HMBC
P<u>H</u>	3.04 (*d*)[b)c)]	N<u>H</u> (3.52) vw[d)]	^{31}<u>P</u>(–63.8) s[d)] ^{15}<u>N</u>$_{H}$ (−261.1) w[d)]	^{13}<u>C</u>N$_2$ (191.5) w[d)e)] ^{13}<u>C</u>H$_{3\ C=N}$ (28.6) w[d)f)]
C<u>H</u>$_{3\ NH}$	1.47(*s*)		^{31}<u>P</u>(–63.7) vw[d)] ^{15}<u>N</u>$_{H}$ (−261.1) s[d)] ^{13}<u>C</u>H$_{3\ NH}$ (30.5) s[d)]	^{13}<u>C</u>H$_{3\ NH}$ (30.5) s[d)] ^{13}<u>C</u>$_{quar\ NH}$ (52.1) s[d)g)] ^{13}<u>C</u>N$_2$ (191.5) vw[d)]
C<u>H</u>$_{3\ C=N}$	1.81(*s*)		^{31}<u>P</u>(–63.8) m[d)] ^{15}<u>N</u>$_{=C}$ (−120.2) s[d)] ^{13}<u>C</u>H$_{3\ C=N}$ (28.5) s[d)]	^{13}<u>C</u>H$_{3\ C=N}$ (28.8) s[d)] ^{13}<u>C</u>$_{quar\ C=N}$ (52.1) s[d)g)] ^{13}<u>C</u>N$_2$ (191.5) vw[d)]
N<u>H</u>	3.53 (*br*)	P<u>H</u> (3.04) vw[d)]	^{31}<u>P</u>(–63.8) vw[d)] ^{15}<u>N</u>$_{H}$ (−261.1) m[d)h)]	^{13}<u>C</u>N$_2$ (191.5) s[d)] ^{13}<u>C</u>H$_{3\ NH}$ (30.5) m[d)]

[a)] singlet (*s*), doublet (*d*), broad (*br*); [b)] $^{1}J_{P,H}$ = 153 Hz; [c)] intensities of the N<u>H</u> (3.53), uncovered P<u>H</u> (3.04), C<u>H</u>$_{3\ C=N}$ (1.81) and C<u>H</u>$_{3\ NH}$ resonances (1.47 ppm) 1.0: 1.0: 9.0: 9.2; [d)] correlations: strong (s), medium (m), weak (w), very weak (vw); [e)] $^{1}J_{P,C}$ = 92 Hz; [f)] no HMBC correlation with <u>C</u>H$_{3\ NH}$; [g)] unresolved HMBC correlations of both the C<u>H</u>$_3$ signals at 1.47 and 1.81 ppm with the coinciding signals of the quaternary carbon atoms at 52.30 and 52.37 ppm; [h)] $^{1}J_{15N,H}$ = 70.0 Hz.

b) *N,N′*-di-*tert*-butylcarbodiimide dissolved in [d_6]benzene

^{1}H atom	δ-value (ppm)	^{1}H- COSY	HMQC(^{15}N), HSQC(^{13}C)	HMBC
C<u>H</u>$_3$	1.16 (*s*)[a)]	—	^{13}<u>C</u>H$_3$ (31.0) s[b)] ^{15}N$_{=C}$ (−264.9) s[b)]	^{13}<u>C</u>H$_3$ (30.9) s[b)] ^{13}<u>C</u>$_{quar}$ (53.9) s[b)]

[a)] singlet (*s*); [b)] correlations: strong (s).

In the ^{13}C NMR spectrum of complex **IV** (**Table 4.6**) two signals in the high field region at 28.8 and 30.5 ppm were observed. They are attributed to the methyl carbon atoms of the *tert*-butyl substituents. They are split into doublet due to coupling with the phosphorus atom ($^{4}J_{P,C}$ = 1 Hz for the NH part and $^{4}J_{P,C}$ = 9 Hz for the N=C part. Two very close signals at 52.30 and 52.37 pm were observed in the ^{13}C NMR spectrum. They assigned to the quarternary carbon atoms but because they are very close to each other it was impossible to distinguish between them. The carbonyl carbon atom (^{13}<u>C</u>N$_2$) was found as expected at low field as doublet at 191.8 ppm with $^{1}J_{P,C}$ of 92 Hz.

Table 4.6 Compilation of $\delta^{13}C$ (ppm) and $^{n}J_{P,C}$ values (Hz) of **IV** and the starting compound *N,N′*-di-*tert*-butylcarbodiimide

^{13}C-atom	**complex IV** $\delta^{13}C$[a)]	***N,N′*-di-*tert*-butylcarbodiimide** $\delta^{13}C$[a)]
$^{13}\underline{C}N_2$	191.8 (*d*), $^{1}J_{P,C}$ = 92	138.8
$^{13}\underline{C}_{quar}$[b)]	52.4 (*d*), $^{3}J_{P,C}$ = 1[c)]	54.1
$^{13}\underline{C}_{quar}$[b)]	52.3 (*d*), $^{3}J_{P,C}$ = 1[c)]	—
$^{13}\underline{C}H_{3\ NH}$	30.8 (*d*), $^{4}J_{P,C}$ = 1	—
$^{13}\underline{C}H_{3\ C=N}$	28.7 (*d*), $^{4}J_{P,C}$ = 9	31.1
other nuclei		
^{31}P	–63.7 (*s*)[d)]	—
$^{15}N_{H}$	—	—
$^{15}N_{=C}$	—	—
^{7}Li	0.75 (*s*)	—

[a)] multiplicity: singlet (*s*), doublet (*d*); [b)] no discrimination between $^{13}\underline{C}_{quar\ NH}$ and $^{13}\underline{C}_{quar\ C=N}$ possible; [c)] unresolved singlets in thf solution; [d)] doublet in the ^{1}H coupled ^{31}P NMR spectrum ($^{1}J_{P,H}$ = 153 Hz).

4.3.3. *Crystal data, Data Collection and Structure Analysis*

Colourless rod-shaped crystals suitable for an X-ray structure analysis were formed when a concentrated tetrahydrofuran solution of compound **IV** was kept for several days at −13 ºC. Data for the structure determination of complex **IV** was collected at 293K. Further details on data collection and refinement are described in the experimental section. At the end the atomic coordinates of hydrogen atoms could either be taken from a difference Fourier map and refined together with their isotropic replacement parameters or were calculated on the basis of an idealized geometry which mean a C–H distance of 96 and 97 pm for the methyl and methylene groups, respectively, tetrahedral angles and staggered arrangement of bonds at carbon. Already in this section it has to be pointed out that one of the two tetrahydrofuran ligand shows a disorder in such that one of the carbon atoms distributed over two positions (**Figure 8.6.1**) Crystallographic parameters and details of data collection have been summarized in **Table 4.7**.

Atomic coordinates and isotropic as well as anisotropic displacement parameters are given in **Table 8.6.2**. of the Appendix. Selected distances, bond angles, and torsion angles have been put together in **Table 4.8**.

Table 4.7 Crystal data and details of structure refinement for bis[μ-(*N,N′*-di-*tert*-butyl-*C*-phosphanidatoformamidin)-1κ^1*P*; 2κ^1*P′*;1:2κ^2*N*; 1:2κ^2*N′*]-1,2-bis(tetrahydrofuran-*O*)dilithium (**IV)**

Diffractometer	$P2_1$
Empirical formula; molecular weight	$C_{26}H_{56}Li_2N_4O_2P_2$; 532.57
Decomposition point (ºC)	167
Wavelength (pm)	71.073
Temp. of measurement (K)	293 ± 2
Crystal shape; crystal size (mm)	colourless rods; 0.4 x 0.2 x 0.2
Crystal system; space group [45]	monoclinic; *P*2$_1$*/c (No. 14)*
Unit cell dimensions: a/pm	884.14(3)
b/pm	1671.56(4)
c/pm	1154.65(3)
β/deg	103.632(2)
Volume (10^{-30}m^3); Z	1658.38(8); 2 dimers
Calculated density (10^3 kg/m^3)	1.067
Absorption coefficient μ (mm^{-1})	0.157
F(000)	584
Θ-Range for data collection (deg)	3.04 to 28.29
Limiting indices	$-11 \le h \le 11$; $-22 \le k \le 22$; $-15 \le l \le 15$
Systematic absences	*h0l: l* = 2*n*+1
	0k0: k = 2n+1
Scan mode; scan width (deg)	Wyckoff scan; 0.8
Velocity (deg s^{-1})	3.0 to 60.0
Reflections collected	7976
Unique reflections	4086
Completeness to θ_{max}	0.993
Refinement method	Full-matrix least-squares on F^2
Data used	4086
Parameters refined (n)	187
Restraints	1
Goodness-of-fit (GOF) on F^2	1.043
Final R-indices:	
R1/ wR2 using all data	0.0612; 0.1293
with [I > 2 σ (I)]	0.0493; 0.1236
Largest diff. peak; deepest hole (10^{-30}e.m^{-3})	0.723; −0.710

Table 4.8 Selected distances (pm), bond angles (deg), torsion angles and intramolecular contacts as well as least-squares planes and angles between these planes for bis[μ-(*N,N′*-di-*tert*-butyl-*C*-phosphanidatoformamidin)-1κ^1*P*;2κ^1*P′*;1:2-κ^2*N*;1:2κ^2*N′*-1,2-bis(tetrahydrofuran*O*)dilithium (**IV**).

a) Bond lengths

Amidinate-ligand				Tetrahydrofuran-ligand	
	n = 1	*n* = 2	mean		
P1–C1	179.5(2)	----		O3–C32A/C	147.3(3)/146.8(4)
P1–H1	128.4(3)	----		O3–C35	141.7(2)
C1–N*n*	129.8(2)	146.1(2)		C32A/C–C33	139.6(4)/ 149.3(5)
N2–H2	92.0	----		O33–C34	150.6(3)
N*n*–C*n*1	148.3(2)	150.2(2)	149.3	C34–C35	150.8(2)
N*n*–Li	204.3(3)	210.2(3)	207.3	Intramolecular contacts	
Li–O3	193.9(3)	—		C1···Li1	237.3(3)
Li–P1′ [a)]	261.4(3)	—		N1···N2	226.1(2)
C*n*1–C*n*2	152.6(3)	151.9(2)	152.6		
C*n*1–C*n*3	152.2(2)	152.6(2)			
C*n*1–C*n*4	153.1(2)	153.2(2)			

a) Symmetry operation: –x+1; –y; –z.

b) Bond angles

Amidinate-ligand				Coordination at lithium	
	n = 1	*n* = 2	mean		
C1–P1–H1	100.1(1)	—		N1–Li–N2	66.1(1)
C1– P1–Li1′	104.2(1)	—		N 1–Li–O3	123.6(2)
H1–P1–Li′	85.4(1)			N2–Li–O3	134.8(2)
N1–C1–N2	110.1(1)			N1–Li–P1′	125.6(1)
N*n*–C1–P1	133.6(1)	116.3(1)	125.0	N2–Li–P1′	108.4(1)
C1–N*n*–C*n*1	87.5(1)	81.4(1)	121.0		
C1–N*n*–Li	87.5(1)	37.5(7)	48.4		

c) Characteristic least-squares planes and deviations (pm) from these planes.
Atoms defining a least-square plane are marked with an asterisk (*).

A: *Amidinate-Ligand*

N1*	C1*	N2*	P1	H1	Li′	H2	C11	C12	C22	Li	O3
0.0	0.0	0.0	–11.5	10.7	–119.0	–31.3	13.9	24.9	174.6	–119.0	–127.1

B_A: *Disordered tetrahydrofuran -Ligand (with C32A)*

O3*	C32A*	C34*	C35*	C33	Li	N1	N2
2.1	–1.3	1.3	–2.0	47.9	–35.7	–95.3	77.1

B_c: *Disordered tetrahydrofuran-Ligand (with C32C)*

C32C*	C33*	C34*	C35*	O3	Li	N1	N2
1.9	–2.9	2.9	–1.8	–46.6	–109.6	–126.2	–17.3

e) Angle between the planes:
A/N1–Li–N2 43.3°; C1–N1–Li/C1–N2–Li 38.7°; N1–Li–N2/B_A 58.7°; N1–Li–N2/B_C 31.5°

4.3.4 *Discussion of Bond Lengths and Angles*

An X-ray structure analysis reveals that **IV** crystallized from tetrahydrofuran as a dimeric complex (**Figure 4.6 a)**). Each monomeric unit comprises a $1\lambda^3\sigma^3$-phosphaguanidinato chelate ligand and a lithium ion that is in contact with an additional tetrahydrofuran molecule (**Figure 4.6 b)**). The lithium coordination sphere comprises two *N*- and one *O*-donor atoms from the phosphaguadinate and THF ligands in the same monomeric unit and a *P*-donor atom which belongs to the phosphanido group in the second monomeric unit to give a coordination number of four.

a)

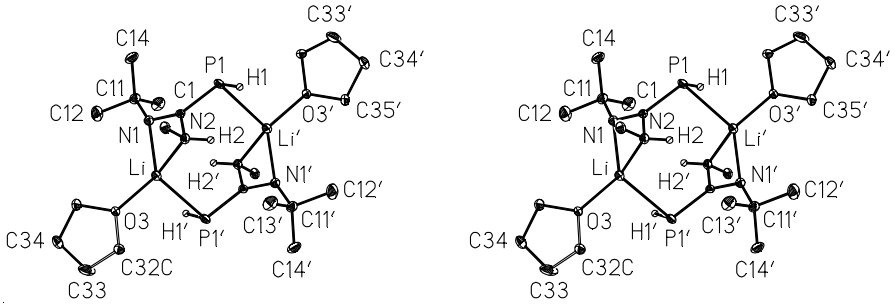

b)

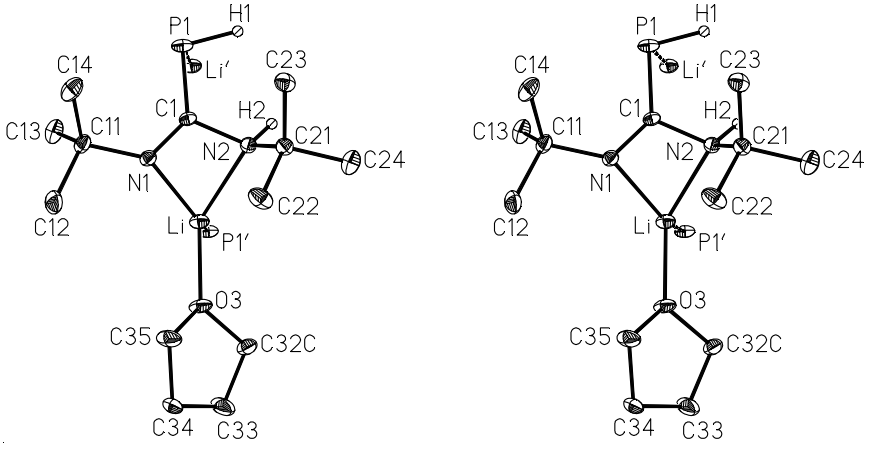

Figure 4.6 Stereoscopic views of the dimeric complex bis[μ-(*N,N′*-di-*tert*-butyl-*C*-phosphanidatoformamidin)-1κ^1*P*; 2κ^1*P′*;1:2κ^2*N*; 1:2κ^2*N′*-1,2-bis(tetrahydrofuran-*O*)dilithium **IV** (a) and of a single monomeric subunit (b). Thermal ellipsoids are at 30% probability; all hydrogen atoms except for H1 and H2 are omitted for clarity. In a) only the quarternary carbon atoms C21 and C21′ of the *tert*-butyl groups at N2 and N2′ respectively, are shown. For the carbon atom C32 of the tetrahydrofuran ligand only one of the two calculated split-positions A and C is shown.

the P–C distance of 179.5 (2) pm is slightly shortened with respect to the standard single bond value (183.5 pm) but still in agreement with the average P–C distances of 180.6 pm found in the Phosphanidyl(*N*-aryl)iminoformiat-entity of the complex (1,2-Dimethoxyethan-1κ^2*O,O′*)(1,2-dimethoxyethan-2κ^2*O,O′*)-(*Z*)-[phosphanidyl-*N*-(2,4,6-tri-*tert*-butylphenyl)imin-oformiato-1κ^2- *N,O*-2κ*P*]dilithium prepared in our research group [79]. The P–Li distances in the same complex range between 250 and 257 pm, the P–Li bond distance of 261.4(3) pm in **IV** is somewhat longer but still consistent with values observed for other compounds such as (1,2-dimethoxyethane)lithium phosphanides $[(\text{dme-}O,O'\text{)Li–PH}_2]_\infty$ (254 and 260 pm) [136] and $[(\text{diglyme-}O,O'\text{)Li–P(H)CH}_3]_\infty$(253 pm) [137]. Distances of 264 and 266 pm were also known for the lithium phosphanide $[(\text{thf})_2$ Li–P(H)Mes$]_\infty$[138].

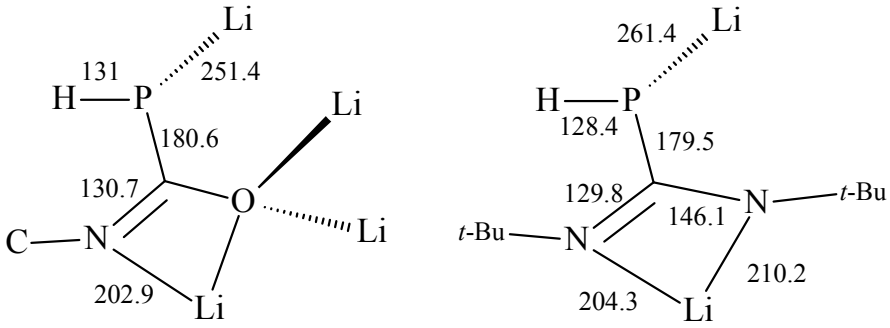

Furthermore, the P–Li distance of 261.4 pm in **IV** is very close to value of 262.5(5) pm reported by *Coles* and co-workers for the phosphaguanidinato complex Li($Ph_2PC\{N^iPr\}_2$)(TMEDA) [19]. According to the Cambridge Crystal Data Centre (CCDC), Li–P distances can reach from 172 to 318 pm with a mean of 2.57 pm [130].

In contrast to the N⋯C⋯N moiety in **III** (π-delocalization over the three atoms), the C–N bond lengths in **IV** are no longer equal but differ considerably. The values of 129.8 and 146.1 pm indicate the presence of localized C=N(R) double and C–N(H)R single bonds. As to be expected the mesomerism within the bent N⋯C⋯N group is disrupted by the protonation of one of its nitrogen atoms. The average N–Li distance of 207.3 (3) pm differs slightly (by 3.3 pm) from the mean value of 204.0 pm determined by X-ray structure analyses of lithium amides and –imides [109]. The Li–O distances of 193.9 (3) pm is shorter than the standard value of 196 pm reported for oxygen donor atoms on tetrahedrally coordinated lithium centres [139]. **Figure 4.8** give stereoscopic views of the molecular packing; no intermolecular contacts significantly shorter than *van der waals* distances were found.

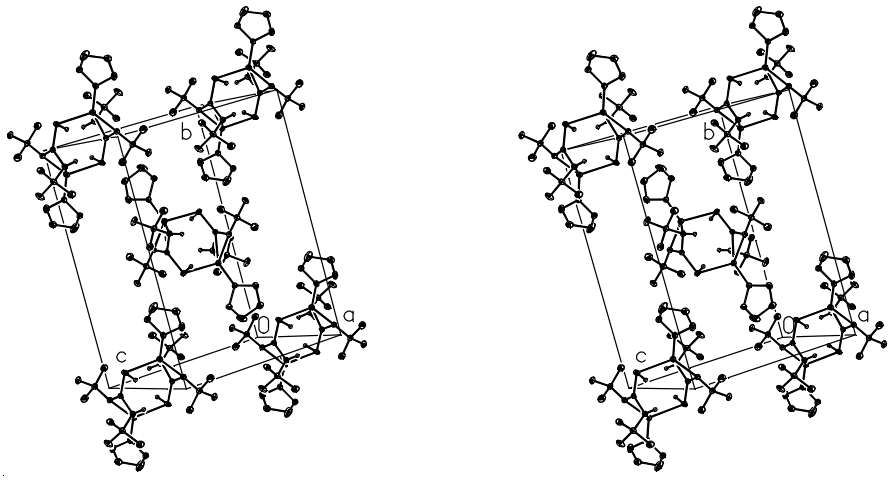

Figure 4.7 Unit cell content of the dimeric complex **IV** in stereoscopic view. Thermal ellipsoids are at 30% probability; hydrogen atoms except those in PH- and NH-groups have been omitted for clarity. Only one position of the disordered tetrahydrofuran carbon atom is depicted.

4.4 *Reaction of (1,2-Dimethoxyethane)lithium Phosphanide with* N,N′*-dicyclohexyl- and diisopropylcarbodiimide*

4.4.1 *Preparation and Reaction Mechanism*

A solution of *two* equivalents of lithium phosphanide dissolved in 1,2-dimethoxyethane and a solution of one equivalent of the corresponding diorganylcarbodiimides dissolved in the same solvent were combined dropwise with stirring at –70 °C. The mixtures were allowed to warm up slowly to room temperature. No change in colour was observed but the completion of the reaction can be inferred from the ^{31}P NMR spectra which show doublets at −154.3 and −140.0 ppm for the dicyclohexyl (**V**) and the diisopropyl derivative (**VI**), respectively. For the dicyclohexyl complex (**V**), crystals suitable for an X-ray structure analysis were obtained from a concentrated tetrahydrofuran solution which had been stored at −13 °C for one week. Crystals of the diisopropyl derivative (**VI**) were isolated from a concentrated tetrahydropyran solution left for three weeks at –13 °C. Both complexes were isolated in very good yield.

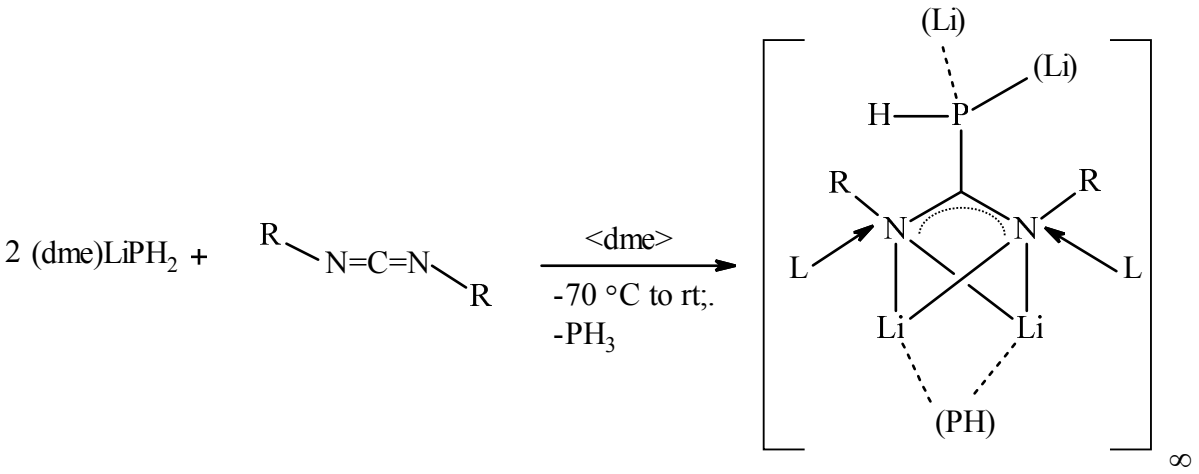

V (R = cyclohexyl;
L = tetrahydrofuran
VI (R = isopropyl;
L = tetrahydropyran

Unexpectedly, the reactions of dicyclohexyl- or diisopropylcarbodiimide with *two* equivalents of (1,2-dimethoxyethane)lithiumphosphanide led to the formation of the corresponding coordination polymer. Each monomeric unit in both polymers consists of a phosphaguanidinato ligand which coordinated through the negatively charged phosphorus atom to a lithium atom from another monomer. The reaction mechanism proceeds presumably via an initial nuecleophilic addition of the phosphanide anion to the carbodiimides leading to

phosphaguanidinato complex which are subsequently deprotonated by a second equivalent of lithiumphosphanide to yield the observed coordination polymers.

4.4.2 *NMR Spectroscopic Characterization*

The ^{31}P NMR spectra of both complexes show doublets at −154.3 ppm (**V**) and −140.0 ppm (**VI**), respectively. $^{1}J_{P,H}$ coupling constants of 157 and 159 Hz are in compliance with the presence of a negatively charged P–H group. In addition, these values are in agreement with that of 149 Hz measured for the *tert*-butyl complex (**IV**). Each spectrum contains further a broad singlet at −109.3 (**V**) and −131.2 (**VI**) ppm, respectively. The origin of these signals could not be established. The ^{1}H and ^{13}C NMR spectra were not very informative due to the relatively low solubility and high moisture and oxygen sensitivity.

4.4.3 *Crystal data, Data Collection and Structure analysis*

Data for the structure determination of the two polymeric complexes **V** and **VI** were collected at 100K ±2 on a Kappa II Dou diffractometer. Further details for the structure determinations of complexes **V** and **VI** are described in the experimental part. At the end the atomic coordinates of hydrogen atoms could either be taken from a difference Fourier map and refined together with their isotropic replacement parameters or were calculated on the basis of an idealized geometry. That means a C–H distance of 98 or 99 pm for the methyl and methylene groups, respectively, C–H distance of 100 pm for the CH groups of the isopropyl or cyclohexyl substituents as well as tetrahedral angles and a staggered arrangement of bonds at carbon. Crystallographic parameters and details of data collection have been summarized in **Table 4.9**. The Atomic coordinates and isotropic as well as anisotropic displacement parameters are given in **Table 8.7.2** for **V** and **8.8.2** for **VI** of the Appendix. A complete listing of bond lengths, bond angles and characteristic torsion angles of the complex **V** and **VI**, respectively, have been put together in **Tables 8.7.1** and **8.8.1**. It should be pointed out that one of the tetrahydrofuran ligands in complex **V** is disordered; two carbon atoms (C33 and C34) were distributed over two positions (C33A, C33C and C34A and C34C) (**Figure 8.7.1**).

Table 4.9 Crystal data and details of structure refinement for *catena*-poly[μ-(*N,N′*-dicyclohexyl-*C*-phosphanidato-1*:2*κ^2*P*-formamidinato-1:2κ^2*N,*1:2 κ^2*N′*)-1,2-bis(tetrahydrofuran-*O*]dilithium (**V**) and *catena*-poly[μ-(*N,N′*-diisopropyl-*C*-phosphanidato-1*:2*κ^2*P*-formamidinato-1:2κ^2*N,*1:2κ^2*N′*)-1,2-bis(tetrahydropyrane-*O*]dilithium (**VI)**

Compound	**V**	**VI**
Diffractometer	Kappa II Dou	Kappa II Dou
Empirical formula; Molecular weight	$C_{21}H_{39}Li_2N_2O_2P$; 396.39	$C_{17}H_{35}Li_2N_2O_2P$; 344.32
Decomposition point (ºC)	97	94
Wavelength (pm)	71.073	71.073
Temp. of measurement (K)	100 ± 2	100 ± 2
crystal size (mm)	0.73 x 0.45 x 0.16	0.51 x 0.28 x 0.22
Crystal system	monoclinic	orthorhombic
Space group [45]	*P2$_1$/c (No. 14)*	*P2$_1$2$_1$2$_1$ (No. 19)*
Unit cell dimensions a/pm	1132.23(4)	1053.47(5)
b/pm	1117.69(4)	1177.92(5)
c/pm	1911.28(8)	1677.65(8)
β/deg	97.765(2)	90
Volume (10^{-30}m^3); Z	2396.5(2); 4	2081.8(2); 4
Calculated density (10^3 kg/m^3)	1.099	1.099
Absorption coefficient μ (mm^{-1})	0.131	0.141
F(000)	864	752
Θ-Range for data collection (deg)	1.82 to 28.49	1.73 to 30.55
Limiting indices	$-15 \le h \le 15$	$-15 \le h \le 15$
	$-14 \le k \le 14$	$-16 \le k \le 12$
	$-25 \le l \le 25$	$-23 \le l \le 23$
Systematic absences	*h0l: l* = 2*n*+1	*h00: h* = 2*n*+1
	0k0: k = 2n+1	*0k0: k* = 2*n*+1
		00l: l = 2*n*+1
Scan modes; scan width (deg)	Omega + Phi; wide scan	Omega + Phi; wide scan
Velocity (deg s^{-1})	0.1	0.1
Reflections collected	40652	22483
Unique reflections [R(int.)]	6024 [0.0358]	6323 [0.0535]
Completeness to θ_{max}	0.993	0.997
Max. and minimum transmission	0.9794; 0.9105	0.9695; 0.9314
Refinement method	[a]	[a]
Data used	6024	6323
Parameters refined (n)	276	227
Restraints	50	0
Goodness-of-fit (GOF) on F^2	1.045	1.004
Final R-indices:		
R1/ wR2 using all data	0.0657; 0.1161	0.0747; 0.0918
with [I > 2 σ (I)]	0.0407; 0.1050	0.0459; 0.0845
extinction coefficient	—	0.0015(6)
Largest diff. peak;	0.370	0.281
deepest hole (10^{-30}e.m^{-3})	−0.242	−0.289

Table 4.10 Selected distances (pm), bond angles (deg), intramolecular distances and torsion angles as well as least-squares planes and angles between these planes for *catena*-poly[μ-(*N,N′*-dicyclohexyl-*C*-phosphanidato-1*:2*κ^2*P*-formamidinato-1:2κ^2*N,*1:2κ^2*N′*)-1,2-bis(tetrahydrofuran)-*O*]dilithium (**V)**

The positions of marked atoms are generated by applying the following symmetry operations: (′) –x, y – 0.5, –z + 0.5; (″) –x, y + 0.5, –z + 0.5

a) Distances

Amidinate ligand							
	n = 1	*n* = 2	mean		*n* = 1	*n* = 2	mean
P1–H1	129.1	—	—	N*n*–Li3	206.8(3)	206.2(3)	203.8
P1–C1	182.2(1)	—	—	N*n*–Li4	199.8(3)	202.4(3)	
C1–N*n*	135.4(2)	135.1(2)	135.3	P1–Li3″	259.9(3)		266.2
N*n*–C*n*1	145.0(2)	145.1(2)	145.1	P1–Li4″	272.2(2)		

b) Bond angles

Amidinate ligand				Coordination at lithium			
	n = 1	*n* = 2	mean		*n* = 3	*n* = 4	mean
C1–P1–H1	98.9	—	—	N1–Li*n*–N2	64.8(1)	66.7(1)	65.8
C1–P1–Li3″	102.7(1)	—	—	N1–Li*n*–O*n*1	115.6(1)	133.6(1)	130.0
C1–P1–Li4″	152.5(1)	—	—	N2–Li*n*–O*n*1	126.4(1)	144.5(1)	
H1–P1–Li3″	92.6	—	—	N1–Li*n*–P1′	113.3(1)	110.9(1)	105.8
H1–P1–Li4″	94.9	—	—	N2–Li*n*–P1′	100.9(1)	98.0(1)	
Li3″–P1–Li4″	52.9(1)	—	—	O*n*1–Li*n*–P1′	122.4(1)	98.5(1)	110.5

Table 4.11 Selected distances (pm), bond angles (deg), intramolecular distances and torsion angles as well as least-squares planes and angles between these planes for *catena*-poly[μ-(*N,N′*-diisopropyl-*C*-phosphanidato-1*:2*κ^2*P*-formamidinato-1:2κ^2*N,*1:2κ^2*N′*)-1,2-bis(tetrahydropyran)-*O*]dilithium (**VI)**

The positions of marked atoms are generated by applying the following symmetry operations: (′) –x + 1, y + 0.5, –z + 1.5; (″) –x + 1, y – 0.5, –z + 1.5

a) Distances

Amidinate ligand							
	n = 1	*n* = 2	mean		*n* = 1	*n* = 2	mean
P1–H1[a)]	128.5(20)	—	—	N*n*–Li3	203.3(3)	207.2(3)	205.3
P1–C1	183.6(1)	—	—	N*n*–Li4	207.5(3)	207.8(3)	207.7
C1–N*n*	134.7(2)	135.4(2)	135.1	P1–Li3″	267.7(3)	—	—
N*n*–C*n*1	145.4(2)	145.5(2)	145.5	P1–Li4″	257.0(3)	—	—

b) Bond angles

Amidinate ligand			Coordination at lithium		
			n = 3	*n* = 4	mean
C1–P1–H1[a)]	99.9(8)	N1–Li*n*–N2	65.3(9)	64.5(9)	64.9
C1–P1–Li3″	149.5(8)	N1–Li*n*–O*n*1	124.5(2)	114.8(1)	126.8
C1–P1–Li4″	127.0(7)	N2–Li*n*–O*n*1	138.0(2)	129.8(1)	
H1–P1–Li3″	108.8(8)	N1–Li*n*–P1′	109.8(1)	112.4(1)	105.0
H1–P1–Li4″	105.4(8)	N2–Li*n*–P1′	97.2(1)	100.4(1)	
Li3″–P1–Li4″	54.8(8)	O*n*1–Li*n*–P1′	113.0(1)	121.8(1)	117.4

4.4.4 *Discussion of Bond Lengths and Angles*

The X-ray structure determinations reveal that **V** and **VI** crystallized as coordination polymeric compounds. In each of the monomeric unit (**Figures 4.8** and **4.9**) which consists of phosphaguanidinato ligand, P–C bond distances of 182.2(1) and 183.6(1) pm in **V** and **VI**, respectively, were observed. These values are close to the standard P–C single bond distance of 183.5 pm and by 4 pm longer than in **IV** (179.5(2) pm)**.** The C–N bond distances vary in a narrow range between 134.7(2) pm in **VI** and 135.4 (2) pm in **V**, which suggests an almost ideal delocalization of π-bonding contributions over the N···C···N unit. This situation is similar to that observed in **III** which has an average C–N bond length of 132.8 pm but in contrast to that found for **IV** which has two different C–N bond lengths of 129.8 and 146.1 pm indicating a localized single and double bond.

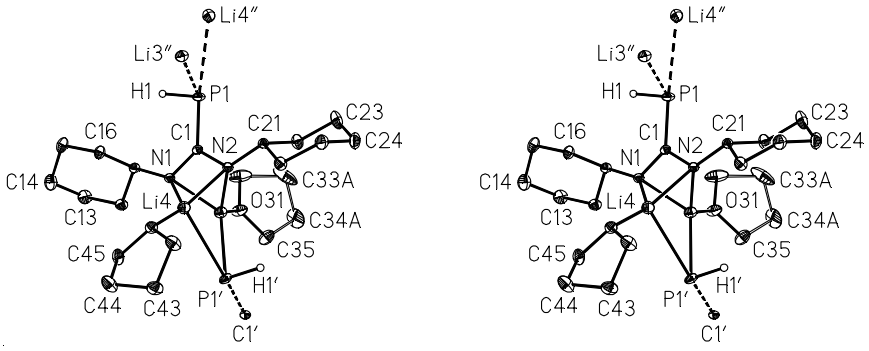

Figure 4.8 Monomeric unit of the complex *catena*-poly[μ-(*N,N′*-dicyclohexyl-*C*-phosphanidato-1*:2* κ^2*P*-formamidinato-1:2 κ^2*N,*1:2 κ^2*N′*)-1,2-bis(tetrahydrofuran-*O*]dilithium **V** in stereoscopic view**.** Thermal ellipsoids are at 30% probability; except for the PH-groups all hydrogen atoms are omitted for clarity. For the carbon atoms C33 and C34 of one tetrahydrofuran ligand two split-positions A and C (not depicted) were calculated. Absent atom numbering has to be complemented logically.

Each of the nitrogen atoms in the chelate ligand (N1 and N2) binds to two lithium atoms (Li3 and Li4) and adopts thus a tetrahedral coordination sphere. The N–Li distances in **V** vary in a narrow range between 199.8(3) pm and 206.8(3) pm, and those in **VI** between 203.3(3) and 207.8(3) pm. These values compared very well with that observed for complex **IV** (204.3(3) pm and 210.2(3) pm) and for the four coordinate lithium atom in **III** (201.9(5) pm and 203.7(5) pm).

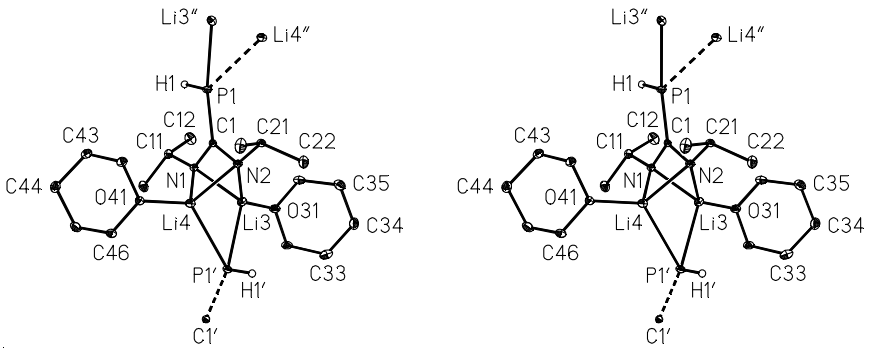

Figure 4.9 Monomeric unit of the complex *catena*-poly[μ-(*N,N′*-diisopropyl-*C*-phosphanidato-1*:2*κ^2*P*-formamidinato-1:2κ^2*N,*1:2κ^2*N′*)-1,2-bis(tetrahydropyrane-*O*]dilithium **VI** in stereoscopic view**.** Thermal ellipsoids are at 30% probability; except for the PH-groups all hydrogen atoms are omitted for clarity. Absent atom numbering has to be complemented logically.

Since **V** and **VI** can be regarded as special representatives of functionalized amidinato- or guanidinato ligands, it is worthy to shed some light on the general coordination modes of these species. The coordination modes of the amidinato- and bidentate guanidinato-ligands in complexes with alkali metal ions can be classified into three general classes [142]:

α) Monodentate mode: the ligand coordinates one metal atom through one nitrogen atom (*Type I*)

β) Bidentate mode: the ligand coordinates also one metal through both nitrogen atoms (*Type II*).

γ) Bimetallic bridging modes: the ligand coordinates to two metal atoms in μ-η^1:η^1- or μ-η^2:η^2- coordination modes (*type III* and *IV*, respectively).

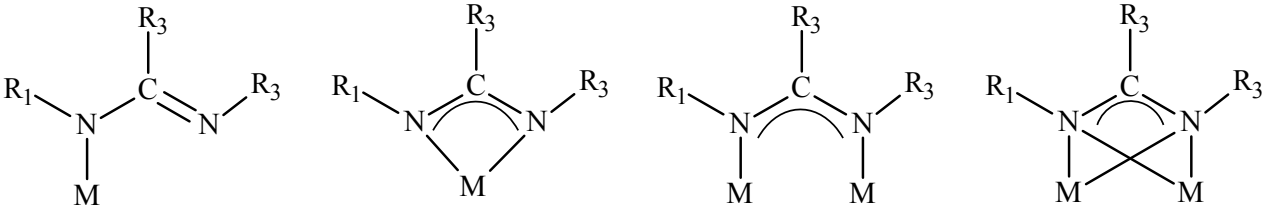

Type I *Type II* *Type III* *Type IV*

A quick literature review shows in particular the μ-η^2:η^2-coordination is predominant in complexes of sodium and potassium [142, 143 and ref. therein]. While only few lithium complexes of this type are known, two prominent examples include the solvent free dimeric

guanidinato complex $\{Li[CyNC(N(SiMe_3)_2)NCy]\}_2$ (*Arnold* complex) [140] and the lithated benzamidinate complex (*Eisen* complex) [141] were found in the literature.

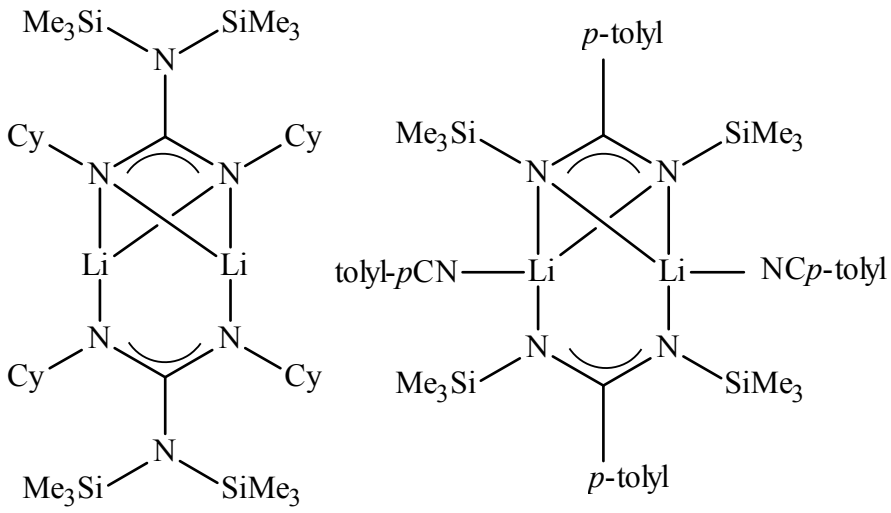

Arnold complex *Eisen* complex

For the sake of comparison, the structural features of the two complexes will be discussed in detail: The most characteristic feature of the *Arnold* complex is that one of the guanidinato ligands coordinates in μ-η^1,η^1-fashion and the second one in a μ-η^2,η^2-fashion. The second guanidinato ligands exhibits a similar coordination mode as the tridentate *P,N,N*-ligand in **V** and **VI**. The C–N and N–Li distances in the *Arnold* complex vary in rather narrow ranged between 131(1) and 135(2) pm and 196(4) and 203(3) pm, respectively. It should be noted that in this complex there is some disorder in the lithium positions but this does not affect the overall interpretation of the structure.

The low temperature X-ray analysis of *Eisen* complex reveals the same coordination motif. The C–N bond distances of 132.0(5) pm and 133.6(5) pm shows a uniform π-delocalization in the amidinato unit. The N–Li bond distances, however, are remarkably longer than in the *Arnold* complex and they vary between 210.8(1) pm and 226.0(9) pm.

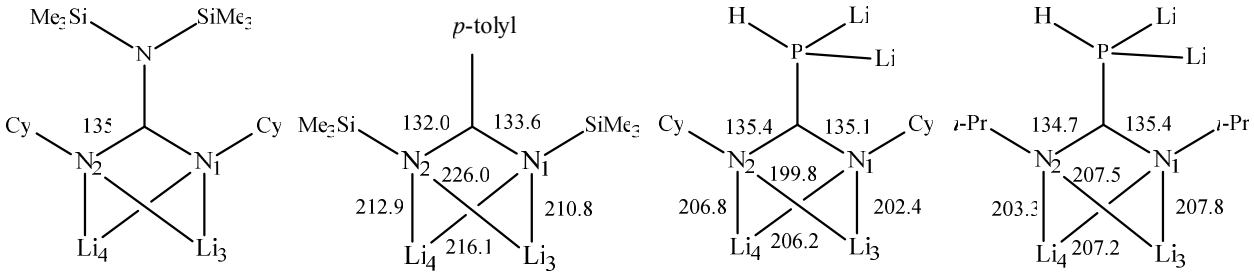

***Arnold* complex** ***Eisen* complex** **V** **VI**

Figures 4.10 and **4.11** show stereoscopic views of the strands of each complex, these strands are both cases directed along the [010] axes and can be generated from the monomer by applying rotary reflections along the appropriate 2_1-axes in the space group $P2_1/c$ (for **V**) and $P2_12_12_1$ (for **VI**), respectively. The strands **V** are arranged in a slightly distorted tetragonal rod packing and those in **VI** in a hexagonal rod packing (**Figure 4.12**).

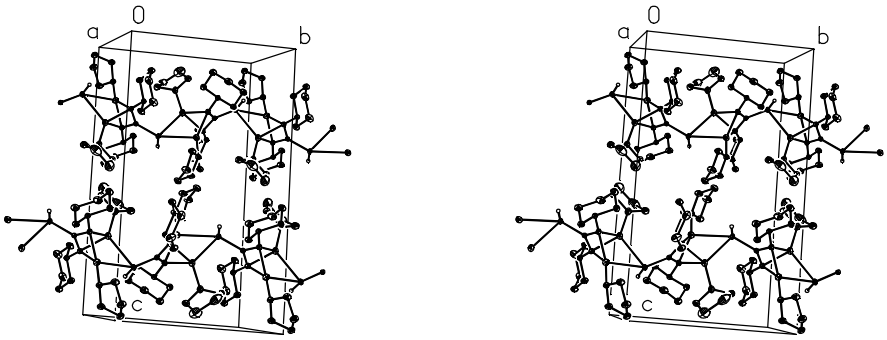

Figure 4.10 Two strands of the coordination polymeric complex **V** in stereoscopic view. The strands directed along [010] are generated from the monomer by applying the symmetry operation of the twofold screw axis (2_1-axis) of space group $P2_1/c$. They are interrelated by the symmetry operation of the glide planes c or the centre of inversion in e.g. (0.5, 0.5, 0.5).

Thermal ellipsoids are at 30% probability; except for the PH-groups hydrogen atoms have been omitted for clarity. Only one position of the disordered tetrahydrofuran carbon atom is depicted.

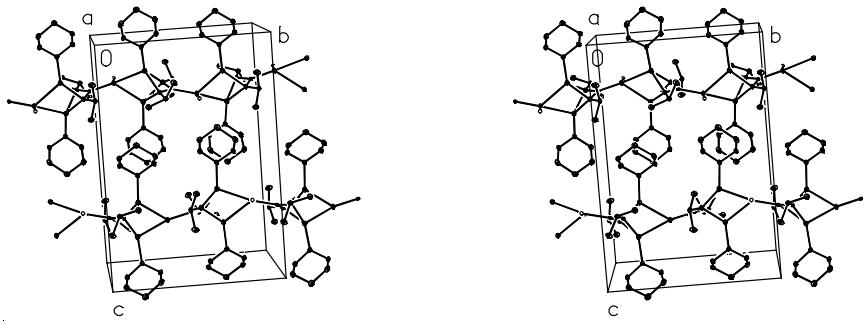

Figure 4.11 Two strands of the coordination polymeric complex **VI** in stereoscopic view. The strands directed along [010] are generated from the monomer by applying the symmetry operation of the two fold screw axis (2_1-axis) of space group $P2_12_12_1$. They are interrelated by the symmetry operation of the two other 2_1-axis along [100] and [010], respectively.

a)

b)

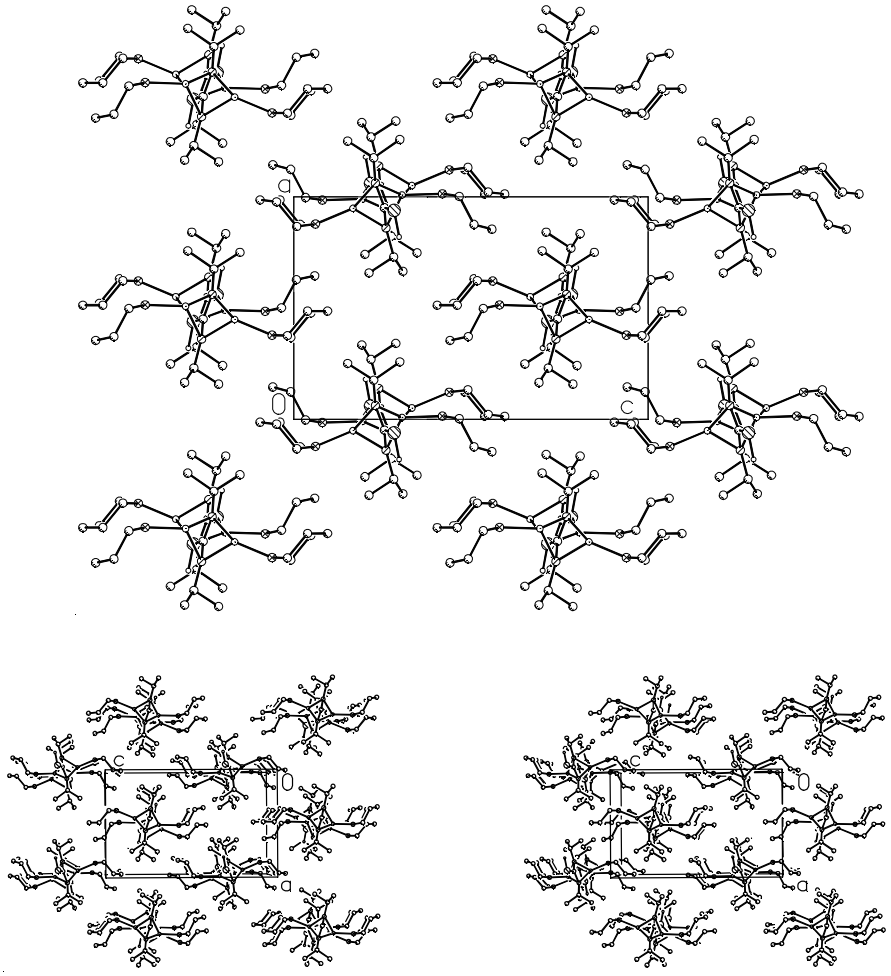

Figure 4.12 Non-stereoscopic (a) and stereoscopic view (b) of the strands of the coordination polymeric complex **VI** viewed along [0$\bar{1}$0]. The strands build up a hexagonal rod packing.

5. Experimental Section

5.1 General Considerations

All manipulations were conducted under argon (purity > 99.998%) on a vacuum line (evacuated to 1.10^{-3} mbar) using standard Schlenk techniques. *n*-Butyl lithium (1.6 M solution in n-hexane), benzonitrile, *tert*-butyl-chloro-di(phenyl)silane and carbodiimides R−N=C=N−R (R = $H_3CC_6H_4$, $C(CH_3)_3$, $CH(CH_3)_2$ and C_6H_{11}) were purchased from *Aldrich Chemical Co*. in 95.0 to 99.5 % purity. Bis(η^5-pentamethylcyclopentadienyl)zirconium dichloride was purchased from *Strem Co.* and used as received. Aluminiumphosphanide (80% wt) was purchased from *Detia Degesch Gmbh* Company. Phosphane (PH_3), (1,2-Dimethoxyethane-*O,O'*)lithium phosphanide and 1-[(1,2-Dimethoxyethane-*O,O'*)lithium-amido]benzylidenphosphane were synthesized according to published procedures [39].
The solvents 1,2-dimethoxyethane, toluene, tetrahydrofuran, and hexane were refluxed over sodium/benzophenone and distilled under argon prior to use [144 a)]. Anhydrous tetrahydropyran (99% purity) was used as received without further purification.
NMR samples were prepared in 5 mm or 10 mm tubes flame-sealed under argon. The spectra were recorded on *Bruker* instruments:
AV250 (^1H: 200.133, ^{13}C: 62.897, ^{31}P: 101.256 MHz) and
AV400 (^1H: 400.137, ^{13}C: 100.614, ^{31}P: 161.977, ^{29}Si: 79.495, ^{15}N: 40.561 MHz).

Chemical shifts were referenced to external TMS (_Xi_ = 100.000000 MHz) using the following secondary standards:

^1H *NMR*: d_6-benzene (internal; $\delta(C_6D_5H)$ = 7.15 ppm); d_8-Tetrahydrofurane (internal; δ = 1.73 ppm)
^{13}C *NMR*: TMS (external, δ = 0.0 ppm)
^{31}P *NMR*: 85% aqueous H_3PO_4, external; δ = 0.00 ppm.
^{29}Si *NMR*: tetramethylsilane, external; δ = 0.00 ppm.
^{15}N *NMR*: nitromethane, external; δ = 0.00 ppm.

All nuclear resonance spectra were recorded at room temperature unless otherwise stated. All coupling constants (*J)* are reported in (Hz) and given as absolute values. For the multiplicity of the resonance signals, the following abbreviations are applied:
s: singlet, d: doublet, t: triplet, q: quartet, m: multiplet, dd: doublet of doublets.

Elemental analyses were carried out with the ICP AES analysing technique at a *Perkin-Elmer Series II Analyzer 2400*. Mass spectra were obtained at a mass spectrometer *micrOTOF-Q* of the company *Bruker Daltonnics*. Melting points were determined using *Büchi B-545* melting point apparatus with samples sealed in capillaries under argon.

IR spectra were obtained using a *Nicolet 6700 FT-IR* instrument; solid state IR measurements were performed with an ATR unit (smart orbit diamond crystal) whereas measurements for the samples dissolved in 1,2-Dimethoxyethane was performed in transmission using CaF_2 window. The following abbreviations for intensities are used:
vw: very weak, w: weak, m: medium, s: strong, vs: very strong, br: broad, sh: shoulder.

Single crystals for X-ray structure determinations were separated directly from the solution at room temperature under argon and covered with polyfluorinated polyether oil (*RS 3000, Riedel-de-Haën*) in order to protect them from atmospheric moisture and oxygen. The oil 'freezes' at reduced temperatures and keeps the crystal static in the X-ray beam. Oxidation by air during data collection does not occur as the crystals are cooled down to –100 ± 3 °C in a stream of nitrogen [144 b)]. Intensities were collected on the four-circle diffractometers P21 (*Syntex, Cupertino, USA*), P4 (*Siemens Analytical X-ray Instruments Inc., Madison, Wisconsin, USA*), and Bruker (*Kappa Apex II Dou) using graphite monochromatized Mo-Kα-radiation (λ = 71.073 pm*). For the treatment of data, the determination of a structure model by applying statistical methods and the subsequent refinement of the structure model, the software package SHELXTL, version 5.10 was employed. The sub-program XP served for an analysis of the molecular geometry and the preparation of the drawings [43, 44].

Data of Structure Refinement

Data for a structure determination were collected on a P4 (for **I** and **III**), Bruker (*Kappa Apex II Dou)* (for **V** and **VI**) or P21 diffractometer (for **IV**) using graphite monochromatized MoK_α radiation (λ = 71.073). On the basis of unit cell dimensions and statistical tests on the distribution of E-values, the triclinic space group $P\bar{1}$ was chosen. To solve the crystal structure with statistical methods, the software package SHELXTL version 5.1 was applied [43, 44]. This package also includes the program XP for an analysis of the molecular geometry and the preparation of drawings. All phosphorus, nitrogen, silicon, lithium, oxygen and carbon atoms were located step by step and their positions as well as their isotropic replacement parameters were refined by full-matrix least-squares calculations. Thereafter, the structure determination was continued by introducing individual anisotropic U_{ij}-values. At the end of the structure refinement, the atomic coordinates of hydrogen atoms were calculated on the basis of an idealized. Furthermore, the riding model applied ensures that a change in the carbon position is automatically transferred to the adjacent hydrogen atoms. Individual isotropic U-values for these hydrogen atoms were adopted from the respective carbon atoms and increased by a corresponding factors. To take into account the incorporation of hydrogen atoms, the parameters of all heavier atoms were refined again, and final agreement factors of R1 and wR2 were calculated.

DFT Calculation

The Gaussian 03 [145] package was used for all energy and frequency calculations. The energies of the model compounds were minimized by using density functional theory with the functional B3LYB [146] starting from the crystallographically determined geometry. An energy consistent, quasi-relativistic pseudopotential of the Stuttgart/Cologne group with an optimized (8s7p6d2f1g)/[6s5p3d2f1g] valence basis set was employed for the heavier atom zirconium (N = 28), [147] where N denotes the number of core electrons. For the lighter atoms carbon, hydrogen, nitrogen and phosphorus the basis sets 6-31G* (for the model compound $Cp_2Zr\{N=C(C_6H_5)P=C(C_6H_5)NH\}$ ($\mathbf{II_{Mod.}}$)) or 6-311+G* (for the negatively charged chelate ligand $\{N=C(C_6H_5)P=C(C_6H_5)NH\}^{-2}$ ($\mathbf{L^{-2}}$)) were used. The natural bond orbital analysis employed the Gaussian 03 adaptation of the NBO program [148].

5.2 Preparation of (1,2-Dimethoxyethane-*O*,*O*′)lithium Phosphanide According to Ref. [149]

A solution of concentrated sulphuric acid (100 ml) in water (200 ml) was added dropwise over a period of 2 h with vigorous stirring to a solid mixture of 80% aluminium phosphanide (10g, 0.138 mol) and paraffin at room temperature. Gaseous phosphane evolved (~3.4 g, about 75% yield) and was passes through a KOH drying tube long enough (32 cm) to remove moisture completely. Without any further isolation it was reacted at −70 ºC with a vigorously stirred solution of *n*-butyl lithium (50 ml of an 1.6 M hexane, 0.08 mol) in 100 ml of 1,2-dimethoxyethane. (1,2-Dimethoxyethane-*O*,*O*′)-lithium phosphanide (7.5 g, 0.058 mol about 72% yield) precipitated immediately as the solvents removed under reduced pressure. The solvent (1,2-dimethoxyethane) : Li–PH_2 ratio was determined by NMR spectroscopy.

Characterization by NMR (solution in d_8-tetrahydrofuran)

^{31}P-NMR: δ = −287.9 (t, $^1J_{PH}$ = 148 Hz)

^{1}H-NMR: δ = −1.4 (d, $^1J_{PH}$ = 148 Hz); 3.3 (s, OCH_3, DME); 3.4 (s, OCH_2, DME)

5.2.1 2-[(1,2-Dimethoxyethane-*O*,*O*′)lithiumamido]-2-phenyl-1$\lambda^3\sigma^2$-phosphaalkene

A solution of benzonitrile (3.2 ml; 31.06 mmol) in 20 ml of 1,2-dimethoxyethane was added dropwise with stirring to a cooled solution (−60 ºC) of (1,2-dimethoxyethane-*O*,*O*′)lithium phosphanide (4.04 g; 31.06 mmol) in 30 ml of the same solvent. Within 24 hours the reaction mixture was allowed to warm up to room temperature. Without any further purification the deep red solution was used for various reactions.

Characterization by *NMR* (solution of the solid product in d_8-tetrahydroduran)

^{31}P{^{1}H}-NMR, *Z*-isomer**:** δ = −28.5 (s); *E*-isomer: −50.0 (s)

^{31}P-NMR, *Z*-isomer**:** δ = −29.3 (d, $^1J_{P,H}$ = 147 Hz); *E*-isomer: −50.1 (d, $^1J_{P,H}$= 150 Hz)

^{1}H-NMR: δ = 3.3 (s, OCH_3, DME); 3.5 (s, OCH_2, DME);
Z-isomer: δ = 2.8 (d, $^{1}J_{P,H}$ = 144 Hz, *H*P); 7.3 (brd, *H*N); 7.8 (d, $^{3}J_{P,H}$ = 6 Hz C–H$_{ortho}$); 7.1 – 7.2 (brd, C–H$_{meta}$, C–H$_{para}$)
E-isomer: δ = 2.7 (d, $^{1}J_{P,H}$ = 149 Hz, *H*P); 6.0 (d, $^{3}J_{P,H}$ = 19 Hz, *H*N); 7.58 (d, $^{3}J_{P,H}$ = 7 Hz, C–H$_{ortho}$); 7.10 – 7.15 (brd, C–H$_{meta}$, C–H$_{para}$)

^{13}C-NMR:
Z-isomer: δ = 124.4 (d, $^{3}J_{CP}$ = 10 Hz, C$_{ortho}$); 124.8 (s, C$_{meta}$); 125.1 (s, C$_{para}$); 149.4 (d, $^{2}J_{CP}$ = 25 Hz, C$_{ipso}$); 208.8 (d, $^{1}J_{CP}$ = 70 Hz, P=*C*)
E-isomer: δ = 123.2 (d, $^{3}J_{CP}$ = 8 Hz, C$_{ortho}$); 124.5 (s, C$_{meta}$); 125.1 (s, C$_{para}$); 149.2 (d, $^{2}J_{CP}$ = 19 Hz, C$_{ipso}$); 209.4 (d, $^{1}J_{CP}$ = 52 Hz, P=*C*)
δ = 56.1 (s, O*C*H$_3$, DME); 69.9 (s, O*C*H$_2$, DME);

5.3 Procedures for the preparation of new compounds

5.3.1 *Z*-[*N*,*P*-Bis(*tert*-butyldiphenylsilyl)-2-amino-2-phenyl-1λ^{3}σ^2-phosphaalkene] (I.2)

A solution of 2-[(1,2-dimethoxyethane-*O*,*O*′)lithiumamido]-2-phenyl-1λ^{3}σ^2-phosphaalkene (10 ml; 3.2 mmol) in 15 ml of 1,2-dimethoxyethane was added dropwise with stirring to a cooled (−60 ºC) solution of *tert.*-butyl(chlor)diphenylsilane (0.97 g; 3.5 mmol) in 15 ml of the same solvent. The reaction mixture was left to warm up slowly overnight, the colour of the still stirred solution had changed from red to orange. The solvent was then removed under reduced pressure and the residue was treated with 20 ml of toluene. After filtration the solution was concentrated to about 10 ml and stored in a refrigerator at −13 ºC. Within one week yellow crystals (1.9 g; 3.1 mmol; 88% yield) had precipitated.

Characterization

Yellow solid, melting point 176 ºC (decomposition).

Elemental analysis: $C_{39}H_{44}NPSi_2$ (613.3 g/mol)
calc.: C 76.30%, H 7.22%, N 2.28%, found: C 74.90%, H 7.26%, N 2.37%.

NMR (solution in d_8-THF; (*Z*)- and (*E*)-isomers are present in the solution with an intensity ratio of about 7:1)

Data for (*Z*)-isomer:

$^{31}P\{^{1}H\}$: δ = 45.5 ppm (s, ^{29}Si satellites: $^{1}J_{Si,P}$ = 81 Hz, $^{13}C_{ipso}$(P=C–C_6H_5) satellites: $^{2}J_{P,C}$ = 27 Hz)

^{1}H: δ = 0.0 (s, $(H_3C)_3$CSiN); 0.87 (s, $(H_3C)_3$CSiP); 6.1 (br, s, N*H*); phenyl substituent at P=C: 6.4 (pt, ^{3}J(H,H) = 8 Hz, C–H_{meta}); 6.6 (pt, ^{3}J(H,H) = 8 Hz, C–H_{para}); 6.7 (pd, ^{3}J(H,H) = 8 Hz, C–H_{ortho}); phenyl substituent at Si(NH): 7.0 (m, C–H_{ortho}); 7.0 (m, C–H_{meta}); 7.1 (m, C–H_{para}) ; phenyl substituent at Si(P): 7.3 (m, C–H_{para}); 7.3 (m, C–H_{meta}); 8.1 (pdpd, C–H_{ortho})

^{13}C: δ = 17.9 (s, $(H_3C)_3C$Si(NH); 19.5 (d, $^{2}J_{P,C}$ = 16 Hz, $(H_3C)_3C$Si(P)); 26.3 (s, $(H_3C)_3$CSi(NH)); 27.3 (d, $^{3}J_{P,C}$ = 4 Hz, $(H_3C)_3$CSi(P)); phenyl substituent at P=C: 126.7 (s, C_{meta}); 127.7 (s, C_{para}); 128.6 (d, $^{3}J_{P,C}$ = 11 Hz, C_{ortho}); 144.2 (d, $^{2}J_{P,C}$ = 28 Hz, C_{ipso}); phenyl substituent at Si(P): 128.4 (s, C_{meta}); 130.0 (s, C_{para}); 134.5 (d, $^{2}J_{P,C}$ = 2 Hz, C_{ipso}); 137.3 (s, C_{ortho}); phenyl substituent at Si(NH): 127.5 (s, C_{meta}); 129.5 (s, C_{para}); 133.5 (s, C_{ipso}); 135.8 (s, C_{ortho}); 208.9 (d, $^{1}J_{CP}$ = 78 Hz, P=*C*)

^{29}Si: δ = −3.9 (d, $^{1}J_{P,Si}$ = 81 Hz); −11.6 (d, $^{3}J_{P,Si}$ = 3 Hz)

Data for (*E*)-isomer:

$^{31}P\{^{1}H\}$: δ = 85.4 ppm (d, $^{3}J_{P,H(N)}$ = 22 Hz; ^{29}Si satellites: $^{1}J_{Si,P}$ = 77 Hz)

^{1}H: δ = 0.4 (s, $(H_3C)_3$CSiP); 0.86 (s, $(H_3C)_3$CSiN); 6.1 (br, d, $^{3}J_{P,H(N)}$ = 22 Hz N*H*); phenyl substituent at P=C: 6.3 (pt, C–H_{meta}); 6.6 (pt, C–H_{para}); 6.6 (pd, C–H_{ortho}); phenyl substituent at Si(NH): 7.3 (m, C–H_{meta}); 7.3 (pt, C–H_{para}); 7.8 (m, C–H_{ortho}) ; phenyl substituent at Si(P): 7.0 (pt, C–H_{meta}); 7.0 (undetc, C–H_{para}); 7.2 (m, C–H_{ortho})

^{13}C: δ = 18.7 (s, $(H_3C)_3C$Si(NH); 20.4 (d, $^{2}J_{P,C}$ = 19 Hz, $(H_3C)_3C$Si(P)); 27.1 (s, $(H_3C)_3$CSi(NH)); 27.7 (d, $^{3}J_{P,C}$ = 5 Hz, $(H_3C)_3$CSi(P)); phenyl substituent at P=C: 126.7 (s,

C_{para}); 127.3 (s, C_{meta}); 127.7 (d, $^{3}J_{P,C}$ = 2 Hz, C_{ortho}); 149.0 (d, $^{2}J_{P,C}$ = 27 Hz, C_{ipso}); phenyl substituent at Si(P): 126.9 (s, C_{meta}); 129.6 (s, C_{para}); 136.4 (d, $^{2}J_{P,C}$ = 2 Hz, C_{ortho}); 136.4 (d, $^{2}J_{P,C}$ = 2 C_{ipso}); phenyl substituent at Si(NH): 127.7 (s, C_{meta}); 129.7 (s, C_{para}); 136.7 (s, C_{ortho}); 136.8 (s, C_{ipso}); 209.4 (d, $^{1}J_{CP}$ = 76 Hz, P=*C*)

^{29}Si NMR signals are not detectable.

IR-Spectrum (nujol):

3366 w br, 3053 s, 3028 s, 1604 m, 1460 s, 1392 m, 1367 m, 1252 m

Characteristic Masses (%) from the Mass Spectrum:

$\{M\}^{+}(^{13}C)$	616.3	19.8
$\{M\}^{+}(^{13}C)$	615.3	54.9
$\{M\}^{+}$	614.3	100
$\{^{t}BuPh_2SiPC(Ph)N(H)SiPh_2\}^{+}$	565	15.4
$\{^{t}BuPh_2SiPC(Ph)N(H)SiPhH_2\}^{+}$	481	23.1
$\{^{t}BuPh_2SiPC(Ph)NH_2\}^{+}$	376	4.4
$\{^{t}BuPh_2SiN(H)C(Ph)(H)\}^{+}$	344	3.3
$\{^{t}BuPh_2SiPC(H)NH_2-2H\}^{+}$	297	25.3

5.3.2 *2-[(*tert*-Butyldiphenylsilyl)amino]-2-phenyl-1$\lambda^3\sigma^2$-phosphaalkene {(Z)-/(E)-I.1} by Decomposition of Compound (Z)-/(E)-I.2*

(*Z*)-/(*E*)-I.1 is generated when a solution of crystalline 1$\lambda^3\sigma^2$-phosphaalkene **I.2** in [d_8]tetrahydrofuran is kept in a sealed NMR tube for about six months at +55 ºC in a drying oven. The decomposition was monitored ^{31}P NMR spectroscopically. The structure of the reaction by-products $\mathbf{I}_{eli}$ formed from the eliminated (*tert*-butyldiphenylsilyl) group at phosphorus is still unknown. ^{1}H, ^{13}C, ^{31}P, and ^{29}Si NMR data were taken from a 400.13 MHz, 100.61 MHz, 161.98 MHz, and 79.50 MHz spectrum, respectively. ^{13}C chemical shift values are listed in **Table 2.9** for comparison.

Data for (*Z*)-isomer:

$^{31}P\{^{1}H\}$: δ = 43.8 ppm (d, $^{1}J_{P,H}$ = 150 Hz)

^{1}H: δ = 0.83 (s, $(H_3C)_3CSiN$); 3.63 (dd, $^{1}J_{P,H}$ = 150 Hz, $^{4}J_{H,H(N)}$ = 1 Hz, (*H*P)); 5.76 (br, s, N*H*); phenyl substituent at P=C: 7.19 (m, C–H_{meta}); 7.57 (m, C–H_{ortho}); 7.67 (m, C–H_{para}); phenyl substituent at Si(NH): 7.14 (m, C–H_{para}); 7.14 (m, C–H_{meta}); 7.56 (m, C–H_{ortho})

^{13}C: δ = 19.1 (s, $(H_3C)_3CSi(NH)$; 26.5 (s, $(H_3C)_3CSi(NH)$); phenyl substituent at P=C: 125.7 (d, $^3J_{P,C}$ = 15 Hz, C_{ortho}); 128.6 (s, C_{meta}); 136.4 (d, $^5J_{P,C}$ = 2 Hz C_{para}); 145.0 (d, $^2J_{P,C}$ = 27 Hz, C_{ipso}); phenyl substituent at Si(NH): 127.5 (s, C_{meta}); 129.3 (s, C_{para}); 137.1 (s, C_{ipso}); 135.1 (s, C_{ortho}); 200.1 (d, $^1J_{P,C}$ = 54 Hz, P=*C*)

^{29}Si: δ = −9.63 (s)

Data for (*E*)-isomer:

$^{31}P\{^1H\}$: δ = 66.8 ppm (dd, $^1J_{P,H}$ = 154 Hz, $^3J_{P,H(N)}$ = 19 Hz)

^1H: δ = 0.89 (s, $(H_3C)_3CSiN$); 3.61 (dd, $^1J_{P,H}$ = 154 Hz, $^4J_{H,H(N)}$ = 3 Hz, (*H*P)); 5.72 (br, dd, $^1J_{P,H(N)}$ = 20 Hz, $^4J_{H,H(P)}$ = 3 Hz N*H*); phenyl substituents at P=C and at Si(NH): not detectable due to low concentration.

^{13}C: The concentrations of (***E***)-**I.1** is too low as to detect the corresponding ^{13}C NMR signals.

^{29}Si: δ = −9.9 (s)

Signals arising from unidentified side products ($\mathbf{I}_{eli.}$):

^1H: δ = 0.86 (s); 7.21 (m, C–H_{meta}); 7.22 (m, C–H_{para}); 7.69 (m, C–H_{ortho})

^{13}C: δ = 18.5 (m) ; 26.7 (m); 128.1 (s); 128.6 (s, C_{meta}); 129.9 (s); 135.9 (s);

^{29}Si: δ = −9.6 (s)

5.3.3 *Formation of (Z)-/(E)-Isomeric 2-Amino-2-phenyl-1λ³σ²-phosphaalkene* H~P=C(C_6H_5)–NH_2 (I.0) *in Reactions of 2-(Lithiumamido)-2-phenyl-1λ³σ²-phosphaalkene (1) with Acids*

(*Z*)-/(*E*)-Isomeric 2-Amino-2-phenyl-1λ³σ²-phosphaalkene H~P=C(C_6H_5)–NH_2 (**I.0**) was obtained when a 1,2-dimethoxyethane solution of (***Z***)-/(***E***)-**1** was treated with different proton sources such as neat trifluoromethanesulfonic acid or triethylammonium chloride. similar results were also obtained in a reaction of (***Z***)-/(***E***)-**1** with (*tert*-butyldimethylsilyl)trifluoromethanesulfonate where it was found that a major part of the silyl ester had accidentally been hydrolysed.

Preparation of the samples

Sample A. An equivalent amount of neat trifluoromethanesulfonic acid (0.3 ml; 3.2 mmol) was added dropwise with stirring to a cold (−78 ºC) 1,2-dimethoxyethane solution of 2-(lithiumamido)-2-phenyl-1$\lambda^3\sigma^2$-phosphaalkene (**1**) (10 ml; 3.2 mmol). After warming up slightly within a few hours the colour of the reaction mixture had changed from red to orange. A small part of the still cold solution was transferred with a pipette into a cooled NMR tube. After sealing the tube the spectrum was taken at +28 ºC. Perceptible decomposition of (***Z***)-/(***E***)-**I.0** occurred within several days. For an optimization of the NMR experiments, however, most of the solvent 1,2-dimethoxyethane had to be removed *in vacuo* at −40 ºC and replaced by [d_8]tetrahydrofuran (*Sample A'*).

Sample B. An equivalent amount of largely hydrolysed (*tert*-butyldimethylsilyl)trifluoromethanesulfonate (0.75 ml, 3.2 mmol) in 1,2-dimethoxyethane was added dropwise with stirring to a cold (−78 ºC) 1,2-dimethoxyethane solution of **1** (10 ml; 3.2 mmol). After warming up to room temperature over night the colour had changed from deep red to orange. The spectrum of the sealed sample was taken at +28 ºC.

Sample C. An equivalent amount of triethylammonium chloride (0.45 g; 3.2 mmol) in 1,2-dimethoxyethane was added at room temperature dropwise with stirring to a 1,2-dimethoxyethane solution of **1** (10 ml; 3.2 mmol). Within a few minutes the colour of the reaction mixture changed from red to orange. A small part of the solution was transferred with a pipette into an NMR tube. After sealing the spectrum of the sample was taken at +28 ºC.

Sample D. A 1,2-dimethoxyethane solution of an equivalent amount of **1** (10 ml; 3.2 mmol) was added at −78 ºC dropwise with stirring to *tert*-butylchlorodiphenylsilane (0.97 g; 3.5 mmol) in 1,2-dimethoxyethane. Within a few minutes the colour of the reaction mixture changed from deep red to orange. A small part of the still cold solution was transferred with a pipette into an NMR tube. The spectrum was taken at +28 ºC. For an isolation of crystalline (*Z*)-*N*,*P*-bis(*tert*-butyldiphenylsilyl)-2-amino-2-phenyl-1$\lambda^3\sigma^2$-phosphaalkene {(***Z***)-**I.2**} see the experimental part section **5.3.1**.

Further ^{31}P NMR signals observed in the 1,2-dimethoxyethane solutions of *Samples A, B, C, and D*

Compound or signal	*Sample*	δ ^{31}P	multiplicity[a] $\{^1H\}/^1H$ coupl.	$J_{P,P}$	$^1J_{P,H}$	$J_{P,H}$	$J_{P,H(N)}$	intens. ratio
E	*A*	51.5	(*s*)/(*s*)	–	–	–	–	0.70
	B	52.4	(*s*)/(*s*)	–	–	–	–	0.33
	C	53.7	(*s*)/(*s*)[b]	–	–	–	–	0.36
F	*A*	177.8	(*s*)/(*s*)	–	–	–	–	0.35
	B	178.2	(*s*)/(*s*)	–	–	–	–	0.33
	C	179.6	(*s*)/(*s*)[b]	–	–	–	–	0.37
G	*B*	18.2	(*s*)/(*d*)	–	141	–	–	4.78
H	*B*	45.5	(*d*)/(*dd*)	294	–	10	–	1.38
I	*B*	93.7	(*d*)/(*d*)	295	–	–	–	1.53
J	*B*	49.0	(*s*)/(*dd*)	–	162	19	–	6.18
K	*B*	84.2	(*s*)/(*t*)	–	–	6	–	1.79
L	*C*	–3.0	(*d*)/(*d*)	173[b]	–	–	–	0.15
M	*C*	–186.5	(*d*)/(*dt*)	174	197	–	–	0.20
n[c]	*D*	–57.9	(*d*)/(*d*)	206	–	–	–	1.87
o[c]	*D*	–48.6	(*d*)/(*d*)	206	–	–	–	1.66
p[d]	*D*	2.3	(*d*)/(*d*)	206	–	–	–	1.01
q[d]	*D*	5.5	(*d*)/(*d*)	206	–	–	–	0.83
R	*D*	88.6	(*s*)/(*m*)[e]	–	–	–	–	0.94

[a] singlet (*s*), doublet (*d*), triplet (*t*), quartet (*q*), multiplet (*m*); [b] half-width of each resonance 35 Hz; [c] signals *n* and *o* in an intensity ratio of 1.0 : 0.89; [d] signals *p* and *q* in an intensity ratio of 1.0: 0.82; [e] unstructured multiplet (essentially three lines).

5.3.4 Diphosphanes (*Z*)-I.01 and (*Z*)-I.02 Originating from a Dimerisation of the Phosphaalkenes (*Z*)-/(*E*)-I.0

These compounds were generated during the formation of the unsubstituted (*Z*)-/(*E*)-isomeric 2-amino-2-phenyl-1$\lambda^3\sigma^2$-phosphaalkene (**I.0**) from the reaction of ligand **1** with acids. Monitoring an NMR sample of **I.0** in a sealed NMR tube for one week shows the generation of the two diastereomers **(*Z*)-I.01** and **(*Z*)-I.02**. These compounds could not be isolated, their structures were determined in solution by 2D NMR spectroscopy. For more details see **Section 2.6**.

5.3.5 [*N*,*N*′-(1-Amido-3-imido-1,3-diphenyl-2λ^{3}σ^2-phospha-1-propene)bis(η^5-pentamethylcyclopentadienyl)zirconium] (II)

A solution of 2-[(1,2-dimethoxyethane-*O*,*O*′)lithiumamido]-2-phenyl-1λ^{3}σ^2-phosphaalkene (2.0 g; 8.6 mmol) in 20 ml of 1,2-dimethoxyethane was added dropwise with stirring to a cooled (−60 ºC) suspension of bis(η^5-pentamethylcyclopentadienyl)zirconium dichloride (2.0 g; 4.6 mmol) in 20 ml of toluene. With continuous stirring the suspension was allowed to warm up to room temperature overnight; its colour had changed from deep red to wine-red. The solvents and phosphine which had been formed in the reaction were removed under reduced pressure and the residue was treated with 15 ml of cold toluene. After filtration to remove lithium chloride, the filtrate was concentrated to about half of its volume and stored in a refrigerator at −13 ºC. After one week red crystals (2.5 g; 4.2 mmol, 48 % yield) had precipitated.

Characterization

Wine-red solid; melting point 103 ºC.

Elemental analysis: $C_{34}H_{41}N_2PZr$ (599.94 g/mol),
calc.: C 68.06%; H 6.90%; N 4.67%, found: C 68.94%; H 7.03%; N 3.81% (too low presumably because of nitride formation).

NMR (solution in d_6-benzene)

$^{31}P\{^1H\}$: δ = 38.4 ppm (s)

^1H: δ = 1.8 (s, 30H, CCH_3); 6.2 (br, s, N*H*); phenyl substituent at P=C–NH: 7.1 (pt of pts, $^3J(H_p,H_m)$ = 8 Hz, $^4J(H_p,H_o)$ = 1 Hz, C–H_{para}); 7.2 (pt, $^3J(H_m,H_p)$ = 8 Hz, $^3J(H_m,H_o)$ = 8 Hz, $^5J(H_m,P)$ = 1 Hz, C–H_{meta}); 7.9 (m, $^4J(H_o,H_p)$ = 1 Hz, $^3J(H_o,H_m)$ = 8 Hz, $^4J(H_o,P)$ = 1 Hz, C–H_{ortho}); phenyl substituent at P–C=N: 7.2 (m, $^3J(H_p,H_m)$ = 8 Hz, $^4J(H_p,H_o)$ = 1 Hz, C–H_{para}); 7.3 (m, $^3J(H_m,H_p)$ = 8 Hz, $^3J(H_m,H_o)$ = 8 Hz, $^5J(H_m,P)$ = 1 Hz, C–H_{meta}); 8.4 (m, $^4J(H_o,H_p)$ = 1 Hz, $^3J(H_o,H_m)$ = 8 Hz, $^4J(H_o,P)$ = 3 Hz, C–H_{ortho}). For further details see **Table 3.1**.

$^{13}C\{^{1}H\}$: δ = 11.4 (s, CCH_3); 119.2 (s, *C*-CH_3); 188.1 (d, $^{1}J_{CP}$ = 72 Hz, N=*C*−P); 204.1, $^{1}J_{CP}$ = 75 Hz, N−*P*=*C*); phenyl substituent at P=C–NH: 127.2 (d, $^{3}J_{C,P}$ = 12 Hz, C_{ortho}); 129.0 (s, C_{meta}); 129.1 (d, $^{5}J_{C,P}$ = 2 Hz, C_{para}); 148.4 (d, $^{2}J_{C,P}$ = 35 Hz, C_{ipso}); phenyl substituent at P–C=N: 126.9 (d, $^{3}J_{C,P}$ = 16 Hz, C_{ortho}); 128.8 (d, $^{4}J_{C,P}$ = 1 Hz, C_{meta}); 130.0 (d, $^{5}J_{C,P}$ = 2 Hz, C_{para}); 142.1 (d, $^{2}J_{C,P}$ = 40 Hz, C_{ipso}). For further details see **Table 3.2**.

^{15}N: δ = −281.0 (s, ^{15}N=C); −170.0 (d, $^{1}J_{15N,H}$ = 63 Hz)

IR-Spectrum (nujol):

3251 m, 2901 m br, 1553 m, 1494 s, 1485 s, 1446 s, 1375 s, 1336 s, 1196 w sh, 1176 m, 1074 w, 1027 w, 903 w, 881 s, 805 m, 764 m, 746 s, 692 s.

Characteristic Masses (%) from the Mass Spectrum:

$\{M\}^{+}(Zr^{94})$	601.2	25.3	$\{Cp^*_2ZrN(H_2)N(H)CH_3\}^{+}(Zr^{94})$	408	91.2
$\{M\}^{+}(Zr^{92})$	600.2	34.1	$\{Cp^*_2ZrN(H_2)N(H)CH_3\}^{+}(Zr^{92})$	407	91.2
$\{M\}^{+}(Zr^{91})$	599.2	61.0	$\{Cp^*_2ZrNC(H)(Ph)NH_2\}^{+}(Zr^{91})$	481.2	40.0
$\{Cp^*ZrN(H)C(Ph)PCN-3CH_3\}^{+}(Zr^{91})$	409.2	100	$\{Cp^*_2ZrNC(H)(Ph)NH_2\}^{+}(Zr^{92})$	481.2	19.8
$\{Cp^*ZrN(H)C(Ph)PCN-3CH_3\}^{+}(Zr^{92})$	410.2	35.2	$\{Cp^*_2ZrNC(H)(Ph)NH_2\}^{+}(Zr^{94})$	481.2	15.4
$\{Cp^*ZrN(H)C(Ph)PCN-3CH_3\}^{+}(Zr^{94})$	411.2	31.9	$\{PhCPCPh-2H\}^{+}$	207.1	7.7
$\{Cp^*_2ZrN(H_2)NH\}^{+}(Zr^{91})$	391.2	94.5	$\{PhCPCH\}^{+}$	121.1	2.2
$\{Cp^*_2ZrN(H_2)NH\}^{+}(Zr^{92})$	392.2	38.5	$\{Cp^*_2ZrNC(H)(Ph)NH_2\}^{+}(Zr^{91})$	481.2	40.0
$\{Cp^*_2ZrN(H_2)NH\}^{+}(Zr^{94})$	393.2	34.1	$\{Cp^*_2ZrNC(H)(Ph)NH_2\}^{+}(Zr^{92})$	481.2	19.8
$\{Cp^*_2ZrN(H_2)N(H)CH_3\}^{+}(Zr^{91})$	406	91.2	$\{Cp^*_2ZrNC(H)(Ph)NH_2\}^{+}(Zr^{94})$	481.2	15.4

5.3.6 bis(1,2-dimethoxyethane)-1κ^2*O*^{1},*O*^{2};2κ^2*O*^{3},*O*^{4}]{bis[μ-*N*,*N*′-bis(4-methylphenyl)}-*C*-phosphanylformamidinato]-1:2κ^4*N*^{1}, *N*^{2};1κ^2*N*^{3};*N*^{4}}dilithium III

1,3-Di-*p*-tolylcarbodiimde (3.8 g, 17.1 mmol) in 20 ml of 1,2-dimethoxyethane was added dropwise with stirring to a cooled (−70 ºC) solution of (1,2-dimethoxyethane-*O*,*O*′) lithium phosphanide (2.2 g, 16.9 mmol) in 20 ml of the same solvent. After stirring for additional day the reaction mixture had taken a pale-yellow colour. Slow concentration of the solution under reduced pressure resulted in the precipitation of pale yellow crystals on the wall of the flask; they were suitable for an X-ray analysis. After removing the solvent almost completely pale-yellow crystals of [bis(1,2-dimethoxyethane)-1κ^2*O*^{1},*O*^{2}; 2κ^2*O*^{3},*O*^{4}]{bis[μ-*N*,*N*′-bis(4-methylphenyl)}-*C*-phosphanylformamidinato]-1:2 κ^4*N*^{1}, *N*^{2};1κ^2*N*^{3};*N*^{4}}dilithium (5.9g, 16.8 mmol) were obtained in quantitative 98% yield.

Characterization

Colour: pale-yellow solid

Melting point: 147 ºC (decomposition)

Elemental analysis: $C_{19}H_{26}LiN_2O_2P$ (352.2 g/mol)

cal.: C 64.77%, H 7.44%, N 7.95% found: C 64.27%, H 6.94%, N 8.11%

NMR (solution in d_8-THF):

^{31}P-NMR: δ = −152.2 (t, $^1J_{PH}$ = 210 Hz)

^{1}H-NMR: δ = 2.3 (s, $H_3CC_6H_4$); 3.0 (*d*, $^1J_{PH}$ = 210 Hz H_2P); 3.3 (s, OCH_3, DME); 3.5 (s, OCH_2, DME); 6.9 (*pd*, $^1J_{HH}$ = 8 Hz, *meta*-C_6H_4); 6.7 (*pd*, $^1J_{HH}$ = 8 Hz, *ortho*-C_6H_4)

^{13}C-NMR: δ = 20.3 (s, $H_3CC_6H_4$); 58.3 (s, OCH_3, DME); 72.2 (s, OCH_2, DME); 123.4 (s, *ortho*-C_6H_4); 128.3 (s, *para*-C_6H_4); 128.9 (s, C_6H_4*meta*-C_6H_4); 152.1 (s, *ipso*-C_6H_4); 165.5 (*d*, $^1J_{CP}$ = 36 Hz, *C*N2)

IR-Spectrum (nujol):

3339 m br, 3021 m, 3212 w, 1716 s, 1591 s, 1460 w, 1363 w, 1313 m, 1248 m, 1224 m, 943 w, 893 w, 789 w, 742 w, 705 w.

Characteristic Masses (%) from the Mass Spectrum:

$\{M+H-2(DME)\}^+$	511	24.7
$\{(H_3CC_6H_4)NC(PH_2)NH(C_6H_4CH_3)Li_2-H\}^+$	271	3.4
$\{(H_3CC_6H_4)NC(PH_2)NH(C_6H_4CH_3)-H\}^+$	257	14.6
$\{(H_3CC_6H_4)NCN(C_6H_4CH_3)+H\}^+$	225	100
$\{(H_3CC_6H_4)NH_2\}^+$	108	1.1

5.3.7 [*tert*-butyl-[(*tert*-butylamino)phosphanylidenemethyl]amino]-(tetrahydrofuran-*O)*-lithium IV

A similar procedure to that described for **5.3.3** was used here, except that (3.3 mL, 16.9 mmol) of *N,N'*-di-*tert*-butylcarbodiimide was employed instead of 1,3-di-*p*-tolylcarbodiimde. The reaction was not accompanied by colour change. After the solvent was

almost completely removed under reduced pressure, and the residue obtained recrystallized from tetrahydrofuran (r.t. to −13 ºC) colourless crystals were isolated in almost 98% yield (4.3 g, 16.4 mmol).

Note: Solutions of compound **IV**, prepared from stoichiometric amounts of lithium phosphanide ($LiPH_2$·dme) and *N,N'*-di-*tert*-butylcarbodiimide between −70 ºC and room temperature in 1,2-dimethoxyethane, turned out to be thermally very stable. They can be stored in a refrigerator at −13 ºC for more than two years without noticeable decomposition. For NMR studies a portion of such a solution (~1.0 ml) was filled into an NMR tube and concentrated in vacuo. Thereafter the remaining volume (~0.1 ml) was diluted with an appropriate amount of [d_6]benzene. In very low concentrations the sample contains phosphine [PH_3; ^{1}H: −0.32; ^{31}P: –241.8; $^1J_{P,H}$= 187.9] and lithium phosphanide [$LiPH_2$; ^{1}H: 1.68; ^{31}P: –288.8 ppm; $^1J_{P,H}$= 157.6 Hz].

Characterization

Colour: colourless solid

Melting point: 167 ºC (decomposition)

Elemental analysis: $C_{13}H_{28}LiN_2O_2P$ (266.2 g/mol)

Cal.: C 58.64%, H 10.60%, N 10.52% Found: C 57.30%, H 10.83%, N 10.51%

NMR (solution in d_8-THF)

^{31}P-NMR: δ = −63.8 (d, $^1J_{PH}$ = 153 Hz)

^{1}H-NMR: δ = 1.5 (s, CH_3 NH); 1.8 (s, CH_3 C=N); 3.0 (d, $^1J_{PH}$ = 153 Hz, P*H*); 3.5 (s br, N*H*); 1.7 (m, CH_2CH_2, THF); 3.5 (m, OCH_2, THF)

^{13}C-NMR: δ = 28.7 (*d*, $H_3C_{C=N}$); 30.8 (*d*, H_3C_{NH}); 52.3 (d, $C_{quar\ NH}$); 52.4 (d, $C_{quar\ N=C}$); 24.7 (m, CCH_2, THF); 66.8 (m, OCH_2, THF); 191.8 (d, $^1J_{CP}$ = 92 Hz, *P=C*);

IR-Spectrum (Nujol):

3313 w br, 2237 vs, 1499 vs, 1433 s, 1883 vs, 1353 s, 1109 s, 1051 m, 1008 m, 939 s, 786 m, 716 m.

Characteristic Masses (%) from the Mass Spectrum:

$\{[M]_2Li_2.THF-H\}^+$	461.3	9.7
$\{[M]_2Li_2.THF-C_4H_9\}^+$	407.3	3.5
$\{[MH_2+H]Li.THF-2C_4H_9\}^+$	157.1	100
$\{H_2NC(H)N(H)^tBu\}^+$	101.1	5.4

5.3.8 *Catena*-poly[μ-(*N,N′*-dicyclohexyl-*C*-phosphanidato-1*:2*κ²*P*-formamidinato-1:2κ²*N*,1:2κ²*N′*)-1,2-bis(tetrahydrofuran-*O*]dilithium (V)

A similar procedure to that described for **5.3,3** was used here, except that (3.5 mL, 7.4 mmol) of *N,N′*-dicyclohexylcarbodiimide was employed instead of 1,3-di-*p*-tolylcarbodiimde. Under vacuum the solvent was removed almost completely from the still colourless solution. Since attempts to recrystallize the remaining white solid from tetrahydrofuran as a solvent failed, the solvent was removed partially and small amounts of tetrahydropyran was added. Keeping the solution mixture for three weeks at −13 ºC resulted in a precipitation of colourless crystals of complex **VI** in 57% yield (3.7g, 9.6 mmol).

Characterization

Colour: colourless solid
Melting point: 97 ºC (decomposition)
Elemental analysis: $C_{17}H_{27}Li_2N_2OP$ (388.2 g/mol)
Cal.: C 63.75%, H 8.50%, N 8.75% Found: C 62.76%, H 10.20%, N 9.95%
The values were calculated for monomer with one tetrahydrofuran molecule

NMR (solution in d_8-THF)

^{31}P-NMR: δ = −154.3 (d, $^1J_{PH}$ = 157 Hz)

5.3.9 *catena*-poly[μ-(N,N′-diisopropyl-C-phosphanidato-1*:2*κ²P-formamidinato-1:2κ²N,1:2κ²N′)-1,2-bis(tetrahydropyran)-O]dilithium (VI)

A similar procedure to that described for **5.3.3** was used here, except that (2.7 mL, 17.4 mmol) of *N,N′*-di-isopropylcarbodiimide was employed instead of 1,3-Di-*p*-tolylcarbodiimde. After stirring for one day the solvent was removed from the still colourless

solution and a white residue (2.7 g, 10.6 mmol) was obtained in about 63% yield. Attempt to recrystallized the white solid from tetrahydrofuran was failed, but by removing almost all tetrahydrofuran solvent molecules and addition of small amount of tetrahydropyran led to the isolation of colourless crystals of complex **V** suitable for an X-ray analysis within three weeks when the solution was stored at −13 ºC.

Characterization

Colour: colourless solid

Melting point: 101 (decomposition)

Elemental analysis: $C_{12}H_{25}LiN_2OP$ (251.2 g/mol)

Cal.: C 57.36%, H 10.03%, N 11.15% Found: C 53.8%, H 9.86%, N 15.96%

NMR (solution in d_8-THF)

^{31}P-NMR: $\delta = -140.0$ (d, $^1J_{PH} = 159$ Hz)

6. Summary

This thesis reports on the investigations of products obtained from the well-known (1,2-dimethoxyethane)lithiumphosphanide and either an organonitrile or a diorganocarbodiimide, respectively. In previous work it had been established that the reactions with pivalo- and benzonitrile give almost quantitative yields of the appropriate 2-[*N*-(1,2-dimethoxyethane)lithiumamido]-2-organyl-1$\lambda^3\sigma^2$-phosphaalkenes. Of these the phenyl compound **1** was chosen for further research. It was reacted with *tert*-butylchlorodiphenylsilane (**2**), bis(η^5-pentamethylcyclopentadienyl)zirconium dichloride (**3**), and trifluoromethylsulfonic acid. The acidification furnished thermally labile 2-amino-2-phenyl-1$\lambda^3\sigma^2$-phosphaalkene (**I**.**0**) as a mixture of (*Z*)-/(*E*)-isomers. 2D NMR spectroscopic methods gave evidence that **I.0** dimerizes via an insertion of the P=C unit of one molecule into the P–H bond of another to form the diastereomeric 1-[(*C*-amino-*C*-phenyl)methylphosphanyl]-2-amino-2-phenyl-1$\lambda^3\sigma^2$-phosphaalkenes (*Z*)-**I**.**01** and (*Z*)-**I**.**02**.

Depending on the substituent at nitrogen, the reactions of diorganylcarbodiimides with (1,2-dimethoxyethane)lithiumphosphanide furnished compounds of very different composition and structure. A dimeric *N*-lithiated monophosphaguanidine ($Li_{solv}NR)C(=NR)PH_2$ (R = 4-CH_3-C_6H_4; **III**) is formed from bis(*p*-methylphenyl)carbodiimide. In contrast, reaction with di-*tert*-butylcarbodiimide yields the corresponding phosphanide tautomer (Li_{solv})HP–C(=NR)(–NHR) {R= $C(CH_3)_3$; **IV**}. Finally, dicyclohexyl - and diisopropylcarbodiimide react with (1,2-dimethoxyethane)lithiumphosphanide in a molar ratio of 1 : 2 to furnish *N*,*P*-dilithiated monophosphaguanidines ($Li_{solv}NR)C(=NR)(PHLi_{solv})$ [R = C_6H_{11}, **V**; R= $CH(CH_3)_2$, **VI**]. X-ray structure analyses show these compounds to crystallize as coordination polymers.

The majority of the new phosphorus compounds are sensitive to moisture and protolyze

---

Note: Arabic numerals for known compounds, Roman ones for new compounds

immediately with traces of water. They are usually pyrophoric and ignite in air. Products like the parent phosphaalkene **I.0** featuring low molecular weight and a sterically unprotected P=C–N skeleton are thermally unstable, cannot be isolated in a pure form and are therefore characterized in solution.

The $1\lambda^3\sigma^2$-phosphaalkene **1**, which is readily accessible according to **Eq. 1** [39], exists in solution as a dynamically exchanging mixture of stereoisomers which had been tentatively assigned as species featuring *Z* and *E* configurated P=C double bonds.

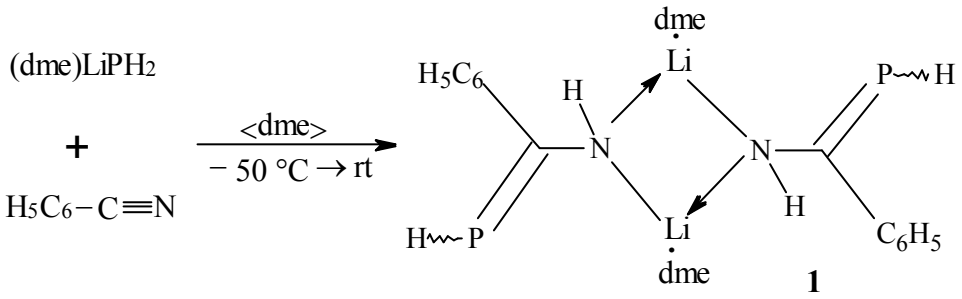

Eq. 1

A strong broadening of the doublet at −50.0 ppm, however, indicates an exchange phenomenon which up to now has not been studied in detail. A detailed multinuclear NMR spectroscopic study at 213K gave evidence, that the equilibrium mixture contains altogether four distinguishable stereoisomers. This number of isomers can only be explained by the assumption of a restricted rotation around the P=C as well as the C–N bond and leads to the configurational isomers shown in **Scheme 1**.

Unequivocal configurational assignment was feasible based on an analysis of the magnitude of the $^1J_{P,H}$ coupling constants which are larger for the ***E*(P=C)** than for the ***Z*(P=C)** isomers, the ^{1}H NMR chemical shifts of the N–H protons, as well as the exclusive observation of $^1H(C_{ortho}),^{31}P$ HMQC correlations in the ***Z*(P=C)** isomers. On raising the temperature the NMR signals of the ***E*(P=C),*Z*(C–N)** and ***Z*(P=C),*Z*(C–N)** isomers on the one hand and of the ***E*(P=C),*E*(C–N)** and ***Z*(P=C),*E*(C–N)** on the other hand begin to coalesce and finally give the room temperature spectrum.

Configuration/ conformation *E*(C–N)

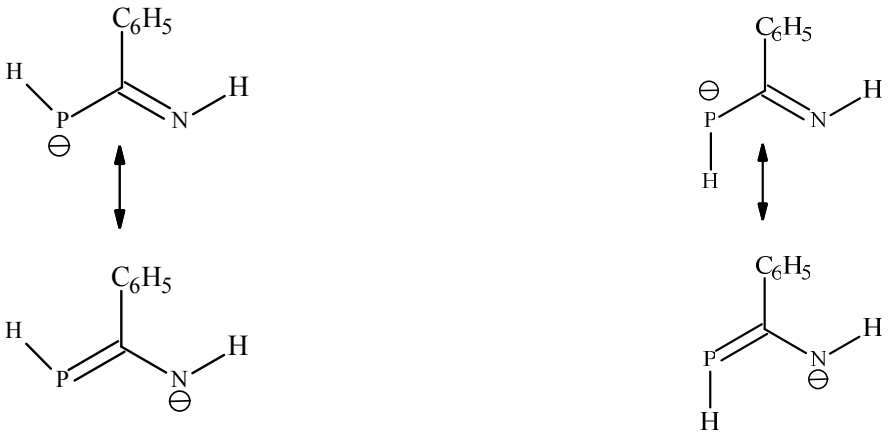

Isomer	***E*(P=C),*E*(C–N)**	***E*/*Z*(P=C),*E*(C–N)**	***Z*(P=C),*E*(C–N)**
temperature	213K	303K	213K
δ $^{31}P\{^{1}H\}$ (*intensity*)	−32.1 ppm (*2.1*)	−26.5 ppm (*10.0*)	−25.6 ppm (*10.0*)

Configuration/ conformation *Z*(C–N)

Isomer	***E*(P=C),*Z*(C–N)**	***E*/*Z*(P=C),*Z*(C–N)**	***Z*(P=C),*Z*(C–N)**
temperature	213K	303K	213K
δ $^{31}P\{^{1}H\}$ (*intensity*)	−35.4 ppm (*0.8*)	−48.1 ppm (*2.8*)	−55.9 ppm (*2.5*)

Scheme 1 Mesomeric anion (**a)**) of four different isomers (**b)** and **c)**) detected at 213K in the $^{31}P\{^{1}H\}$ NMR spectrum of a 1,2-dimethoxyethane solution of compound **1**

Reaction of $1\lambda^3\sigma^2$-phosphaalkene **1** with an equimolar amount of *tert*-butylchlorodiphenylsilane (**2**) furnished unexpectedly the (***Z***)-/(***E***)-isomers of *N*,*P*-bis(*tert*-butyldiphenylsilyl)-2-amino-2-phenyl-$1\lambda^3\sigma^2$-phosphaalkene (**I.2**) as major product. Crystals of the (*Z*)-isomer suitable for an X-ray structure determination were obtained from toluene at −13 °C. From the NMR spectrum of a [d_8]tetrahydrofuran solution an intensity ratio of 7:1 was inferred for the mixture of (*Z*)- and (*E*)-isomers.

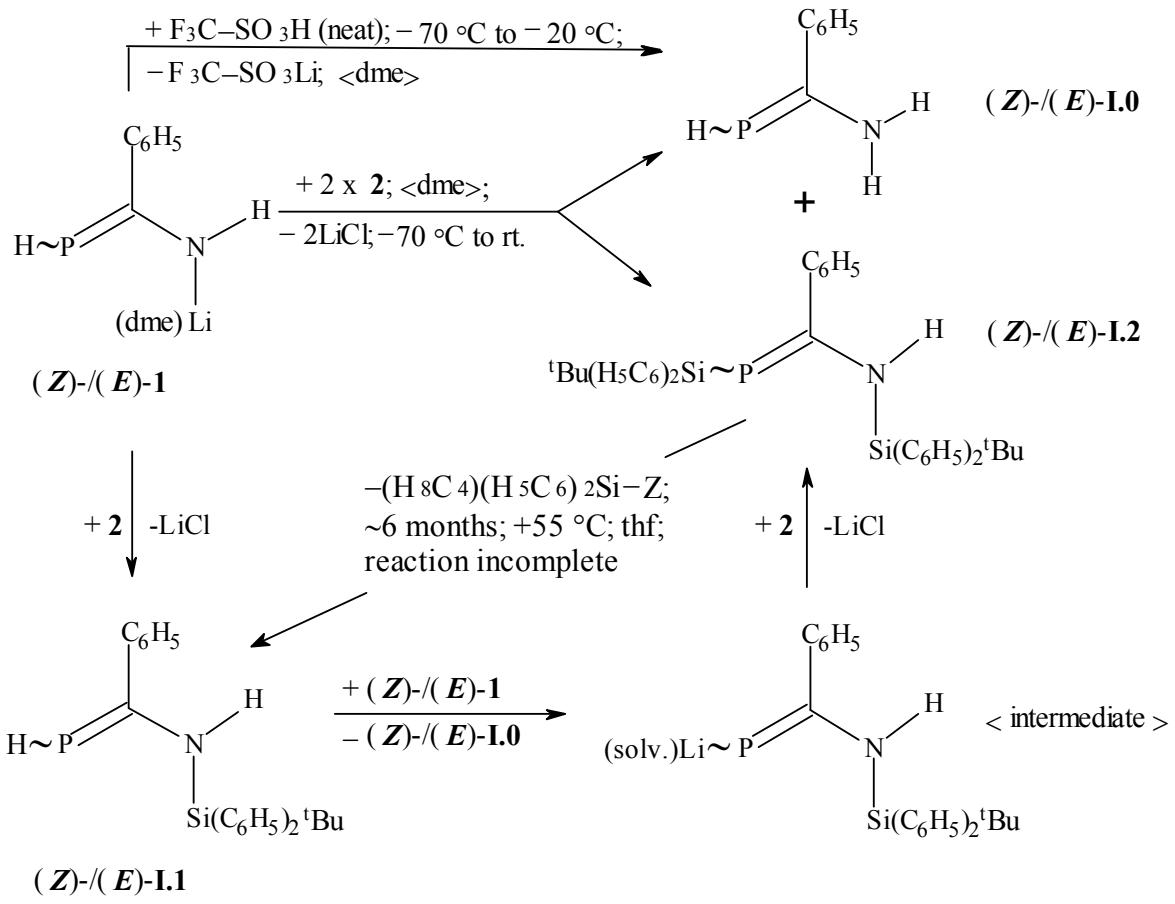

Scheme 2 Formation of 2-amino-2-phenyl-1$\lambda^3\sigma^2$-phosphaalkene (**I.0**) and its *N*-mono- (**I.1**) and *N*,*P*-disilylated derivates (**I.2**)
2 : ^{t}Bu(H_5C_6)$_2$Si–Cl; (H_8C_4)(H_5C_6)$_2$Si–Z: compound of unknown composition and structure

Quite obviously, the disilylation of the lithium derivative **1** to give compound **I.2** entails the generation of the transient monosubstituted *N*-(*tert*-butyldiphenylsilyl)-2-amino-2-phenyl-1$\lambda^3\sigma^2$-phosphaalkene **I.1** and the *unsubstituted* 2-amino-2-phenyl-1$\lambda^3\sigma^2$-phosphaalkene **I.0,** all of which could be detected in a ^{31}P NMR spectrum of the reaction mixture recorded two hours after commencement (**Figure 1)**.

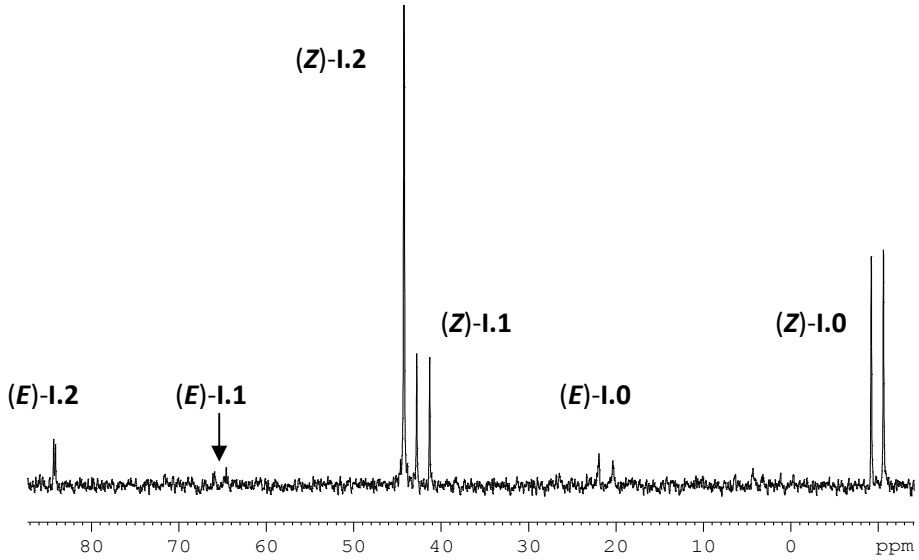

Figure 1 ^{31}P NMR spectrum of a sample taken at room temperature from the reaction of compound **1** with the chlorosilane **2** in 1,2-dimethoxyethane

Unexpectedly, phosphaalkene **I.2** was found to be unstable in [d_8]tetrahydrofuran. Monitoring a solution in a sealed NMR tube at +55 °C revealed that the decay was rather slow and remained incomplete even after six months. Application of 2D NMR spectroscopic techniques permitted to identify the phosphorus-containing decomposition products as the (***Z***)-/(***E***)-isomers of the *N*-monosilylated $1\lambda^3\sigma^2$-phosphaalkene **I.1.** In addition, formation of a further, phosphorus-free by-product was observed but its constitution could not yet be established.
An equilibrium mixture containing (***Z***)- and (***E***)-**I.0** in a ratio of 1 : 0.2 was independently accessible via reaction of a [d_8]tetrahydrofuran solution of **1** with neat trifluoromethylsulfonic acid at −40 °C in 1,2-dimethoxyethane proved to be advantageous for detailed 2D NMR analyses. Even if the products could not be isolated, their identity was unequivocally confirmed by extensive multinuclear NMR studies.

The ^{31}P NMR signal of (*E*)-**I.0** shows an unusual temperature dependence which becomes manifest in a change of the multiplicity from a doublet of triplets at 293K to a doublet of doublets with an increased $^3J_{P,Ha(N)}$ coupling of 21 Hz at 213K (**Figure 2**). This phenomenon can be explained with the eventual freezing of the NH_2-group rotation which is fast on the NMR time scale at higher temperature and slow at low temperature and implies that at 213K the rotation around C–N bond become restricted due to high energy barrier.

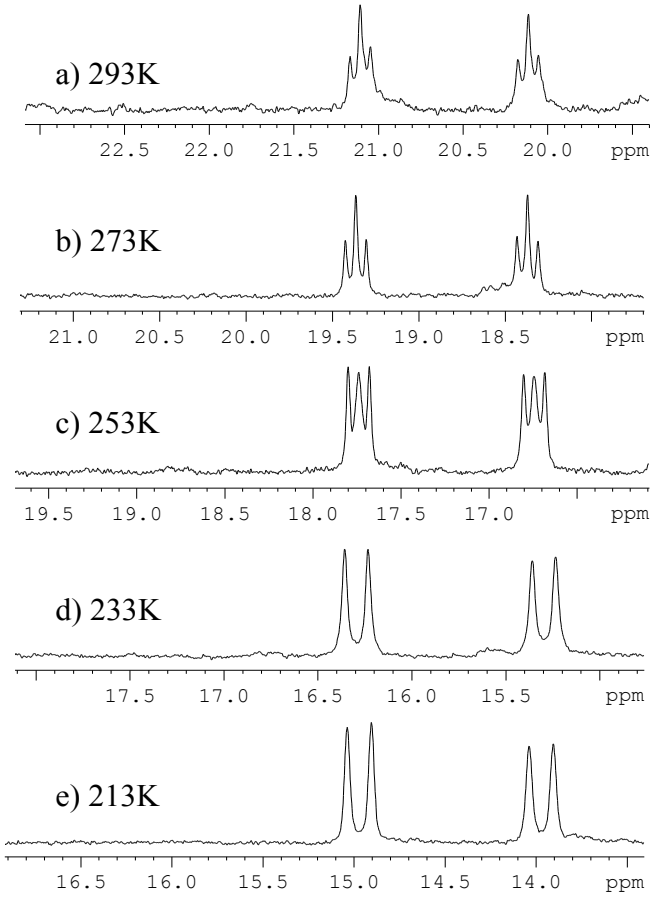

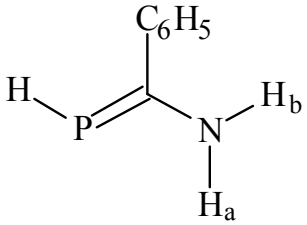

(***E***)-**I.0**

Figure 2 Temperature dependence of the ^{31}P NMR spectrum of isomer (***E***)-**I.0**

The unsubstituted 1-$\lambda^3\sigma^2$-phosphaalkene (***Z***)-/(***E***)-**I.0** is unstable at room temperature in [d_8]tetrahydrofuran and slowly forms two new compounds which were tentatively assigned as the diastereomeric phosphaalkenes **I.01** and **I.02** based on incomplete spectroscopic evidence. The reaction mechanism proceeds presumably via an acid catalyzed insertion of the P–H group of one molecule into the P=C unit of a second one (**Eq. 2**).

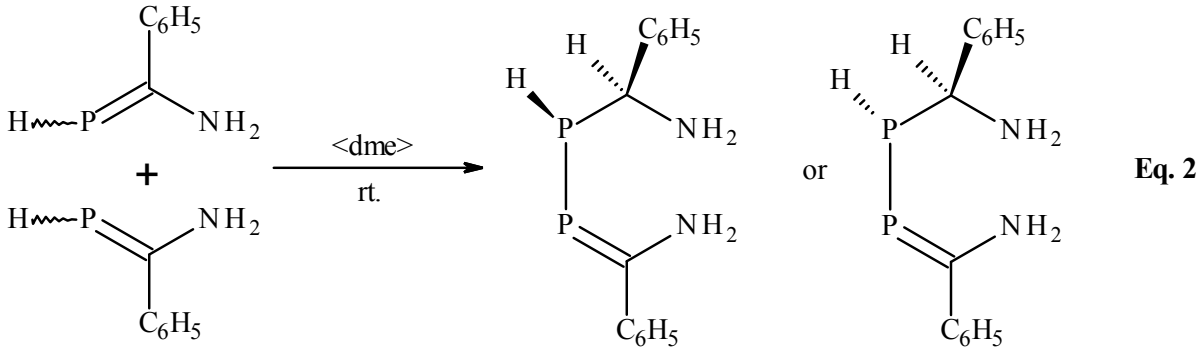

Eq. 2

(***Z***)-/(***E***)-**I.0**

S$_{(P)}$,S$_{(C)}$-(*Z*)-I.01
or
R$_{(P)}$,R$_{(C)}$-(*Z*)-I.01

R$_{(P)}$,S$_{(C)}$-(*Z*)-I.02
or
S$_{(P)}$,R$_{(C)}$-(*Z*)-I.02

Reaction of (***Z***)-/(***E***)-**1** with an equimolar amount of solid bis(η^5-pentamethylcyclopentadienyl)zirconium dichloride afforded the complex [*N,N'*-(1-amido-3-imido-1,3-diphenyl-2λ^{3}σ^2-phospha-1-propene)bis(η^5-pentamethylcyclopentadienyl)zirconium] (**II**) which was isolated in the form of crystalline solvates with toluene (**II·C$_7$H$_8$**) or hexane (**2II· *n*-C$_6$H$_{14}$**), respectively. The identity of the products was established from comprehensive NMR spectroscopic studies and single-crystal X-ray structure determinations.

Unfortunately, the symmetry of space group *C*2/*c* prevented a precise determination of bond lengths and angles in the solvate (**II·C$_7$H$_8$**). The complex molecules are placed on a twofold axis; consequently the P–C=N and P=C–N(H) entities of the chelate ligand are superimposed. A close inspection of the crystal packing reveals that complex and solvent molecules are arranged in a slightly distorted PtS-type structure. Hexane solvate (**2II· *n*-C$_6$H$_{14}$**) on the other hand shows no sign of disorder and the bond lengths of the P–C=N and P=C–N(H) entities of the six-membered chelate ring are clearly distinguishable (**Figure 3**).

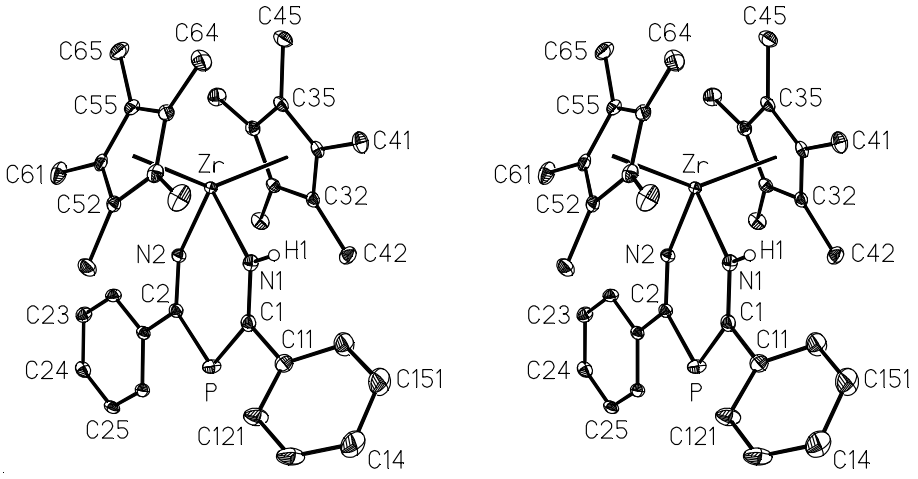

Figure 3 Structure of the two components of the solid state adduct [*N,N'*-(1-amido-3-imido-1,3-diphenyl-2λ^{3}σ^2-phospha-1-propene)]bis(η^5-pentamethylcyclopentadienyl)zirconium– *n*-hexane (1 / 0.5) (≙ **2 II·*n*-C$_6$H$_{14}$**) in stereoscopic view
Complex molecule **II**. With regard to the disordered phenyl substituent numbered C1*m*... (m = 1→ 6) only the conformer with carbon atoms of the higher occupancy factor of 0.524 is depicted.

DFT calculations on the model compound [*N,N′*-(1-amido-3-imido-1,3-diphenyl-2$\lambda^3\sigma^2$-phospha-1-propene)bis(cyclopentadienyl)zirconium] confirmed the interpretation of the bonding situation that had been derived from the structural features. Quantumchemical DFT calculations with the functional B3LYP employing different basis sets for the heavier atom Zr (quasi-relativistic pseudopotential) and the lighter atoms C, H, N, and P (6-31G*) were performed using the bis(η^5-cyclopentadienyl) complex as a model compound. The conformity of experimentally determined and calculated molecular parameters is found to be within the scope of expectation:

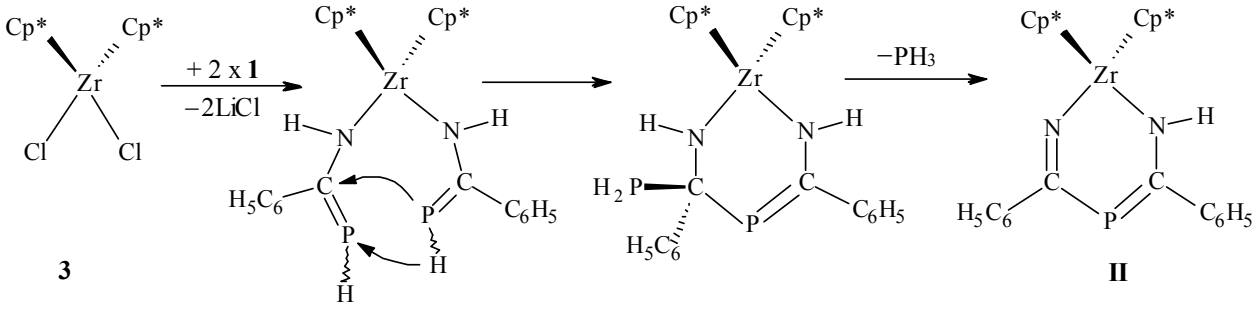

Scheme 3 Template-like formation of the [*N,N′*-(1-amido-3-imido-1,3-diphenyl-2$\lambda^3\sigma^2$-phospha-1-propene)] ligand at the zirconium centre

The formation of the [1-amido-3-imido-1,3-diphenyl-2$\lambda^3\sigma^2$-phospha-1-propene] dianion, a totally new type of chelate ligand compared to similar ligands reported by *Stephan* (N=C–P(R)–C=N) [90] and *Bergman* (N=C–N=C–(O,S)) [105], is best explained by assuming a template-like reaction. The chlorine atoms of zirconium complex **3** are first replaced by the N–H groups of two 2-amino-2-phenyl-1$\lambda^3\sigma^2$-phosphaalkene substituents. Next, the close vicinity of the two H~P=C entities enables a straightforward addition of the P–H unit of one ligand to the P=C bond of the other so that the chelate ring is closed by establishing a new P–C bond. Migration of a hydrogen atom from nitrogen to the PH_2 group results in an elimination of a PH_3 molecule and the formation of a C=N bond (**Scheme** 3).

Last, but not least, reactions of the diorganylcarbodiimides **4** - **7** with (1,2-dimethoxy-ethane)lithiumphosphanide opened new and fascinating vistas in organophosphorus chemistry. Nucleophilic attack of the phosphanide anion at the *sp*-hybridized carbon atom of the *diorganylcarbodiimide* molecule results in the formation of a strong P–C bond. Consequently, several lithium monophosphaguanidinates (**III** - **VI**) could be isolated and their crystal structures could be solved (**Scheme 4**). The outcome of these reactions differs considerably from that of (dme)$LiPH_2$ with *bis(trimethylsilyl)carbodiimide* to give the coordination polymer (tetrahydrofuran)lithium cyano(trimethylsilyl)amide $[(thf)Li(Me_3Si)N–C{\equiv}N]_\infty$ and different trimethylsilylphosphanes $(Me_3Si)_{3-x}PH_x$ ($x = 0 \rightarrow 2$) by a straightforward *N*,*P*-trimethylsilyl transfer [109].

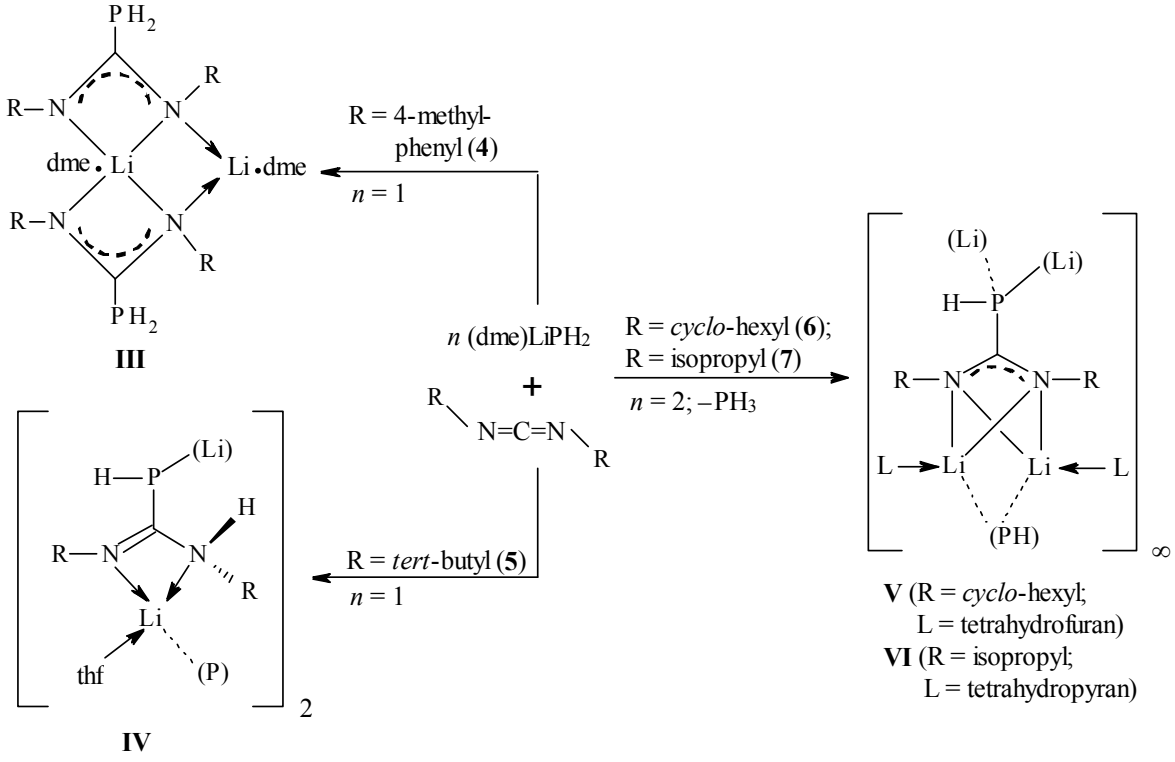

Scheme 4 Monophosphaguanidates isolated from reactions of the diorganylcarbodiimides **4** - **7** with (1,2-dimethoxyethane)lithiumphosphanide
Dotted bonds and element symbols in brackets refer to symmetry related positions.

The molecular structure of **III** is noteworthy due to the presence of one dme-complexed lithium cation of coordination number 6 is surrounded by four nitrogen atoms of both the bent bidentate monophosphaguanidinate anions, the second dme-complexed lithium cation of coordination number 4 gets in contact with only one nitrogen atom of each mesomeric N⋯C⋯N entity. On the whole, the different coordination of both lithium cations can best be described as that of a lithium lithiate.

Provided that the solid state structure of complex **III** is retained in e.g. a tetrahydrofuran solution, the detection of only one ^{7}Li NMR signal even at low temperature might be explained by the assumption that the arms of the phosphaguanidinate ligand can fluctuate rather fast from the six-coordinate to the four-coordinate lithium cation and vice versa (**Figure 4**). The ^{7}Li chemical shift value changes only slightly from 1.1 ppm at 298K to 0.5 ppm at 193K.

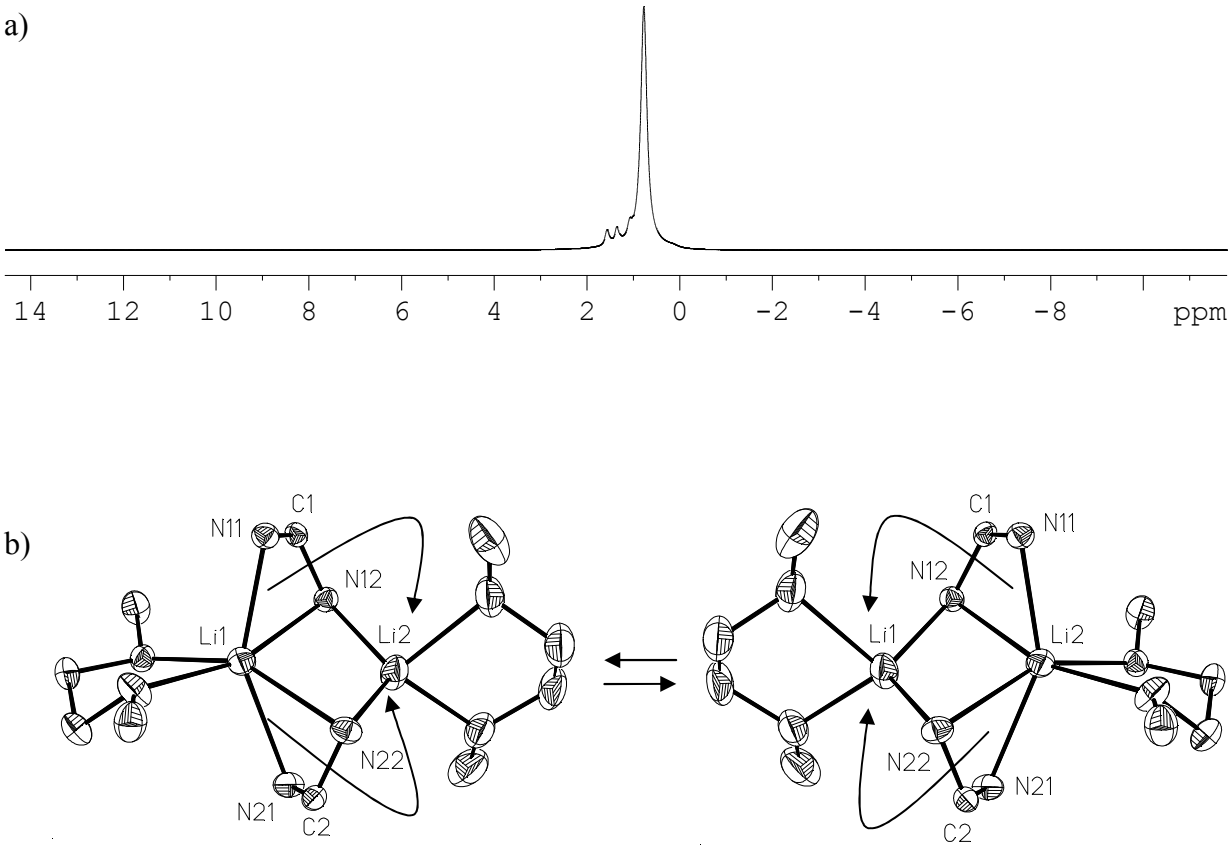

Figure 4 ^{7}Li NMR studies on complex **III** in solution
a) ^{7}Li NMR spectrum of complex **III** at 253K dissolved in [d_8]tetrahydrofuran
b) Fluctuation of the [μ-(*C*-phosphanylformamidinato)] ligands of complex **III** between six and four coordinate lithium cations
For the sake of simplicity the organyl substituents at nitrogen, the PH_2 groups at carbon and the hydrogen atoms of the 1,2-dimethoxyethane ligands have not been depicted.

The reaction of di-*tert*-butylcarbodiimide (**5**) with (1,2-dimethoxyethane)lithiumphosphanide in 1,2-dimethoxyethane furnished the dimeric complex **IV**. The nucleophilic attack of the phosphanide anion at the *sp*-hybridized carbon atom is most likely followed by a 1,3-hydrogen shift from phosphorus to nitrogen. The four-coordinate lithium cation is in contact with both the formally neutral nitrogen atoms of the *N,N',P*-tridentate chelate ligand *C*-phosphanidatoformamidin, a tetrahydrofuran molecule and the neighbouring PH-group of the second monomeric unit (**Figure 5**). In contrast to the N⋯C⋯N moiety of compounds **III**, **V** and **VI** the C–N bond lengths are no longer equal but differ considerably.

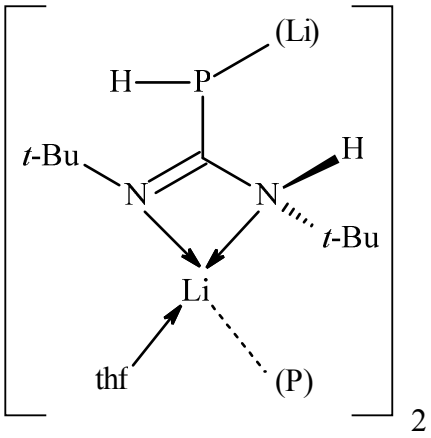

Figure 5 The dimeric complex bis[μ-(*N,N'*-di-*tert*-butyl-*C*-phosphanidatoformamidin)-1κ^1*P*; 2κ^1*P'*;1:2κ^2*N*; 1:2κ^2*N'*]1,2-bis(tetrahydrofuran-*O*)dilithium (**IV**).

The reactions of di-*cyclo*-hexyl- (**6**) and diisopropylcarbodiimide (**7**) with *two* equivalents of (1,2-dimethoxyethane)lithiumphosphanide in 1,2-dimethoxyethane yield the dilithium complexes **V** and **VI**. Whereas the first equivalent is used for the formation of the P–C bond via a nuecleophilic attack of the phosphanide anion at the *sp*-hybridized carbon atom, the second one deprotonates the freshly introduced phosphanyl group.

Crystals of complexes **V** and **VI** suitable for X-ray structure analyses precipitated at −13 °C from a rather concentrated tetrahydrofuran or tetrahydropyran solution. The phosphorus atom of the PH group as well as the two nitrogen atoms of the bent (R)–N⋯C⋯N–(R) entity are in close contact with both lithium cations (**Figure 6**). In the solid state both compounds build up coordination polymers; parallel strands are aligned along [0$\bar{1}$0] resulting in a tetragonal or hexagonal rod packing (**Figure 7**).

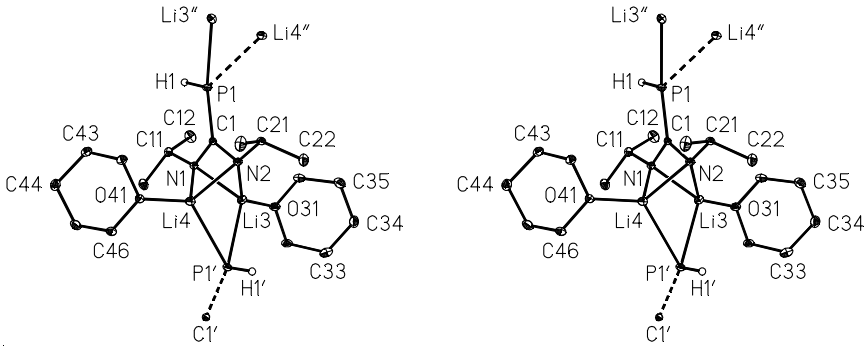

Figure 6 Monomeric unit of the complex *catena*-poly[μ-(*N,N′*-diisopropyl-*C*-phosphanidato-1*:2*κ^2*P*-formamidinato-1:2κ^2*N,*1:2κ^2*N′*)-1,2-bis(tetrahydropyran-*O*]dilithium **(VI)** in stereoscopic view**.** Thermal ellipsoids are at 30% probability; except for the PH-groups all hydrogen atoms are omitted for clarity. The structure of complex **V** is found to be almost identical to that of **VI**.

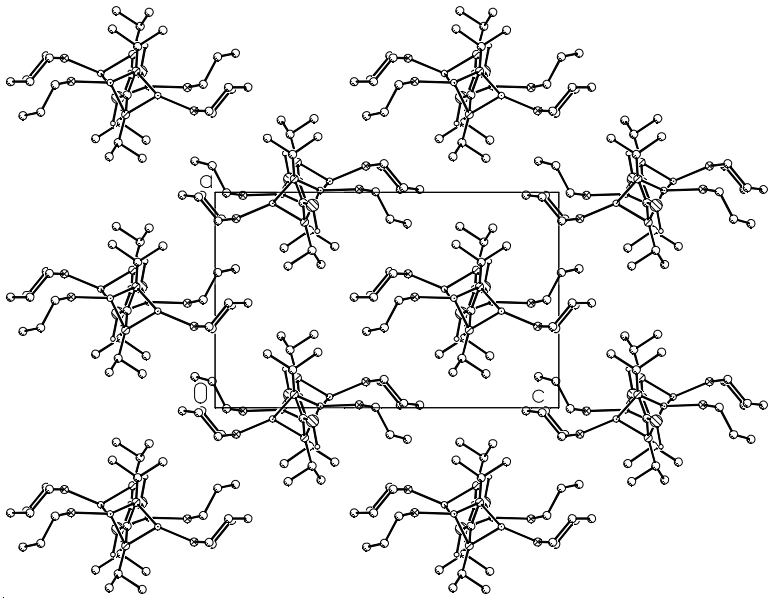

Figure 7 Strands of the coordination polymer **VI** viewed along [0$\bar{1}$0]. The strands build up a hexagonal rod packing.

The investigations on monophosphaguanidinates synthesized from diorganylcarbodiimides and (1,2-dimethoxyethane)lithiumphosphanide are still at the starting stage. Three different structure types with respect to only four different organyl substituents awake our curiosity in finding out how many other types could be realized just by varying the organic group or the additional ligands at lithium. Furthermore, the reactivity of the new complexes has not yet been explored. Protonation, silylation or exchange of lithium for other metals are obvious possibilities.

7. Zusammenfassung

Die vorliegende Dissertation berichtet über die Untersuchungen von Verbindungen, die aus dem bekannten (1,2-Dimethoxyethan)lithiumphosphanid und entweder Organonitrilen oder Diorganocarbodiimiden erhalten wurden. In früheren Arbeiten wurde festgestellt, daß die Reaktionen mit Pivalo- und Benzonitril nahezu quantitative Ausbeuten der entsprechenden 2-[*N*-(1,2-Dimethoxyethan)lithiumamido]-2-organyl-1$\lambda^3\sigma^2$-phosphaalkene ergeben. In dieser Arbeit wurde die Phenylverbindung **1** für weitere Untersuchungen ausgewählt und mit *tert*-Butylchlordiphenylsilan (**2**), Bis(η^5-pentamethylcyclopentadienyl)zirconiumdichlorid (**3**) und Trifluormethylsulfonsäure umgesetzt. Die Versauerung lieferte thermisch labiles 2-Amino-2-phenyl-1$\lambda^3\sigma^2$-phosphaalken (**I.0**) als Gemisch aus (*Z*)-/(*E*)-Isomeren. 2D-NMR-spektroskopische Methoden zeigten, dass **I.0** über eine Insertion der P=C-Einheit eines Moleküls in die P–H-Bindung eines weiteren dimerisiert, was zur Bildung der diastereomeren 1-[(*C*-Amino-*C*-phenyl)methylphosphanyl]-2-Amino-2-phenyl-1$\lambda^3\sigma^2$-phosphaalkenes (***Z***)-**I.01** und (***Z***)-**I.02** führt.

Die Reaktionen zwischen Diorganylcarbodiimiden und (1,2-Dimethoxyethan)lithiumphosphanid lieferten, je nach Substituenten am Stickstoff, unterschiedliche Verbindungen mit ungewöhnlichen Zusammensetzungen bzw. Strukturen. Aus Bis(*p*-methylphenyl)carbodiimid wurde ein dimeres *N*-lithiiertes Monophosphaguanidin (Li_{solv}NR)C(=NR)PH_2 (R = 4-CH_3-C_6H_4; **III**) gebildet. Die Umsetzung mit Di-*tert*-butylcarbodiimid ergibt jedoch das entsprechende Phosphanid-Tautomer (Li_{solv})HP-C(=NR)(–NHR) {R = $C(CH_3)_3$; **IV**}. Weiterhin wurde Dicyclohexyl- und Diisopropylcarbodiimid mit (1,2-Dimethoxyethan)lithiumphosphanid im Molverhältnis von 1 : 2 ungesetzt, um *N*,*P*-lithinierte Monophosphaguanidine (Li_{solv}NR)C(=NR)(PHLi_{solv}) [R = C_6H_{11}, **V**; R = $CH(CH_3)_2$; **VI**] zu erhalten. Röntgenstrukturanalysen zeigen, dass diese Verbindungen als Koordinationspolymere kristallisieren.

Die neuen Phosphorverbindungen sind meistens empfindlich gegenüber Feuchtigkeit und

---

Anmerkung: arabische Ziffern für bekannte Verbindungen, römische für neue Verbindungen.

protolysieren selbst mit geringen Mengen von Wasser sofort. Sie sind zudem meist pyrophor und entzünden sich spontan an Luft. Produkte wie die Ausgangsverbindung **I.0** mit einem niedrigem Molekulargewicht und einer sterisch ungeschützten P=C–N-Einheit sind thermisch labil, weshalb sie nicht in reiner Form isoliert und nur in der Lösung charakterisiert werden konnten.

Das $1\lambda^3\sigma^2$-Phosphaalken **1**, liegt nach Gl. 1 [39], in der Lösung als dynamisches Gleichgewicht von Stereoisomeren vor, welches vorläufig den Spezies mit *Z* und *E* konfigurierten P=C-Doppelbindungen zugeordnet wurden.

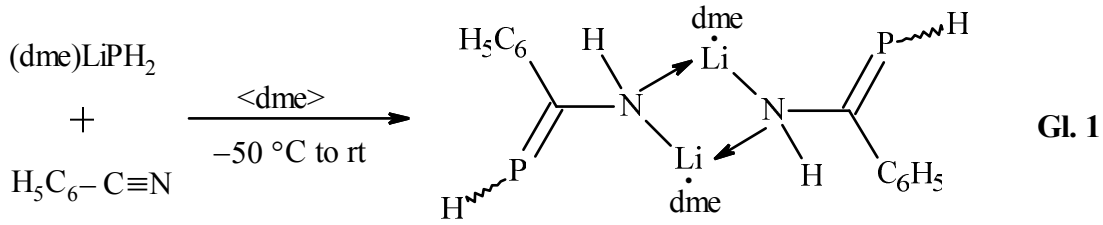

Gl. 1

1

Eine starke Verbreiterung des Dubletts bei −50,0 ppm legt jedoch Austauschphänome nahe, die bisher nicht im Detail untersucht wurden. Eine detaillierte multinukleare NMR-spektroskopische Untersuchung bei 213K zeigte, dass die Gleichgewichtsmischung insgesamt vier unterscheidbare Stereoisomere enthält. Diese Anzahl von Isomeren lässt sich nur durch die Annahme einer gehinderten Rotation um die P=C-sowie die C–N-Bindung erklären, was auf die in **Schema 1** gezeigten Konfigurationsisomere schließen lässt.

Die eindeutige Konfigurationszuordnung basiert auf einer Analyse der $^1J_{P,H}$-Kopplungskonstanten, die für das *E*(P=C)-Isomer größer sind als für die *Z*(P=C)-Isomere, den ^{1}H-NMR-chemischen Verschiebungen der N–H-Protonen sowie die ausschließlich in den ***Z*(P=C)**-Isomeren beobachteten $^1H(C_{ortho})$,^{31}P HMQC-Korrelationen. Bei Erhöhung der Temperatur begannen die NMR-Signale der ***E*(P = C)-**, ***Z*(C-N)-** und ***Z*(P=C)-**, ***Z*(C-N)-** als auch der ***E*(P=C)-**, ***E*(C-N)-** und ***Z*(P=C)-**, ***E*(C-N)-**Isomere zu koaleszieren und was schließlich zu dem bei Raumtemperatur beobachteten Spektrum führt.

Konfiguration/ konformation *E*(C–N)

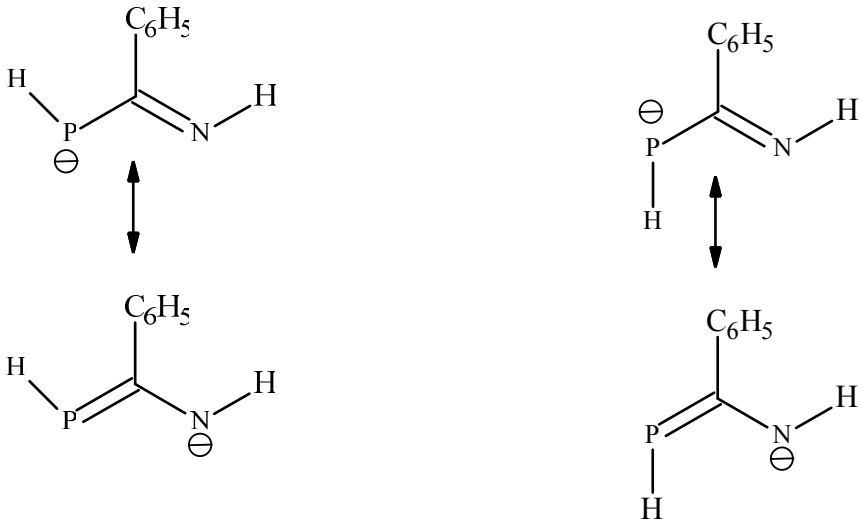

Isomer	***E*(P=C),*E*(C–N)**	***E*/*Z*(P=C),*E*(C–N)**	***Z*(P=C),*E*(C–N)**
Temperatur	213K	303K	213K
δ ^{31}P{^{1}H} (*Intensität*)	−32.1 ppm (*2.1*)	−26.5 ppm (*10.0*)	−25.6 ppm (*10.0*)

Konfiguration/ konformation *Z*(C–N)

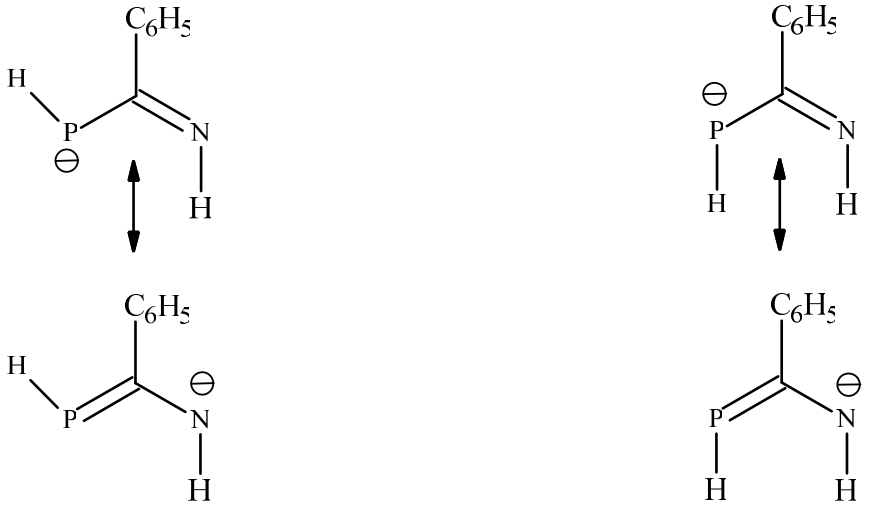

Isomer	***E*(P=C),*Z*(C–N)**	***E*/*Z*(P=C),*Z*(C–N)**	***Z*(P=C),*Z*(C–N)**
Temperatur	213K	303K	213K
δ ^{31}P{^{1}H} (I*ntensität*)	−35.4 ppm (*0.8*)	−48.1 ppm (*2.8*)	−55.9 ppm (*2.5*)

Schema 1 Mesomeres von vier verschiedenen Isomeren bei 213 K im ^{31}P erfaßt {^{1}H}-NMR-Spektrum einer 1,2-Dimethoxyethan-Lösung von Verbindung **1**

Die Umsetzung von $1\lambda^3\sigma^2$-Phosphaalken **1** mit einer äquimolaren Menge von *tert*-Butylchlordiphenylsilan (**2**) lieferte unerwartet die (*Z*)-/(*E*)-Isomere des *N*,*P*-Bis(*tert*-butyldiphenylsilyl)-2-amino-2-phenyl-$1\lambda^3\sigma^2$-Phosphaalken (**I.2**) als Hauptprodukt (**Schema 2**). Für die Röntgenstrukturbestimmung geeignete Kristalle des (*Z*)-Isomers wurden aus Toluol bei −13 °C erhalten. Aus dem NMR-Spektrum einer [d_8]Tetrahydrofuran-Lösung wurde für das Gemisch aus (*Z*)- und (*E*)-Isomeren ein Intensitätsverhältnis von 7: 1 abgeleitet.

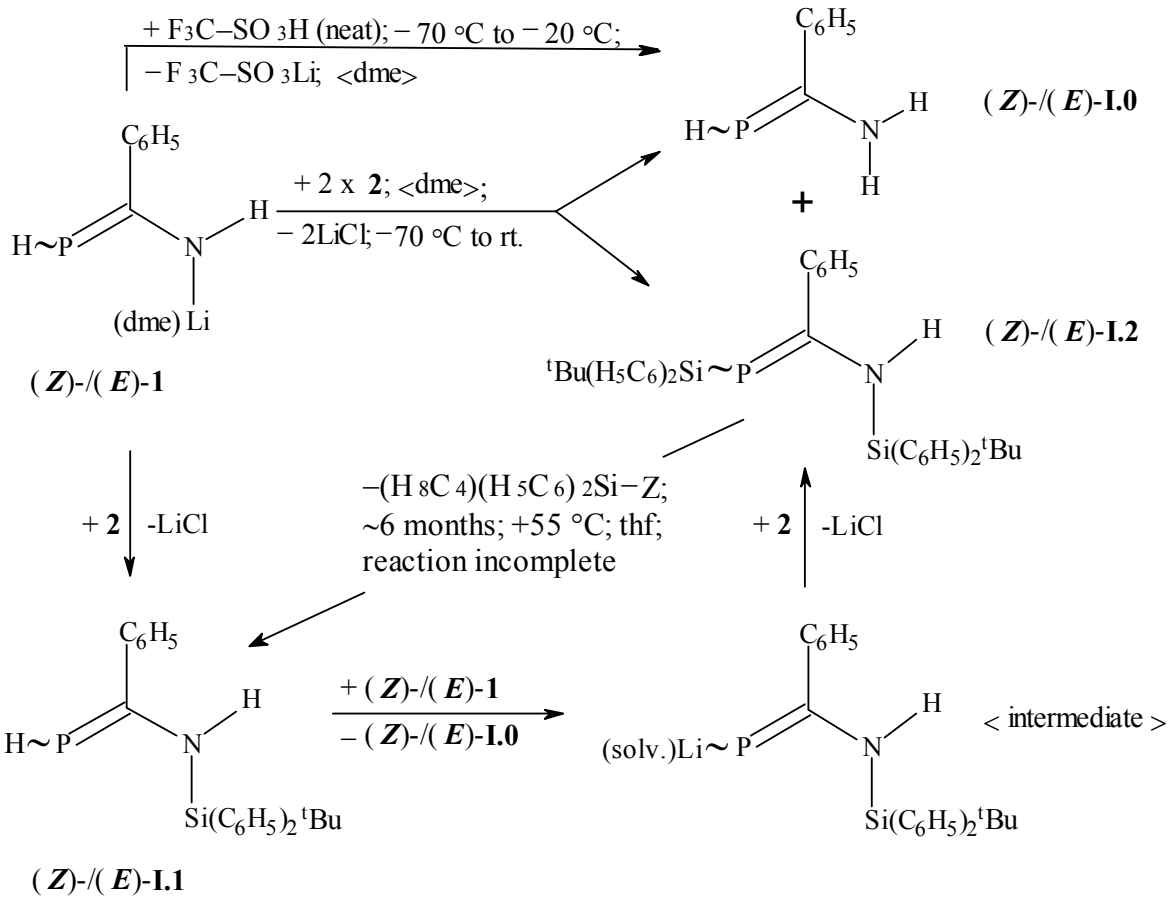

Scheme 2 Bildung von 2-Amino-2-phenyl-$1\lambda^3\sigma^2$-phosphaalken (**I.0**) und dessen *N*-Mono- (**I.1**) und *N*,*P*-disilylierten Derivaten (**I.2**)
2: ^{t}Bu(H_5C_6)$_2$Si-Cl; (H_8C_4)(H_5C_6)$_2$Si-*Z*: Verbindung der unbekannter Zusammensetzung und Struktur

Ganz offensichtlich entsteht bei der Disilylierung des Lithiumderivats **1** zur Verbindung **I.2** vorübergehend das monosubstituierte *N*-(*tert*-Butyldiphenylsilyl)-2-amino-2-phenyl-$1\lambda^3\sigma^2$-phosphaalken **I.1** und unsubstituiertes 2-Amino-2-phenyl-$1\lambda^3\sigma^2$-phosphaalken **I.0**. Die drei Produkte wurden in einem ^{31}P-NMR-Spektrum der Reaktionsmischung zwei Stunden nach Beginn der Reaktion nachgewiesen (**Abbildung 1**).

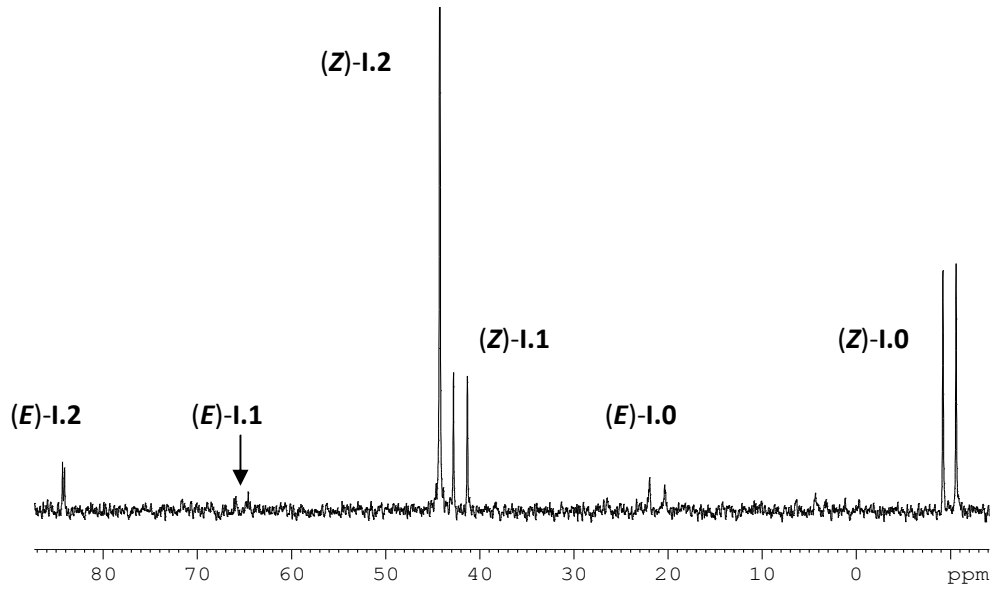

Abbildung 1 ^{31}P-NMR-Spektrum einer bei Raumtemperatur entnommenen Probe aus der Reaktion von Verbindung **1** mit dem Chlorsilan **2** in 1,2-Dimethoxyethan

Unerwarteterweise erwies sich Phosphaalken **I.2** in [d_8]Tetrahydrofuran als instabil. Die NMR-spektroskopische Kontrolle einer unter Luftausschluss versiegelten Lösung bei +55 °C ergab, dass der Zerfall eher langsam ablief und auch nach sechs Monaten noch nicht vollständig abgeschlossen war. 2D-NMR-Spektroskopie ermöglichte die Zuordnung der phosphorhaltigen Zersetzungsprodukte als (*Z*)-/(*E*)-Isomere des *N*-monosilylierten $1\lambda^3\sigma^2$-Phosphaalkens **I.1**. Darüber hinaus wurde die Bildung eines weiteren, phosphorfreien Nebenproduktes beobachtet, dessen Zusammensetzung jedoch nicht abschließend geklärt werden konnte.

Schwerpunkt der vorliegenden Arbeit war die Herstellung von **I.0**. Durch behandeln einer Lösung von **1** in [d_8]Tetrahydrofuranlösung mit reiner Trifluormethylsulfonsäure bei −40 °C in 1,2-Dimethoxyethan konnte eine Gleichgewichtsmischung aus (***Z***)-und (***E***)-**I.0** im Verhältnis 1 : 0,2 zugänglich gemacht und mittels 2D-NMR-Analysen nachgewiesen werden. Auch wenn die Produkte nicht isoliert werden konnten, wurde ihre Identität durch umfangreiche multinukleare NMR-Untersuchungen eindeutig bestätigt.

Das ^{31}P-NMR-Signal von (***E***)-**I.0** zeigte eine ungewöhnliche Temperaturabhängigkeit, die sich in einer Veränderung der Multiplizität von einem Dublett von Tripletts bei 293 K zu einem Dublett von Dubletts mit einer erhöhten $^3J_{P,Ha(N)}$-Kopplung von 21 Hz bei 213 K manifestiert (**Abbildung 2**). Dieses Phänomen lässt sich mit der hohen Energiebarriere und

dem daraus resultierenden Einfrieren Rotation der NH_2-Gruppe um die C–N-Bindung bei 213 K begründen, welche bei höheren Temperaturen deutlich schneller, relativ zur NMR-Zeitskala abläuft.

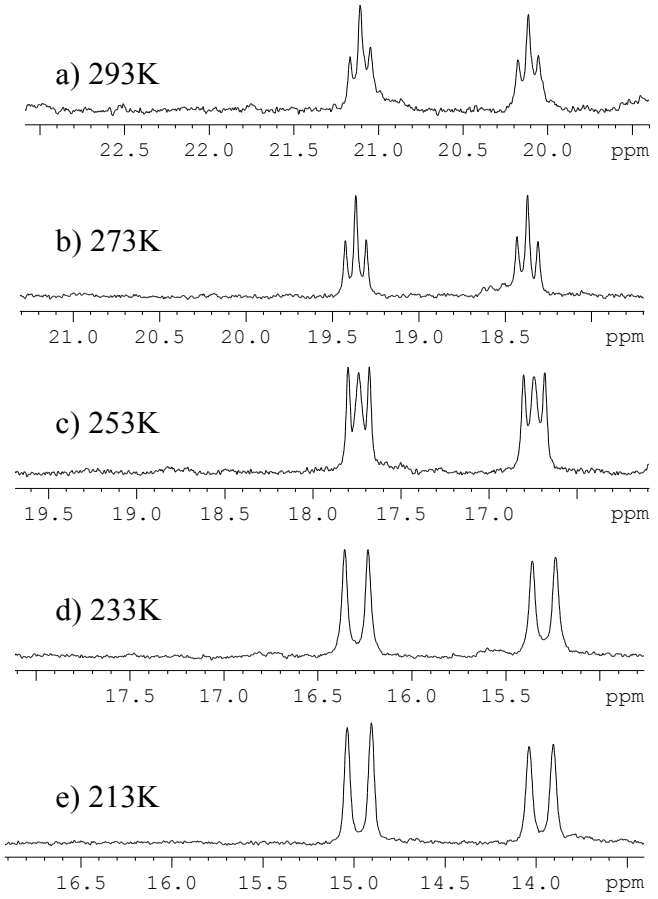

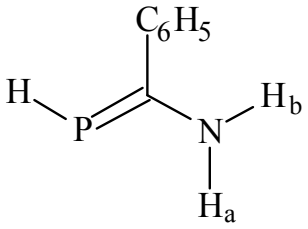

(***E***)-**I.0**

Abbildung 2 Temperaturabhängigkeit des ^{31}P-NMR-Spektrums von Isomer (***E***)-**I.0**

Das unsubstituierte 1-$\lambda^3\sigma^2$-Phosphaalken (***Z***)-/(***E***)-**I.0** ist bei Raumtemperatur in [d_8] Tetrahydrofuran instabil und wandelt sich langsam in zwei neue Verbindungen um, die aufgrund der unvollständigen NMR-Untersuchungen vorläufig als diastereomere Phosphaalkene **I.01** und **I.02** zugeordnet wurden. Vermutlich verläuft der Reaktionsmechanismus über eine säurekatalysierte Insertion der P–H-Gruppe eines Moleküls in die P=C-Einheit eines zweiten (**Gleichung 2**).

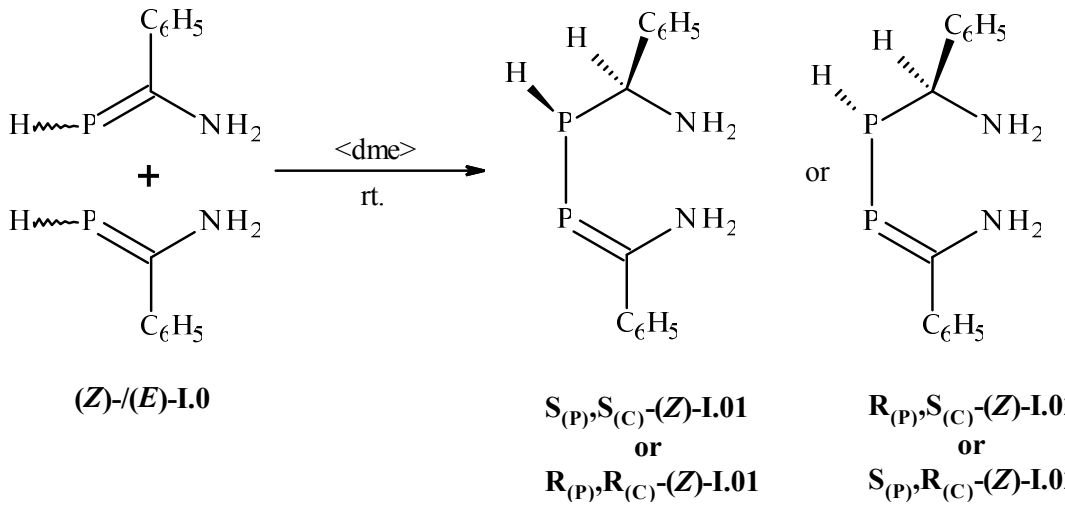

Gl. 2

(*Z*)-/(*E*)-I.0

$S_{(P)},S_{(C)}$-(*Z*)-I.01
or
$R_{(P)},R_{(C)}$-(*Z*)-I.01

$R_{(P)},S_{(C)}$-(*Z*)-I.02
or
$S_{(P)},R_{(C)}$-(*Z*)-I.02

Die Umsetzung von (***Z***)-/(***E***)-**1** mit einer äquimolaren Menge von festem Bis(η^5-pentamethylcyclopenadienyl)zirconiumdichlorid lieferte den Komplex [*N*,*N*'-(1-Amido-3-imido-1,3-Diphenyl-2$\lambda^3\sigma^2$-phospha-1-propen)bis(η^5-pentamethylcyclopentadienyl)zirconium] (**II**), der in Form von kristallinen Solvaten mit Toluol (**II·C_7H_8**) oder Hexan (**2II·*n*-C_6H_{14}**) isoliert wurde. Die Identität der Produkte wurde aus umfassenden NMR-spektroskopischen Untersuchungen und Röntgenstrukturbestimmungen eindeutig bestimmt.

Leider verhinderte die Symmetrie der Raumgruppe *C*2/*c* eine genaue Bestimmung von Bindungslängen und -winkeln in (**II·C_7H_8**). Die komplexen Moleküle liegen auf einer zweizähligen Achse, wodurch sich die P–C=N- und P=C–N(H)-Einheiten des Chelatliganden überlagern. Eine genaue Inspektion der Kristallpackung zeigt, dass Komplexe und Lösungsmittelmoleküle in einer leicht verzerrten PtS-Struktur angeordnet sind. Das Hexansolvat (**2II·*n*-C_6H_{14}**) zeigt dagegen keine Verzerrung und die Bindungslängen der P–C=N- und P=C–N(H)-Einheiten des sechsgliedrigen Chelatrings sind deutlich zu unterscheiden (**Abbildung 3)**.

DFT-Berechnungen an der Modellverbindung [*N*,*N*'-(1-Amido-3-imido-1,3-diphenyl-2$\lambda^3\sigma^2$-phospha-1-propen)bis(cyclopentadienyl)zirconium] bestätigten die Interpretation der Bindungssituation, die aus der den Strukturmerkmalen abgeleitet wurde. Die quantenmechanischen DFT-Berechnungen mit dem Dichtefunktional B3LYP mit unterschiedlichen Basissätzen für das Schweratom Zr (quasi-relativistisches Pseudopotential) und die leichteren Atome C, H, N sowie P (6-31G*) wurden unter Verwendung des Bis(η^5-cyclopentadienyl)-Komplexes als Modell-Verbindung durchgeführt. Die Übereinstimmung

der experimentell ermittelten und berechneten molekularen Parameter liegen im Rahmen der Erwartung.

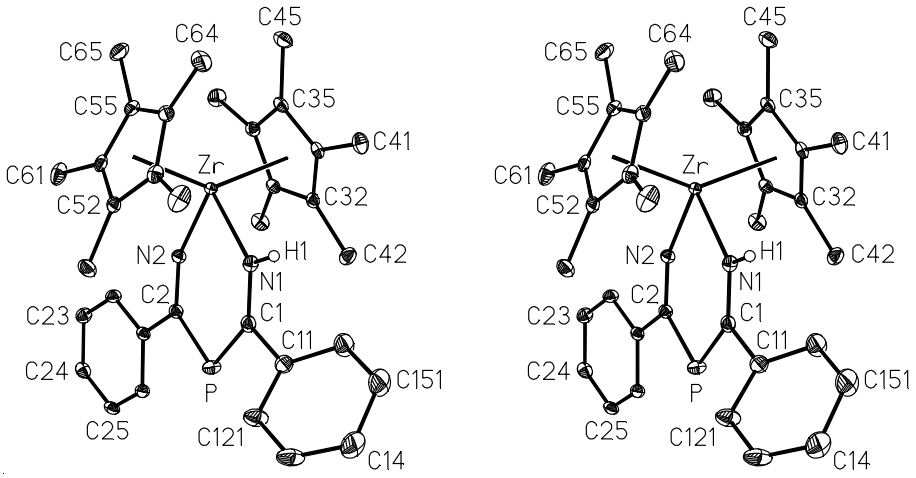

Abbildung 3 Struktur der beiden Komponenten des Festkörperaddukts [*N*,*N*′-(1-Amido-3-imido-1,3-diphenyl-2$\lambda^3\sigma^2$-phospha-1-propen)]bis(η^5-pentamethylcyclopentadienyl)zirconium-*n*-Hexan (1/0,5) (≙ **2II• *n*-C_6H_{14}**) in stereoskopischer Ansicht

Komplexes Molekül **II**. In Bezug auf den fehlgeordneten Phenylsubstituenten mit der Bezeichnung C1*m* ... (*m* = 1 → 6) ist nur das Konformer den Kohlenstoffatomen des höheren Besetzungsfaktors von 0.524 ist dargestellt.

Die Bildung des [1-Amido-3-imido-1,3-diphenyl-2$\lambda^3\sigma^2$-phospha-1-propen]-Dianions, ein völlig neuen Art von Chelatligand, lässt sich vorzugsweise mit den ähnlichen Liganden von Stephan (N=C–P(R)–C=N) [90] und Bergman (N=C–N=C–(O, S)) [105] vergleichen und wird am besten durch die Annahme einer schablonenartigen Reaktion erklärt (**Schema 3**). Die Chloratome des Zirconiumkomplexes **3** werden zunächst durch die N–H-Gruppen von zwei 2-Amino-2-phenyl-1$\lambda^3\sigma^2$-phosphaalken-Substituenten ersetzt. Als nächstes ermöglicht die räumliche Nähe der beiden H~P=C-Einheiten eine einfache Addition der P–H-Einheit eines Liganden an die P=C-Bindung des anderen, so dass der Chelatring durch die Bildung einer neuen P–C-Bindung geschlossen wird. Die Wanderung eines Wasserstoffatoms vom Stickstoff zu einer PH_2-Gruppe führt zur nachfolgenden Eliminierung eines PH_3-Moleküls und der Ausbildung einer C=N-Bindung (**Schema 3**).

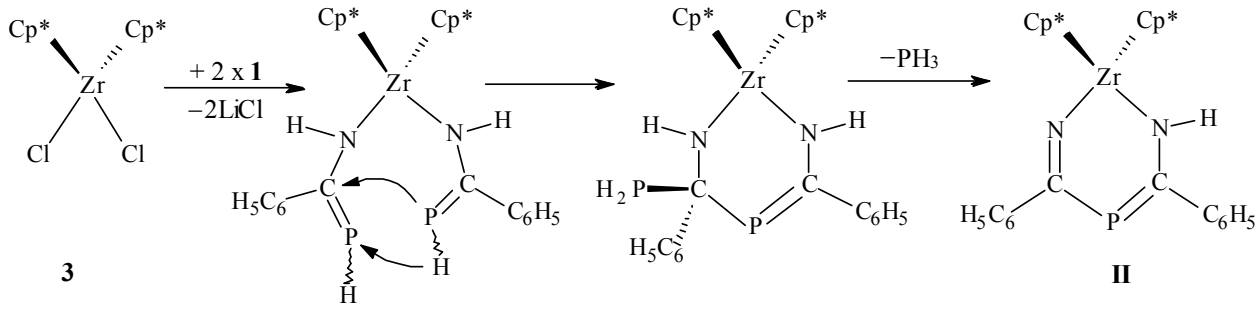

Schema 3 Templat-ähnliche Bildung der [*N*,*N*′-(1-amido-3-imido-1,3-diphenyl-2$\lambda^3\sigma^2$-phospha-1-propen)] Ligand am Zirconium.

Abschließend haben die Reaktionen der Diorganylcarbodiimide **4** - **7** mit (1,2-Dimethoxyethan)lithiumphosphanid neue und faszinierende Möglichkeiten in der Organophosphorchemie eröffnet. Der nukleophile Angriff des Phosphanidanions am *sp*-hybridisierten Kohlenstoffatom des Diorganylcarbodiimidmoleküls führt zur Bildung einer starken P–C-Bindung. Darüber hinaus konnten mehrere Lithiummonophosphaguanidinate (**III-VI**) isoliert und ihre Kristallstrukturen bestimmt werden (**Schema 4**). Die Ergebnisse der Reaktionen in der vorliegenden Arbeit unterscheiden sich erheblich von der Reaktionen von (dme)LiPH_2 mit Bis(trimethylsilyl)carbodiimid zu Herstellung des Koordinationspolymeren (Tetrahydrofuran)lithiumcyano(trimethylsilyl)amids $[(thf)Li(Me_3Si)N–C{\equiv}N]_\infty$ und verschiedener Trimethylsilylphosphane $(Me_3Si)_{3-x}PH_x$ (x = 0→2) durch einen direkten *N*,*P*-Trimethylsilyl-Transfer [109].

Die molekulare Struktur von **III** ist bemerkenswert aufgrund des Vorhandensein eines dme-komplexierten Lithiumkations mit der Koordinationszahl 6. Die Koordinationssphäre des Lithiums besteht aus aus vier Stickstoffatomen, welche aus verzerrt zweizähnigen Monophosphaguanidinat-Anionen kommen und dem DME Molekül. Das zweite dme-komplexierte Lithiumkation der Koordinationzahl 4 hat nur zu jeweils einem Stickstoffatom der mesomeren N⋯C⋯N-Einheit Kontakt. Zusammenfassend können die unterschiedlichen Koordinationen beider Lithiumkationen am besten als Lithiumlithiat beschrieben werden.

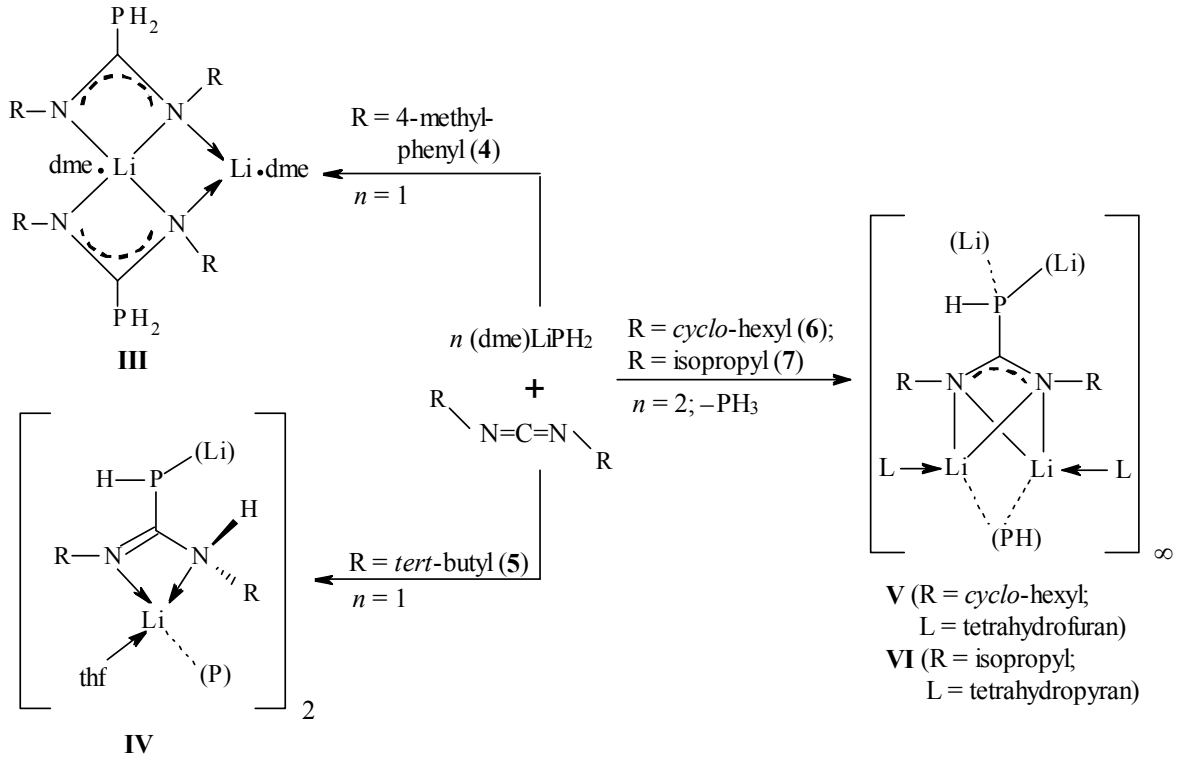

Schema 4 Monophosphaguanidate, isoliert aus Reaktionen der Diorganylcarbodiimide **4** - **7** mit (1,2-Dimethoxyethan) lithiumphosphanid (gestrichelte Bindungen und Elementensymbole in Klammern beziehen sich auf symmetriebezogene Positionen)

Ausgehend von der Annahme, dass die Festkörperstruktur von Komplex **III** in z.B. einer Tetrahydrofuran Lösung erhalten bleibt, kann die Beobachtung eines einzelenen ^{7}Li-NMR-Signal damit erklärt werden, dass die Arme des Phosphaguanidinat-Liganden recht schnell von der Sechserkoordination in die Viererkoordination wechseln können und umgekehrt (**Abb. 4**). Die chemische Verschiebungswert von ^{7}Li ändert sich nur geringfügig von 1,1 ppm bei 298 K auf 0,5 ppm bei 193 K.

a)

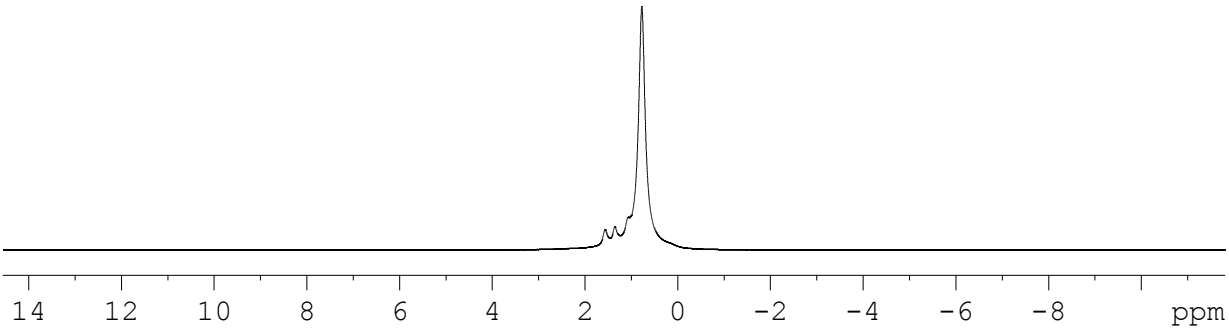

b)

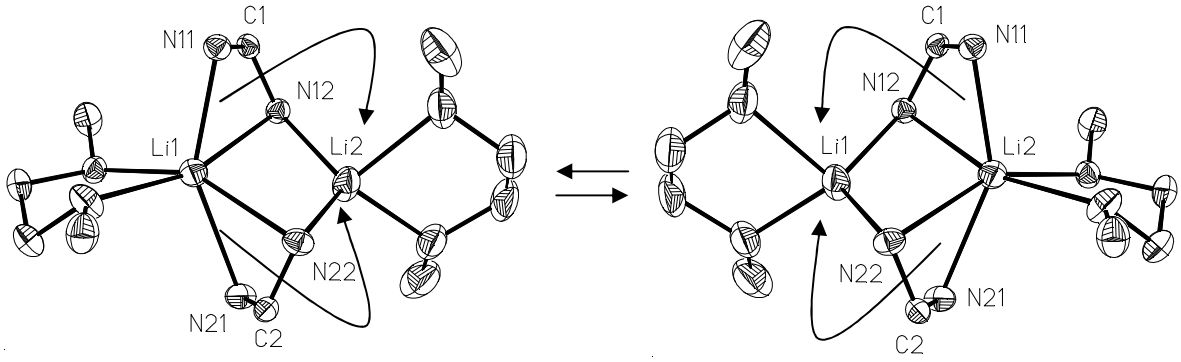

Abbildung 4 ^{7}Li-NMR-Untersuchungen an Komplex **III** in Lösung

a) ^{7}Li-NMR-Spektrum von Komplex **III** bei 253K, gelöst in [d_8]Tetrahydrofuran

b) Fluktuation der [μ-(*C*-Phosphanylformamidinato)]-Liganden von Komplex **III** zwischen sechsfach und vierfachkoordinierten-Lithiumkationen

Zur bessern Übersicht wegen sind die Organyl-Substituenten am Stickstoff, die PH_2-Gruppen am Kohlenstoff und die Wasserstoffatome der 1,2-Dimethoxyethanliganden nicht dargestellt.

Die Umsetzung von Di-tert-butylcarbodiimid (**5**) mit (1,2-Dimethoxyethan) lithiumphosphanid in 1,2-Dimethoxyethan liefert den dimeren Komplex **IV**. Der nukleophile Angriff des Phosphanidanions am *sp*-hybridisierten Kohlenstoffatom wird höchstwahrscheinlich durch eine 1,3-Wasserstoff-Verschiebung von Phosphor zu Stickstoff gefolgt. Das vierfach koordinierte Lithiumkation zeigt sowohl Kontakt mit den formal neutralen Stickstoffatomen des *N*-,*N'*-,*P*-tridentat-Chelatliganden C-Phosphanidatoformamidin, als auch zu einem Tetrahydrofuran-Molekül sowie der benachbarten PH-Gruppe der zweiten Monomereinheit in Verbindung **IV** (**Abbildung 5**). Im Gegensatz zu der N···C···N-**IV** Einheit der Verbindungen **III**, **V** und **VI** sind die C–N-Bindungslängen nicht mehr identisch, sondern unterscheiden sich erheblich.

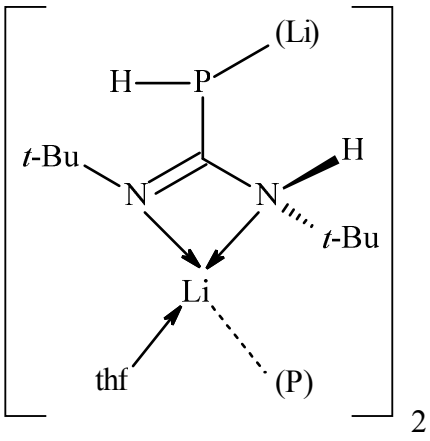

Abbildung 5 Dimer Komplex Bis[μ-(*N,N'*-di-*tert*-butyl-*C*-phospha- nidatoformamidin)-1κ^1*P*; 2κ^1*P'*;1:2κ^2*N*; 1:2κ^2*N'*]1,2-bis(tetrahydrofuran-*O*)dilithium (**IV)**

Die Reaktionen von Dicyclohexyl- (**6**) und Diisopropylcarbodiimid (**7**) mit zwei Äquivalenten (1,2-Dimethoxyethan)lithiumphosphanid in 1,2-Dimethoxyethan ergeben die Dilithiumkomplexe **V** und **VI**. Während das erste Äquivalent für die Bildung der P–C-Bindung über einen nukleophilen Angriff des Phosphanid-Anions am *sp*-hybridisierten Kohlenstoffatom benötigt wird, deprotoniert das zweite die zuvor eingeführte Phosphanylgruppe.

Kristalle der Komplexe **V** und **VI**, die für Röntgenstrukturanalysen geeignet waren, wurden bei −13 °C aus einer eher konzentrierten Tetrahydrofuran- oder Tetrahydropyran-Lösung erhalten. Das Phosphoratom der PH-Gruppe sowie die beiden Stickstoffatome der gebogenen (R)–N⋯C⋯N–(R)-Einheit zeigen einen kurzen Kontakt mit beiden Lithiumkationen (**Abbildung 6**). Beide Verbindungen liegen im Festkörper als Koordinationspolymere vor; Parallele Stränge werden entlang [010] ausgerichtet, was zu einer tetragonalen oder sechseckigen Stabpackung führt (**Abbildung 7**).

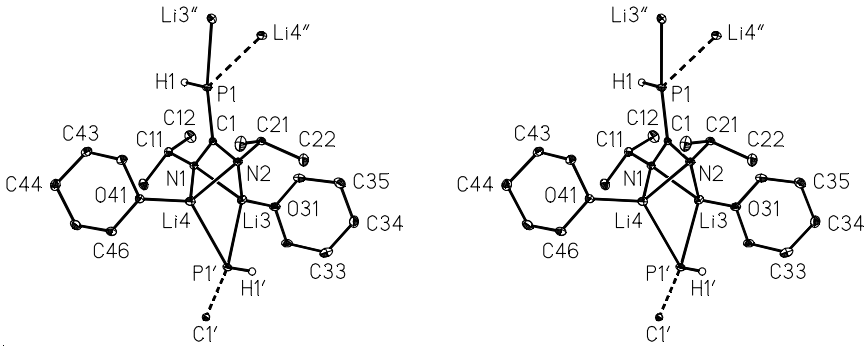

Abbildung 6 Monomere Einheit des komplexen *Catena*-Poly[μ-(*N*,*N*′-Diisopropyl-*C*-phosphanidato-1*:2*κ^{2}P-Formamidinato-1:2κ^2*N*,1:2κ^2*N*′)-1,2-Bis(Tetrahydropyran-*O*]Dilithium (**VI**) in stereoskopischer Ansicht wurden Thermische Ellipsoide sind mit einer Wahrscheinlichkeit von 30%, dargestellt, mit Ausnahme der PH-Gruppen wurden alle Wasserstoffatome zur besseren Übersicht weggelassen. Die Struktur des Komplexes **V** ist nahezu identisch mit der von **VI**.

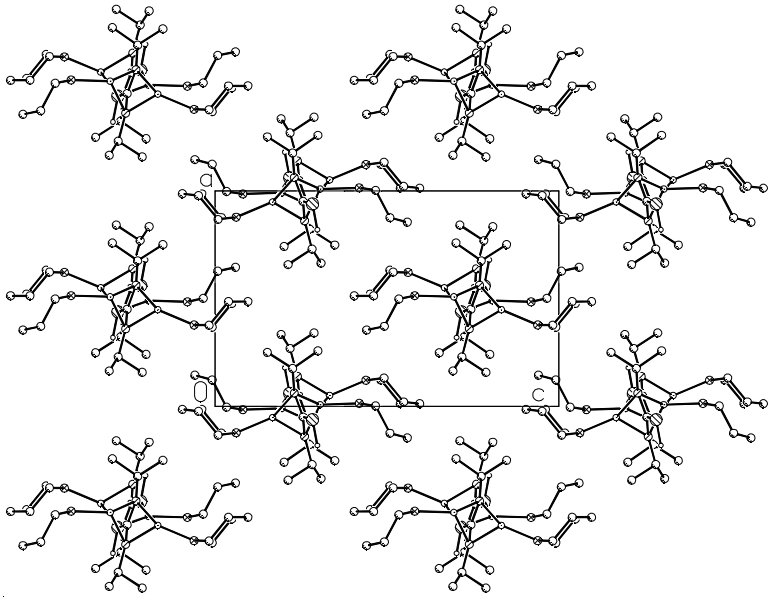

Abbildung 7 Stränge des Koordinationspolymers **VI** bei [010]. Die Stränge bauen eine hexagonale Stabpackung auf.

8. Appendix

8.1 *General Crystallographic Information*

Four-circle diffractometer $P2_1$ (Syntex, Cupertino, USA), Bruker (*Kappa Apex II Dou)*, and P4 (Siemens Analytical X-ray Instruments Inc., Madison, Wisconson, USA); Mo-Kα radiation with graphite monochromator (λ = 71.073 nm); control of intensity and orientation by two measurements after a period of 98 reflections; registration of the background at the beginning and at the end of the measurement with an overall duration equal to the time of measurement; application of the software package program SHELXTL, version 5.1 from the company Bruker AXS Inc., Madison, Wisconsin [118-120] for the treatment of data, determination of structures with statistical methods and subsequent refinements: calculation of the quality factors R1 and wR2 using measured values with $F > 4\sigma$ (F_o); full-matrix least squares refinement on F2; several cycles of refinement with complete matrix and following difference Fourier synthesis; minimizing of the function $\Sigma w (F_o^2 - F_c^2)^2$. The quality factors are defined by the following formulas with m (number of reflections) and n (number of parameters):

$$wR = \{\Sigma [w(Fo - | Fc |)^2] / \Sigma [w(Fo^2]\} 1/2$$

$$wR_2 = \{\Sigma [w(Fo^2 - Fc^2)^2] / \Sigma [w(Fo^2)^2]\} 1/2$$

$$R = R_1 = \Sigma | Fo - | Fc || / \Sigma Fo$$

$$GOF = \{\Sigma [w(Fo^2 - Fc^2)^2] / (m - n\} 1/2$$

The anisotropic displacement parameters U_{ij} ($10^{-23} m^2$) refer to the expression:
$e[-2\pi^2 (a^{*2} h^2 U_{11} + b^{*2} k^2 U_{22} + c^{*2} l^2 U_{33} + 2b^* c^* k l U_{23} + 2a^* c^* h l U_{13} + 2 a^* b^* h k U_{12})]$;
The equivalent isotropic U_{eq} value is defined as one-third of the trace of the orthogonalized U_{ij} tensor [149].

8.2 *Z*-[*N*,*P*-bis(*tert*-butyldiphenylsilyl)-2-amino-2-phenyl-1$\lambda^3\sigma^2$-phosphaalkene] {(***Z***)-**I.2**}

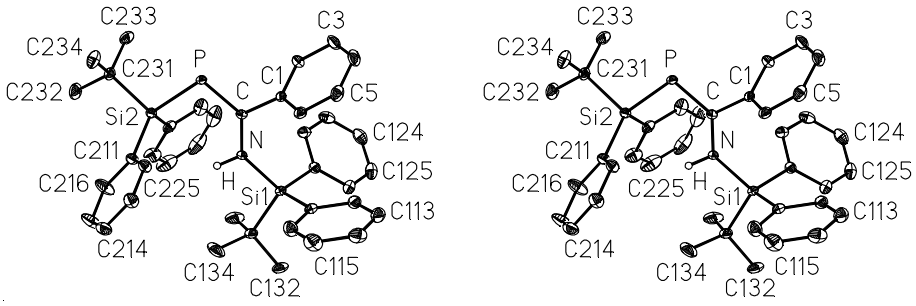

Table 8.2.1 Bond lengths (pm) and bond angles (deg), characteristic torsion angles as well as least-squares planes and angles between these planes for *Z*-[*N*,*P*-bis(*tert*-butyldiphenylsilyl)-2-amino-2-phenyl-1$\lambda^3\sigma^2$-phosphaalkene] {(***Z***)-**I.2**}

a) Bond lengths

PCN-skeleton		C-phenyl		mean	Si–C_6H_5	*m* = 1	*m* = 2	mean
P–C	172.7(2)	C1–C2	139.8(2)	138.9	Si*m*–C*m*11	187.7(2)	189.1(2)	188.5
P–Si2	226.4(1)	C1–C6	139.1(2)		Si*m*–C*m*21	187.7(2)	189.4(2)	
C–C1	149.7(2)	C2–C3	138.7(9)		Si–$C(CH_3)_3$	*m* = 1	*m* = 2	mean
C–N	137.4(2)	C3–C4	137.9(3)		Si*m*–C*m*31	190.2(2)	190.8(2)	190.5
N–Si1	177.2(1)	C4–C5	138.3(3)					
N–H	88.0	C5–C6	139.3(2)					

Si-phenyl, *mn* =	11[a]	12[a]	21[a]	22[a]	Si–*t*-butyl[b]	
C*mn*1–C*mn*2	139.3(2)	139.9(2)	139.6(2)	138.8(3)	C131–C132	153.4(2)
C*mn*1–C*mn*6	140.2(2)	140.4(2)	139.9(2)	139.7(3)	C131–C133	153.4(3)
C*mn*2–C*mn*3	138.8(2)	138.5(3)	138.7(2)	139.4(3)	C131–C134	153.1(3)
C*mn*3–C*mn*4	137.5(3)	138.2(3)	137.8(3)	136.2(4)	C231–C132	153.1(2)
C*mn*4–C*mn*5	137.9(3)	138.9(3)	136.8(3)	137.8(4)	C231–C133	153.8(2)
C*mn*5–C*mn*6	138.6(3)	138.5(3)	139.4(3)	138.8(3)	C231–C134	153.5(2)

mean: [a] 138.7; [b] 153.4

b) Bond angles

C–P–Si2	106.1(1)	N–Si1–C111	111.7(1)	P–Si2–C211	111.0(1)
N–C–P	128.6(1)[c]	N–Si1–C121	109.3(1)	P–Si2–C221	110.0(1)
P–C–C1	114.1(1)[c]	N–Si1–C131	103.4(1)	P–Si2–C231	103.9(1)
N–C–C1	117.2(1)[c]	C111–Si1–C121	110.7(1)	C211–Si2–C221	112.0(1)
C–N–Si1	134.4(1)	C111–Si1–C131	112.0(1)	C211–Si2–C231	110.7(1)
C–N–H	112.8	C121–Si1–C131	109.5(1)	C221–Si2–C231	108.9(1)
Si1–N–H	112.8				

[c] sum of angles at C: 359.9°

Phenyl substituents			*m*,*n*=1	*m*=1, *n*=2	*m*=2, *n*=1	*m*,*n*=2
C–C1–C2	119.9(1)	Si*m*–C*mn*1–C*mn*2	122.9(1)	120.8(1)	119.4(1)	119.7(1)[d]
C–C1–C6	121.2(1)	Si*m*–C*mn*1–C*mn*6	119.9(1)	122.0(1)	124.6(1)	123.9(2)[d]
C2–C1–C6	118.8(2)	C*mn*2–C*mn*1–C*mn*6	117.1(2)	117.0(2)	116.0(1)	116.5(2)[e]
C1–C2–C3	120.3(2)	C*mn*1–C*mn*2–C*mn*3	121.5(2)	121.5(2)	122.3(2)	121.8(2)[f]
C2–C3–C4	120.4(2)	C*mn*2–C*mn*3–C*mn*4	120.0(2)	120.5(2)	120.2(2)	120.5(2)[g]
C3–C4–C5	119.7(2)	C*mn*3–C*mn*4–C*mn*5	120.0(2)	119.3(2)	119.1(2)	119.2(2)[g]
C4–C5–C6	120.4(2)	C*mn*4–C*mn*5–C*mn*6	120.0(2)	120.2(2)	120.9(2)	120.5(2)[g]
C5–C6–C1	120.5(2)	C*mn*5–C*mn*6–C*mn*1	121.3(2)	120.2(2)	121.5(2)	121.5(2)[d]

mean: [d] 121.7; [e] 116.7; [f] 121.6; [g] 120.0

t-Butyl substituents	*m* = 1	*m* = 2		*m* = 1	*m* = 2
Si*m*–C*m*31–C*m*32	108.7(1)	110.2(1)[h]	C*m*32–C*m*31–C*m*33	108.4(2)	109.0(2)[i]
Si*m*–C*m*31–C*m*33	108.7(1)	109.2(1)[h]	C*m*32–C*m*31–C*m*34	108.5(2)	109.4(2)[i]
Si*m*–C*m*31–C*m*34	113.4(1)	110.1(1)[h]	C*m*33–C*m*31–C*m*34	109.0(2)	108.9(2)[i]

mean: [h] 110.1; [i] 108.9

c) Characteristic torsion angles [j]

P–C–C1–C2	–55.2(2)	N–Si1–C111–C112	–118.8(1)
P–Si2–C211–C212	8.7(2)	N–Si1–C121–C122	–10.9(2)
P–Si2–C221–C222	–20.8(2)	N–Si1–C131–C132	–173.8(1)
P–Si2–C231–C232	178.3(1)	C111–Si1–C131–C133	–53.8(1)
C211–Si2–C231–C234	58.3(2)	C121–Si1–C131–C134	–47.9(2)
C221–Si2–C231–C233	–58.6(1)	C111–Si1–C121–C122	–134.3(1)
C211–Si2–C221–C222	–144.7(1)		

[j] The torsion angle A–B–C–D is defined as positive when on viewing along the B–C bond, atom A must be rotated clockwise to eclipse atom D [46 and 47].

d) Characteristic least-squares planes and deviations (pm) from these planes
Atoms defining a least-squares plane are marked with an asterisk (*).

*A: *PCN-skeleton*										
N*	C*	P*	Si1	H	C132	C111	C1	C4	Si2	C232	C211
0.0	0.0	0.0	40.1	–25.7	71.5	–91.3	–5.7	–22.7	30.0	58.0	–113.0

B_1: *phenyl substituent 11*						
C111*	C112*	C113*	C114*	C115*	C116*	Si1
0.3	0.0	–0.2	0.2	0.0	–0.3	–5.5

B_2: *phenyl substituent 12*						
C121*	C122*	C123*	C124*	C125*	C126*	Si1
–0.6	0.1	0.4	–0.4	–0.1	0.6	10.9

B_3: *phenyl substituent 21*						
C211*	C212*	C213*	C214*	C215*	C216*	Si2
0.7	–0.1	–0.4	0.3	0.3	–0.8	–1.6

B_4: *phenyl substituent 22*						
C221*	C222*	C223*	C224*	C225*	C226*	Si2
0.7	–0.5	–0.1	0.5	–0.3	–0.3	1.8

C: *C-phenyl*						
C1*	C2*	C3*	C4*	C5*	C6*	C
0.2	–0.1	–0.1	0.3	–0.2	0.0	–9.2
D: *Si2PCNC1-skeleton*						
Si2*	P*	C*	N*	C1*		
5.5	−7.4	−0.2	−3.8	5.8		
Angles (deg) between different planes						
A/B_1 79.2; A/B_2 68.8; A/B_3 65.4; A/B_4 69.7; A/C 56.7; B_1/B_2 50.6; B_3/B_4 45.3; D/CNSi1 22.8						

Table 8.2.2 Atomic Coordinates, Equivalent Isotropic Displacement Parameters, and Anisotropic Displacement Parameters with Estimated Standard deviations in Parentheses for *Z*-[*N*,*P*-bis(*tert*-butyldiphenylsilyl)-2-amino-2-phenyl-1$\lambda^3\sigma^2$-phosphaalkene] {(***Z***)-**I.2**}

Atom	X/a·10^4	Y/b·10^4	Z/c·10^4	U(eq)	U11	U22	U33	U23	U13	U12
P	9349(1)	8077(1)	2154(1)	23(1)	14(1)	31(1)	20(1)	–4(1)	–3(1)	–9(1)
N	11768(2)	7705(2)	2828(1)	22(1)	13(1)	28(1)	23(1)	–7(1)	–2(1)	–7(1)
Si1	12772(1)	8141(1)	3333(1)	21(1)	17(1)	25(1)	21(1)	–1(1)	–6(1)	–9(1)
Si2	11385(1)	7203(1)	1358(1)	21(1)	19(1)	23(1)	18(1)	1(1)	–2(1)	–8(1)
C	10173(2)	8209(2)	2779(1)	20(1)	15(1)	21(1)	22(1)	–1(1)	–2(1)	–8(1)
C1	8967(2)	8918(2)	3340(1)	22(1)	17(1)	29(1)	21(1)	–6(1)	–1(1)	–13(1)
C2	7611(2)	10407(2)	3303(1)	29(1)	23(1)	29(1)	31(1)	–5(1)	1(1)	–9(1)
C3	6431(2)	11035(2)	3809(1)	39(1)	26(1)	37(1)	45(1)	–16(1)	8(1)	–9(1)
C4	6582(2)	10197(2)	4356(1)	41(1)	34(1)	57(1)	35(1)	–20(1)	14(1)	–26(1)
C5	7912(2)	8719(2)	4398(1)	37(1)	41(1)	56(1)	22(1)	–3(1)	1(1)	–32(1)
C6	9105(2)	8079(2)	3893(1)	27(1)	23(1)	36(1)	26(1)	–2(1)	–4(1)	–17(1)
C111	12678(2)	7232(2)	4117(1)	24(1)	21(1)	29(1)	27(1)	2(1)	–9(1)	–13(1)
C112	11937(2)	8122(2)	4653(1)	30(1)	30(1)	33(1)	28(1)	0(1)	–5(1)	–15(1)
C113	11840(2)	7418(2)	5223(1)	38(1)	36(1)	51(1)	26(1)	0(1)	–3(1)	–21(1)
C114	12487(2)	5805(3)	5269(1)	44(1)	39(1)	52(1)	34(1)	17(1)	–8(1)	–19(1)
C115	13224(3)	4888(2)	4747(1)	48(1)	53(1)	34(1)	49(1)	13(1)	–8(1)	–15(1)
C116	13316(2)	5592(2)	4177(1)	38(1)	43(1)	29(1)	36(1)	0(1)	–4(1)	–13(1)
C121	11855(2)	10340(2)	3391(1)	24(1)	22(1)	26(1)	24(1)	–1(1)	–1(1)	–11(1)
C122	10775(2)	11353(2)	2989(1)	30(1)	25(1)	33(1)	32(1)	3(1)	–6(1)	–13(1)
C123	10168(2)	12972(2)	3000(1)	39(1)	29(1)	31(1)	49(1)	8(1)	–7(1)	–9(1)
C124	10615(2)	13634(2)	3413(1)	41(1)	40(1)	27(1)	49(1)	–4(1)	8(1)	–15(1)
C125	11696(3)	12657(2)	3815(1)	39(1)	50(1)	40(1)	33(1)	–9(1)	4(1)	–28(1)
C126	12310(2)	11037(2)	3801(1)	32(1)	38(1)	37(1)	27(1)	–1(1)	–6(1)	–22(1)
C131	14928(2)	7282(2)	2922(1)	29(1)	18(1)	38(1)	31(1)	–2(1)	–5(1)	–13(1)
C132	15983(2)	7417(3)	3347(1)	39(1)	25(1)	55(1)	42(1)	5(1)	–14(1)	–22(1)
C133	14933(2)	8259(3)	2336(1)	53(1)	24(1)	93(2)	35(1)	14(1)	–2(1)	–25(1)
C134	15674(2)	5546(3)	2745(1)	61(1)	34(1)	42(1)	45(1)	12(1)	14(1)	–3(1)
C211	13063(2)	5167(2)	1527(1)	26(1)	21(1)	27(1)	24(1)	2(1)	–1(1)	–7(1)
C212	12822(2)	4341(2)	2047(1)	29(1)	27(1)	27(1)	27(1)	1(1)	0(1)	–11(1)
C213	13993(2)	2835(2)	2193(1)	37(1)	40(1)	29(1)	32(1)	5(1)	–5(1)	–12(1)
C214	15458(2)	2101(2)	1820(1)	41(1)	31(1)	30(1)	47(1)	2(1)	–9(1)	–2(1)
C215	15732(3)	2873(3)	1304(1)	55(1)	28(1)	44(1)	61(1)	6(1)	12(1)	2(1)
C216	14552(2)	4379(2)	1153(1)	50(1)	34(1)	42(1)	45(1)	12(1)	14(1)	–3(1)
C221	12147(2)	8679(2)	1176(1)	29(1)	35(1)	39(1)	21(1)	7(1)	–10(1)	–23(1)
C222	11166(3)	10233(2)	1365(1)	41(1)	60(1)	37(1)	33(1)	6(1)	–9(1)	–30(1)
C223	11678(4)	11359(3)	1247(1)	59(1)	106(2)	52(1)	42(1)	10(1)	–17(1)	–55(2)
C224	13171(4)	10963(4)	934(1)	65(1)	113(2)	88(2)	44(1)	27(1)	–32(1)	–86(2)
C225	14167(3)	9435(4)	732(1)	63(1)	65(2)	107(2)	49(1)	27(1)	–17(1)	–67(2)
C226	13664(3)	8309(3)	849(1)	47(1)	41(1)	62(1)	46(1)	9(1)	–5(1)	–33(1)
C231	10383(2)	7141(2)	682(1)	28(1)	32(1)	33(1)	21(1)	–2(1)	–5(1)	–16(1)
C232	11612(3)	6611(3)	95(1)	44(1)	51(1)	61(1)	22(1)	–8(1)	0(1)	–28(1)
C233	8987(2)	8801(2)	574(1)	42(1)	44(1)	44(1)	34(1)	4(1)	–22(1)	–15(1)
C234	9703(3)	5993(3)	825(1)	44(1)	60(1)	53(1)	36(1)	–5(1)	–7(1)	–40(1)

Atom	X/a·10^4	Y/b·10^4	Z/c·10^4	U(eq)	Atom	X/a·10^4	Y/b·10^4	Z/c·10^4	U(eq)
H	12442	7008	2545	27	H13C	17104	6951	3145	59
H6	10017	7064	3926	33	H13B	15938	6854	3735	59
H5	8013	8137	4774	44	H13A	15581	8532	3433	59
H4	5776	10634	4703	50	H222	10116	10538	1581	49
H3	5514	12047	3779	47	H223	10981	12412	1386	71
H2	7497	10994	2928	35	H224	13521	11730	857	78
H116	13821	4951	3820	46	H225	15206	9151	509	75
H115	13670	3774	4778	58	H22È	14367	7263	705	56
H114	12426	5323	5659	52	H216	14764	4881	788	60
H113	11327	8050	5582	46	H215	16741	2376	1046	66
H112	11487	9237	4628	36	H214	16266	1073	1920	49
H126	13057	10383	4075	39	H213	13783	2308	2551	44
H125	12015	13100	4099	47	H212	11822	4827	2311	34
H124	10189	14746	3423	49	H23I	9203	5961	473	66
H123	9439	13631	2721	47	H23H	8889	6351	1192	66
H122	10450	10920	2702	36	H23G	10582	4935	901	66
H13I	16743	5201	2505	92	H23F	8499	8785	215	62
H13H	14972	5427	2498	92	H23E	9404	9550	497	62
H13G	15785	4899	3121	92	H23D	8167	9127	939	62
H13F	16046	7857	2130	80	H23C	11064	6671	–256	66
H13E	14484	9367	2446	80	H23B	12460	5520	148	66
H13D	14273	8176	2056	80	H23A	12099	7302	18	66

8.3 [(1-amido-3-imido-1,3-diphenyl-2$\lambda^3\sigma^2$-phospha-1-propene-*N,N′*)bis(η^5-pentamethylcyclopentadienyl)zirconium]–toluene (1/1) (≙ **II·C$_7$H$_8$**)

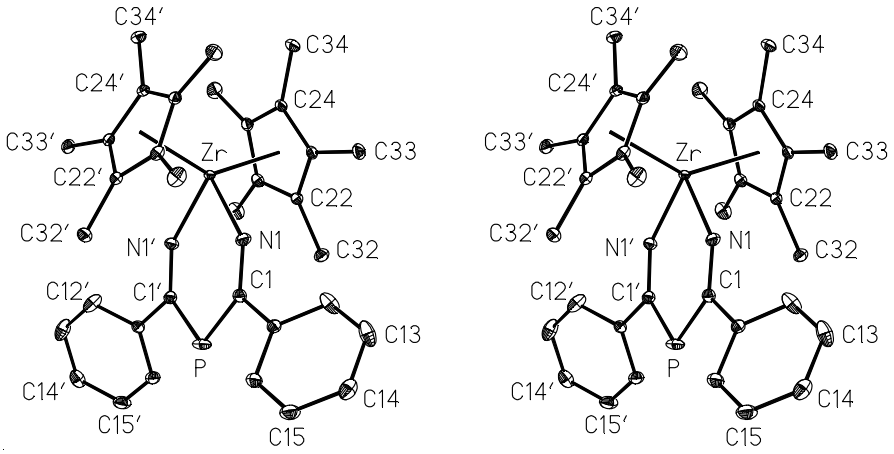

Table 8.3.1 Distances (pm) and bond angles (deg), characteristic torsion angles and intramolecular contacts as well as least-squares planes and angles between these planes for [(1-amido-3-imido-1,3-diphenyl-2$\lambda^3\sigma^2$-phospha-1-propene-*N,N′*)bis(η^5-pentamethylcyclopentadienyl)zirconium]–toluene (1/1) (≙ **II·C$_7$H$_8$**)

Due to space group symmetry the molecular structure of the zirconium complex exhibits a twofold axis. As a consequence the P–C=N and P=C–N(H) fragments are superimposed and the chelate ligand is found to be disordered. Similarly, the solvent molecule toluene adopts two different positions in centrosymmetric voids of the unit cell. The following table comprises data of two different structure determinations at (100 ±2)K and ambient temperature obtained with crystals of (**II·C$_7$H$_8$**)$_{Hex}$ and (**II·C$_7$H$_8$**)$_{Tol}$, respectively. Well known parameters of the phenyl substituent and the η^5-pentamethylcyclopentadienyl ligand as well as the toluene molecule are also included in detail in order to demonstrate the high quality of both data sets.

M_{Cp}: centre of the η^5-pentamethylcyclopentadienyl ligand; (′): symmetry operation (–x+1; y; –z+3/2).

a) Distances

chelate ligand at zirconium			
	(**II·C$_7$H$_8$**)$_{Hex}$ / (**II·C$_7$H$_8$**)$_{Tol}$		(**II·C$_7$H$_8$**)$_{Hex}$ / (**II·C$_7$H$_8$**)$_{Tol}$
Zr–N1	210.2(2) / 210.4(2)	C1···C1′	280.5 / 281.9
N1–C1	130.3(3) / 130.2(2)	N1···N1′	275.5 / 276.2
P–C1	179.3(2) / 180.1(2)	Zr···M_{Cp}	224.5 / 224.9
C1–C11	150.2(3) / 150.1(2)		
phenyl substituent			
	(**II·C$_7$H$_8$**)$_{Hex}$ / (**II·C$_7$H$_8$**)$_{Tol}$		(**II·C$_7$H$_8$**)$_{Hex}$ / (**II·C$_7$H$_8$**)$_{Tol}$
C11–C12[a)]	139.1(3) / 139.2(3)	C13–C14	137.3(4) / 137.7(3)
C11–C16	138.9(3) / 139.4(3)	C14–C15	137.3(4) / 137.8(3)
C12–C13	138.6(3) / 138.5(3)	C15–C16	138.0(4) / 138.9(3)

η^5-pentamethylcyclopentadienyl ligand			
	(II·C$_7$H$_8$)$_{Hex}$ / **(II·C$_7$H$_8$)**$_{Tol}$		**(II·C$_7$H$_8$)**$_{Hex}$ / **(II·C$_7$H$_8$)**$_{Tol}$
C21–C22[b)]	141.5(3) / 141.4(2)	C21–C31[c)]	149.8(3) / 149.8(2)
C21–C25	141.9(3) / 142.5(2)	C22–C32	149.6(3) / 149.9(2)
C22–C23	142.4(3) / 142.3(2)	C23–C33	150.0(3) / 150.3(2)
C23–C24	141.8(3) / 142.0(2)	C24–C34	150.1(3) / 150.2(2)
C24–C25	142.0(3) / 142.4(2)	C25–C35	150.1(3) / 150.6(2)
toluene molecul[e)]			
	(II·C$_7$H$_8$)$_{Hex}$ / **(II·C$_7$H$_8$)**$_{Tol}$		**(II·C$_7$H$_8$)**$_{Hex}$ / **(II·C$_7$H$_8$)**$_{Tol}$
C41–C42[d)]	137.4(8) / 140.5(8)	C44–C45	136.1(9) / 144(1)
C41–C46	140.1(8) / 139.9(8)	C45–C46	137.5(9) / 140.3(9)
C42–C43	139.2(8) / 139.6(9)	C41–C47	152.2(7) / 150.4(7)
C43–C44	136.9(9) / 143(1)		

mean values: [a)]C–C$_{phenyl}$ 138.2 / 138.2; [b)]C–C$_{cycl.}$ 141.9 / 142.1; [c)]C–CH$_3$ 149.9 / 150.2; [d)]C–C$_{cycl}$ 137.9 / 142.4; [e)] refinement of bond length and bond angles within a given limit;

b) Bond angles

chelate ligand			
	(II·C$_7$H$_8$)$_{Hex}$ / **(II·C$_7$H$_8$)**$_{Tol}$		**(II·C$_7$H$_8$)**$_{Hex}$ / **(II·C$_7$H$_8$)**$_{Tol}$
M$_{Cp}$′···Zr···M$_{Cp}$	139.5 / 139.6	N1–C1–P[a)]	127.3(2) / 127.2(2)
N1–Zr···M$_{Cp}$	105.8 / 104.5	N1–C1–C11	118.8(2) / 119.2(2)
N1–Zr–N1′	81.8(1) / 82.0(2)	P–C1–C11	113.8(1) / 113.5(1)
Zr–N1–C1	140.1(2) /140.1(2)	C1′–P–C1	102.9(1) / 103.0(1)
phenyl substituents			
	(II·C$_7$H$_8$)$_{Hex}$ / **(II·C$_7$H$_8$)**$_{Tol}$		**(II·C$_7$H$_8$)**$_{Hex}$ / **(II·C$_7$H$_8$)**$_{Tol}$
C1–C11–C12[b)]	121.7(2) / 120.2(2)	C12–C13–C14	120.5(2) / 120.1(2)
C1–C11–C16	120.6(2) / 121.8(2)	C13–C14–C15	119.6(2) / 119.6(2)
C12–C11–C16	117.7(2) / 118.0(2)	C14–C15–C16	120.1(2) / 120.5(2)
C11–C12–C13	120.7(2) / 121.2(2)	C15–C16–C11	121.4(2) / 120.5(2)
η^5-pentamethylcyclopentadienyl ligand			
	(II·C$_7$H$_8$)$_{Hex}$ / **(II·C$_7$H$_8$)**$_{Tol}$		**(II·C$_7$H$_8$)**$_{Hex}$ / **(II·C$_7$H$_8$)**$_{Tol}$
C22–C21–C25[c)]	108.3(2) / 108.3(2)	C23–C22–C32	126.2(2) / 126.2(2)
C21–C22–C23[c)]	107.6(2) / 107.7(2)	C22–C23–C33	125.8(2) / 125.8(2)
C22–C23–C24[c)]	108.4(2) / 108.5(2)	C24–C23–C33	125.6(2) / 125.4(2)
C23–C24–C25[c)]	107.6(2) / 107.6(2)	C23–C24–C34	124.6(2) / 125.1(2)
C24–C25–C21[c)]	108.1(2) / 107.9(2)	C25–C24–C34	126.7(2) / 126.2(2)
C25–C21–C31	124.9(2) / 124.6(2)	C24–C25–C35	127.0(2) / 127.0(2)
C22–C21–C31	126.5(2) / 126.8(2)	C21–C25–C35	124.2(2) / 124.4(2)
C21–C22–C32	126.1(2) / 126.0(2)		
toluene molecul[e)]			
	(II·C$_7$H$_8$)$_{Hex}$ / **(II·C$_7$H$_8$)**$_{Tol}$		**(II·C$_7$H$_8$)**$_{Hex}$ / **(II·C$_7$H$_8$)**$_{Tol}$
C46–C41–C42[c)]	117.2(5) / 117.4(5)	C44–C45–C46	121.0(7) / 121.3(7)
C41–C42–C43	122.0(6) / 123.5(8)	C45–C46–C41	120.5(6) / 121.1(7)
C42–C43–C44	119.3(6) / 119.3(8)	C42–C41–C47	121.1(6) / 121.7(5)
C43–C44–C45	119.9(8) / 117.4(7)	C46–C41–C47	121.7(6) / 120.8(6)

Sum of angles at [a)] C1 359.9 / 359.9; [b)] C11 360.0 / 360.0; [c)] C21 359.7 / 359.7; C22 359.9 / 359.9; C23 359.8 / 359.7; C24 358.9 / 358.9; C25 359.3 / 359.3; [d)] C41 360.0 / 359.9

c) Characteristic torsion angles[f] for (**II**·C_7H_8)$_{Tol}$[g]

C1′–P–C1–N1	–3.2	C1–N1–Zr···M_{Cp}	–106.9
P–C1–C11–C16	144.0	P–C1–N1–Zr	7.5

[f] The torsion angle A–B–C–D is defined as positive if, when viewed along the B–C bond, atom A must be rotated clockwise to eclipse atom D [46 and 47]; [g] almost identical values for (**II**·C_7H_8)$_{Hex}$

d) Characteristic least-squares planes and deviations (pm) from these planes for (**II**·C_7H_8)$_{Tol}$[g]

Atoms defining a least-squares plane are marked with an asterisk (*). The six-membered chelate heterocycle adopts a slight twist conformation.

A: *chelate heterocycle*								
P*	C1*	N1*	C1′*	N1′*	Zr*	C11	C16	M_{Cp}
0.0	2.9	–2.9	–2.9	2.9	0.0	4.4	–63.6	–212.6

B: *phenyl substituent*								
C11*	C12*	C13*	C14*	C15*	C16*	C1	N1	P
–0.5	–0.1	0.5	–0.3	–0.2	0.6	–8.6	47.2	–105.4

C: *η5-pentamethylcyclopentadienyl ligand*									
C21*	C22*	C23*	C24*	C25*	C31	C32	C33	C34	C35
–0.4	–0.2	0.7	–0.9	0.8	–13.5	–7.2	–10.4	–28.8	–16.6

D: *toluene molecule*						
C41*	C42*	C43*	C44*	C45*	C46*	C47
–0.2	1.3	–1.0	–0.5	1.6	–1.2	1.9

Angles (deg) between different planes
A/B 34.0; A/C 20.1; B/C 51.4

Table 8.3.2 Atomic Coordinates, Equivalent Isotropic Displacement Parameters, and Anisotropic Displacement Parameters with Estimated Standard deviations in Parentheses for [(1-amido-3-imido-1,3-diphenyl-2$\lambda^3\sigma^2$-phospha-1-propene-*N*,*N*′)bis(η^5-pentamethylcyclopentadienyl)zirconium] (**II**)

Solvate (**II**·C_7H_8)$_{Tol}$

Atom	X/a·10^4	Y/b·10^4	Z/c·10^4	U(eq)	U11	U22	U33	U23	U13	U12	Occu. Factor
Zr	5000	9087(1)	7500	12(1)	13(1)	8(1)	16(1)	0	4(1)	0	0.5
P	5000	12763(1)	7500	22(1)	34(1)	10(1)	22(1)	0	–1(1)	0	0.5
N(1)	4514(1)	10543(2)	8012(1)	26(1)	19(1)	14(1)	42(1)	–4(1)	–8(1)	2(1)	
C(1)	4532(1)	11735(2)	8041(1)	17(1)	17(1)	16(1)	19(1)	0(1)	–1(1)	–1(1)	
C(11)	4085(1)	12381(2)	8545(1)	17(1)	17(1)	16(1)	18(1)	3(1)	0(1)	1(1)	
C(12)	3359(1)	11878(2)	8726(1)	29(1)	34(1)	35(1)	19(1)	–3(1)	5(1)	–17(1)	
C(13)	2908(1)	12491(2)	9160(1)	33(1)	26(1)	53(1)	20(1)	2(1)	7(1)	–15(1)	
C(14)	3182(1)	13609(2)	9430(1)	27(1)	27(1)	33(1)	23(1)	7(1)	9(1)	9(1)	
C(15)	3909(1)	14111(2)	9270(1)	30(1)	36(1)	17(1)	41(1)	–2(1)	18(1)	1(1)	
C(16)	4358(1)	13509(2)	8828(1)	26(1)	24(1)	17(1)	41(1)	–4(1)	14(1)	–2(1)	
C(21)	4168(1)	8922(2)	6294(1)	17(1)	17(1)	18(1)	17(1)	–1(1)	1(1)	–4(1)	
C(22)	3610(1)	9390(2)	6711(1)	17(1)	14(1)	15(1)	20(1)	–2(1)	0(1)	–1(1)	
C(23)	3479(1)	8457(2)	7183(1)	16(1)	13(1)	15(1)	22(1)	–4(1)	4(1)	–3(1)	
C(24)	3946(1)	7405(2)	7052(1)	17(1)	15(1)	13(1)	23(1)	–4(1)	5(1)	–3(1)	
C(25)	4388(1)	7701(2)	6508(1)	18(1)	15(1)	16(1)	23(1)	–6(1)	6(1)	–2(1)	
C(31)	4426(1)	9531(2)	5684(1)	27(1)	30(1)	32(1)	20(1)	3(1)	5(1)	–5(1)	
C(32)	3197(1)	10624(2)	6643(1)	23(1)	20(1)	18(1)	30(1)	–1(1)	–3(1)	3(1)	
C(33)	2873(1)	8519(2)	7684(1)	23(1)	18(1)	22(1)	31(1)	–7(1)	11(1)	–3(1)	
C(34)	3846(1)	6148(2)	7337(1)	24(1)	23(1)	14(1)	37(1)	–1(1)	8(1)	–4(1)	
C(35)	4885(1)	6838(2)	6136(1)	26(1)	25(1)	26(1)	30(1)	–12(1)	11(1)	1(1)	
C(41)	2814(3)	6821(5)	10361(2)	22(1)	28(2)	23(3)	18(2)	–10(2)	9(2)	–7(2)	0.5
C(42)	1941(4)	6995(7)	10254(4)	27(1)	21(3)	30(5)	31(5)	–10(3)	5(3)	–1(3)	0.5
C(43)	1530(5)	7864(7)	9804(4)	46(2)	59(4)	40(4)	31(4)	–11(3)	–12(3)	23(3)	0.5
C(44)	2010(5)	8626(7)	9427(3)	46(2)	78(5)	30(4)	26(3)	–5(3)	–1(3)	1(3)	0.5
C(45)	2901(6)	8453(7)	9535(4)	47(2)	86(6)	29(4)	25(3)	–3(2)	4(3)	–14(4)	0.5
C(46)	3286(5)	7564(7)	9991(4)	28(1)	31(4)	31(5)	23(4)	–10(3)	8(3)	–7(3)	0.5
C(47)	3233(3)	5894(4)	10863(2)	26(1)	31(2)	26(2)	20(2)	5(2)	1(2)	5(2)	0.5

Atom	X/a·10^4	Y/b·10^4	Z/c·10^4	U(eq)	Atom	X/a·10^4	Y/b·10^4	Z/c·10^4	U(eq)
H12	3173	11118	8552	35	H33A	3061	7987	8062	27
H13	2420	12146	9269	40	H33B	2845	9346	7844	27
H14	2878	14024	9718	33	H33C	2328	8265	7465	27
H15	4101	14858	9459	36	H34A	4347	5681	7325	29
H16	4844	13861	8720	31	H34B	3749	6218	7800	29
H31A	4394	10405	5732	32	H34C	3379	5742	7070	29
H31B	4990	9300	5648	32	H35A	5429	7182	6120	32
H31C	4057	9278	5281	32	H35B	4947	6065	6370	32
H32A	3020	10842	7066	28	H35C	4597	6716	5680	32
H32B	3587	11224	6530	28					
H32C	2718	10595	6289	28					

Table 8.3.3 Atomic Coordinates, Equivalent Isotropic Displacement Parameters, and Anisotropic Displacement Parameters with Estimated Standard deviations in Parentheses for [(1-amido-3-imido-1,3-diphenyl-2$\lambda^3\sigma^2$-phospha-1-propene-*N*,*N′*)bis(η^5-pentamethylcyclopentadienyl)zirconium] (**II**)

Solvate (**II**·C_7H_8)$_{Hex.}$

Atom	X/a·10^4	Y/b·10^4	Z/c·10^4	U(eq)	U11	U22	U33	U23	U13	U12	Occu. Factor
Zr	5000	9076(1)	7500	13(1)	14(1)	9(1)	18(1)	0	4(1)	0	0.5
P	5000	12751(1)	7500	25(1)	38(1)	12(1)	24(1)	0	1(1)	0	0.5
N1	4513(1)	10533(2)	8010(1)	28(1)	20(1)	16(1)	43(1)	–2(1)	–8(1)	2(1)	
C1	4534(1)	11727(2)	8039(1)	19(1)	19(1)	16(1)	21(1)	–1(1)	–1(1)	0(1)	
C11	4086(1)	12367(2)	8547(1)	19(1)	19(1)	19(1)	19(1)	4(1)	–1(1)	2(1)	
C12	4360(2)	13490(2)	8830(1)	29(1)	27(1)	18(1)	43(2)	–4(1)	15(1)	–2(1)	
C13	3913(2)	14093(2)	9271(1)	34(1)	42(1)	19(1)	44(1)	–3(1)	19(1)	1(1)	
C14	3187(2)	13597(2)	9432(1)	30(1)	29(1)	35(1)	26(1)	6(1)	9(1)	12(1)	
C15	2910(2)	12485(3)	9160(1)	35(1)	29(1)	56(2)	21(1)	3(1)	7(1)	–11(1)	
C16	3356(2)	11876(2)	8724(1)	32(1)	37(1)	36(1)	22(1)	–2(1)	4(1)	–17(1)	
C21	4172(1)	8910(2)	6297(1)	20(1)	19(1)	21(1)	21(1)	–2(1)	1(1)	–4(1)	
C22	3613(1)	9379(2)	6715(1)	18(1)	16(1)	15(1)	23(1)	–3(1)	0(1)	–1(1)	
C23	3481(1)	8442(2)	7186(1)	18(1)	14(1)	15(1)	25(1)	–5(1)	3(1)	–3(1)	
C24	3951(1)	7395(2)	7053(1)	19(1)	16(1)	14(1)	27(1)	–3(1)	5(1)	–3(1)	
C25	4391(1)	7694(2)	6509(1)	19(1)	17(1)	17(1)	24(1)	–6(1)	4(1)	–2(1)	
C31	4427(2)	9525(3)	5688(1)	30(1)	32(1)	34(1)	24(1)	3(1)	6(1)	–6(1)	
C32	3197(2)	10608(2)	6647(1)	26(1)	21(1)	21(1)	32(1)	0(1)	–4(1)	5(1)	
C33	2877(1)	8503(2)	7686(1)	24(1)	19(1)	22(1)	32(1)	–7(1)	11(1)	–3(1)	
C34	3848(2)	6141(2)	7340(1)	26(1)	23(1)	14(1)	42(2)	–1(1)	8(1)	–4(1)	
C35	4888(2)	6836(2)	6138(1)	30(1)	27(1)	29(1)	35(2)	–12(1)	11(1)	0(1)	
C41	2802(3)	6844(5)	10352(3)	33(1)	28(2)	23(3)	18(2)	–10(2)	9(2)	–7(2)	0.5
C42	1947(4)	7001(6)	10259(3)	31(1)	21(3)	30(5)	31(5)	–10(3)	5(3)	–1(3)	0.5
C43	1544(4)	7862(6)	9804(3)	42(1)	59(4)	40(4)	31(4)	–11(3)	–12(3)	23(3)	0.5
C44	2012(4)	8593(7)	9448(4)	49(2)	78(5)	30(4)	26(3)	–5(3)	–1(3)	1(3)	0.5
C45	2861(4)	8473(7)	9542(4)	52(2)	86(6)	29(4)	25(3)	–3(2)	4(3)	–14(4)	0.5
C46	3260(4)	7601(6)	9975(3)	35(1)	31(4)	31(5)	23(4)	–10(3)	8(3)	–7(3)	0.5
C47	3230(3)	5898(5)	10853(3)	34(1)	31(2)	26(2)	20(2)	5(2)	1(2)	5(2)	0.5
Za	3922	8364	6752	40							
Zb	6079	8364	8249	40							

Atom	X/a·10^4	Y/b·10^4	Z/c·10^4	U(eq)	Atom	X/a·10^4	Y/b·10^4	Z/c·10^4	U(eq)
H(1)	4200(30)	10320(50)	8370(30)	33	H(42)	1664	6454	10525	38
H(12)	4834(16)	13850(20)	8713(13)	27(7)	H(43)	944	7885	9767	51
H(13)	4090(16)	14830(30)	9483(14)	45(8)	H(44)	1731	9170	9126	59
H(14)	2861(17)	14040(20)	9699(14)	39(8)	H(45)	3177	9068	9331	62
H(15)	2365(18)	12120(20)	9259(14)	48(8)	H(46)	3851	7494	9978	43
H(16)	3155(17)	11130(20)	8520(14)	41(8)	H(471)	3825	5928	10857	50
H(311)	4367(16)	10390(30)	5728(13)	40(7)	H(472)	3108	6073	11300	50
H(312)	4055(18)	9260(20)	5263(15)	43(8)	H(473)	3025	5096	10715	50
H(313)	4957(18)	9340(20)	5644(14)	41(8)	H(341)	4310(17)	5620(20)	7316(13)	7(7)
H(321)	3036(17)	10880(20)	7032(15)	40(8)	H(342)	3767(17)	6150(20)	7809(15)	6(7)

H(322)	2700(20)	10610(30)	6339(16)	56(9)	H(343)	3394(18)	5730(20)	7110(15)	44(8)
H(323)	3566(18)	11220(30)	6523(14)	46(8)	H(351)	5444(16)	7120(20)	6101(13)	32(7)
H(331)	2846(16)	9310(20)	7843(13)	35(7)	H(352)	4610(18)	6720(30)	5695(15)	48(8)
H(332)	3066(16)	7930(20)	8090(13)	36(7)	H(353)	4959(18)	6030(30)	6356(15)	46(8)
H(333)	2333(16)	8270(20)	7478(12)	34(7)					

8.4 **[**(1-amido-3-imido-1,3-diphenyl-2$\lambda^3\sigma^2$-phospha-1-propene-*N*,*N*′)bis(η^5-pentamethylcyclopentadienyl)zirconium]–*n*-hexane (2 / 2 x 0.5) (≙ **2II**· ***n*-C_6H_{14}**)

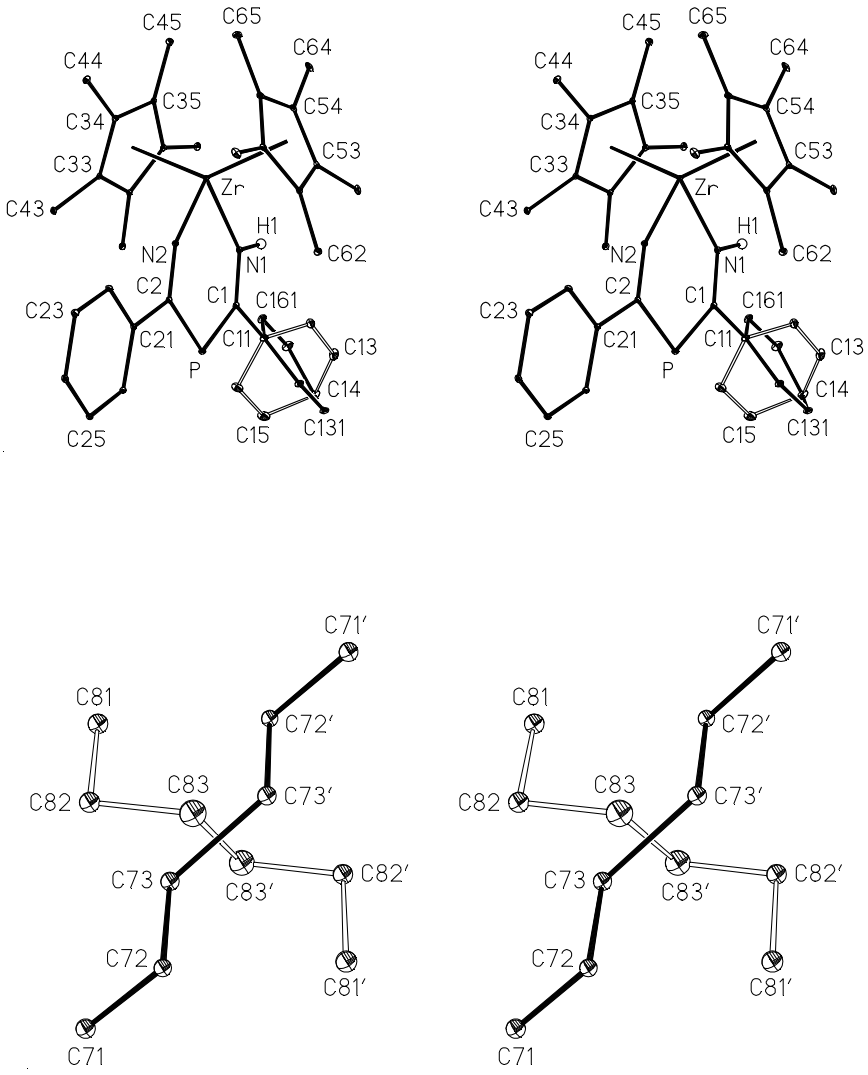

Figure 8.4.1 Disordered solvent molecule. Displacement ellipsoids are of 2% probability.

Table 8.4.1 Bond lengths (pm) and bond angles (deg), characteristic torsion angles, intramolecular and intermolecular contacts as well as least-squares planes and angles between these planes for **[**(1-amido-3-imido-1,3-diphenyl-2$\lambda^3\sigma^2$-phospha-1-propene-*N*,*N*′)bis(η^5-pentamethylcyclopentadienyl)zirconium]–*n*-hexane (2 / 2 x 0.5) (≙ **2II· *n*-C_6H_{14})**
Well known parameters of the phenyl substituents and the η^5-pentamethylcyclopentadienyl ligands as well as the *n*-hexane molecule are also included in detail in order to demonstrate the high quality of the data sets.
M_{Cp3}, M_{Cp5} : centres of the η^5-pentamethylcyclopentadienyl ligands; C73' and C83' : symmetry operation (–x, –y+2, –z).

a) Bond lengths

chelate ligand at zirconium

	n = 1	*n* = 2				
Zr–N*n*	221.2(2)	199.6(2)	N1–H1	0.92	Zr···M_{Cp3}	224.7
N*n*–C*n*	131.9(3)	128.1(3)	C1···C2	282.5(2)	Zr···M_{Cp5}	224.3
P–C*n*	176.9(2)	183.5(2)	N1···N2	275.6(2)		
C*n*–C*n*1	150.5(3)	150.2(3)				

phenyl substituents (*n* = 1: atoms partially disordered[a)])

	n = 2[c)]	*n* = 1[d)]		*n* = 1[d)]
C*n*1–C*n*2	139.3(3)	132.8(6)	C*n*1–C*n*21	139.5(5)
C*n*1–C*n*6	140.0(3)	145.7(7)	C*n*1–C*n*61	140.3(5)
C*n*2–C*n*3	138.6(3)	138.7(8)	C*n*21–C*n*31	139.4(6)
C*n*3–C*n*4	138.3(3)	123.2(7)	C*n*31–C*n*4	132.4(6)
C*n*4–C*n*5	138.4(3)	147.6(8)	C*n*4–C*n*51	143.5(7)
C*n*5–C*n*6	138.7(3)	138.2(8)	C*n*51–C*n*61	138.3(7)

η^5-pentamethylcyclopentadienyl ligands

	n = 3	*n* = 5		*n* = 3	*n* = 5
C*n*1–C*n*2	142.6(3)	141.5(3)	C*n*1–C(*n*+1)1	150.5(3)	150.1(3)
C*n*1–C*n*5	142.1(3)	141.7(3)	C*n*2–C(*n*+1)2	149.9(3)	149.7(3)
C*n*2–C*n*3	140.8(3)	142.2(3)	C*n*3–C(*n*+1)3	150.2(3)	149.9(3)
C*n*3–C*n*4	142.2(3)	141.1(3)	C*n*4–C(*n*+1)4	150.2(3)	150.8(3)
C*n*4–C*n*5	142.4(3)	141.6(3)	C*n*5–C(*n*+1)5	149.6(3)	150.2(3)

Solvent molecule *n*-hexane (disordered[b)])

	n = 7[e)]	*n* = 8[f)]		*n* = 7[e)]	*n* = 8[f)]
C*n*1–C*n*2	143(1)	148(2)	C*n*3–C*n*3'	171(3)	165(5)
C*n*2–C*n*3	141(1)	137(2)			

occupancy factor for [a)] C121, C131, C151, C161 *0.524(4)* and for C12, C13, C15, C16 *0.476(4),* [b)] for C71, C72, C73 *0.587(6)* and for C81, C82, C83 *0.413(6)*; mean C–C bond lengths for [c)] *n* = 2: 138.9; [d)] *n* = 1: 137.7 and 138.9; [e)] *n* = 7: 152; [f)] *n* = 8: 150

d) Bond angles

chelate ligand at zirconium

	n = 1	*n* = 2		*n* = 1	*n* = 2
M_{Cp3}···Zr···M_{Cp5}	139.2	—	N*n*–C*n*–P	131.1(2)	122.5(2)
N*n*–Zr···M_{Cp3}	104.0	106.4	N*n*–C*n*–C*n*1	116.9(2)	120.9(2)
N*n*–Zr···M_{Cp5}	103.8	106.7	P–C*n*–C*n*1	112.0(2)	116.6(2)
N1–Zr–N2	81.7(2)	—	C*n*1–P–C2	103.2(1)	—
Zr–N*n*–C*n*	133.0(2)	148.5(2)			

phenyl substituents (n = 1: atoms partially disordered[a)])				
	n = 2[a)]	n = 1[b)]		n = 1[b)]
Cn–Cn1–Cn2	119.6(2)	124.2(3)	Cn–Cn1–Cn21	120.9(3)
Cn–Cn1–Cn6	121.9(2)	119.2(3)	Cn–Cn1–Cn61	120.5(3)
Cn2–Cn1–Cn6	118.5(2)	116.6(4)	Cn21–Cn1–Cn61	117.8(3)
Cn1–Cn2–Cn3	120.8(2)	123.0(6)	Cn1–Cn21–Cn31	120.3(4)
Cn2–Cn3–Cn4	120.2(2)	123.5(6)	Cn21–Cn31–Cn4	121.6(5)
Cn3–Cn4–Cn5	119.7(2)	119.4(4)	Cn31–Cn4–Cn51	119.3(4)
Cn4–Cn5–Cn6	120.3(2)	118.3(6)	Cn4–Cn51–Cn61	118.6(5)
Cn5–Cn6–Cn1	120.5(2)	119.1(6)	Cn51–Cn61–Cn1	120.9(5)
η^5-pentamethylcyclopentadienyl ligands				
	n = 3[c)h)]	n = 5[d)i)]		n = 3[e)h)] n = 5[f)i)]
Cn5–Cn1–Cn2	107.9(2)	108.4(2)	Cn1–Cn2–C(n+1)2	126.6(2) 126.5(2)
Cn1–Cn2–Cn3	108.1(2)	107.4(2)	Cn3–Cn2–C(n+1)2	125.2(2) 126.0(2)
Cn2–Cn3–Cn4	108.4(2)	108.3(2)	Cn2–Cn3–C(n+1)3	126.0(2) 126.8(2)
Cn3–Cn4–Cn5	107.7(2)	108.1(2)	Cn4–Cn3–C(n+1)3	125.4(2) 124.5(2)
Cn4–Cn5–Cn1	107.8(2)	107.7(2)	Cn3–Cn4–C(n+1)4	125.1(2) 123.8(2)
			Cn5–Cn4–C(n+1)4	126.5(2) 127.3(2)
Cn2–Cn1–C(n+1)1	126.3(2)	125.9(2)	Cn4–Cn5–C(n+1)5	125.3(2) 127.1(2)
Cn5–Cn1–C(n+1)1	125.5(2)	125.9(2)	Cn1–Cn5–C(n+1)5	125.7(2) 123.8(2)
solvent molecule *n*-hexane (disordered)				
	n = 7[g)]	n = 8[g)]		n = 7 n = 8
Cn1–Cn2–Cn3	103(1)	99(2)	Cn4–Cn5–Cn1	116(1) 105(3)

mean C–C–C bond angles for [a)] n = 2: 120.2 ; [b)] n = 1: 120.4 and 120.0; [c)] n = 3: 108.0; n = 5: 108.0; C–C–CH_3 for [e)] n = 3: 125.8; [f)] n = 5: 125.7; [g)] n = 7: 110; n = 8: 102; sum of angles at Cnm for [h)] n = 3, m = 1: 359.7; 2: 359.9; 3: 359.8; 4: 359.3; 5: 358.8; [i)] n = 5 , m = 1: 359.7; 2: 359.9; 3: 359.6; 4: 359.2; 5: 358.6

c) Characteristic torsion angles[j)]

C2–P–C1–N1	–0.4	N1–Zr–N2–C2	–3.2	P–C1–C11–C16	37.8
P–C1–N1–Zr	0.3	Zr–N2–C2–P	3.7	P–C1–C11–C161	141.9
C1–N1–Zr–N2	0.7	N2–C2–P–C1	–0.9	P–C2–C21–C26	–4.9
				C1–N1–Zr···M_{Cp3}	–104.2

[j)] The torsion angle A–B–C–D is defined as positive if, when viewed along the B–C bond, atom A must be rotated clockwise to eclipse atom D [64 and 47].

d) Characteristic least-squares planes and deviations (pm) from these planes
Atoms defining a least-squares plane are marked with an asterisk (*).

A_1: *Chelate heterocycle*												
P*	C1*	N1*	C2*	N2*	Zr*	C11	C14	C16	C21	C24	C26	M_{Cp3}	M_{Cp5}
–0.5	0.5	0.2	–0.7	1.5	–0.9	1.7	9.3	–76.1	–0.2	9.5	–9.8	–212.9	207.9

A_2: *Chelate heterocycle*												
C1*	N1*	C2*	N2*	P	Zr	C11	C14	C16	C21	C24	C26	M_{Cp3}	M_{Cp5}
0.6	–0.6	–0.6	0.7	0.5	–2.9	2.4	11.1	–74.4	0.3	10.8	– 8.2	–215.3	205.4

B_1: *Phenyl substituent* (*n* = 1; disordered)								
C11*	C12*	C13*	C14*	C15*	C16*	C1	N1	P
1.9	–1.3	0.2	0.1	0.7	–1.7	5.5	–64.0	105.9

B_{11} : *Phenyl substituent* (*n* = 1; disordered)								
C11*	C121*	C131*	C14*	C151*	C161*	C1	N1	P
–6.1	3.2	3.9	–7.8	4.6	2.1	–3.2	7.7	–113.1

B_2: *Phenyl substituent* (*n* = 2)								
C21*	C22*	C23*	C24*	C25*	C26*	C2	N2	P
0.9	–0.7	–0.1	0.7	–0.5	–0.3	5.4	–0.2	23.4

C_1: η^5-Pentamethylcyclopentadienyl ligand (*n* = 3)										
C31*	C32*	C33*	C34*	C35*	C41	C42	C43	C44	C45	Zr
–1.7	0.8	0.4	–1.4	1.9	5.7	11.8	12.2	12.6	33.4	–224.7

C_2: η^5-Pentamethylcyclopentadienyl ligand (*n* = 5)										
C51*	C52*	C53*	C54*	C55*	C61	C62	C63	C64	C65	Zr
–3.6	–1.1	1.4	1.6	–1.2	3.0	5.0	18.9	24.8	26.0	224.9

Angles (°) between least-squares planes:
A_2/B_1 36.9; A_2/B_{11} 42.9; B_1/B_{11} 79.7; A_2/B_2 5.3; A_1/C_1 19.7; A_1/C_2 21.0; C_1/C_2 40.3

e) Intramolecular and intermolecular contacts shorter than the sum of corresponding van der waals radii (N 160, C 170, P 180 pm)

Intramolecular			
C12···N1	294	C22···N2	285	C16···P	305	C26···P	310

Intermolecular					
C15···C121	(1–x; 1–y; –z)[a]	331	C71···C121	(1–x; 2–y; z)	326
C25···C51	(x; y–1; z)	331	C81···C16	(x; y+1; z)	281
C25···C32	(1+x; y; z)	332	C81···C15	(x; y+1; z)	329
C71···C13	(x; y; z)	293	C82···C15	(x; y+1; z)	258[b]
C71···C12	(x; y; z)	309	C82···C16	(x; y+1; z)	270

[a] Symmetry operation to create the second atom. [b] The very short H821···H15 contact (124.2 pm) is considered to be not realistic because of highly uncertain carbon positions of the disordered solvent molecule

a)

b)

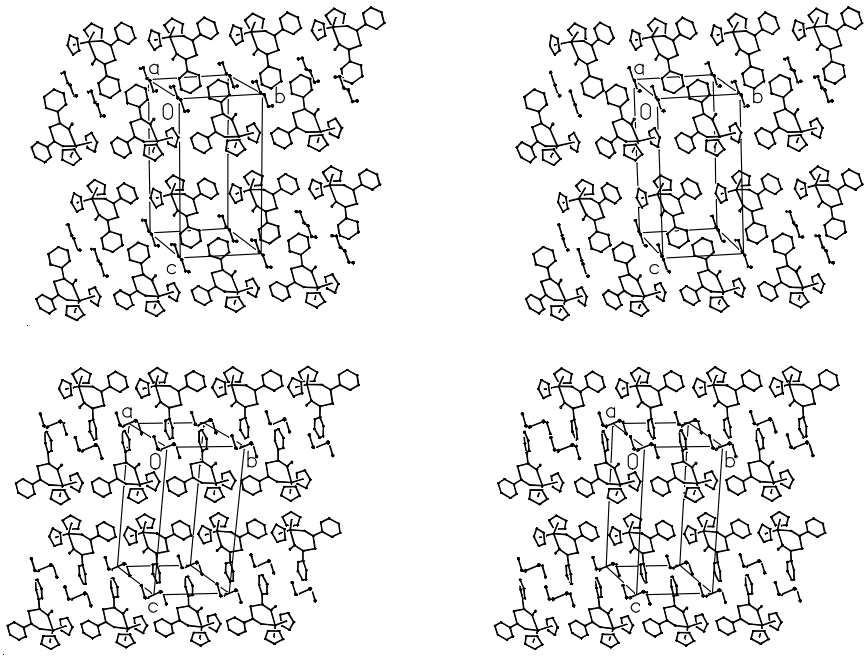

Figure 8.4.2 Structure of the solid state adduct (**2II**·***n*-C$_6$H$_{14}$**)** in detail
In contrast to **Figure 3.10** only one position of the disordered phenyl substituent and the disordered centrosymmetric *n*-hexane molecule are depicted:
a) *n*-hexane molecule C7*n* (*n* = 1→ 3) and phenyl substituent C1*m* (*m* = 1→ 6)
b) *n*-hexane molecule C8*n* (*n* = 1→ 3) and phenyl substituent C1*m*/C1*m**1 (*m* = 1, 4; m* = 2, 3, 5, 6)

Table 8.4.2 Comparison between characteristic molecular data obtained from different structure determinations of **[***N,N′*-(1-amido-3-imido-1,3-diphenyl-2$\lambda^3\sigma^2$-phospha-1-propene)bis(η^5-pentamethylcyclopentadienyl)zirconium] (**II**)
Because of space group symmetry in the solid state adduct (**II**·C$_7$H$_8$**)** the chelate ligand has a twofold axis and is found to be disordered.

	(**2II**·***n*-C$_6$H$_{14}$**)**	mean	(**II**· C$_7$H$_8$)$_{Hex}$ / (**II**·C$_7$H$_8$)$_{Tol}$	mean
Zr–N1	221.2	**210.4**	210.2 / 210.4	**210.3**
Zr–N2	199.6			
N1–C1	131.9	**130.0**	130.3 / 130.2	**130.3**
N2–C2	128.1			
P–C1	176.9	**180.2**	179.3 / 180.1	**179.7**
P–C2	183.5			
C1–C11	150.5	**150.4**	150.2 / 150.1	**150.2**
C2–C21	150.2			
Zr···M$_{Cp3}$	224.7	**224.5**	224.5 / 224.9[a)]	**224.7**
Zr···M$_{Cp5}$	224.3			
N1–Zr–N2	81.7	**81.7**	81.8 / 82.0	**81.9**

Zr–N1–C1	133.0	**140.8**	140.1 / 140.1	**140.1**
Zr–N2–C2	148.5			
N1–C1–P	131.1	**126.8**	127.3 / 127.2	**127.3**
N2–C2–P	122.5			
N1–C1–C11	116.9	**118.9**	118.8 / 119.2	**119.0**
N2–C2–C21	120.9			
P–C1–C11	112.0	**114.3**	113.8 / 113.5	**113.7**
P–C2–C21	116.6			
C1–P–C2	103.2	**103.2**	102.9 / 103.0[b)]	**103.0**

Table 8.4.3 Atomic Coordinates, Equivalent Isotropic Displacement Parameters, and Anisotropic Displacement Parameters with Estimated Standard deviations in Parentheses for [(1-amido-3-imido-1,3-diphenyl-2$\lambda^3\sigma^2$-phospha-1-propene-*N*,*N′*)bis(η^5-pentamethylcyclopentadienyl)zirconium] (**II**)

Solvate (**2II**·***n*-C$_6$H$_{14}$**)

Atom	X/a·10^4	Y/b·10^4	Z/c·10^4	U(eq)	U11	U22	U33	U23	U13	U12	Occu. Factor
Zr	2601(1)	8257(1)	2914(1)	14(1)	13(1)	14(1)	15(1)	0(1)	1(1)	6(1)	
P	4428(1)	5677(1)	1903(1)	23(1)	29(1)	25(1)	20(1)	−1(1)	3(1)	15(1)	
N(1)	2674(2)	7455(2)	1835(1)	19(1)	19(1)	20(1)	17(1)	2(1)	1(1)	5(1)	
N(2)	3892(2)	7079(2)	3074(1)	18(1)	17(1)	19(1)	20(1)	1(1)	1(1)	8(1)	
C(1)	3318(2)	6594(2)	1545(1)	21(1)	17(1)	22(1)	20(1)	1(1)	2(1)	4(1)	
C(2)	4523(2)	6213(2)	2827(1)	18(1)	16(1)	17(1)	20(1)	2(1)	3(1)	6(1)	
C(11)	3105(3)	6306(3)	775(1)	27(1)	26(1)	36(1)	19(1)	−4(1)	−1(1)	12(1)	
C(12)	3056(8)	7317(7)	344(3)	46(2)	69(5)	38(3)	25(3)	−2(2)	−2(3)	16(3)	0.48
C(13)	2913(9)	7037(8)	−366(3)	57(2)	76(5)	63(5)	21(3)	5(3)	−5(3)	14(4)	0.48
C(14)	2765(4)	5816(4)	−656(2)	55(1)	53(2)	83(3)	19(1)	−13(2)	−3(1)	18(2)	
C(15)	2766(1)	4575(9)	−239(3)	70(3)	112(7)	70(5)	37(4)	−22(4)	−9(4)	48(5)	0.48
C(16)	2899(9)	4821(8)	469(3)	56(2)	93(6)	55(4)	30(3)	−11(3)	−13(3)	41(4)	0.48
C(121)	4325(6)	6462(6)	366(2)	34(1)	42(3)	51(3)	19(2)	3(2)	5(2)	29(3)	0.52
C(131)	4116(6)	6229(6)	−348(3)	39(1)	52(3)	55(4)	25(3)	2(2)	10(2)	35(3)	0.52
C(151)	1535(7)	5885(8)	−268(3)	51(1)	44(3)	81(5)	26(3)	−7(3)	−10(2)	22(3)	0.52
C(161)	1722(6)	6096(6)	442(3)	38(1)	31(3)	55(3)	25(3)	0(2)	0(2)	13(2)	0.52
C(21)	5418(2)	5614(2)	3285(1)	17(1)	15(1)	15(1)	22(1)	3(1)	4(1)	5(1)	
C(22)	5649(2)	6082(2)	3982(1)	22(1)	24(1)	18(1)	26(1)	0(1)	3(1)	11(1)	
C(23)	6516(3)	5589(3)	4412(1)	24(1)	28(1)	25(1)	21(1)	0(1)	−1(1)	11(1)	
C(24)	7153(3)	4607(3)	4154(1)	23(1)	21(1)	22(1)	30(1)	7(1)	1(1)	10(1)	
C(25)	6909(2)	4106(2)	3466(1)	22(1)	19(1)	17(1)	33(1)	4(1)	8(1)	9(1)	
C(26)	6050(2)	460(2)	3032(1)	20(1)	19(1)	18(1)	22(1)	1(1)	4(1)	7(1)	
C(31)	−232(2)	7127(2)	2705(1)	19(1)	11(1)	22(1)	22(1)	4(1)	1(1)	4(1)	
C(32)	205(2)	5877(2)	2778(1)	18(1)	13(1)	19(1)	20(1)	2(1)	3(1)	3(1)	

C(33)	760(2)	5951(2)	3461(1)	18(1)	15(1)	19(1)	19(1)	5(1)	4(1)	6(1)	
C(34)	665(2)	7238(2)	3820(1)	19(1)	17(1)	22(1)	18(1)	2(1)	3(1)	7(1)	
C(35)	2(2)	7937(2)	3356(1)	19(1)	13(1)	19(1)	24(1)	7(1)	4(1)	6(1)	
C(41)	−967(3)	7448(3)	2074(1)	27(1)	22(1)	33(1)	26(1)	7(1)	−4(1)	8(1)	
C(42)	15(3)	44631(3)	2244(1)	27(1)	27(1)	22(1)	27(1)	−2(1)	5(1)	2(1)	
C(43)	1241(3)	4800(3)	3776(1)	26(1)	27(1)	24(1)	29(1)	11(1)	4(1)	12(1)	
C(44)	986(3)	7626(3)	4579(1)	29(1)	33(1)	35(1)	19(1)	1(1)	3(1)	12(1)	
C(45)	−634(3)	9094(3)	3559(1)	29(1)	22(1)	28(1)	39(1)	5(1)	7(1)	13(1)	
C(51)	4864(2)	10451(2)	3417(1)	21(2)	20(1)	13(1)	25(1)	−2(1)	−4(1)	3(1)	
C(52)	5113(2)	10333(2)	2706(1)	20(1)	17(1)	13(1)	28(1)	1(1)	0(1)	3(1)	
C(53)	4010(2)	10703(2)	2343(1)	22(1)	24(1)	14(1)	25(1)	4(1)	−1(1)	5(1)	
C(54)	3103(2)	11056(2)	2827(1)	23(1)	20(1)	13(1)	36(1)	1(1)	−2(1)	7(1)	
C(55)	3629(2)	10906(2)	3494(1)	23(1)	22(1)	16(1)	28(1)	−5(1)	1(1)	4(1)	
C(61)	582(2)	10268(3)	3996(1)	34(1)	36(1)	26(1)	37(1)	−2(1)	−17(1)	9(1)	
C(62)	6355(3)	9966(3)	2393(2)	31(1)	20(1)	28(1)	46(1)	2(1)	11(1)	7(1)	
C(63)	3923(3)	10890(3)	1585(1)	36(1)	48(1)	25(1)	29(1)	11(1)	−2(1)	6(1)	
C(64)	1961(3)	11728(3)	2648(2)	37(1)	28(1)	19(1)	68(1)	8(1)	−3(1)	12(1)	
C(65)	3232(3)	11462(2)	4168(1)	38(1)	36(1)	28(1)	42(1)	−14(1)	7(1)	4(1)	
C(71)	3100(1)	10155(1)	−348(6)	145(5)							0.59
C(72)	1610(1)	9970(1)	−579(5)	115(3)							0.59
C(73)	945(1)	10193(2)	35(6)	135(4)							0.59
C(81)	640(2)	12080(2)	781(8)	152(7)							0.41
C(82)	1290(2)	11880(2)	118(1)	147(7)							0.41
C(83)	50(3)	10760(3)	−190(2)	232(1)							0.41

Atom	X/a·10^4	Y/b·10^4	Z/c·10^4	U(eq)	Atom	X/a·10^4	Y/b·10^4	Z/c·10^4	U(eq)
H(1)	2200(3)	7740(3)	1488(1)	32(7)	H(611)	6561	11259	4163	51
H(12)	3122	8274	530	55	H(612)	6365	9635	3830	51
H(13)	2929	7829	−643	68	H(613)	5193	9792	4371	51
H(14)	2610	5478	−1129	66	H(621)	7246	10893	2368	47
H(15)	2677	3632	−453	84	H(622)	6028	9493	1929	47
H(16)	2858	4032	753	67	H(623)	6603	9272	2679	47
H(22)	5206	6748	4165	26	H(631)	2869	10446	1414	54
H(23)	6673	5927	4885	29	H(632)	4503	10382	1344	54
H(24)	7755	4278	4448	28	H(633)	4340	11964	1501	54
H(26)	5890	4254	2561	23	H(641)	2479	12734	2483	56
H(121)	5303	6729	575	41	H(642)	1412	11804	3058	56
H(131)	4963	6370	−620	47	H(643)	1251	11084	2286	56
H(151)	612	5788	−493	61	H(651)	3226	10770	4523	56
H(161)	903	6099	707	46	H(652)	2232	11509	4120	56
H(411)	−605	7088	1661	41	H(653)	3978	12467	4303	56
H(412)	−713	8535	2065	41	H(711)	3658	9997	−740	217
H(413)	−2062	6930	2085	41	H(712)	3043	9419	−8	217
H(421)	867	4309	2286	41	H(713)	3620	11175	−136	217
H(422)	−23	4991	1784	41	H(721)	1633	10726	−910	137
H(423)	−924	3778	2312	41	H(722)	1060	8949	−798	137
H(431)	350	3951	3901	38	H(731)	1464	11255	211	162
H(432)	1887	5256	4189	38	H(732)	1124	9554	382	162
H(433)	1802	4440	3443	38	H(811)	1431	12793	1094	228
H(441)	230	6866	4834	44	H(812)	205	11112	988	228

H(442)	947	8616	4693	44	H(813)	−152	12480	701	228
H(443)	1990	7650	4705	44	H(821)	1608	12806	−140	177
H(451)	−693	9650	3158	43	H(822)	2144	11556	181	177
H(452)	19	9795	3922	43	H(831)	179	10647	−691	278
H(453)	−1645	8596	3730	43	H(832)	−866	10983	−120	278

8.5 [bis(1,2-dimethoxyethane)-1κ^2*O*^{1},*O*^{2};2κ^2*O*^{3},*O*^{4}]{bis[μ-*N*,*N*′-bis(4-methylphenyl)}-*C*-phosph-a nylformamidinato]1:2κ^4*N*^{1}, *N*^{2};1κ^2*N*^{3};*N*^{4}}dilithium **III**.

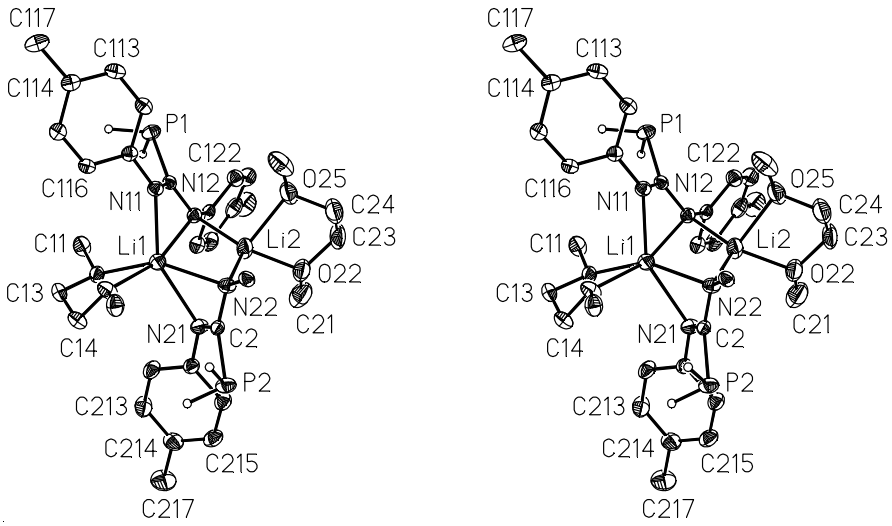

Figure 8.5.1 Non-stereoscopic (a) and stereoscopic view (b) of the complex [bis(1,2-dimethoxyethane)-1κ^2*O*^{1},*O*^{2};2κ^2*O*^{3},*O*^{4}]{bis[μ-*N*,*N*′-bis(4-methylphenyl)}-*C*-phosphanylform-amidinato]-1:2κ^4*N*^{1}, *N*^{2};1κ^2*N*^{3};*N*^{4}}dilithium **III**. Thermal ellipsoids are at 30% probability; except for the PH_2-groups all hydrogen atoms are omitted for clarity. Only the *ipso* carbon of the phenyl group at N22 is shown. Absent atom numbering has to be complemented logically.

Table 8.5.1 Bond lengths (pm) and bond angles (deg), characteristic torsion angles as well as least-squares planes and angles between these planes for [bis(1,2-dimethoxyethane)-1κ^2*O*^{1},*O*^{2};2κ^2*O*^{3},*O*^{4}]{bis[μ-*N*,*N*′-bis(4-methylphenyl)}-*C*-phosphanylform-amidinato]1:2κ^4*N*^{1}, *N*^{2};1κ^2*N*^{3};*N*^{4}}dilithium **III**.

a) Bond lengths

Amidinate ligands

	n = 1	*n* = 2	mean		*m*/*n* = 1	*m*/*n* = 2	mean
P*n*–C*n*	188.9(2)	188.2(2)	188.6	Li1–N11	211.6(5)	—	—
P*n*–H*n*1	134(3)	128(3)	132.0	Li1–N1*m*		232.6(5)	233.2
P*n*–H*n*2	129(2)	138(3)		Li1–N2*m*	231.7(5)	235.2(5)	
C*n*–N*n*1	132.5(3)	131.9(3)	132.8	Li2–N*n*2	201.9(5)	203.7(5)	202.8
C*n*–N*n*2	133.5(3)	133.2(3)			*m* = 2	*m* = 5	
N*n*1–C*n*11	140.5(3)	140.8(3)	140.9	Li1–O1*m*	212.0(5)	222.4(5)	217.2
N*n*2–C*n*21	141.2(3)	140.9(3)		Li2–O2*m*	200.0(5)	208.6(6)	204.3

1,2-Dimethoxyethan-ligands

	n = 1	*n* = 2	mean	Contact with complex skeleton			
C*n*1–O*n*2	142.3(3)	140.7(5)	142.2	Li1···C1	253.6(5)	Li2···N21	262.5(6)
C*n*6–O*n*5	141.0(3)	144.6(4)		Li1···C2	260.3(5)	Li1···Li2	260.7(6)
O*n*2–C*n*3	141.9(3)	145.4(4)	142.1	Li2···C1	294.2(6)	Li2···C121	278.2(5)
O*n*5–C*n*4	141.8(3)	139.2(4)		Li2···C2	266.3(5)		
C*n*3–C*n*4	148.8(4)	148.9(6)	148.9				

4-Methylpheny substituents

	n = 1	*n* = 2		*n* = 1	*n* = 2	mean
C*n*11–C*n*12	139.6(3)	138.2(4)	C*n*21–C*n*22	139.3(4)	139.6(3)	138.9
C*n*11–C*n*16	140.2(3)	140.4(3)	C*n*21–C*n*26	139.3(3)	139.9(3)	
C*n*12–C*n*13	138.6(4)	138.3(4)	C*n*22–C*n*23	138.4(4)	139.1(4)	
C*n*15–C*n*16	137.8(3)	137.5(4)	C*n*25–C*n*26	138.6(4)	137.7(3)	
C*n*13–C*n*14	139.0(4)	139.0(4)	C*n*23–C*n*24	138.2(4)	138.2(4)	
C*n*14–C*n*15	139.4(3)	138.0(4)	C*n*24–C*n*25	138.5(4)	138.7(3)	
C*n*14–C*n*17	151.4(3)	151.9(4)	C*n*24–C*n*27	151.8(4)	150.7(3)	151.5

b) Bond angles

Amidinate-ligands				Coordination at Li1		
	n = 1	*n* = 2	mean			mean
C*n*–P*n*–H*n*1	98.0(1)	94.0(1)	96.0	N11–Li1–N12	61.2(1)	59.3
C*n*–P*n*–H*n*2	98.0(1)	94.0(1)		N21–Li1–N22	57.4(1)	
H*n*1–P*n*–H*n*2	97.0(2)	100.0(2)	99.0	O12–Li1–O15	76.2(2)	—
N*n*1–C*n*–P*n*	122.2(2)	122.2(2)	121.8	N11–Li1–N21	148.6(2)	155.2
N*n*2–C*n*–P*n*	120.6(2)	122.1(2)		N12–Li1–O15	163.4(2)	
N*n*1–C*n*–N*n*2	117.0(2)	115.5(2)	116.3	N22–Li1–O12	153.6(2)	
C*n*–N*n*1–C*n*11	121.2(2)	122.3(2)	121.8	N11–Li1–N22	104.0(2)	—
C*n*–N*n*2–C*n*21	121.4(2)	123.4(2)	122.4	N12–Li1–N22	95.6(2)	—
C*n*–N*n*1–Li1	92.0(2)	86.9(8)	86.8	N12–Li1–N21	93.5(2)	—
C*n*–N*n*2–Li1	83.0(2)	85.1(2)		N11–Li1–O12	102.4(2)	102.7
C*n*11–N*n*1–Li1	139.9(2)	137.4(2)	139.2	N21–Li1–O15	102.9(2)	
C*n*21–N*n*2–Li1	145.5(2)	134.1(2)		N11–Li1–O15	104.0(2)	101.8
C*n*–N*n*2–Li2	121.3(2)	102.4(2)		N21–Li1–O12	99.6(2)	
C*n*21–N*n*2–Li2	107.0(2)	124.9(2)		N12–Li1–O12	98.4(2)	96.9
Li1–N*n*2–Li2	73.4(2)	72.5(2)	73.0	N22–Li1–O15	95.3(2)	

Coordination at Li2						
N12–Li2–N22	117.3(2)	O22–Li2–O25	81.8(2)	N21–Li2–O25	163.9(2)	
N12–Li2–O22	123.5(2)	N12–Li2–O25	101.3(2)	N21–Li2–N12	92.5(2)	
N22–Li2–O22	114.0(2)	N22–Li2–O25	109.7(3)	N21–Li2–N22	55.8(2)	
				N21–Li2–O22	97.5(2)	

p-Tolyl groups	*n* = 1	*n* = 2		*n* = 1	*n* = 2	mean
N*n*1–C*n*11–C*n*12	124.1(2)	119.5(2)[a)]	N*n*2–C*n*21–C*n*22	122.7(2)	124.7(2)	123.8[a]
N*n*11–C*n*1–C*n*16	119.1(2)	123.7(2)[a)]	N*n*2–C*n*21–C*n*26	119.7(2)	117.9(2) 119.1[a)]	
C*n*12–C*n*11–C*n*16	116.8(2)	116.8(2)	C*n*22–C*n*21–C*n*26	117.6(2)	117.2(2)	117.1
C*n*11–C*n*12–C*n*13	121.4(2)	121.3(3)	C*n*21–C*n*22–C*n*23	121.1(3)	120.7(2)	121.1
C*n*11–C*n*16–C*n*15	121.3(2)	121.4(3)	C*n*21–C*n*26–C*n*25	120.7(3)	120.8(2)	
C*n*12–C*n*13–C*n*14	121.4(2)	121.8(3)	C*n*22–C*n*23–C*n*24	121.8(3)	121.9(2)	121.8
C*n*16–C*n*15–C*n*14	121.7(2)	121.7(3)	C*n*26–C*n*25–C*n*24	121.7(3)	122.4(2)	
C*n*13–C*n*14–C*n*15	117.2(2)	116.9(3)	C*n*23–C*n*24–C*n*25	117.0(2)	116.8(2)	117.0
C*n*13–C*n*14–C*n*17	121.4(2)	121.2(3)	C*n*23–C*n*24–C*n*27	121.7(3)	121.8(2)	121.5
C*n*15–C*n*14–C*n*17	121.4(2)	121.9(3)	C*n*25–C*n*24–C*n*27	121.3(3)	121.3(2)	

1,2-Dimethoxyethan-ligands

	n = 1	*n* = 2		*n* = 1	*n* = 2	mean
Li*n*–O*n*2–Cn1	124.1(2)	124.1(2)	Li*n*–O*n*5–Cn6	129.8(2)	120.6(2)	124.7
Li*n*–O*n*2–Cn3	114.4(2)	110.3(3)	Li*n*–O*n*5–Cn4	105.2(2)	105.7(3)	108.9
C*n*1–O*n*2–Cn3	111.4(2)	114.8(3)	C*n*6–O*n*5–Cn4	114.1(2)	112.2(3)	113.1
O*n*2–C*n*3–Cn4	108.5(2)	107.9(3)	O*n*5–C*n*4–Cn3	107.5(2)	107.3(2)	107.8

[a)] mean were calculated using the higher and lower angel each

c) Torsion angles

	n = 1	*n* = 2		*n* = 1	*n* = 2
Li1–N*n*1–C*n*–P*n*	148.4(2)	137.6(2)	O25–Li2–N22–C221	–7.4(4)	—
Li1–N*n*2–C*n*–P*n*	150.9(2)	–138.2(2)	O25–Li2–N12–C1	–58.6(3)	—
N*n*1–C*n*–P*n*–H*n*1	–36.8	–36.8			
N*n*1–C*n*–P*n*–H*n*2	–135.4	137.1	Li*n*–O*n*2–C*n*3–C*n*4	–28.7(3)	33.1(4)
C*n*–N*n*1–C*n*11–C*n*12	167.1(3)	136.8(3)	O*n*2–C*n*3–C*n*4–O*n*5	55.9(3)	–56.3(4)
C*n*–N*n*2–C*n*21–C*n*22	60.3(3)	48.4(3)	C*n*3–C*n*4–O*n*5–Li*n*	–53.7(2)	49.9(3)
Li2–N*n*2–C*n*21–C*n*22	–85.1(3)	–92.2(3)	Cn*4*–On*5*–Li*n*–O*n*2	29.4(2)	–25.3(3)
N11–Li1–N22–C2	–173.9(2)	—	O*n*5–Li*n*–O*n*2–C*n*3	0.1(2)	–5.1(3)
N11–Li1–N22–C221	52.7(3)	—			

b) Characteristic least-squares planes and deviations (pm) from these planes.
Atoms defining a least-square plane are marked with an asterisk (*).

A: *Amidinate-Ligand 1*										
N11*	C1*	N12*	P1	C111	C114	C117	C121	C124	C127	Li1
0.0	0.0	0.0	14.1	–5.9	–3.1	4.1	4.3	18.0	30.4	94.4
B: *Amidinate-Ligand 2*										
N21*	C2*	N22*	P2	N211	N214	N217	N221	N224	N227	Li1
0.0	0.0	0.0	12.5	–10.1	25.0	30.9	2.6	16.4	27.8	142.3
C: *Amidinate 1 as chelating*										
Li1*	N11*	N12*	C1	P1	C111	C121				
0.0	0.0	0.0	34.5	140.2	26.6	35.8				
D: *Amidinate 2 as chelating*										
Li1*	N21*	N22*	C2	P2	C211	C221				
0.0	0.0	0.0	49.1	188.5	34.2	42.5				
E: *Four ring Li2N2-Heterocycles*										
Li1*	N12*	Li2*	N22*	N11	N21	O12	O15	O22	O25	
–6.1	7.7	–9.2	7.6	177.4	–193.4	–99.1	26.5	–113.2	149.7	
F: *1,2-Dimethoxyethan-Chelating 1*										
Li1*	O12*	C13*	O15*	C14	C11	C16	N11	N21	N12	N22
–0.1	0.1	–0.1	0.1	67.4	–71.7	18.1	–202.3	224.1	–64.1	100.2
G: *1,2-Dimethoxyethan-Chelating 2*										
Li2*	O22*	C23*	O25*	C24	C21	C26	N12	N22		
–2.9	0.4	–3.6	0.24	64.4	–57.6	55.4	–173.9	169.8		
H*: p-Tolyl-Substituent 11*										
C111*	C112*	C113*	C114*	C115*	C116*	N11	C117			
–3.0	0.2	0.7	–2.3	1.2	1.4	–7.5	–10.8			
I: *p-Tolyl-Substituent 12*										
C121*	C122*	C123*	C124*	C125*	C126*	N12	C127			
2.5	–1.2	–1.1	2.0	–0.7	–1.5	2.6	9.8			
J: *p-Tolyl-Substituent 21*										
C211*	C212*	C213*	C214*	C215*	C216*	N21	C217			
2.0	-0.6	–1.0	1.2	0.2	–1.8	1.6	2.2			
K: *p-Tolyl-Substituent 22*										
C221*	C222*	C223*	C224*	C 225*	C226*	N22	C227			
0.2	–1.9	-0.1	1.6	–1.0	–1.0	0.3	5.8			
D: Angle between the least-square planes										
C/D 84:7º; C/F 78:7º; D/F 76:9º; C/E 73:5º; D/E 86:8º; E/F 30:6º; E/G 82:9º; A/C 29:8º; B/D 44:0º; C/H 27:9º; C/I 33:5º; D/J 15:4º; D/K 17:0º										

Table 8.5.2 Atomic Coordinates, Equivalent Isotropic Displacement Parameters, and Anisotropic Displacement Parameters with Estimated Standard deviations in Parentheses for [bis(1,2-dimethoxyethane)-1κ^2*O*^{1},*O*^{2};2κ^2*O*^{3},*O*^{4}]{bis[μ-*N*,*N*′-bis(4-methylphenyl)}-*C*-phosphanylformamidinato]1:2κ^4*N*^{1}, *N*^{2};1κ^2*N*^{3};*N*^{4}}dilithium **III**.

Atom	X/a·10^4	Y/b·10^4	Z/c·10^4	U(eq)	U11	U22	U33	U23	U13	U12
P1	8193(1)	657(1)	4055(1)	42(1)	54(1)	34(1)	42(1)	5(1)	–4(1)	–24(1)
C1	8599(2)	1894(2)	3603(1)	31(1)	25(1)	26(1)	39(1)	5(1)	–6(1)	–9(1)
Li2	8054(5)	3582(4)	2333(3)	54(1)	54(3)	38(2)	82(4)	20(2)	–33(3)	–24(2)
P2	10747(1)	5616(1)	1658(1)	44(1)	54(1)	48(1)	42(1)	4(1)	–4(1)	–33(1)
C2	10041(2)	4492(2)	2024(1)	31(1)	33(1)	32(1)	31(1)	6(1)	–10(1)	–14(1)
Li1	10274(5)	2908(4)	3074(3)	42(1)	38(2)	39(2)	48(2)	8(2)	–8(2)	–15(2)
N11	8839(2)	2602(2)	4043(1)	33(1)	36(1)	32(1)	35(1)	2(1)	–6(1)	–16(1)
C111	8629(2)	2548(2)	4886(1)	31(1)	35(1)	25(1)	34(1)	1(1)	–4(1)	–12(1)
C112	7367(3)	2527(2)	5363(2)	39(1)	34(1)	40(1)	45(2)	–3(1)	–5(1)	–16(1)
C113	7246(3)	2427(2)	6191(2)	41(1)	38(1)	37(1)	45(2)	–5(1)	8(1)	–17(1)
C114	8362(3)	2370(2)	6584(1)	36(1)	45(2)	26(1)	36(1)	–4(1)	0(1)	–14(1)
C115	9588(3)	2460(2)	6114(1)	35(1)	38(1)	31(1)	38(1)	–3(1)	–6(1)	–13(1)
C116	9720(3)	2552(2)	5289(1)	33(1)	30(1)	32(1)	37(1)	–2(1)	0(1)	–14(1)
N12	8767(2)	2040(2)	2808(1)	33(1)	34(1)	31(1)	34(1)	3(1)	–8(1)	–13(1)
C121	8582(3)	1309(2)	2285(1)	33(1)	38(1)	29(1)	34(1)	7(1)	–12(1)	–12(1)
C126	9703(3)	755(2)	1667(2)	43(1)	45(2)	45(2)	39(1)	3(1)	–12(1)	–16(1)
C125	9550(3)	28(2)	1150(2)	52(1)	62(2)	53(2)	34(1)	–5(1)	–9(1)	–12(2)
C124	8274(4)	–167(2)	1218(2)	52(1)	80(2)	43(2)	41(2)	4(1)	–26(2)	–25(2)
C123	7144(3)	431(2)	1807(2)	52(1)	62(2)	53(2)	56(2)	9(1)	–23(2)	–35(2)
C122	7284(3)	1156(2)	2330(2)	43(1)	42(2)	42(1)	47(2)	0(1)	–9(1)	–17(1)
N22	8912(2)	4678(2)	2613(1)	36(1)	37(1)	31(1)	40(1)	–2(1)	0(1)	–15(1)
C221	8107(2)	5732(2)	2986(1)	33(1)	30(1)	33(1)	38(1)	1(1)	–6(1)	–16(1)
C226	7723(3)	5772(2)	3824(1)	36(1)	35(1)	32(1)	39(1)	8(1)	–4(1)	–11(1)
C225	6920(3)	6773(2)	4224(2)	37(1)	33(1)	41(1)	34(1)	0(1)	–4(1)	–10(1)
C224	6449(2)	7780(2)	3826(2)	37(1)	27(1)	36(1)	45(2)	–5(1)	–9(1)	–9(1)
C223	6784(3)	7735(2)	2995(2)	43(1)	45(2)	33(1)	49(2)	8(1)	–15(1)	–9(1)
C222	7576(3)	6732(2)	2576(2)	41(1)	47(2)	41(1)	33(1)	4(1)	–12(1)	–14(1)
N21	10688(2)	3452(2)	1753(1)	40(1)	40(1)	33(1)	41(1)	3(1)	3(1)	–11(1)
C211	11827(3)	3138(2)	1093(1)	37(1)	38(1)	39(1)	34(1)	2(1)	–4(1)	–14(1)
C216	11796(3)	3727(2)	368(2)	45(1)	50(2)	49(2)	34(1)	3(1)	–9(1)	–16(1)
C215	12944(3)	3392(3)	–257(2)	54(1)	67(2)	63(2)	34(2)	8(1)	–8(1)	–30(2)
C214	14157(3)	2442(3)	–213(2)	57(1)	50(2)	83(2)	37(2)	–8(2)	3(1)	–27(2)
C213	14163(3)	1831(3)	491(2)	59(1)	46(2)	69(2)	41(2)	–5(1)	–4(1)	–1(2)
C212	13025(3)	2170(2)	1129(2)	49(1)	51(2)	51(2)	31(1)	4(1)	–1(1)	–6(1)
O22	7279(3)	3908(2)	1299(2)	73(1)	73(2)	77(2)	87(2)	36(1)	–45(1)	–39(1)
C21	7979(5)	3297(4)	579(3)	97(1)	128(4)	105(3)	85(3)	35(3)	–54(3)	–63(3)
O25	5857(2)	4160(2)	2813(2)	71(1)	44(1)	52(1)	119(2)	26(1)	–28(1)	–18(1)
C23	5718(4)	4243(4)	1453(3)	96(2)	73(3)	112(3)	131(4)	60(3)	–73(3)	–51(3)
C24	5156(4)	4862(4)	2236(3)	91(1)	55(2)	83(3)	144(4)	46(3)	–44(3)	–29(2)
C26	5336(4)	4651(3)	3612(3)	85(1)	49(2)	68(2)	137(4)	–10(2)	–5(2)	–25(2)
C117	8261(3)	2202(2)	7483(2)	50(1)	72(2)	46(2)	36(1)	–2(1)	4(1)	–31(2)
O12	12193(2)	1473(1)	3079(1)	37(1)	38(1)	34(1)	42(1)	6(1)	–14(1)	–15(1)
C11	12226(3)	366(2)	3208(2)	52(1)	48(2)	36(1)	77(2)	5(1)	–19(2)	–16(1)
O15	11645(2)	3505(2)	3669(1)	48(1)	33(1)	40(1)	69(1)	–5(1)	0(1)	–15(1)
C13	13255(3)	1647(2)	3437(2)	42(1)	30(1)	45(2)	49(2)	–2(1)	–11(1)	–10(1)
C14	13087(3)	2838(2)	3333(2)	44(1)	31(1)	46(2)	54(2)	–7(1)	–1(1)	–15(1)
C16	11444(3)	4602(2)	3882(2)	49(1)	47(2)	39(2)	59(2)	0(1)	–18(1)	–10(1)
C127	8145(5)	–1009(3)	675(2)	81(1)	119(3)	69(2)	68(2)	–12(2)	–31(2)	–43(2)
C227	5611(3)	8870(2)	4279(2)	51(1)	47(2)	38(2)	60(2)	–9(1)	–13(1)	–5(1)
C217	15422(4)	2064(4)	–904(2)	94(1)	73(3)	141(4)	50(2)	–7(2)	21(2)	–33(3)

Atom	X/a·10^4	Y/b·10^4	Z/c·10^4	U(eq)	Atom	X/a·10^4	Y/b·10^4	Z/c·10^4	U(eq)
H11	9080(30)	390(20)	4604(15)	47(7)	H10G	8096	2513	661	145
H12	9030(20)	–87(19)	3519(14)	33(6)	H10H	8931	3344	419	145
H21	12080(30)	4960(20)	1600(17)	63(9)	H10I	5459	3576	1477	115
H22	10520(30)	6060(20)	2420(15)	48(7)	H10J	5292	4729	1017	115
H12A	6574	2583	5114	47	H20A	14232	1152	3178	50
H13A	6381	2397	6496	49	H20B	13133	1468	4016	50
H15A	10352	2459	6368	42	H20C	13772	2996	3611	53
H16A	10567	2619	4989	39	H20D	13287	3003	2755	53
H22A	10581	877	1599	51	H20E	12246	4580	4139	73
H23A	10335	–349	738	62	H20F	10533	4929	4257	73
H25A	6247	342	1855	62	H20G	11412	5058	3397	73
H26A	6483	1556	2726	52	H20H	13228	–157	3182	79
H32A	8019	5100	4121	43	H20I	11801	166	2791	79
H33A	6680	6774	4794	44	H20J	11671	328	3738	79
H35A	6464	8409	2703	52	H14A	7325	2158	7708	75
H36A	7756	6729	2005	49	H14B	8352	2832	7733	75
H42A	10965	4370	308	54	H14C	9039	1506	7592	75
H43A	12900	3825	–731	64	H24A	7177	–1031	813	121
H45A	14971	1162	535	70	H24B	8870	–1751	749	121
H46A	13069	1730	1600	59	H24C	8305	–788	113	121
H10A	5353	5558	2202	109	H34A	5484	8726	4858	76
H10B	4099	5063	2379	109	H34B	4662	9221	4115	76
H10C	4285	4871	3738	127	H34C	6141	9370	4160	76
H10D	5580	5311	3635	127	H44A	16176	1381	–755	141
H10E	5789	4103	4004	127	H44B	15811	2653	–1023	141
H10F	7398	3610	155	145	H44C	15093	1914	–1382	141

8.6 Bis[μ-(*N,N′*-di-*tert*-butyl-*C*-phosphanidatoformamidin)-1κ^1*P*; 2κ^1*P′*;1:2κ^2*N*; 1:2κ^2*N′*-1,2-bis(tetrahydrofuran-*O*)dilithium **IV**

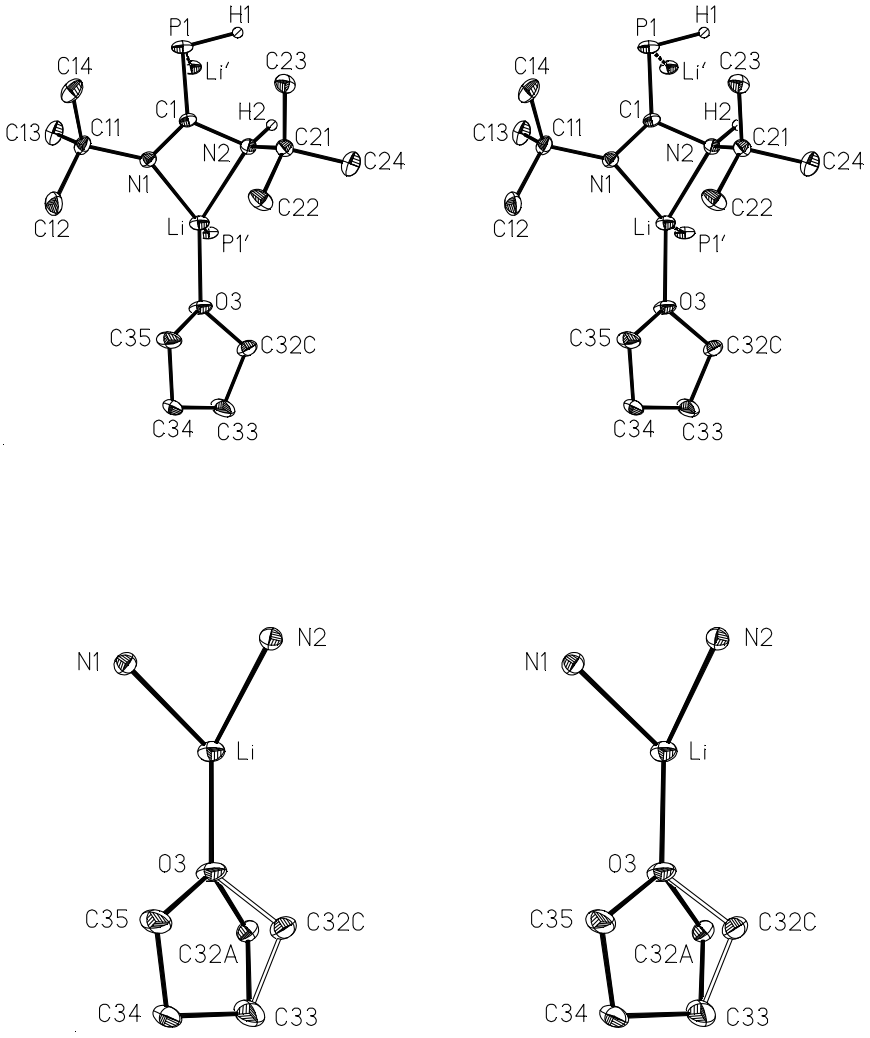

Figure 8.6.1 Stereoscopic view of the split-positions of the tetrahydrofuran carbon C32. Thermal ellipsoids are at 30% probability; all hydrogen atoms are omitted for clarity.

Table 8.6.1 Bond lengths (pm) and bond angles (deg), characteristic torsion angles and Intramolecular contacts as well as least-squares planes and angles between these planes for bis[μ-(*N,N′*-di-*tert*-butyl-*C*-phosphanidatoformamidin)-1κ^1*P*;2κ^1*P′*;1:2-κ^2*N*;1:2κ^2*N′*-1,2-bis(tetrahydrofu-ran-*O*)dilithium (**IV**).

a) Bond lengths

Amidinate-ligand				Tetrahydrofuran-ligand	
	n = 1	*n* = 2	mean		
P1–C1	179.5(2)	----		O3–C32A/C	147.3(3)/146.8(4)
P1–H1	128.4	----		O3–C35	141.7(2)
C1–Nn	129.8(2)	146.1(2)		C32A/C–C33	139.6(4)/ 149.3(5)
N2–H2	92.0	----		O33–C34	150.6(3)
N*n*–C*n*1	148.3(2)	150.2(2)	149.3	C34–C35	150.8(2)
N*n*–Li	204.3(3)	210.2(3)	207.3	Intramolecular contacts	
Li–O3	193.9(3)	—		C1···Li1	237.3(3)
Li–P1′ [a)]	261.4(3)	—		N1···N2	226.1(2)
C*n*1–C*n*2	152.6(3)	151.9(2)	152.6		
C*n*1–C*n*3	152.2(2)	152.6(2)			
C*n*1–C*n*4	153.1(2)	153.2(2)			

a) Symmetry operation: –x+1; –y; –z.

b) Bond angles

Amidinate-ligand				Coordination at lithium	
	n = 1	*n* = 2	mean		
C1–P1–H1	100.1(1)	—		N1–Li–N2	66.1(1)
C1– P1–Li1′	104.2(1)	—		N 1–Li–O3	123.6(2)
H1–P1–Li′	85.4			N2–Li–O3	134.8(2)
N1–C1–N2	110.1(1)			N1–Li–P1′	125.6(1)
N*n*–C1–P1	133.6(1)	116.3(1)	125.0	N2–Li–P1′	108.4(1)
C1–N*n*–C*n*1	87.5(1)	81.4(1)	121.0		
C1–N*n*–Li	87.5(1)	37.5(7)	48.4		
C*n*1–N*n*–Li	138.6(1)	117.0(1)	127.8	Tetrahydrofuran-ligand	
N*n*–C*n*1–C*n*2	104.8(1)	111.5(1)	109.3	Li–O3–C32A/C	122.8(2)/122.2(2)
N*n*–C*n*1–C*n*3	111.6(1)	112.3(1)		C35–O3–C32A/C	106.0(2)/106.7(2)
N*n*–C*n*1–C*n*4	111.2(1)	104.6(1)		O3–C32A/C–C33	107.8(2)/103.2(2)
C*n*2–C*n*1–C*n*3	109.1(1)	109.8(1)	109.6	C32A/C–C33–C34	103.8(2)/108.0(2)
C*n*2–C*n*1–C*n*4	108.8(1)	108.9(1)		C33–C34–C35	103.2(1)
C*n*3–C*n*1–C*n*4	111.2(1)	109.7(1)		C34–C35–O3	107.7(1)
C1–N2–H2	108.4(1)			Li–O3–C35	128.7(1)
C21–N2–H2	105.4(1)				
Li–N2–H2	125.0(1)				

c) Torsion angles

N1–C1–P1–Li′	–99.3(2)	C1–N2–C21–C24	–167.0(1)	O3–C32A/C–C33–C34	34.1(3)/–23.2(4)
N2–C1–P1–Li′	75.4(1)	C1–N1–C11–C12	–173.5(2)	C32A/C–C33–C34–C35	–30.5(3)/5.0(3)
N2–C1–P1–H1	–12.4(2)	P1–C1–N1–Li	139.3(2)	C33–C34–C35–O3	16.1(2)
N1–C1–N2–H2	158.9	P1–C1–N2–Li	–141.0(1)	C34–C35–O3–C32A/C	3.7(3)/–31.7(3)
C11–N1–C1–P1	–11.5(2)	C1–N1–Li–P1′	–71.5(2)	C35–O3–C32A/C–C33	–24.3(3)/33.8(4)
C21–N2–C1–P1	102.9(1)	C1–N2–Li–P1′	99.6(1)		
		N1–Li–O3–C35	–1.6(3)		

e) Characteristic least-squares planes and deviations (pm) from these planes.
Atoms defining a least-square plane are marked with an asterisk (*).

A: *Amidinate-Ligand*											
N1*	C1*	N2*	P1	H1	Li′	H2	C11	C12	C22	Li	O3
0.0	0.0	0.0	–11.5	10.7	–119.0	–31.3	13.9	24.9	174.6	–119.0	–127.1

B_A: *Disordered tetrahydrofuran -Ligand (with C32A)*							
O3*	C32A*	C34*	C35*	C33	Li	N1	N2
2.1	–1.3	1.3	–2.0	47.9	–35.7	–95.3	77.1

B_c: *Disordered tetrahydrofuran-Ligand (with C32C)*							
C32C*	C33*	C34*	C35*	O3	Li	N1	N2
1.9	–2.9	2.9	–1.8	–46.6	–109.6	–126.2	–17.3

e) Angle between the planes:
A/N1–Li–N2 43.3°; C1–N1–Li/C1–N2–Li 38.7°; N1–Li–N2/B_A 58.7°; N1–Li–N2/B_C 31.5°

Table 8.6.2 Atomic Coordinates, Equivalent Isotropic Displacement Parameters, and Anisotropic Displacement Parameters with Estimated Standard deviations in Parentheses for bis[μ-(*N,N′*-di-*tert*-butyl-*C*-phosphanidatoformamidin)-1κ^1*P*; 2κ^1*P′*;1:2κ^2*N*; 1:2κ^2*N′*-1,2-bis(tetrahydrofuran-*O*)-dilithium **IV**

Atom	X/a·10^4	Y/b·10^4	Z/c·10^4	U(eq)	U11	U22	U33	U23	U13	U12
P1	6196(1)	999(1)	1538(1)	25(1)	33(1)	20(1)	20(1)	0(1)	4(1)	–11(1)
N1	3809(2)	–82(1)	1803(1)	22(1)	25(1)	19(1)	23(1)	–1(1)	9(1)	–1(1)
N2	6086(2)	–654(1)	1686(1)	21(1)	21(1)	21(1)	21(1)	2(1)	7(1)	–1(1)
Li	3885(3)	–1050(2)	739(2)	25(1)	30(1)	22(1)	23(1)	–1(1)	9(1)	–7(1)
O3	2667(2)	–2012(1)	757(1)	31(1)	43(1)	23(1)	33(1)	–9(1)	24(1)	–15(1)
C1	5213(2)	85(1)	1719(1)	18(1)	24(1)	17(1)	14(1)	–1(1)	4(1)	–3(1)
C11	2672(2)	531(1)	1981(2)	27(1)	32(1)	21(1)	30(1)	–1(1)	15(1)	4(1)
C12	1279(2)	55(1)	2172(2)	43(1)	35(1)	36(1)	68(1)	2(1)	30(1)	6(1)
C13	2152(2)	1060(1)	885(2)	38(1)	45(1)	35(1)	37(1)	4(1)	13(1)	13(1)
C14	3325(2)	1033(1)	3095(2)	38(1)	56(1)	32(1)	32(1)	–7(1)	21(1)	6(1)
C21	6786(2)	–1067(1)	2843(1)	23(1)	23(1)	24(1)	23(1)	4(1)	5(1)	–1(1)
C22	5558(2)	–1505(1)	3323(2)	37(1)	30(1)	44(1)	35(1)	18(1)	4(1)	–9(1)
C23	7680(2)	–491(1)	3785(1)	29(1)	28(1)	30(1)	25(1)	5(1)	0(1)	–3(1)
C24	7911(2)	–1682(1)	2528(2)	39(1)	43(1)	33(1)	42(1)	5(1)	9(1)	11(1)
C32A	2297(5)	–2575(2)	–252(3)	26(1)	29(2)	23(1)	26(2)	–8(1)	10(2)	–5(1)
C32C	3062(6)	–2774(2)	269(5)	24(1)	23(2)	21(2)	30(3)	–3(2)	9(2)	–2(2)
C33	1597(3)	–3248(1)	114(3)	57(1)	33(1)	52(1)	90(2)	–44(1)	23(1)	–20(1)
C34	682(2)	–2914(1)	950(2)	31(1)	22(1)	31(1)	41(1)	1(1)	8(1)	–9(1)
C35	1625(2)	–2195(1)	1483(2)	41(1)	43(1)	39(1)	52(1)	–18(1)	34(1)	–19(1)

Atom	X/a·10^4	Y/b·10^4	Z/c·10^4	U(eq)	Atom	X/a·10^4	Y/b·10^4	Z/c·10^4	U(eq)
H1	7590(30)	737(16)	1660(20)	65(8)	H23B	6977	–99	3966	34
H2	6910(30)	–542(12)	1351(18)	33(5)	H23C	8148	–784	4494	34
H12A	869	–268	1482	52	H24A	7353	–2029	1910	47
H12B	1603	–284	2857	52	H24B	8717	–1409	2254	47
H12C	490	417	2297	52	H24C	8366	–1993	3221	47
H13A	3016	1373	775	46	H32A	3241	–2728	–487	31
H13B	1778	730	196	46	H32B	1595	–2326	–929	31
H13C	1334	1408	994	46	H32C	3918	–3036	818	29
H14A	3706	685	3762	46	H32D	3338	–2695	–488	29
H14B	4161	1361	2966	46	H33A	917	–3512	–560	68
H14C	2518	1368	3258	46	H33B	2373	–3627	520	68
H22A	4819	–1126	3488	44	H34A	–357	–2758	523	37
H22B	5031	–1884	2742	44	H34B	604	–3300	1560	37
H22C	6046	–1781	4044	44	H35A	2200	–2313	2289	49
H23A	8476	–229	3487	34	H35B	945	–1744	1509	49

8.7 *Catena*-poly[μ-(*N,N′*-dicyclohexyl-*C*-phosphanidato-1*:2* κ^2P-formamidinato-1:2 κ^2N,1:2 κ^2N')-1,2-bis(tetrahydrofuran-*O*]dilithium **V**

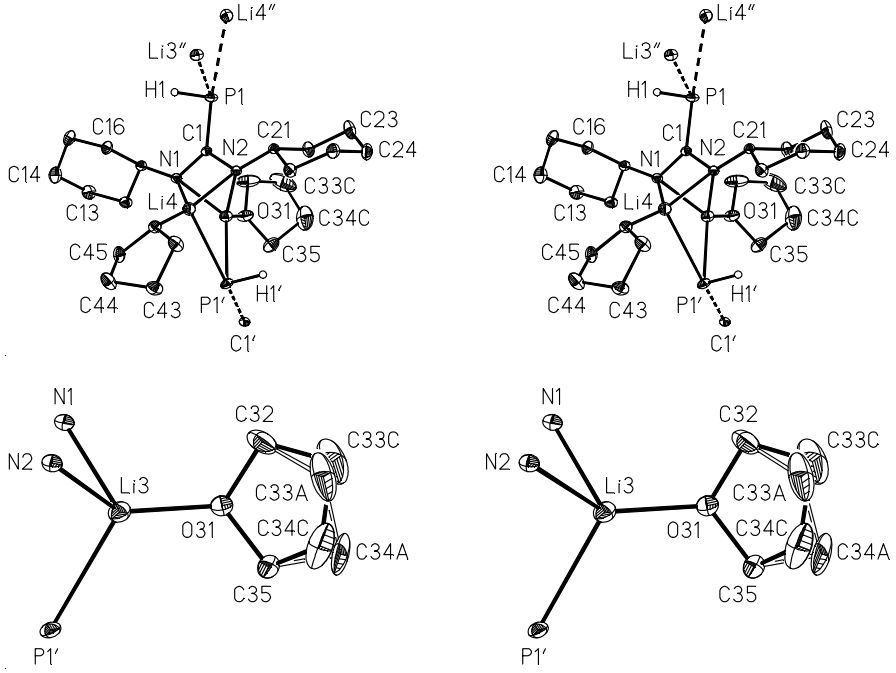

Figure 8.7.1 Split-positions A and C of the tetrahydrofuran carbons C33 and C34. Thermal ellipsoids are at 30% probability; all hydrogen atoms are omitted for clarity.

Table 8.7.1 Bond lengths (pm) and bond angles (deg), characteristic intramolecular distances and torsion angles as well as least-squares planes and angles between these planes for *catena*-poly[μ-(*N,N′*-dicyclohexyl-*C*-phosphanidato-1*:2*κ^2P-formamidinato-1:2κ^2N,1:2κ^2N')-1,2-bis(tetrahydrofuran)-*O*]dilithium (**V**)

The positions of marked atoms are generated by applying the following symmetry operations: (′) –x, y – 0.5, –z + 0.5; (″) –x, y + 0.5, –z + 0.5

a) Bond lengths

Amidinate ligand							
	n = 1	*n* = 2	mean		*n* = 1	*n* = 2	mean
P1–H1	129.1	—	—	N*n*–Li3	206.8(3)	206.2(3)	203.8
P1–C1	182.2(1)	—	—	N*n*–Li4	199.8(3)	202.4(3)	
C1–N*n*	135.4(2)	135.1(2)	135.3	P1–Li3″	259.9(3)		266.2
N*n*–C*n*1	145.0(2)	145.1(2)	145.1	P1–Li4″	272.2(2)		
Tetrahydrofuran ligands				Cyclohexyl substituents			
	n = 3	*n* = 4	mean		*n* = 1	*n* = 2	mean
Li*n*–O*n*1	190.0(3)	191.5(3)	190.8	C*n*1–C*n*2	152.9(2)	152.9(2)	152.6
O*n*1–C*n*2	141,4(2)	144.2(2)	142.8	C*n*1–C*n*6	152.9(2)	152.2(2)	
O*n*1–C*n*5	142.2(2)	144.4(2)	143.3	C*n*2–C*n*3	153.0(2)	152.7(2)	
C*n*2–C*n*3	[a]	150.2(2)	152.2	C*n*3–C*n*4	152.3(2)	152.3(2)	
C*n*3–C*n*4		151.4(2)		C*n*4–C*n*5	152.2(2)	151.6(2)	
C*n*4–C*n*5		151.3(2)		C*n*5–C*n*6	153.0(2)	152.6(2)	

Characteristic intramolecular distances

Li3···Li4 237.1(4)	C1···Li3 231.4(3)	C1···Li4 235.1(3)	mean 233.1

[a] tetrahydofuran ligand (*n* = 3) partially disordered: C32–C33A 162(1); C32–C33C 143.6(7); C33A–C34A 154(1); C33C–C34C 154.5(9); C34A–C35 151.3(4); C34C–C35 151.6(4); for the sake of completeness: C33A–C34C 123.9; C33C–C34A 167.9

b) Bond angles

Amidinate ligand				Coordination at lithium			
	n = 1	*n* = 2	mean		*n* = 3	*n* = 4	mean
C1–P1–H1	98.9	—	—	N1–Li*n*–N2	64.8(1)	66.7(1)	65.8
C1–P1–Li3″	102.7(1)	—	—	N1–Li*n*–O*n*1	115.6(1)	133.6(1)	130.0
C1–P1–Li4″	152.5(1)	—	—	N2–Li*n*–O*n*1	126.4(1)	144.5(1)	
H1–P1–Li3″	92.6	—	—	N1–Li*n*–P1′	113.3(1)	110.9(1)	105.8
H1–P1–Li4″	94.9	—	—	N2–Li*n*–P1′	100.9(1)	98.0(1)	
Li3″–P1–Li4″	52.9(1)	—	—	O*n*1–Li*n*–P1′	122.4(1)	98.5(1)	110.5
P1–C1–N*n*	128.1(1)	122.1(1)	125.1	Cyclohexyl substituents			
N1–C1–N2	109.7(1)				*n* = 1	*n* = 2	mean
C1–N*n*–C*n*1	122.0(1)	121.7(1)	121.9	N*n*–C*n*1–C*n*2	108.5(1)	112.3(1)	110.2
C1–N*n*–Li3	82.3(1)	82.5(1)	82.4	N*n*–C*n*1–C*n*6	111.8(1)	108.1(1)	
C1–N*n*–Li4	86.8(1)	85.9(1)	86.4	C*n*2–C*n*1–C*n*6	109.8(1)	109.4(1)	109.6
C*n*1–N*n*–Li3	135.7(1)	134.1(1)	134.9	C*n*1–C*n*2–C*n*3	112.0(1)	112.2(1)	111.6
C*n*1–N*n*–Li4	138.7(1)	141.1(1)	139.9	C*n*2–C*n*3–C*n*4	111.2(1)	110.9(1)	
Li3–N*n*–Li4	71.3(1)	70.9(1)	71.1	C*n*3–C*n*4–C*n*5	111.1(1)	110.6(1)	
				C*n*4–C*n*5–C*n*6	111.0(1)	111.4(1)	
				C*n*5–C*n*6–C*n*1	112.4(1)	113.1(1)	

Tetrahydrofuran ligands							
	n = 3	*n* = 4	mean		*n* = 3	*n* = 4	mean
Li*n*–O*n*1–C*n*2	122.6(1)	119.5(1)	120.1	O*n*1–C*n*2–C*n*3	[a]	106.3(1)	105.1
Li*n*–O*n*1–C*n*5	123.4(1)	114.8(1)		O*n1*–C*n5*–C*n*4		104.9(1)	
C*n*2–O*n*1–C*n*5	109.6(1)	109.1(1)	109.4	C*n*2–C*n*3–C*n*4	[a]	102.3(1)	102.1
				C*n*3–C*n*4–C*n*5		101.5(1)	

[a] tetrahydofuran ligand (*n* = 3) partially disordered: O31–C32–C33A 98.4(6), O31–C32–C33C 108.9(3); O31–C35–C34A 112.9(5), O31–C35–C34C 98.9(3); C32–C33A–C34A 105.7(9), C32–C33C–C34C 101.8(5); C33A–C34A–C35 98.2(8), C33C–C34C–C35 102.8(4); for the sake of completeness: C32–C33A–C34C 106.9, C32–C33C–C34A 108.2; C33A–C34C–C35 113.0, C33C–C34A–C35 97.3(8)

c) Torsion angles

Amidinate ligand			Tetrahydrofuran ligands		
	n = 1	*n* = 2			
P1–C1–N*n*–C*n*1	–5.0(2)	2.9(2)	N2–Li3–O31–C32	–35.9(3)	
P1–C1–N*n*–Li3	135.0(1)	–135.2(1)	N1–Li4–O41–C42	–168.7(2)	
P1–C1–N*n*–Li4	–153.4(1)	153.6(1)			
C1–N*n*–C*n*1–C*n*2	154.5(1)	–88.3(2)	O31–C32–C33A–C34A	39.1(1)	*en*[a]
C*n*1–N*n*–Li3–O31	35.4(2)	–50.2(2)	C32–C33A–C34A–C35	–28.1(2)	
C*n*1–N*n*–Li4–O41	–13.3(3)	24.9(3)	C33A–C34A–C35–O31	8.3(2)	
C*n*1–N*n*–Li3–P1′	–113.1(2)	94.8(2)	C34A–C35–O31–C32	18.2(8)	

C*n*1–N*n*–Li4–P1′	112.4(2)	–92.1(2)	C35–O31–C32–C33A	–33.7(5)	
C1–N1–Li4–O41	124.4(2)				
C1–N1–Li4–P1′	–109.9(1)		O31–C32–C33C–C34C	–10.4(9)	b)
C1–N2–Li3–O31	77.4(2)		C32–C33C–C34C–C35	32.2(1)	
C1–N2–Li3–P1′	–137.7		C33C–C34C–C35–O31	–41.3	
			C34C–C35–O31–C32	36.7	
Cyclohexyl substituents[c]			C35–O31–C32–C33C	–17.2	
	n = 1	*n* = 2			
C*n*1–C*n*2–C*n*3–C*n*4	–56.1	57.0	O41–C42–C43–C44	–29.3	*en*[a]
C*n*2–C*n*3–C*n*4–C*n*5	55.7	–56.2	C42–C43–C44–C45	39.1	
C*n*3–C*n*4–C*n*5–C*n*6	–55.3	55.1	C43–C44–C45–C41	–35.6	
C*n*4–C*n*5–C*n*6–C*n*1	55.6	–55.0	C44–C45–O41–C42	18.1	
C*n*5–C*n*6–C*n*1–C*n*2	–54.8	53.8	C45–O31–C42–C43	7.2	
C*n*6–C*n*1–C*n*2–C*n*3	54.9	–54.8			

[a] Approximately envelope (*en*) conformation; [b] conformation between twist and envelope; [c] chair conformation of both cyclohexyl substituents

d) Characteristic least-squares planes and deviations (pm) from these planes
Atoms defining a least-squares plane are marked with an asterisk (*).

A: *Amidinate ligand*								
N1*	C1*	N2*	P1	H1	C11	C21	Li3	Li4
0.0	0.0	0.0	–9.0	18.3	3.0	–0.9	–135.5	100.2
B_1: *Cyclohexyl substituent (n = 1)*								
C12*	C13*	C15*	C16*	C11	C14	N1		
0.2	–0.2	0.2	–0.2	–66.6	66.3	–56.6		
B_2: *Cyclohexyl substituent (n = 2)*								
C22*	C23*	C25*	C26*	C21	C24	N2		
–0.8	0.8	–0.8	0.8	66.1	–66.6	54.0		
C_{3A}: *Tetrahydrofuran ligand (n = 3, disordered A)*								
O31*	C33A*	C34A*	C35*	C32	Li3			
–3.3	2.8	–4.4	4.9	–58.9	105.4			
C_{3C}: *Tetrahydrofuran ligand (n = 4, disordered C)*								
O31*	C32*	C33C*	C34C*	C35	Li3			
–4.0	6.1	–5.6	3.5	–60.9	104.1			
C_4: *Tetrahydrofuran ligand (n = 4)*								
O41*	C42*	C43*	C45*	C44	Li4			
–4.0	3.9	–2.3	2.5	59.6	–134.7			

Angles (deg) between different planes

A/B_1 55.5, A/B_2 58.1; A/N1–Li3–N2 51.0, A/N1–Li4–N2 36.6, A/Li3–N1–Li4 85.5, A/Li3–N2–Li4 86.4; C_{3A}/Li3–P1′–Li4 31.9, C_4/Li3–P1′–Li4 85.5; N1–Li3–N2/N1–Li4–N2 87.7, Li3–N1–Li4/Li3–N2–Li4 83.7; Li3–N1–Li4/Li3–P1′–Li4 29.1, Li3–N2–Li4/Li3–P1′–Li4 54.7

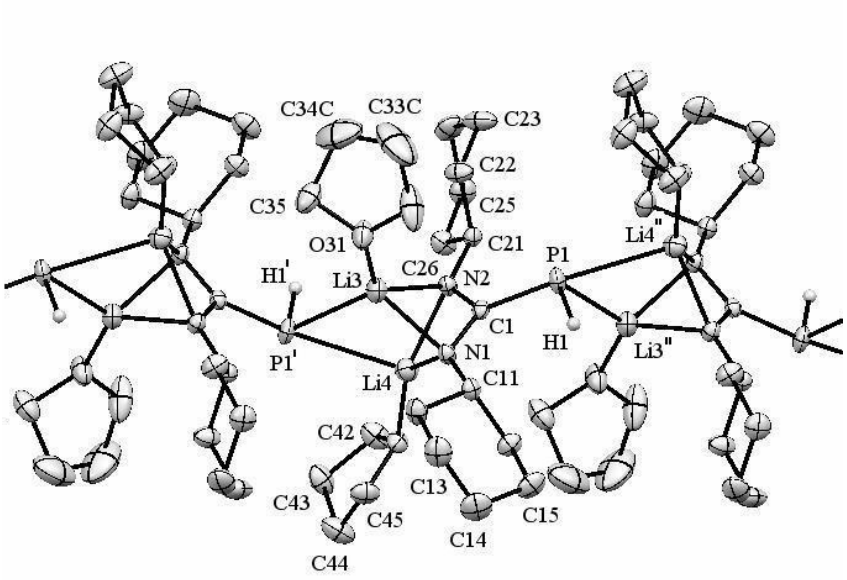

Figure 8.7.2 Solid state structure of the polymeric structure of *catena*-poly[μ-(*N,N′*-dicyclohexyl-*C*-phosphanidato-1*:2*κ^2*P*-formamidinato-1:2κ^2*N,*1:2κ^2*N′*)-1,2-bis(tetrahydrofuran-*O*)]dilithium **V.** Thermal ellipsoids are at 50% probability; except for the PH-groups all hydrogen atoms are omitted for clarity.

a)

b)

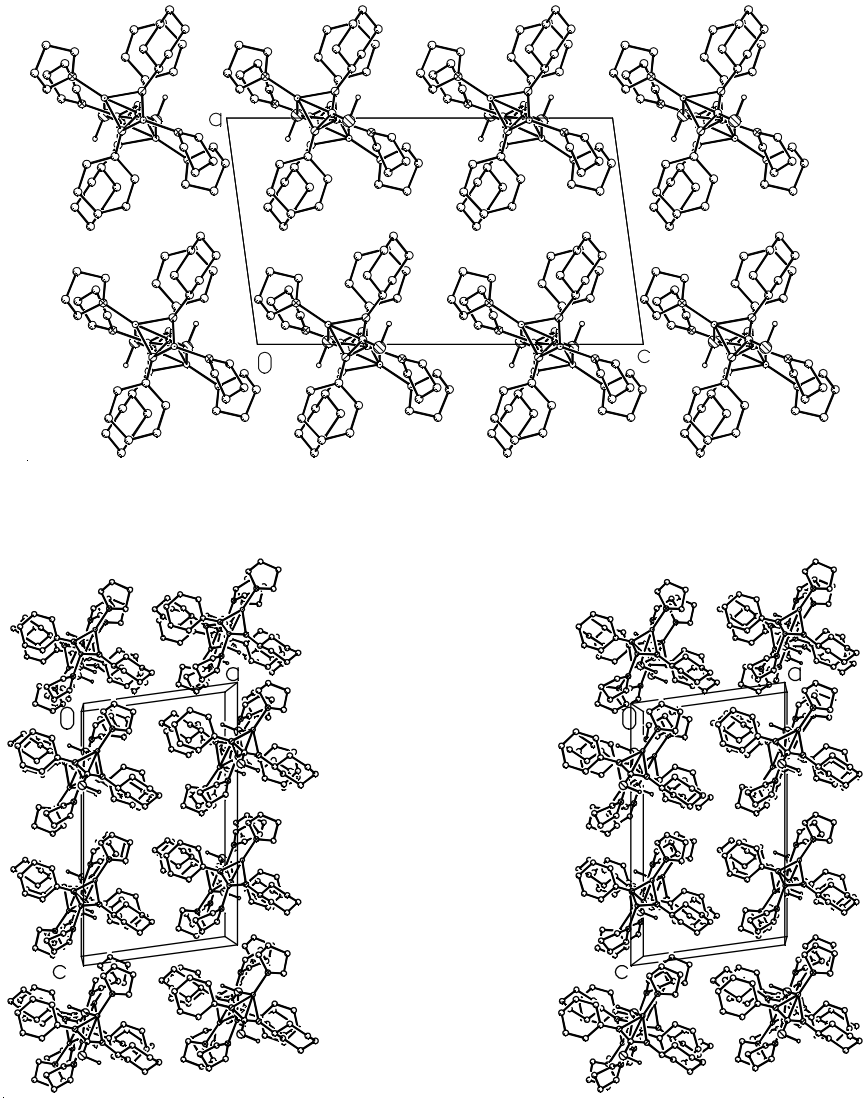

Figure 8.7.3 Non-stereoscopic (a) and stereoscopic view (b) of the strands of the coordination polymeric complex **V** viewed along [0$\bar{1}$0]. The strands are arranged in a slightly distorted tetragonal rod packing.

Table 8.7.2 Atomic Coordinates, Equivalent Isotropic Displacement Parameters, and Anisotropic Displacement Parameters with Estimated Standard deviations in Parentheses for *catena*-poly[μ-(*N,N′*-dicyclohexyl-*C*-phosphanidato-1*:2* κ^2*P*-formamidinato-1:2 κ^2*N,*1:2 κ^2*N′*)-1,2-bis(tetrahydrofuran-*O*]dilithium **V**

Atom	X/a·10^4	Y/b·10^4	Z/c·10^4	U(eq)	U11	U22	U33	U23	U13	U12
P1	128(1)	9115(1)	1846(1)	23(1)	31(1)	14(1)	24(1)	3(1)	–3(1)	–4(1)
C1	–211(1)	7705(1)	2254(1)	17(1)	21(1)	15(1)	16(1)	–1(1)	4(1)	1(1)
N1	–1185(1)	7003(1)	2096(1)	19(1)	20(1)	17(1)	20(1)	3(1)	0(1)	–1(1)
N2	567(1)	7173(1)	2758(1)	19(1)	20(1)	17(1)	20(1)	2(1)	0(1)	–1(1)
Li3	87(2)	5665(2)	2165(1)	28(1)	31(1)	22(1)	32(1)	–1(1)	5(1)	0(1)
Li4	–886(2)	6429(2)	3094(1)	28(1)	28(1)	29(1)	27(1)	4(1)	5(1)	1(1)
O31	629(1)	5234(1)	1301(1)	36(1)	53(1)	23(1)	35(1)	3(1)	16(1)	5(1)
O41	–1834(1)	6382(1)	3851(1)	24(1)	26(1)	25(1)	21(1)	2(1)	5(1)	1(1)
C11	–2183(1)	7361(1)	1582(1)	20(1)	22(1)	19(1)	17(1)	2(1)	–1(1)	–1(1)
C12	–2827(1)	6234(1)	1280(1)	28(1)	29(1)	23(1)	28(1)	–1(1)	–5(1)	–5(1)
C13	–3932(1)	6532(2)	756(1)	35(1)	35(1)	37(1)	30(1)	–3(1)	–12(1)	–5(1)
C14	–4785(1)	7334(2)	1092(1)	39(1)	28(1)	51(1)	34(1)	1(1)	–12(1)	2(1)
C15	–4162(1)	8467(2)	1390(1)	34(1)	29(1)	41(1)	28(1)	1(1)	–6(1)	12(1)
C16	–3053(1)	8166(1)	1910(1)	25(1)	23(1)	30(1)	21(1)	–1(1)	–3(1)	4(1)
C21	1699(1)	7724(1)	3027(1)	18(1)	19(1)	17(1)	19(1)	0(1)	1(1)	0(1)
C22	2688(1)	7387(1)	2592(1)	30(1)	24(1)	39(1)	28(1)	–9(1)	6(1)	–1(1)
C23	3901(1)	7874(2)	2916(1)	40(1)	21(1)	58(1)	43(1)	–13(1)	9(1)	–5(1)
C24	4224(1)	7435(2)	3672(1)	38(1)	21(1)	40(1)	50(1)	–9(1)	–8(1)	5(1)
C25	3261(1)	7772(1)	4116(1)	31(1)	30(1)	35(1)	26(1)	1(1)	–7(1)	0(1)
C26	2042(1)	7314(1)	3787(1)	28(1)	26(1)	35(1)	22(1)	5(1)	–2(1)	–3(1)
C32	852(2)	6088(2)	789(1)	56(1)	115(2)	30(1)	24(1)	3(1)	8(1)	–6(1)
C33A	2230(12)	5745(13)	737(9)	74(4)	91(7)	82(6)	59(7)	–28(5)	47(5)	–58(5)
C33C	1910(9)	5748(7)	499(5)	93(2)	129(5)	85(4)	77(5)	–7(3)	60(4)	–47(3)
C34A	2293(11)	4368(12)	781(8)	67(3)	55(5)	76(6)	83(7)	–23(5)	55(5)	2(4)
C34C	2405(4)	4733(7)	1005(4)	78(2)	56(2)	101(4)	81(3)	–36(3)	23(2)	13(2)
C35	1284(2)	4172(2)	1212(1)	40(1)	53(1)	37(1)	31(1)	–1(1)	10(1)	16(1)
C42	–1278(1)	6104(2)	4556(1)	33(1)	34(1)	42(1)	22(1)	2(1)	–2(1)	–11(1)
C43	–1991(1)	5101(2)	4813(1)	35(1)	41(1)	35(1)	27(1)	9(1)	–4(1)	–8(1)
C44	–3222(2)	5326(2)	4418(1)	41(1)	33(1)	56(1)	32(1)	8(1)	2(1)	–15(1)
C45	–2928(1)	5710(2)	3702(1)	31(1)	21(1)	44(1)	26(1)	1(1)	–1(1)	1(1)

Atom	X/a·10^4	Y/b·10^4	Z/c·10^4	U(eq)	Atom	X/a·10^4	Y/b·10^4	Z/c·10^4	U(eq)
H1	–918(17)	9355(17)	1518(10)	45(5)	H222	2734	6505	2559	36
H11	–1874	7806	1191	23	H321	166	6124	408	67
H121	–2273	5746	1039	33	H322	960	6889	1008	67
H122	–3068	5751	1671	33	H33A	2767	6112	1131	89
H131	–4345	5782	592	43	H33B	2465	6029	285	89
H132	–3685	6940	339	43	H33C	1718	5456	8	112
H141	–5100	6893	1476	47	H33D	2479	6422	510	112
H142	–5467	7552	734	47	H34A	3067	4085	1029	80
H151	–3929	8954	998	40	H34B	2136	3988	310	80

H152	–4719	8945	1633	40	H34C	2920	5055	1422	94
H161	–3299	7760	2327	30	H34D	2866	4148	762	94
H162	–2642	8918	2073	30	H351	1447	3708	1656	48
H21	1600	8613	3020	22	H352	876	3656	833	48
H261	1432	7596	4073	34	H421	–440	5853	4551	40
H262	2046	6428	3800	34	H422	–1286	6811	4867	40
H251	3459	7431	4595	37	H431	–1679	4311	4691	42
H252	3232	8654	4161	37	H432	–1993	5146	5330	42
H241	4991	7794	3879	46	H441	–3642	5966	4644	49
H242	4321	6555	3673	46	H442	–3713	4590	4384	49
H231	3880	8759	2911	48	H451	–3573	6214	3456	37
H232	4518	7610	2629	48	H452	–2817	5005	3405	37
H221	2489	7707	2108	36					

8.8 *Catena*-poly[μ-(*N,N′*-diisopropyl-*C*-phosphanidato-1*:2*κ^2*P*-formamidinato-1:2κ^2*N,*1:-2κ^2*N′*)-1,2-bis(tetrahydropyran)-*O*]dilithium (**VI)**

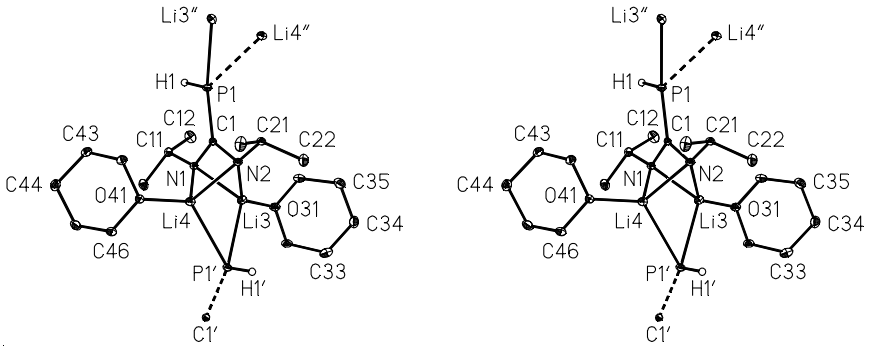

Table 8.8.1 Bond lengths (pm) and bond angles (deg), characteristic intramolecular distances and torsion angles as well as least-squares planes and angles between these planes for *catena*-poly[μ-(*N,N′*-diisopropyl-*C*-phosphanidato-1*:2*κ^2*P*-formamidinato-1:2κ^2*N,*1:2κ^2*N′*)-1,2-bis(tetrahydropyran)-*O*]dilithium (**VI)**

The positions of marked atoms are generated by applying the following symmetry operations: (′) –x + 1, y + 0.5, –z + 1.5; (″) –x + 1, y – 0.5, –z + 1.5

a) Bond lengths

Amidinate ligand							
	n = 1	*n* = 2	mean		*n* = 1	*n* = 2	mean
P1–H1[a)]	128.5(20)	—	—	N*n*–Li3	203.3(3)	207.2(3)	205.3
P1–C1	183.6(1)	—	—	N*n*–Li4	207.5(3)	207.8(3)	207.7
C1–N*n*	134.7(2)	135.4(2)	135.1	P1–Li3″	267.7(3)	—	—
N*n*–C*n*1	145.4(2)	145.5(2)	145.5	P1–Li4″	257.0(3)	—	—

Tetrahydropyran ligands				Isopropyl substituents			
	n = 3	*n* = 4	mean		*n* = 1	*n* = 2	mean
Li*n*–O*n*1	193.1(3)	191.4(3)	192.3	C*n*1–C*n*2	152.6(2)	151.9(2)	152.2
O*n*1–C*n*2	143.7(2)	144.1(2)	143.9	C*n*1–C*n*3	152.5(2)	151.6(2)	
O*n*1–C*n*6	143.1(2)	143.2(2)	143.2	C*n*1–H*n*1[b]	100.0	100.0	
C*n*2–C*n*3	149.9(2)	150.7(2)	151.3				
C*n*3–C*n*4	152.5(2)	151.9(2)		Characteristic intramolecular distances			
C*n*4–C*n*5	151.2(2)	152.3(2)		Li3···Li4	241.7(4)	C1···Li3	238.3(3)
C*n*5–C*n*6	150.9(2)	151.1(2)				C1···Li4	233.2(3)

b) Bond angles

Amidinate ligand				Coordination at lithium			
	n = 1	*n* = 2	mean		*n* = 3	*n* = 4	mean
C1–P1–H1[a]	99.9(8)	—	—	N1–Li*n*–N2	65.3(9)	64.5(9)	64.9
C1–P1–Li3″	149.5(8)	—	—	N1–Li*n*–O*n*1	124.5(2)	114.8(1)	126.8
C1–P1–Li4″	127.0(7)	—	—	N2–Li*n*–O*n*1	138.0(2)	129.8(1)	
H1–P1–Li3″[a]	108.8(8)	—	—	N1–Li*n*–P1′	109.8(1)	112.4(1)	105.0
H1–P1–Li4″[a]	105.4(8)	—	—	N2–Li*n*–P1′	97.2(1)	100.4(1)	
Li3″–P1–Li4″	54.8(8)	—	—	O*n*1–Li*n*–P1′	113.0(1)	121.8(1)	117.4
P1–C1–N*n*	128.2(1)	121.5(1)	124.9	Isopropyl substituents			
N1–C1–N2	110.2(1)	—	—		*n* = 1	*n* = 2	mean
C1–N*n*–C*n*1	122.0(1)	120.3(1)	121.2	N*n*–C*n*1–C*n*2	111.5(1)	108.9(1)	110.0
C1–N*n*–Li3	87.2(1)	85.4(1)	86.3	N*n*–C*n*1–C*n*3	108.4(1)	111.3(1)	
C1–N*n*–Li4	83.0(1)	82.7(1)	82.9	N*n*–C*n*1–H*n*1[b]	109.1	109.0	109.1
C*n*1–N*n*–Li3	136.0(1)	143.6(1)	139.8	C*n*2–C*n*1–C*n*3	109.7(1)	109.8(1)	109.8
C*n*1–N*n*–Li4	137.3(1)	132.6(1)	135.0	C*n*2–C*n*1–H*n*1[b]	109.1	109.0	109.1
Li3–N*n*–Li4	72.1(1)	71.2(1)	71.7	C*n*3–C*n*1–H*n*1[b]	109.1	109.0	

Tetrahydropyran ligands							
	n = 3	*n* = 4	mean		*n* = 3	*n* = 4	mean
Li*n*–O*n*1–C*n*2	122.6(1)	120.2(1)	122.8	C*n*2–C*n*3–C*n*4	110.9(2)	111.0(1)	110.4
Li*n*–O*n*1–C*n*6	122.6(1)	125.6(1)		C*n*3–C*n*4–C*n*5	110.2(1)	109.3(1)	
C*n*2–O*n*1–C*n*6	111.0(1)	112.4(1)	111.7	C*n*4–C*n*5–C*n*6	110.1(1)	110.6(1)	
O*n*1–C*n*2–C*n*3	110.8(1)	111.4(1)	111.6				
O*n*1–C*n*6–C*n*5	111.2(1)	111.9(1)					

[a] hydrogen position refined; [b] hydrogen position calculated

c) Torsion angles

Amidinate ligand			Tetrahydropyran ligand[c]		
	n = 1	*n* = 2		*n* = 3	*n* = 4
P1–C1–N*n*–C*n*1	6.1(2)	1.3(2)	N2–Li3–O31–C32	137.4(2)	
P1–C1–N*n*–Li3	151.0(1)	–151.4(1)	N1–Li4–O41–C42	–47.7(2)	
P1–C1–N*n*–Li4	–136.7(1)	137.0(1)			
C1–N*n*–C*n*1–C*n*2	77.7(2)	–142.4(1)	O*n*1–C*n*2–C*n*3–C*n*4	–56.2(2)	56.1(2)
C*n*1–N*n*–Li3–O31	23.7(3)	–44.0(4)	C*n*2–C*n*3–C*n*4–C*n*5	52.0(2)	–53.9(2)
C*n*1–N*n*–Li4–O41	–32.9(2)	49.1(3)	C*n*3–C*n*4–C*n*5–C*n*6	–52.0(2)	53.3(2)
C*n*1–N*n*–Li3–P1′	–114.8(2)	92.6(2)	C*n*4–C*n*5–C*n*6–O*n*1	57.3(2)	–55.6(2)
C*n*1–N*n*–Li4–P1′	111.9(2)	–98.9(2)	C*n*5–C*n*6–O*n*1–C*n*2	–61.9(2)	57.7(2)
C1–N1–Li4–O41	98.0(2)		C*n*6–O*n*1–C*n*2–C*n*3	61.1(2)	–57.8(2)
C1–N1–Li4–P1′	–117.2(1)				
C1–N2–Li3–O31	94.2(2)				
C1–N2–Li3–P1′	–129.2(1)		[c] chair conformation of both ligands		

d) Characteristic least-squares planes and deviations (pm) from these planes. Atoms defining a least-squares plane are marked with an asterisk (*).								
A: *Amidinate ligand*								
N1*	C1*	N2*	P1	H1	C11	C21	Li3	Li4
0.0	0.0	0.0	7.0	–5.1	–7.2	8.3	–106.8	133.9
B_1: *Tetrahydropyran ligand (n = 3)*								
C32*	C33*	C35*	C36*	C34	O31	Li3		
0.3	–0.2	0.2	–0.3	–64.2	66.7	251.8		
B_2: *Tetrahydropyran ligand (n = 4)*								
C42*	C43*	C45*	C46*	C44	O41	Li4		
0.2	–0.2	0.2	–0.2	66.3	–62.8	–234.7		
Angles (deg) between different planes								
A/N1–Li3–N2 38.2, A/N1–Li4–N2 49.7, A/Li3–N1–Li4 86.0, A/Li3–N2–Li4 87.1; B_1/Li3–P1′–Li4 63.9, B_2/Li3–P1′–Li4 76.6; N1–Li3–N2/N1–Li4–N2 87.8, Li3–N1–Li4/Li3–N2–Li4 82.9; Li3–N1–Li4/Li3–P1′–Li4 28.5, Li3–N2–Li4/Li3–P1′–Li4 54.4								

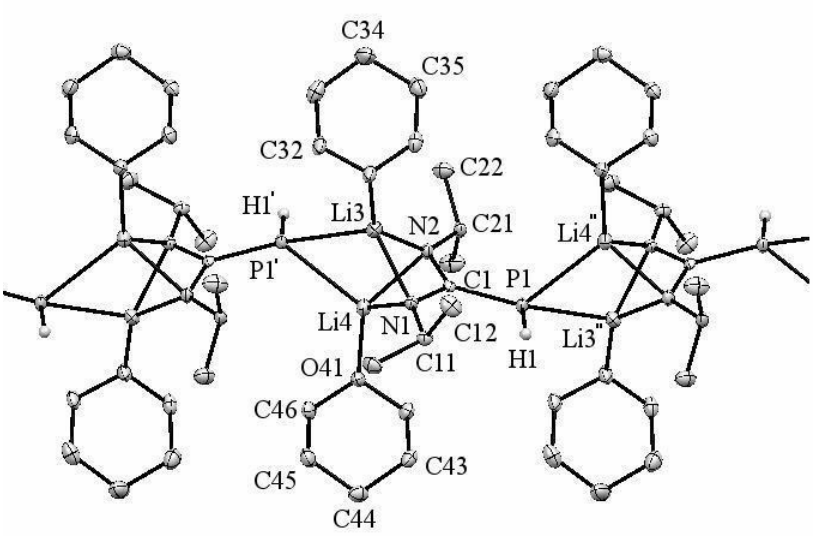

Figure 8.8.1 Solid state structure of the polymeric complex *catena*-poly[μ-(*N,N*′-diisopropyl-*C*-phosphanidato-1*:2*κ^2*P*-formamidinato-1:2κ^2*N*,1:2κ^2*N*′)-1,2-bis(tetrahydropyrane-*O*]di-lithium **VI.** Thermal ellipsoids are at 50% probability; except for the PH-groups all hydrogen atoms are omitted for clarity.

Table 8.8.2 Atomic Coordinates, Equivalent Isotropic Displacement Parameters, and Anisotropic Displacement Parameters with Estimated Standard deviations in Parentheses for *catena*-poly[μ-(*N,N′*-diisopropyl-*C*-phosphanidato-1*:2*κ^2*P*-formamidinato-1:2κ^2*N,*1:2κ^2*N′*)-1,2-bis(tetrahydropyran)-*O*]dilithium (**VI)**

Atom	X/a·10^4	Y/b·10^4	Z/c·10^4	U(eq)	U11	U22	U33	U23	U13	U12
P1	5605(1)	3733(1)	7832(1)	16(1)	17(1)	9(1)	21(1)	1(1)	–3(1)	1(1)
N1	6391(1)	6044(1)	7603(1)	13(1)	13(1)	11(1)	13(1)	0(1)	–1(1)	0(1)
N2	4379(1)	5697(1)	7303(1)	14(1)	14(1)	10(1)	19(1)	1(1)	–2(1)	–1(1)
Li3	5511(3)	6818(2)	6671(2)	19(1)	25(2)	16(1)	16(1)	3(1)	–2(1)	0(1)
Li4	4913(3)	7015(2)	8055(2)	18(1)	24(1)	13(1)	19(1)	0(1)	–1(1)	1(1)
O31	6218(1)	6947(1)	5613(1)	22(1)	38(1)	13(1)	16(1)	2(1)	3(1)	1(1)
O41	4857(1)	7108(1)	9193(1)	18(1)	27(1)	13(1)	15(1)	–2(1)	–3(1)	3(1)
C1	5486(2)	5239(1)	7558(1)	11(1)	16(1)	10(1)	8(1)	–2(1)	2(1)	1(1)
C11	7694(1)	5779(1)	7819(1)	15(1)	14(1)	17(1)	14(1)	0(1)	–1(1)	–1(1)
C12	8416(2)	5255(1)	7122(1)	24(1)	17(1)	30(1)	26(1)	–7(1)	6(1)	–1(1)
C13	8346(2)	6873(1)	8080(1)	22(1)	19(1)	24(1)	22(1)	–3(1)	–3(1)	–7(1)
C21	3238(1)	5004(1)	7255(1)	15(1)	15(1)	10(1)	20(1)	0(1)	–4(1)	–1(1)
C22	2490(2)	5350(2)	6520(1)	24(1)	22(1)	28(1)	20(1)	0(1)	–4(1)	–3(1)
C23	2420(2)	5143(2)	7992(1)	27(1)	20(1)	41(1)	21(1)	4(1)	1(1)	–6(1)
C32	6232(2)	7998(1)	5178(1)	21(1)	33(1)	12(1)	19(1)	4(1)	4(1)	–1(1)
C33	5133(2)	8059(1)	4612(1)	26(1)	23(1)	21(1)	33(1)	8(1)	3(1)	4(1)
C34	5131(2)	7045(2)	4047(1)	30(1)	36(1)	29(1)	26(1)	4(1)	–12(1)	–9(1)
C35	5217(2)	5950(1)	4515(1)	26(1)	31(1)	20(1)	27(1)	–3(1)	2(1)	–6(1)
C36	6324(2)	5998(1)	5085(1)	21(1)	24(1)	13(1)	25(1)	1(1)	5(1)	2(1)
C42	4972(2)	6095(1)	9670(1)	20(1)	24(1)	16(1)	19(1)	4(1)	–1(1)	–2(1)
C43	6238(2)	6045(1)	10086(1)	19(1)	21(1)	17(1)	18(1)	4(1)	2(1)	4(1)
C44	6452(2)	7098(1)	10592(1)	21(1)	19(1)	26(1)	20(1)	–1(1)	–3(1)	5(1)
C45	6280(2)	8151(1)	10076(1)	23(1)	26(1)	17(1)	26(1)	–7(1)	–3(1)	1(1)
C46	5013(2)	8122(1)	9654(1)	21(1)	28(1)	14(1)	22(1)	–3(1)	–1(1)	7(1)

Atom	X/a·10^4	Y/b·10^4	Z/c·10^4	U(eq)	Atom	X/a·10^4	Y/b·10^4	Z/c·10^4	U(eq)
H1	6801(2)	3666(2)	7972(1)	30(5)	H33B	4330	8072	4918	31
H11	7691	5232	8275	18	H34A	4342	7048	3726	36
H12A	8437	5794	6677	36	H34B	5861	7101	3677	36
H12B	7990	4556	6953	36	H35A	4421	5830	4817	31
H12C	9286	5079	7288	36	H35B	5328	5304	4144	31
H13A	7912	7182	8549	33	H36A	6355	5288	5400	25
H13B	8311	7428	7645	33	H36B	7125	6058	4779	25
H13C	9234	6714	8213	33	H42A	4284	6078	10071	23
H21	3490	4189	7203	18	H42B	4876	5419	9323	23
H22A	3005	5216	6042	35	H43A	6271	5363	10430	23
H22B	2274	6158	6554	35	H43B	6924	5981	9685	23
H22C	1710	4900	6489	35	H44A	5838	7112	11038	26
H23A	2152	5937	8040	41	H44B	7320	7086	10818	26
H23B	2910	4927	8465	41	H45A	6972	8190	9677	27
H23C	1670	4655	7948	41	H45B	6330	8839	10414	27
H32A	7037	8061	4876	25	H46A	4944	8789	9298	25
H32B	6189	8642	5556	25	H46B	4324	8170	10053	25
H33A	5186	8770	4299						

9. References

[1] F. Krafft, *Angew. Chem.* **1969**, *81*, 634; *Angew. Chem. Int. Ed. Engl.* **1969**, *8*, 660

[2] a) Y. Wang, Y. Xie, M. Y. Abraham, R. J. Gilliard, P. Wie, H. F. Schaefer, III, P. V. R. Schleyer, G. H. Robinson, *Organometallics,* **2010**, *29*, 4778; b) M. Regitz in: *Multiple Bonds and Low Coordination in Phosphorus Chemistry*, edited by M. Regitz, O. J. Scherer, Georg Thieme, Stuttgart, 1990

[3] T. E. Gier, *J. Am. Chem. Soc.* **1961**, *83*, 1769

[4] K. Dimroth, P. Hoffmann, *Angew. Chem.* **1964**, *76*, 433; *Angew. Chem. Int. Ed. Engl.* **1964**, *3*, 384

[5] G. Märkl, *Angew. Chem.* **1966**, *78*, 907; *Angew. Chem. Int. Ed. Engl.* **1966**, *9*, 846

[6] G. Becker, *Z. Anorg. Allg. Chem.* **1976**, *423*, 242

[7] M. Yoshifuji, I. Shima, N. Inamoto, *J. Am. Chem. Soc.* **1981**, *103*, 4587

[8] Th. C. Klebach, R. Lourens, F. Bickelhaupt, *J. Am. Chem. Soc.* **1978**, *100*, 4886

[9] C. Gerhardt, *Annalen*, **1858,** *108,* 219

[10] J. Barker, M. Kilner, *Coord. Chem. Rev.* **1994**, *133*, 219

[11] M. L. Coles, D. J. Evans, P. C. Junk, M. K. Smith, *Chem. Eur. J.*, **2003**, *9*, 415

[12] M. L. Coles, P. C. Junk, L. M. Louis, *J. Chem. Soc. Dalt. Trans.*, **2002**, 3906

[13] J. Baldamus, C. Berghof, M. L. Cole, E. Hey-Hawkins, P. C. Junk, L. M. Louis, *Eur. J. Inorg. Chem.*, **2002**, 2878

[14] M. Weidenbruch, *Angew. Chem.*, **2006**, *118*, 4052

[15] A. Strecker, Liebigs, *Ann. Chem.*, **1861**, *118*, 151

[16] T. Yamada, X. Liu, U. Engler, H. Yamane, R. Dronskowski, *Chem. Eur. J.*, **2009**, *15*, 5651

[17] P. J. Pailey, S. Pace, *Coord. Chem. Rev.* **2001**, *214*, 91

[18] F. T. Edelmann, *Coordination Chemistry Reviews*, **1994**, *137*, 403

[19] M. E. Mansfield, M. L. Coles, P. C. Junk, *Dalt. Trans.*, **2005**, 2833

[20] H. P. M. M. Ambrosius, A. H. I. M. van der Linden, J. J. Steggerda, *J. Organomet. Chem.* **1981**, *204*, 211

[21] J. Grundy, M. L. Cole, P. B. Hitchcock, *Dalton. Trans.*, **2003**, 2573

[22] D. H. M. W. Thewissen, H. P. M. M. Ambrosius, H. L. M. Van Gaal, J. J. Steggerda, *J. Organomet. Chem.*, **1980**, *192,* 101

[23] E. P. O. Fuchs, H. Heydt, M. Regitz, W. W. Schoeller, T. Bush, *Tetrahedron Lett.* **1989**, *30*, 5111

[24] J. Grobe, D. Le Van, J. Nientiedt, *Z. Naturforsch.*, **1986,** *41b*, 149

[25] J. Grobe, D. Le Van, J. Nientiedt, B. Krebs, M. Dartmann, *Chem. Ber.* **1988**, *121*, 655

[26] J. Grobe, D. Le Van, B. Krebs, R. Fröhlich, A. Schiemann, *J. Organom. Chem.* **1990**, 389, C29

[27] L. Weber, S. Uthmann, H.-G. Stammler, B. Neumann, W. W. Schoeller, R. Boese, D. Bläser, *Eur. J. Inorg. Chem.* **1999**, 2369

[28] A. N. Chernega, A. V. Ruban, V. D. Romanenko, L. N. Markovski, A. A. Korkin, M. Yu. Antipin, Y. T. Struchkov, *Heteroatom Chem.* **1991**, *2*, 229

[29] L. Weber, S. Kleinebekel, A. Rühlicke, H.-G. Stammler, B. Neumann, *Eur. J. Inorg. Chem.* **2000**, 1185

[30] G. Becker, W. Uhl, H.-J. Wessely, *Z. Anorg. Allg. Chem.* **1981**, *479*, 41

[31] G. Becker, O. Mundt, *Z. Anorg. Allg. Chem.* **1980**, *462*, 130

[32] H. Oehme, E. Leissring, H. Meyer, *Tetrahedron Lett.* **1980**, *21*, 1141

[33] L. Weber, *Eur. J. Inorg. Chem.* **2000**, 2425

[34] K. Issleib, H. Schmidt, H. Meyer, *J. Organomet. Chem.* **1978**, *160*, 47

[35] M. Song, B. Donnadieu, M. Soleilhavoup, G. Bertrand, *Chem. Asian J.* **2007**, *2*, 904

[36] T. van Dijk, S. Burck, M. K. Rong, A. J. Rosenthal, M. Nieger, J. C. Slootweg, K. Lammertsma, *Angew. Chem. Int. Ed.* **2014**, *53*, 9068

[37] K. Paasch, M. Nieger, E. Niecke, *Angew. Chem.* **1995**, *107*, 2600; *Angew. Chem. Int. Ed. Engl.* **1995**, *34*, 2369

[38] U. Seidl, *Diplomarbeit*, Stuttgart, **1991**

[39] U. Seidl, *Dissertation*, Stuttgart, **1995**

[40] G. Becker, W. Schwarz, N. Seidler, M. Westerhausen, *Z. Anorg. Allg. Chem.* **1992**, *612*, 72

[41] Prof. Dr. E.u. Würthwein, University of Münster, personal communication

[42] A. Doddi, D. Bockfeld, T. Bannenberg, P. G. Jons, M. Tamm, *Angew. Chem. Int. Ed.* **2014**, *53*, 13568

[43] SHELXTL Version 5.1, *Bruker AXS Inc.*, Madison (WI), USA, **1998**

[44] G. M. Scheldrick, *Acta Cryst.* **2008**, *A64*, 112

[45] T. Hahn (Hrsg.), *International Tables for Crystallography, Volume A: Space-Group Symmetry, Fifth Edition*, Kluwer Academic Publishers, Dordrecht (NL), **2002**

[46] R. S. Cahn, C. Sir Ingold, V. Prelog, *Angew. Chem.*, **1966**, *78*, 413; *Angew. Chem. Int. Ed. Engl.*, 1966, *5*, 385

[47] H. J. Geise, C. Altona, C. Rombers, *Tetrahedron*, **1967**, *23*, 439

[48] M. Regitz, O. J. Scherer, R. Appel, *Multiple bonds and low coordination in phosphorus chemistry*, Thieme Verlag, Stuttgart, **1990**

[49] R. T. Boeré, M. L. Cole, P. C. Junk, J. D. Masuda, G. Wolmershäuser, *Chem. Commun.* **2004**, 2564

[50] L. Pauling, The Nature of the Chemical Bond, 3rd edn., Cornell University Press, Ithaca, NY, **1960**.; L. Pauling, *Die Nature der chemischen Bindung*; 2nd repr. of the 3rd ed., Verlag Chemie, Weinheim., Kapitel 7, Seite 214, **1976**.

[51] V. Schomaker, D. P. Stevenson, *J. Am. Chem. Soc*., **1941**, *63*, 37

[52] L. Pauling, M. L. Huggins, *Z. Kristallogr.* **1934**, *87*, 205

[53] L. Pauling, *The Nature of the Chemical Bond*, Cornell University Press, New York (USA), **1960**

[54] H. Krafft, *Dissertation*, Stuttgart, **2000**

[55] W. Du Mont, L. Müller, R. Martens, P. M. Papathomas, B. A. Smart, H. E. Robertson, D. W. H. Rankin, *Eur. J. Inorg. Chem*., **1999**, 1381

[56] J. Bruckmann, C. Krüger, *Acta Cryst.*, **1995**, *C51*, 1155

[57] M. Westerhausen, R. Löw, W. Schwarz, *J. Organomet.Chem.* **1996**, *513*, 213

[58] H. R. G. Bender, E. Niecke, M. Nieger, *J. Am. Chem. Soc.* **1993**, *115*, 3314

[59] M. Kapitein, M. Balmer, C. von Hänisch, *Phosphorus, Sulfur, and Silicon and the Related Elements*, **2016**, *191:4*, 641

[60] J. Dykema, T. N Truong, M. S. Gordon, *J. Am. Chem. Soc.* **1985**, *107*, 4535

[61] J. Gorbe, D. Le Van, J. Winnemöller, A. H. Maulitz, B. Krebs, M. Läge, *Z. Anorg. Allg. Chem.* **2000**, *626*, 1141

[62] L. Weber, M. Meyer, H. Stammler, B. Neumann, *Organometallics,* **2003**, *22*, 5063

[63] L. Weber, M. Meyer, H. Stammler, B. Neumann, *Chem. Eur. J.*, **2001**, *7*, 5401

[64] R. Blom, A. Haaland, *J. Mol. Struct*., **1985**, *128*, 21

[65] D. Schomburg, *Z. Naturforsch.*, **1986**, *41b*, 1112

[66] J. E. Huheey, Anorganische Chemie, de Gruyter, Berlin, **1988**, P. 278

[67] M. J. Barrow, E. A. V. Ebsworth, *J. Chem. Soc. Dalton Trans*., **1984**, 563

[68] C. Glidewell, D. W. H. Rankin, A. G. Robiette, G. M. Sheldrick*, J. Mol. Struct.*, **1970**, *6*, 231

[69] W. R. Roper, C. J. Wilkins, *Trans. Faraday Soc*., **1962**, *58*, 1686

[70] M. F. Lappert, M. J. Slade, A. Singh, *J. Am. Chem. Soc.* **1983**, *105*, 302

[71] D. Mootz, A. Zinnius, B. Bottche, *Angew. Chem.* **1969**, *81*, 398

[72] J. L. Atwood, D. E. Berry, S. R. Stobart, M. J. Zaworotko, *Inorg. Chem.* **1983**, *22*, 3480

[73] S. Abele, *Dissertation*, Stuttgart, **1994**

[74] P. Oberprantacher, *Dissertation*, Stuttgart, **2000**

[75] G. Becker, J. R. Heek, U. Hübler, W. Schwarz, *Z. Anorg. Allg. Chem.* **1999**, *625*, 2008

[76] K. Hübler, *Dissertation*, Stuttgart, **1994**

[77] M. E. Mansfield, J. Grundy, M. L. Coles, A. G. Avent, P. B. Hitchcock, *J. Am. Chem. Soc*. **2006**, *128*, 13879

[78] G. Becker, M. Rossler, W. Uhl, *Z. Anorg. Allg. Chem.* **1981**, *473*, 7

[79] Z. Pentelencik, *Dissertation*, Stuttgart, **2012**

[80] V. D. Romanenko, T. V. Sarina, N. V. Kolotilo, L. N. Markovsikii, *Zh. Obschch. Khim.*, **1985**, *55*, 1188

[81] M. Bader, *Dissertation*, Stuttgart, **2002**

[82] F. Lindenberg, J. Sieler, E. Hey-Hawkins, *Phosphorus, Sulfur and Silicon* **1996**, *108*, 279

[83] T. W. Mackewitz, C. Peters, U. Bergsträsser, S. Leininger, M. Regitz, *J. Org. Chem*., **1997**, *62*, 7605.

[84] A. Afonin, I. Ushakov, D. Pavlov, A. Ivanov, A. Mikhaleva, *Magn. Reson. Chem*., **2010**, *48*, 685

[85] H. Gunther, *NMR-Spektroskopie*, Georg Thieme Verlag Stuttgart, **1973**

[86] D. W. Stephan, *Angew. Chem.*, **2000**, 112, 322; *Angew. Chem. Int. Ed.*, **2000**, *39*, 314

[87] M. J. Carney, P. J. Walsh, F. J. Hollander, R. G. Bergman, *J. Am. Chem. Soc.*, **1989**, *111*, 8751

[88] M. J. Carney, P. J. Walsh, R. G. Bergman, *J. Am. Chem. Soc.*, **1990**, *112*, 6426

[89] Z. Hou, D. W. Stephan, *Organometallics,* **1993**, *12*, 3158

[90] Z. Hou, T. L. Breen, D. W. Stephan, *J. Am. Chem. Soc.*, **1992**, *114*, 10088

[91] T. L. Breen, D. W. Stephan, *J. Am. Chem. Soc.*, **1995**, *117*, 11914

[92] TOPSPIN-daisy Version 2.0.0

[93] a) S. M. Kirk, H. C. Quilter, A. Buchard, L. H. Thomas, G. Kociok-Kohn, M. D. Jones, *Dalton Trans.*, **2016**, *45*, 13846; b) T. Kawase, T. Okada, T. Enomoto, T. Kikuchi, Y. Miyake, M. Oda, *Bull. Chem. Soc. Jpn.*, **2003**, *76*, 1793

[94] U. Müller, *Anorganische Strukturchemie*, **2008**, P. 249.

[95] P. J. Walsh, F. Hollander, R. G. Bergman, *Organometallics,* **1993**, *12*, 3723

[96] R. L. Zuckerman, S. W. Krska, R. G. Bergman*, J. Am. Chem. Soc.*, **2000**, *122*, 751

[97] M. R. Collier, M. F. Lappert, J. McMeeking, *Inorg. Nucl. Chem. Lett.*, **1971**, *7*, 689

[98] G. Erker, W. Frömberg, J. L. Atwood, W. E. Hunter, *Angew. Chem. Int. Ed.*, **1984**, *23*, 68

[99] G. Erker, W. Frömberg, C. Krüger, E. Raabe, *J. Am. Chem. Soc.*, **1988**, *110*, 2400

[100] D. R. Armstrong , K. W. Henderson, I. Little, C. Jenny, A. R. Kennedy, A. E. McKeown, R. E. Mulvey, *Organometallics*, **2000**, *19*, 4369

[101] K. W. Henderson, A. Hind, A. R. Kennedy, A. E. McKeown, R. E. Mulvey*, J. Organometallic Chem.*, **2002**, *656*, 63

[102] U. Segerer, S. Blaurock, J. Sieler, E. Hey-Hawkins, *Organometallics*, **1999**, *18*, 2842

[103] The Cambridge Structural Database was used to determine the mean Zr–N bond distance in complexes of the type Cp_2ZrNR_2: F. H. Allen, O. Kennard, *Chem. Des. Autom. News*, **1993**, *8*, 31

[104] C. Lefeber, P. Arndt, A. Tillack, W. Baumann, R. Kempe, V. V. Burlakov, U. Rosenthal, *Organometallics*, **1995**, *14*, 3090

[105] M. J. Carney, P. J. Walsh, F. J. Hollander, R. G. Bergman, *Organometallics*, **1992**, *111*, 761

[106] S. E. d'Arbeloff-Wilson, P. B. Hitchcock, J. F. Nixon, H. Kawaguchi, K. Tatsumi, *J. Organomet. Chem*., **2003**, *672*, 1

[107] W. E. Hunter, D. C. Hrncir, R. Van Bynum, R.A. Penttila, J. L. Atwood, *Organometallics.*, 1983, *2*, 750

[108] J. Jeffery, M. F. Lappert, N. T. Luong-Thi, M. Webb, J. L. Atwood, W. E. Hunter, *J. Chem. Soc. Dalton Trans.*, **1981**, 1593

[109] G. Becker, K. Hübler, J. Weidlein, *Z. Anorg. Allg. Chem.* **1994**, *620*, 16

[110] K. Issleib, H. Schmidt, H. Meyer, *J. Organomet. Chem.*, **1980**, *192*, 33

[111] W. -X. Zhang, M. Nishiura, Z. Hou, *Chem. Commun.*, **2006**, 3812

[112] M. R. Crimmin, A. G. M. Barrett, M. S. Hill, P. B. Hitchcock, P. A. Procopiou, *Organometallics.*, **2008**, *27*, 497

[113] W. -X. Zhang, Z. Hou, *Org. Biomol. Chem.*, **2008**, *6*, 1720

[114] M. P. Coles, P. B. Hitchcock, *Chem. Commun.* **2002**, 2794

[115] G. Jin, C. Jones, P. C. Junk, K. -A. Lippert, R. P. Rose, A. Stasch, *New J. Chem.*, **2009**, *33*, 64

[116] O. I. Kolodiazhnyi, *Tetrahydron Lett.*, **1982**, *23(47)*, 4933

[117] O. I. Kolodiazhnyi, *Phosphorus and Sulfur*, **1983**, *18*, 39

[118] O. I. Kolodiazhnyi, *Zh. Obschch. Khim.*, **1983**, *53*, 1093

[119] H. Oehme, , E. Leibring, H. Meyer, Z. *Chem.*, **1981,** *21,* 407

[120]] L. N. Markovski, V. D. Romanenko, Pidvarko *Zh. Obshch. Khim.*, **1982,** *52(8)*, 1925

[121] A. N. Chernega, M. Yu. Antipin, Yu. T. Struchkov, I. E. Boldescul, T. V. Sarina, V. D. Romanenko, *Ukr. Khim. Zh.*, **1985**. *51,* 868

[122] A. N. Chernega., M. Y. Antipin, Y. T. Struchov, I. E. Bodesu, T. V. Sarina, V. D. Romanenko, *Dokl. AKAD. NaukSSSR*, **1984**, *278,* 365

[123] T. M. Al-Shboul, G. Volland, H. Görls, M. Westerhausen, *Z. Anorg. Allg. Chem.*, **2009**, *635*, 1568

[124] R. S. Turbervill, J. M. Goicoechea, *Organomet.*, **2012**, *31*, 2452

[125] K. Issleib, H. Schmidt, Ch. Wirkner, *Synth. React. Inorg. Met-Org. Chem.*, **1981**, *11(3)*, 279

[126]] D. Stalke, U. Klingebiel, G. M. Sheldrick, *J. Organomet. Chem.*, **1988**, *344*, 37

[127] F. T. Edelmann, F. Knösel, F. Pauer, D. Stalke, *J. Orgmet. Chem.*, **1992**, *438*, 1

[128] S. Freitag, W. Kolodziejski, F. Pauer, D. Stalke, *J. Chem. Soc. Dalton Trans.*, **1993**, 3479

[129] C. Knapp, E. Lork, P. G, Watson, R. Mews, *Inorg. Chem.*, **2002**, *41*, 2014

[130] A. Jana, G. Schwab, H. W. Roesky, D. Stalke, *Inorg. Chem.*, **2008**, *47*, 8990

[131] V. M. McConaghie, H. H. Nielsen, *J. Chem. Phys.* **1953**, *21*, 1836

[132] L. S. Bartell, R. C. Hirst, *J. Chem. Phys.* **1959**, *31*, 449

[133] U. Olsher, R. M. Izatt, J. S. Bradshaw, N. K. Dalley, *Chem. Rev*., **1991**, *91*, 137

[134] R. Allmann In: *Homoatomic Rings, Chains and Macromolecules of Main-Group Elements*, edited by A. L. Rheingold, Elsevier Scientific Publishing Company, Amsterdam, **1977**, Chapter 2, Page 33.

[135] K. Issleib, E. Leißring, M. Riemer, *Z. Chem.*, **1983**, *23*, 99

[136] G. Becker, H.-M. Hartmann, W. Schwarz, *Z. Anorg. Allg. Chem.* **1989**, *577*, 9

[137] G. Becker, B. Eschbach, O. Mundt, N. Seidler, *Z. Anorg. Allg. Chem.* **1994**, *620*, 1381

[138] E. Hey, F. Weller, *J. Chem. Soc., Chem. Commun.* **1988**, 782

[139] M. Wenger, T. Armbruster, *Eur. J. Mineral.* **1991**, *3*, 387

[140] G. R. Giesbrecht, A. Shafir, J. Arnold, *J. Chem. Soc. Dalton, Trans*., **1999**, 3601

[141] M. S. Eisen, M. Kapon, *J. Chem. Soc. Dalton, Trans*., **1994**, 3507

[142] P. C. Junk, M. Coles, *Chem. Cummun*., **2007**, 1579

[143] J. Baldamus, C. Berghof, M. Coles, D. J. Evans, E. Hey-Hawkins, P. C. Junk, *J. Chem. Soc. Dalton, Trans*., **2002**, 4185

[144] a) D. D. Perrin, W. L. F. Armarego, *Purification of Laboratory Chemicals*, 3rd Ed., Pergamon Press, Oxford., 1988; b) T. Kottke and D. Stalke, *J. Appl. Crystallogr.*, **1993**,

26, 615.

[145] M. J. Frisch, G. W. Trucks, H. B. Schlegel, G. E. Scuseria, M. A. Robb, J. R. Cheeseman, J. A. Montgomery Jr., T. Vreven, K. N. Kudin, J. C. Burant, J. M. Millam, S. S. Iyengar, J. Tomasi, V. Barone, B. Mennucci, M. Cossi, G. Scalmani, N. Rega, G. A. Petersson, H. Nakatsuji, M. Hada, M. Ehara, K. Toyota, R. Fukuda, J. Hasegawa, M. Ishida, T. Nakajima, Y. Honda, O. Kitao, H. Nakai, M. Klene, X. Li, J. E. Knox, H. P. Hratchian, J. B. Cross, V. Bakken, C. Adamo, J. Jaramillo, R. Gomperts, R. E. Stratmann, O. Yazyev, A. J. Austin, R. Cammi, C. Pomelli, J. W. Ochterski, P. Y. Ayala, K. Morokuma, G. A. Voth, P. Salvador, J. J. Dannenberg, V. G. Zakrzewski, S. Dapprich, A. D. Daniels, M. C. Strain, O. Farkas, D. K. Malick, A. D. Rabuck, K. Raghavachari, J. B. Foresman, J. V. Ortiz, Q. Cui, A. G. Baboul, S. Clifford, J. Cioslowski, B. B. Stefanov, G. Liu, A. Liashenko, P. Piskorz, I. Komaromi, R. L. Martin, D. J. Fox, T. Keith, M. A. Al-Laham, C. Y. Peng, A. Nanayakkara, M. Challacombe, P. M. W. Gill, B. Johnson, W. Chen, M. W. Wong, C. Gonzalez, J. A. Pople, *Gaussian 03, Revision E.01*, Gaussian, Inc., Wallingford CT, 2004

[146] A. D. Becke, *J. Chem. Phys.*, **1993**, *98*, 5648.

[147] (a) Andrae, U. Haeussermann, M. Dolg, H. Stoll, H. Preuss, *Theor. Chim. Acta*, **1990**, *77*, 123 (b) J. M. L. Martin, A. Sundermann, *J. Chem.. Phys.*, **2001**, *114*, 3408

[148] E. D. Glendering, A. E. Reed, J. E. Carpenter, F. Weinhold, NBO Version 3.1

[148] G. M. Sheldrick, *Program system SHELXTL PLUS*, Rel. 4.0, 1989 (*Siemens Analytical X-ray Instruments, Inc., Madison, WI, USA*). Cited in: J. Grobe, D. Le Van, B. Broschk, M. Hegemann, B. Lüth, G. Becker, M. Böhringer, E-U. Würthwein, *J. Organomet. Chem.*, **1997**, *529*, 177.

[149] V. H. Schäfer, G. Fritz, W. Hölderich, *Z. Anorg. Allg. Chem.*, **1977**, *428*, 222

Acknowledgment

Firstly, I would like to express my sincere gratitude to my late advisor Prof. *G. Becker* for the continuous support of my Ph.D study and related research, for his patience, motivation, and immense knowledge. His guidance helped me in all the time of research and writing of this thesis.

A very special gratitude goes out to Prof. *D. Gudat* for not only taking over the supervision of my dissertation after the death of Prof. *G. Becker* but also for his helpful suggestions concerning NMR spectroscopic analysis and writing the thesis.

My sincere thanks also goes to Dr. *K. Hübler*, Dr. *F. Lissner*, and Dr. *O Mundt*, for their insightful comments and help for the X-ray structure analysis. I would also like to thank Prof. *M. Niemeyer* (Mainz University) for his help in doing the DFT Quantum Calculations of the zirconium complex.

I would also like to thank:

Dr. *W. Frey* at the Institute of Organic Chemistry, University of Stuttgart, for his help in the single crystal X-ray measurements, Mrs. *K. Török* and Mr *B. Rau* for NMR spectroscopy measurements, Mrs. *K. Wohlbold* and Mr. *J. Trinkner* for the measurement of mass spectra, Mrs. *B. Förtsch* for carrying out the elementary analysis, Dr *S. Todisco* For doing the NMR spectra simulations of the zirconium complex.

I would like also to thank my family: my parents and brothers and sister for supporting me spiritually throughout writing this thesis and my life in general.

Last but not least special thanks goes also to my wife for her limitless support and help.

Formula and Structure of Newly Prepared Compounds

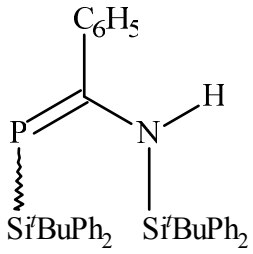

(*Z*)-/(*E*)-**1.2**

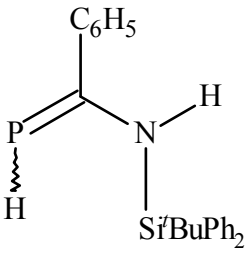

(*Z*)-/(*E*)-**1.1**

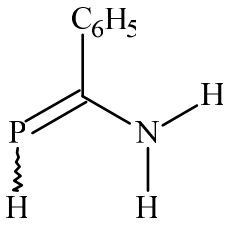

(*Z*)-/(*E*)-**1.0**

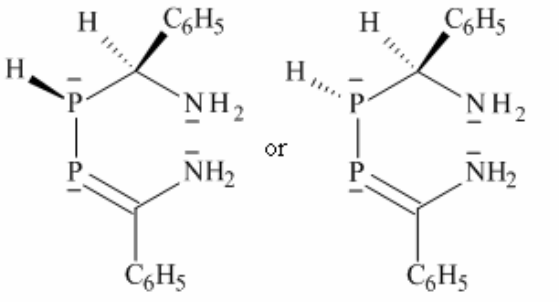

$S_{(P)},S_{(C)}$-(*Z*)-I.01
or
$R_{(P)},R_{(C)}$-(*Z*)-I.01

$R_{(P)},S_{(C)}$-(*Z*)-I.02
or
$S_{(P)},R_{(C)}$-(*Z*)-I.02

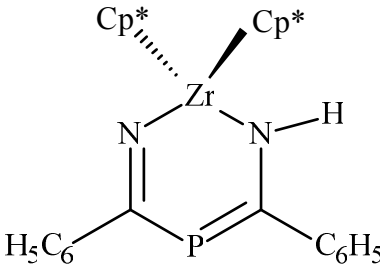

II

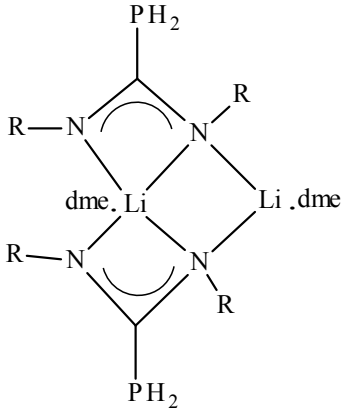

III

R = 4-methyl-phenyl

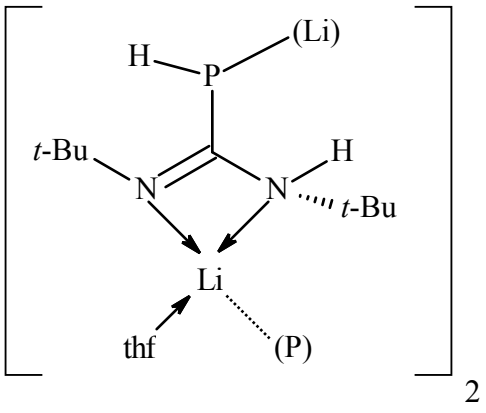

IV

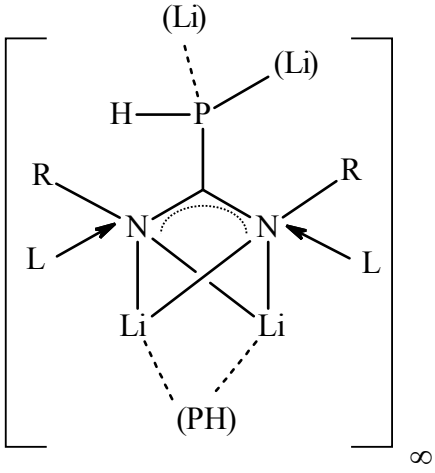

V (R = cyclohexyl;
L = tetrahydrofuran
VI (R = isopropyl;
L = tetrahydropyran

Lebenslauf

Name	Samer Ali Tanash
Gebortstag/-Ort	15.Juli.1976/ Huwwara, Jordanien
Familienstand	Verheiratet
Staatsanghörigkeit	Jordanisch
Adresse	Lüglensheidestr. 29, 70378, Stuttgart
E-Mail	samertanash@yahoo.com

Schulbildung

1982 - 1992	Huwwara Secondary School
1992 - 1994	Irbid Secondary School
Juli 1994	Abschluß: Abitur (Ministry of Education, Jordan)
1994 - 1999	B. Sc. Studium/ Yarmouk Universität-Jordanien
1999 - 2003	M. Sc. Studium/ "Jordan University of Sience and Technology"-Jordanien
2006 - 2007	Gaststudium am Institut für Anorganische Chemie der Universität Stuttgart
2007 - 2017	Promotion am Institut für Anorganische Chemie der Universität Stuttgart

Beschäftigung

2003 - 2004	Chemiker (International Pharmaciutical Research Centre)-Jordanien
2004 - 2006	Chemie Lehrer (Ministry of Education)-Jordanien
2006 - 2012	Wissenschaftliche Hilfskraft am Institut für Anorganische Chemie der Universität Stuttgart